Le cycle biogéochimique du silicium dans l'Océan Austral par les approches isotopiques

Ivia Closset

Thèse de Doctorat
de l'Université Pierre et Marie Curie

Spécialité Biogéochimie Marine

Ecole Doctorale des Sciences de l'Environnement

Le cycle biogéochimique du silicium dans l'Océan Austral par les approches isotopiques

Présentée par
Ivia CLOSSET

Pour l'obtention du grade de
Docteur de L'Université Pierre et Marie Curie

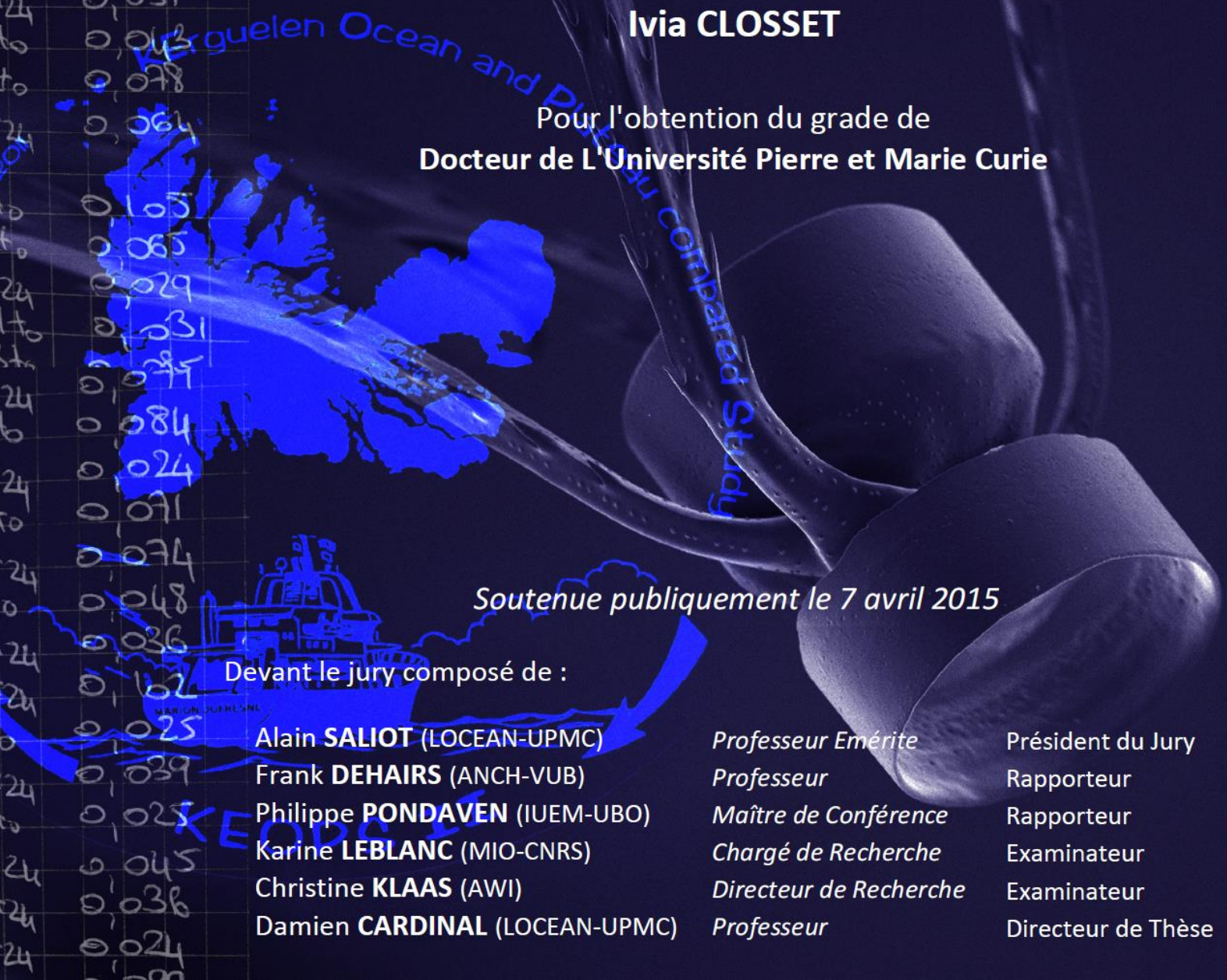

Soutenue publiquement le 7 avril 2015

Devant le jury composé de :

Alain **SALIOT** (LOCEAN-UPMC)	*Professeur Emérite*	Président du Jury
Frank **DEHAIRS** (ANCH-VUB)	*Professeur*	Rapporteur
Philippe **PONDAVEN** (IUEM-UBO)	*Maître de Conférence*	Rapporteur
Karine **LEBLANC** (MIO-CNRS)	*Chargé de Recherche*	Examinateur
Christine **KLAAS** (AWI)	*Directeur de Recherche*	Examinateur
Damien **CARDINAL** (LOCEAN-UPMC)	*Professeur*	Directeur de Thèse

«Voici mon secret.
Il est très simple :
On ne voit bien qu'avec le cœur.
L'essentiel est invisible pour les yeux. »

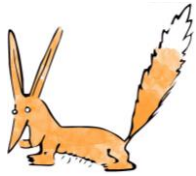

REMERCIEMENTS

Dans le désordre, un immense merci à toutes celles et ceux qui, de près ou de loin, ont contribué à la réalisation de cette thèse.

Mes premiers remerciements vont tout droit à toi Damien, qui m'a encadré pendant ces (un peu plus que) trois années. Merci pour tes encouragements, tes conseils et ton enthousiasme. Tout en me laissant une très grande autonomie, que j'ai beaucoup appréciée, tu as su rester disponible et attentif pour recadrer mon travail, me maintenir parfois les pieds sur terre et me rappeler les échéances. J'ai adoré nos longues discussions le soir (même quand j'étais en retard au judo), faut pas s'étonner si j'ai beaucoup de choses à dire dans les articles après... Merci aussi de m'avoir permis de m'embarquer pour l'aventure KEOPS-2, et d'avoir en partie comblé mon penchant « globe-trotteur » en me permettant de participer à toutes ces conférences. La recherche, c'est aussi savoir transmettre, merci pour ce que tu m'as transmis et pour m'avoir appris à transmettre à mon tour. Merci enfin d'avoir été là aussi dans les moments difficiles, ceux de la recherche et les autres, je t'en suis extrêmement reconnaissante.

Un grand merci également à Frank Dehairs, Karine Leblanc et Mathieu Roy-Barman, membres de mon comité de thèse, pour vos conseils et votre appui scientifique lors de ces réunions annuelles. Merci à vous également de façon plus individuelle : Karine pour nous avoir prise en main avec Marine et nos champs d'ampoules à décanter pendant la campagne KEOPS-2, Frank pour nos discussions pendant les longues heures de filtrations à bord et lors des moments partagés à terre, Mathieu pour tes conseils et tes allers-retours à Gif le samedi pour arrêter le Neptune.

Je tiens très sincèrement à remercier les membres de mon jury d'avoir accepté d'évaluer mon travail. Merci à Alain Saliot d'avoir accepté de présider ce jury, merci à Frank Dehairs et Philippe Pondaven d'avoir accepté la lourde charge de rapporter cette thèse, et merci à Karine Leblanc et Christine Klaas d'avoir accepté de l'examiner.

Parce qu'une thèse implique la production d'une (très) grande quantité de données, je remercie les différentes équipes techniques avec qui j'ai eu un immense plaisir à travailler. Tout particulièrement François Thil (LSCE) avec qui nous avons dû redoubler d'imagination face aux caprices du Neptune, Jacques Navez (MRAC) qui m'a appris à faire des compromis entre stabilité et sensibilité, Irina Djouarev (LOCEAN-IRD) avec qui j'ai même réussi à détraquer le téléphone, et Benoit Villemant et son équipe (ISTeP) pour les (interminables) analyses manuelles sur la délicate colonne de chromatographie anionique. Un grand merci également à l'équipe KEOPS-2 et l'équipage du Marion Dufresne avec qui j'ai partagé pendant 2 mois de mer une sacré aventure, et un certain zef en particulier qui s'est assuré qu'on ne manquait pas de sucreries au labo à 4h du matin, et qu'on a gentiment torturé durant ces 2 mois.

Ce travail est également le fruit de nombreuses discussions. Je pense à François Fripiat, Anne-Julie Cavagna, Andrés Rigual-Hernandez, Marc Elskens, Tom Trull, Céline Ridame et bien d'autres encore… Merci d'avoir éclairé mon chemin au milieu de cette mer de résultats et même dans les profondeurs souvent tortueuses de mes pensées.

Je poursuis en adressant un immense merci…

… Aux habitants présents et passés du 46/00 qui ont tellement contribués au plaisir que j'ai trouvé à faire de la recherche. Vincent, Fanny, Johan, Céline, pour les restos, les bières du mercredi soirs, les jeudis-pâtisserie… ; Virginie et Violaine, grandes sœurs de thèse, qui ont essuyées les pots cassés de l'administration de l'UPMC et de tout le reste avant moi ; merci pour vos précieux conseils et vos « vouis-vouis… tu verras… » compatissants. Julie, Mangalaa, Renaud, Violaine, les suivants (par ordre d'apparition) et à qui je pourrais bientôt dire des « vouis-vouis… tu verras… » compatissants moi aussi ; merci pour la belle bande de patates que nous formons à présent (oui Renaud, c'est toi la patate!), pour ces moments de procrastination partagés au labo ou à l'extérieur, ces parties endiablées de « marcelton », et toutes les bêtises qu'il nous reste à faire pendant ces quelques derniers mois. Pour tout cela, ce n'est pas sans tristesse que je me vois bientôt partir du labo.

… A tous les amis doctorants, ou déjà docteurs, du « dehors » qui vous rappellent qu'il y en a d'autres dans la même galère (et parfois c'est pire !). Tatiana, Marine… pour toutes ces aventures qu'on a partagées, on s'est bien marré quand même mes deux poulettes ! Bon sinon les filles, je suis la plus

âgée, c'est vrai, mais finalement c'est moi la petite dernière, et toc ! Caro, Aless, Mathilde et tous les autres… à vous de jouer maintenant !

… A tous les amis tout court, Marie, Sandrine, Ann-Lor, Greg et Claire, Patrick, Anne, Bergère et tous les autres... Ceux qui, même s'ils ne comprennent pas toujours très bien pourquoi on s'acharne à aller chercher de l'eau en Antarctique alors qu'il suffirait d'ouvrir le robinet de la cuisine… nous encouragent, nous soutiennent et nous rappellent qu'il y a aussi une vie, en dehors de la thèse… Merci pour ces précieux moments à profiter et à penser à autre chose.

… A mes amis judokas (même ceux que j'ai étranglés !). Pour tous ces savoureux moments passés sur le tapis, après l'entrainement, lors des compétitions, et sur les pistes de ski aussi. Même si j'ai progressé en judo, j'ai bien compris que mon cas était désespéré quand j'ai un ballon aux pieds. Merci de m'avoir donné la niaque, de m'avoir appris à me relever quand je tombe, et merci aussi pour tous les nouveaux bleus découverts chaque semaine (même pas mal d'abord !).

… Enfin, à ma famille (de sang, de cœur ou d'adoption). Après tout ce chemin parcouru (sans oublier les nombreux virages parfois à plus de 90°), nous avons toujours partagés les moments de joie comme les moments de doute. Vous avez su à chaque instant avoir les mots qu'il fallait pour me donner confiance et me remonter le moral. Et pour tellement plus… merci !

Et maintenant, Hadjime !

Le cycle biogéochimique du silicium dans l'Océan Austral par les approches isotopiques

Closset Ivia

Sorbonne Universités (UPMC, Univ Paris 06)-CNRS-IRD-MNHN, Laboratoire LOCEAN, Paris, France

Résumé

La biogéochimie de l'Océan Austral joue un rôle crucial dans la régulation de la production primaire marine globale en influençant par exemple la disponibilité des nutriments dans les eaux de surface des basses latitudes. Les variations du cycle du silicium (Si) sont nombreuses et son couplage avec les cycles des autres éléments n'est pas encore bien compris dans cet océan. Nous avons étudié le cycle du Si dans la région naturellement fertilisée en fer de Kerguelen, à l'aide de deux approches isotopiques, permettant d'intégrer différentes échelles spatio-temporelles. Ces analyses suggèrent qu'une pompe de silicium active est rapidement initiée au printemps par la transition d'un mode de production de silice biogénique régénérée à une production dite « nouvelle ». L'évolution saisonnière de la composition isotopique naturelle du Si (δ^{30}Si) est principalement contrôlée par l'équilibre entre les rapports « dissolution sur production » et « Si-supply sur Si-uptake » qui découplent la dynamique isotopique des réservoirs de Si dissous et particulaire (respectivement DSi et BSi). Nous avons identifié une source unique de Si issue des eaux hivernales (WW) du sud-est du Plateau, qui alimente le bloom dans la région. Les échanges hivernaux et estivaux semblent apporter suffisamment de DSi dans la couche de mélange (ML) pour permettre aux diatomées de se développer à des taux élevés de production de BSi (jusqu'à 47.9 mmoles m^{-2} j^{-1}) pendant plus de 80 jours. Nous avons également utilisé les mesures de δ^{30}Si pour retracer les flux saisonniers de BSi vers l'océan profond dans les 3 principales zones de l'Océan Austral. Ces résultats confirment que le δ^{30}Si n'est pas altéré durant la sédimentation des particules. L'évolution saisonnière du δ^{30}Si a permis d'identifier et de quantifier pour la première fois certains processus contrôlant la production des diatomées et leur devenir, tels que les évènements de mélange alimentant la ML en nutriments, ou l'évolution saisonnière de la vitesse de sédimentation des particules. Les variations les plus frappantes ont été mesurées dans la Zone Antarctique où ces vitesses peuvent excéder 200 m j^{-1} en été, et décroitre de façon exponentielle jusqu'à des valeurs très faibles en hiver (<10 m j^{-1}). Ces résultats confirment que le δ^{30}Si du DSi et de la BSi, combinés aux techniques isotopiques de mesure des flux dans la ML, sont des outils prometteurs dans l'amélioration de nos connaissances du cycle du Si et apportent des informations nouvelles à intégrer aux modèles biogéochimiques.

***Mots clés** : Océan Austral, Cycle du silicium, Isotopes, Silice biogénique, Production, Dissolution, Diatomées*

The biogeochemical silicon cycle in the Southern Ocean tracked by isotopic approaches

Closset Ivia

Sorbonne Universités (UPMC, Univ Paris 06)-CNRS-IRD-MNHN, LOCEAN Laboratory, Paris, France

Abstract

Southern Ocean biogeochemistry plays a crucial role on global marine primary production and elemental cycling, impacting the nutrient availability even in low latitude surface waters. Variations in the silicon (Si) cycle are large and its coupling to other nutrient biogeochemical cycles is still not well understood in this ocean. We first investigate the Si cycle in the naturally iron-fertilized Kerguelen area through a combination of two isotopic approaches that integrate different spatio-temporal scales. These analyses suggested that a strong silicon pump was quickly initiated in spring by a switch from regenerated to new biogenic silica production. The seasonal evolution of natural Si isotopic composition ($\delta^{30}Si$) was mainly driven by the balance between the dissolution to production and Si-supply to Si-uptake ratios that decoupled the isotopic dynamics of particulate and dissolved Si-reservoirs (DSi and BSi, repectively). We identified a unique Si-source originated from Winter Water (WW) southeast to the Plateau, fuelling the blooms in the region. Winter and summer water exchanges seemed to bring enough DSi in the Mixed Layer (ML) to allow diatoms growing with relatively high rates of BSi production (up to 47.9 mmol m^{-2} d^{-1}) for more than 80 days, making this area as active as the most productive zones of the world ocean such as coastal upwelling. We also used $\delta^{30}Si$ measurements to track seasonal flows of BSi to the deep sea with an unprecedented temporal resolution and for the three major zones of the open Southern Ocean. These results confirmed that the $\delta^{30}Si$ is well preserved during settling making it an appropriate proxy of the relative Si-utilization by diatoms in the ML. The seasonal evolution of $\delta^{30}Si$ signal allows for the first time to identify and quantify important features about the processes controlling the diatoms' productivity and its fate, such as mixing events that bring nutrients in the ML or the seasonal evolution of particle sinking velocities. The most striking variations were recorded in the Antarctic Zone where sinking rates of BSi can exceed 200 m d^{-1} in summer, and decreased exponentially to very low values in winter (<10 m d^{-1}). These insights confirm that the $\delta^{30}Si$ of DSi and BSi, combined to isotopic technics to measure Si fluxes in the ML, are promising tools to improve our understanding on the Si-biogeochemical cycle and provide new constraints for application to biogeochemical models.

Keywords *: Southern Ocean, Silicon cycle, Silicon isotopes, Biogenic Silica, Production, Dissolution, Diatoms*

AVANT-PROPOS

Contexte de la thèse

Les résultats présentés dans ce manuscrit sont le fruit de 3 années et demie de travail, encadrées par Damien Cardinal au sein de l'équipe « Biogéochimie – Traceurs – Paléoclimats » (BTP) du laboratoire LOCEAN. Ce travail de thèse a débuté avec ma participation à la campagne océanographique KEOPS-2, puis la mise en place progressive du laboratoire de préparation des échantillons pour l'analyse des isotopes du silicium (salle blanche, analyse en routine sur les différents instruments, etc.). Les échantillons de 2 grands projets ont ainsi été préparés, analysés, interprétés et discutés au cours de ces années qui m'ont amenées à échanger et travailler avec de nombreuses personnes. Les résultats présentés dans ce manuscrit sont ainsi le produit de multiples collaborations avec des équipes de recherche qui se trouvent donc étroitement associées à ce travail :

* Le **Laboratoire des Sciences du Climat et de l'Environnement** (LSCE, Gif-sur-Yvette), en particulier les membres de l'équipe GEOTRAC et les personnes en charge de l'instrumentation MC-ICP-MS qui m'ont formée à la délicate utilisation du Neptune^{+}.

* L'**Institut Méditerranéen d'Océanologie** (MIO, Marseille), avec qui l'échantillonnage lors de la campagne et l'analyse des échantillons de production et de dissolution ont été réalisés en étroite collaboration.

* Le **Musée Royal de l'Afrique Centrale** (MRAC, Tervuren), et les personnes en charge du HR-ICP-MS sur lequel ces analyses de flux ont été mesurées, et qui nous ont encadrées lors de nos nombreuses semaines d'analyses.

* L'équipe technique de la **plateforme analytique ALYSES** (IRD, Bondy), en particulier les personnes en charge de l'instrumentation ICP-MS sur lequel j'ai continuellement contrôlé la qualité des protocoles et la propreté de la chimie.

* Les chercheurs de l'**Institut des Sciences de la Terre de Paris** (ISTeP, Paris), qui m'ont permis d'analyser par chromatographie anionique à haute capacité la teneur en sulfates dans la matrice particulièrement complexe des échantillons d'eau de mer.

Ce travail de thèse a également été l'occasion de créer de nombreux échanges, en particulier avec certains membres de l'**Antarctic Climate and Ecosystems Cooperative Research Centre** (ACE-CRC), la **Vrije Universiteit Brussel** (VUB), **Macquarie University**, le **Laboratoire ARAGO** et ne s'achève

pas avec la rédaction de ce manuscrit puisqu'un projet d'ATER me permet de poursuivre cette discussion avec l'analyse d'un nouveau jeu de données.

Soutiens financiers des travaux

Ce travail de thèse a été financé par une bourse du Ministère de l'Enseignement Supérieur et de la Recherche attribuée dans le cadre de l'Ecole Doctorale des Sciences de l'Environnement d'Ile de France (ED 129).

La participation à la campagne océanographique KEOPS-2 (8/10/2011 – 30/11/2011) a été financée par le programme de Recherche Française de l'INSU-CNRS LEFE-CYBER (« Les enveloppes fluides et l'environnment » - « Cycles biogéochimiques, environnement et ressources ») ; le programme SIMI-6 de l'Agence Nationale de la Recherche ; le Centre National d'Etudes Spatiales et l'Institut Polaire Paul-Emile Victor.

L'analyse des échantillons a été financée par le projet MuSiCC (« a **Mu**lti-proxy approach on the marine biogeochemical **Si**licon and **C**arbon **C**ycles ») soutenu par le programme de l'Union Européenne (FP7, CIG Marie Curie).

Valorisation de la thèse

Les résultats présentés dans ce manuscrit sont déjà impliqués dans 2 publications scientifiques :

Closset I., M. Lasbleiz, K. Leblanc, B. Quéguiner, A.-J. Cavagna, M. Elskens, J. Navez, D. Cardinal (2014), Seasonal evolution of net and regenerated silica production around a natural Fe-fertilized area in the Southern Ocean estimated with Si isotopic approaches, Biogeosciences, 11, 5827-5846, doi:10.5194/bg-11-5827-2014. *(Chapitre 1)*.

Rigual-Hernandez A.S., T.W. Trull, S.G. Bray, **I. Closset**, L.K. Armand (2015), Seasonal dynamics in diatom export fluxes to the deep sea in the Australian sector of the Antarctic Zone, Journal of Marine Systems, 142, 62-74. *(Article Annexe 1)*.

D'autres articles liés à ces travaux sont en cours de révision :

Cavagna A-J., F. Fripiat, M. Elskens, F. Dehairs, P. Mangion, L. Chirurgien, **I. Closset**, M. Lasbleiz, L. Flores-Leiva, D. Cardinal, K. Leblanc, C. Fernadez, D. Lefèvre, L. Oriol, S. Blain, B. Quéguiner (2014), Biological productivity

regime and associated N cycling in the vicinity of Kerguelen Island area, Southern Ocean, Biogeosciences Discussion, 11, 18073-18104.

Jacquet S. H. M., F. Dehairs, A.-J. Cavagna, F. Planchon, L. Monin, L. André, **I. Closset**, D. Cardinal (2014), Early season mesopelagic carbon remineralization and transfer efficiency in the naturally iron-fertilized Kerguelen area, Accepted in Biogeosciences.

Enfin, au moins 2 articles incluant les résultats présentés dans ce manuscrit sont actuellement en préparation :

Closset I., D. Cardinal, S. Bray, F. Thil, I. Djouraev, A. S. Rigual-Hernandez, T. Trull (2015), Seasonal variations, origin and fate of settling diatoms in the Southern Ocean tracked by silicon isotope records in deep sediment traps, submitted to Global Biogeochemical Cycles.

Closset I., D. Cardinal, F. Thil, (2015), Controls on seasonal variations of Si isotopic composition of diatoms and seawater related to iron supply and mesoscale activity in the naturally Fe-fertilized Kerguelen area (Southern Ocean), in prep.

SOMMAIRE

INTRODUCTION GENERALE

CHAPITRE I : Evolution Saisonnière de la Production de Silice Biogénique dans l'Océan de Surface

CHAPITRE 2 : Facteurs de Contrôle des Variations Saisonnières des Isotopes du Silicium

CHAPITRE 3 : Variations Saisonnières, Origine et Devenir du Flux de Diatomées dans la Colonne d'eau

SYNTHÈSE et PERSPECTIVES

MATERIEL SUPPLEMENTAIRE et ANNEXES

Introduction Générale

1. L'Océan Austral et son rôle dans le climat

L'océan joue un rôle central dans le système climatique terrestre en absorbant environ ¼ des émissions anthropiques de CO_2 (i.e. 2.5 ± 0.5 GtC an^{-1}), et par conséquent en régulant l'accumulation dans l'atmosphère de ce gaz à effet de serre (Le Quéré et al., 2014). En effet, les variations de la pression partielle de CO_2 atmosphérique (pCO_2) sont le bilan des émissions anthropiques de carbone et l'action d'un certain nombre de processus terrestres et océaniques qui retirent ou émettent du CO_2. Les océans constituent ainsi une mosaïque de régions qui absorbent (zones puits) et qui rejettent (zones sources) du CO_2 dans l'atmosphère (Takahashi et al., 2009). Au niveau global, les régions de hautes latitudes, et en particulier l'Océan Austral, représentent des puits importants de CO_2. Ainsi, même s'il couvre moins de 15% de la surface totale de l'océan mondial, l'Océan Austral serait responsable d'environ un tiers du puits océanique (Gruber et al., 2009 ; Lenton et al., 2013), faisant de lui un acteur majeur dans la régulation du climat actuel. Les capacités d'absorption du CO_2 atmosphérique ne sont pas réparties de façon homogène dans cet océan et dépendent fortement des propriétés physiques et biogéochimiques des eaux de surface.

La majeure partie de l'Océan Austral est constituée d'un courant dirigé vers l'est sur l'ensemble de la colonne d'eau : le Courant Circumpolaire Antarctique (ACC) entourant le continent Antarctique et connectant les trois grands bassins océaniques (Atlantique, Pacifique et Indien). Ce puissant courant est traditionnellement divisé en plusieurs zones océanographiques possédant une saisonnalité et des propriétés physico-chimiques relativement uniformes, et séparées par des fronts hydrologiques (Orsi et al., 1995 ; Sokolov & Rintoul, 2007). On distingue du nord au sud (*Fig. I.1.*) : la Zone Sub-Antarctique (SAZ) située entre le Front Sub-Tropical (STF, non représenté sur la figure) et le Front Sub-Antarctique (SAF) et la Zone du Front Polaire (PFZ) située entre le SAF et le Front Polaire (PF). Ces deux zones constitueraient le puits de CO_2 atmosphérique le plus important de l'ACC dont les capacités d'absorption seraient maximales dans la SAZ, et diminueraient progressivement vers le sud (Metzl et al., 1999 ; Takahashi et al., 2009). Enfin, au sud du PF se trouve la Zone Antarctique (AZ), parfois appelée zone libre de glace en permanence (Permanently Open Ocean Zone, POOZ) puis une zone sous l'influence de la glace de mer (Seasonal Ice Zone, SIZ), qui à l'inverse, représenterait une faible source de CO_2 (Takahashi et al., 2009). L'intensité et la position exacte des fronts varient le plus souvent en réponse à des interactions avec la bathymétrie et sont généralement associées à une forte activité

mésoéchelle (méandres, tourbillons, filaments etc.) stimulant la production primaire (e.g. Sokolov & Rintoul, 2007).

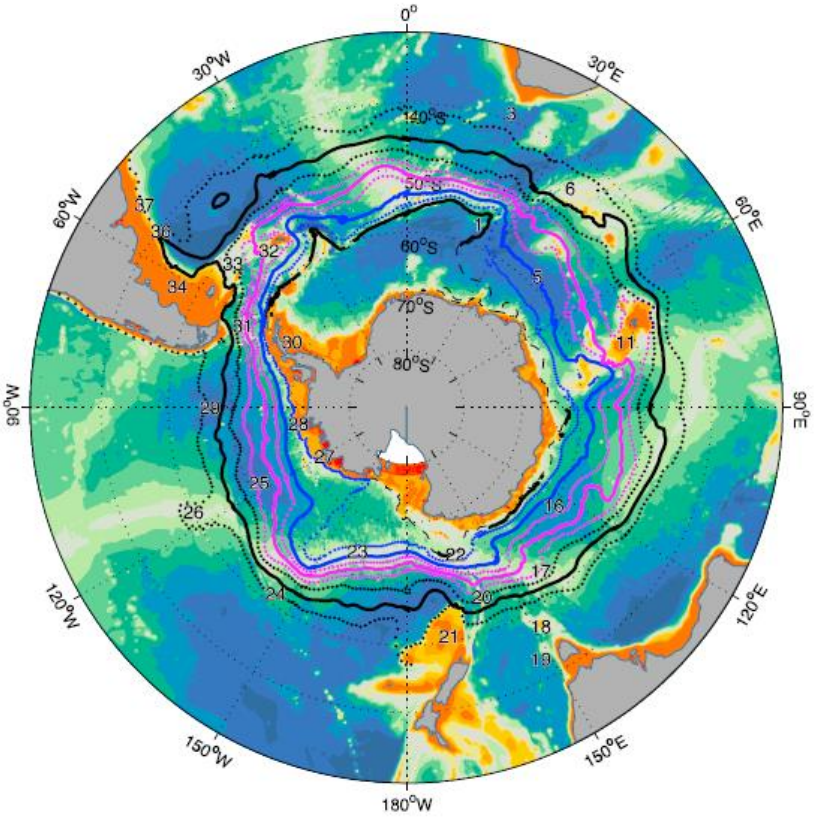

Figure I.1. Carte de la bathymétrie de l'Océan Austral, représentant la position moyenne (en traits pleins) des fronts du Courant Circumpolaire Antarctique (ACC) déterminée à partir des données d'altimetrie (Solokov & Rintoul, 2009). Du nord au sud : Le Front Sub-Antarctique (SAF, noir), le Front Polaire (PF, magenta), le Front Sud de l'ACC (SACCF, bleu), la limite Sud de l'ACC (SB, noir).

Cette structuration frontale particulière est à l'origine de processus de remontée d'eaux profondes riches en nutriments (upwelling), de formation d'eaux denses et de subduction formant des eaux intermédiaires, moteurs de la circulation thermohaline (Marshall & Speer, 2012 ; *Fig. I.2.*). Cette circulation à grande échelle, induite par les différences de densité des masses d'eau, prend ainsi naissance dans l'Océan Austral au sud du PF avec la remontée des eaux profondes circumpolaires (Upper Circumpolar Deep Water, UCDW ; et Lower Circumpolar Deep Water, LCDW) au niveau de la Divergence Antarctique (AD) puis se sépare en deux boucles distinctes (Speer et al., 2000 ; Trull et al., 2001). Une partie de ces eaux migrent vers le sud par transport d'Ekman induit par les vents d'est autour du continent, se refroidissent et forment les Eaux Antarctiques de Fond (Antarctic Bottom Water, AABW) qui vont s'écouler le long de la pente continentale. L'autre partie se dirige en surface vers le nord sous l'effet du transport d'Ekman créé par les régimes de vents d'ouest dominant la Zone

Antarctique, puis subductent pour former les Eaux Antarctiques Intermédiaires (AAIW) et les Eaux Modales Sub-Antarctiques (SAMW) au niveau du PF et du SAF, respectivement. Cette deuxième boucle entraine un export des Eaux de Surface Antarctiques (AASW) et de leurs propriétés physiques et chimiques vers les basses latitudes via la formation des AAIW et SAMW, contrôlant ainsi en partie l'apport de nutriments et donc le développement des organismes phytoplanctoniques (ou production biologique) à ces plus faibles latitudes. Sarmiento et al. (2004) ont en effet montré que les SAMW qui se dispersent à travers tout l'Hémisphère Sud et jusque dans l'Atlantique Nord, représentent la source principale de nutriments dans les régions d'upwelling du Pacifique Equatorial et seraient à l'origine des trois quarts de la production biologique au nord de 30°S. Ainsi, les processus biogéochimiques dominant les eaux de surface antarctiques, tels que la consommation ou le recyclage des nutriments, vont avoir des conséquences importantes sur la disponibilité en nutriments, la production biologique et l'absorption de CO_2 de l'océan mondial.

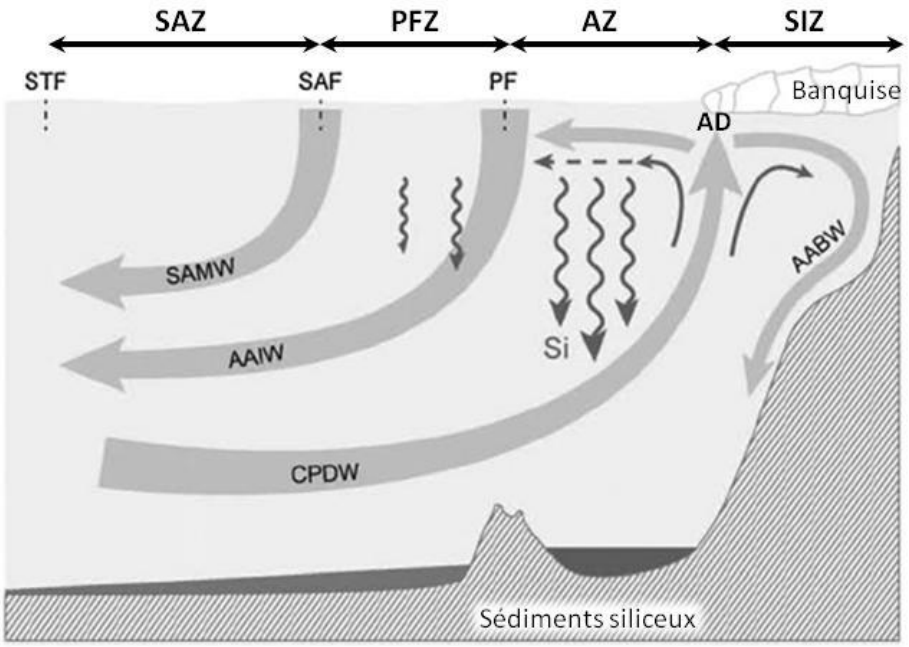

Figure I.2. Schéma de la circulation verticale des masses d'eau dans l'Océan Austral (modifié d'après Tréguer, 2014). Les eaux profondes circumpolaires (CPDW) remontent en surface au niveau de la Divergence Antarctique (AD), et replongent en profondeur dans la Zone de Glace Saisonnière (SIZ) pour former les Eaux Antarctique de Fond (AABW) ; ou migrent vers le nord et plongent en subsurface dans la Zone du Front Polaire (PFZ) en formant les Eaux Antarctiques Intermédiaires (AAIW) ou dans la Zone Sub-Antarctique (SAZ) en formant les Eaux Modales Sub-Antarctique (SAMW). Les lignes en tirets représentent la localisation des fronts : le Front Polaire (PF), le Front Sub-Antarctique (SAF) et le Front Sub-Tropical (STF).

2. Facteurs de contrôle de la fixation et de l'export de carbone dans l'Océan Austral

Dans l'Océan Austral, le transfert de CO_2 atmosphérique vers l'océan s'opère par le biais de l'action combinée de mécanismes appelés pompes à carbone. Les réactions physico-chimiques du CO_2 avec l'eau de mer contrôlées par son équilibre thermodynamique à l'interface air-mer (loi de Henry) et combinées à son transport vertical via la circulation thermohaline, constituent la pompe physique de carbone (ou pompe de solubilité). La dissolution du CO_2 dans l'eau de mer est donc un processus abiologique, favorisé dans les eaux froides des hautes latitudes. La transformation du carbone inorganique dissous (Dissolved Inorganic Carbon ou DIC) par les micro-organismes photosynthétiques, dans la couche éclairée de l'océan (couche euphotique), en carbone organique dissous et particulaire (DOC et POC) constitue la première étape de la pompe biologique de carbone (*Fig. I.3.*). Une grande partie de ce carbone organique est directement reminéralisé à l'échelle saisonnière dans la couche de mélange par les organismes hétérotrophes (bactéries et zooplancton). Le carbone non recyclé dans les couches superficielles de l'océan est quant à lui exporté vers l'océan plus profond où il continue à se reminéraliser et est stocké sur des périodes s'étendant de plusieurs milliers à plusieurs millions d'années en fonction de la profondeur à laquelle il est exporté (Boyd & Trull, 2007 ; *Fig. I.3)*. Cette notion de profondeur d'export (et donc de durée de stockage) dépend fortement des processus physiques et biogéochimiques tels que la vitesse de sédimentation des particules ou l'activité de reminéralisation bactérienne, et implique que seulement une très faible fraction du carbone organique produit en surface atteint les sédiments (François et al., 2002 ; Klaas & Archer, 2002). La pompe biologique de carbone est donc le résultat d'interactions complexes entre les processus biogéochimiques qui contrôlent l'intensité de la production de carbone organique (production primaire) dans l'océan de surface et ceux qui définissent l'efficacité de l'export de cette production en profondeur. L'identification et la quantification des impacts de ces différents processus ainsi que leurs réponses aux variations de l'environnement, en particulier dans les hautes latitudes, est un enjeu majeur de la recherche dans le contexte actuel de changement climatique (Achterberg, 2014).

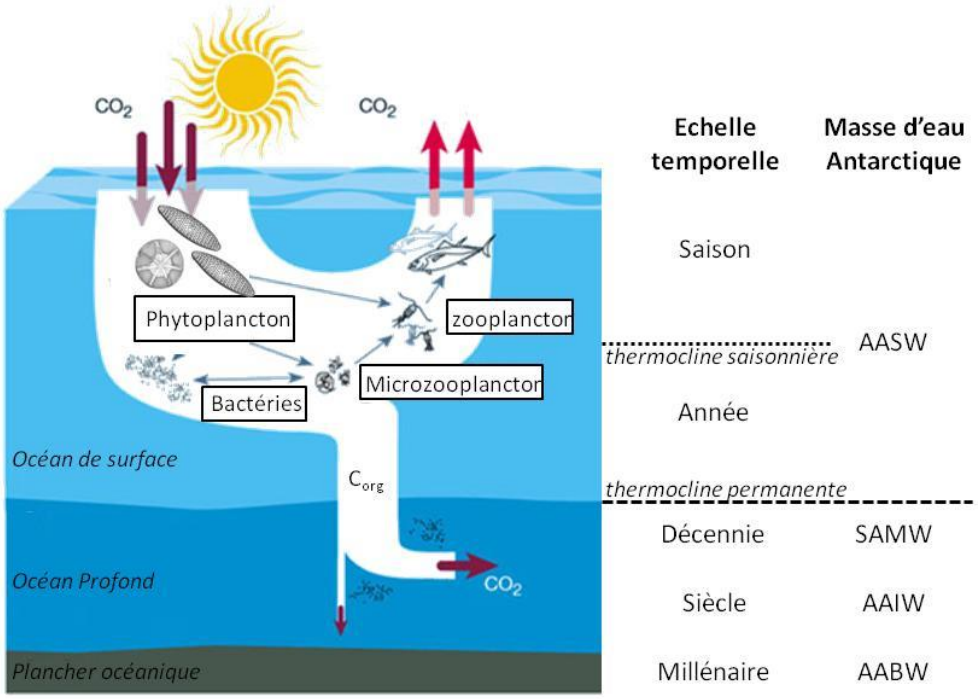

Figure I.3. Représentation schématique de la pompe de carbone biologique et des échelles de temps correspondant aux profondeurs et aux masses d'eau dans lesquelles est exporté et stocké le carbone organique (C_{org}) produit en surface (Adapté d'après Chisholm, 2000 et Boyd & Trull, 2007). De la surface vers le fond : Eau de Surface Antarctique (AASW), Eau Modale Sub-Antarctique (SAMW), Eau Antarctique Intermédiaire (AAIW) et Eau Antarctique de Fond (AABW).

Dans l'Océan Austral, la production primaire et l'export de matière organique sont généralement decouplés et soumis à une très forte saisonnalité (Quéguiner, 2013). En effet, les caractéristiques particulières de cet océan (l'influence de la couverture saisonnière de glace, les périodes irrégulières d'ensoleillement, ainsi que le régime des vents particulièrement intenses dans cette région du globe) génèrent des conditions optimales pour la croissance du phytoplancton en début d'été lorsque la colonne d'eau est fortement stratifiée, que les concentrations en nutriments sont élevées et que l'éclairement est maximum. L'export de matière, en revanche, s'effectue le plus souvent lors d'épisodes de déstabilisation de la couche de mélange induits par les vents violents qui s'établissent plutôt au début de l'automne (Quéguiner, 2013). Cependant, en dépit de concentrations relativement importantes de nutriments (en particulier les nitrates) disponibles dans les eaux de surface en début de saison, les concentrations en chlorophylle *a* (Chl *a*), indicateur de la biomasse phytoplanctonique, et les taux de production primaire nette demeurent relativement faibles (Chl *a* < 0.5 mg m^{-3}, Arrigo et al., 1998 ; Moore & Abbot, 2000 ; Sokolov & Rintoul, 2007). L'océan Austral représente ainsi la plus grande Zone HNLC (High-Nutrient Low-Chlorophyll) à la surface de la planète (Martin, 1990). En effet, durant l'hiver, la circulation thermohaline, combinée à un mélange vertical

particulièrement intense, transporte les eaux profondes vers la surface et représente le mécanisme majeur d'apport de nutriments dans la couche euphotique (Marshall & Speer, 2012). En raison du faible développement phytoplanctonique, les stocks de nitrates (NO_3^-) et phosphates (PO_4^{3-}) présents dans la couche de mélange à la fin de l'été ne sont pas totalement épuisés (e.g. Mosseri et al., 2008). La conséquence majeure de cette situation est que de grandes quantités de nutriments non utilisés (appelés alors préformés) quittent la couche de surface, via la formation des AAIW et SAMW, et sont redistribués dans les eaux de surface des faibles et moyennes latitudes (Sarmiento et al., 2004).

Contrairement à d'autres régions océaniques, la production primaire dans l'Océan Austral serait contrôlée simultanément par différents facteurs limitants au cours de la saison (Boyd et al., 1999 ; 2001). Les faibles conditions d'éclairement induites par un régime de mélange vertical défavorable sont probablement la cause principale de la limitation de la croissance du phytoplancton en hiver ou au début du printemps (Nelson & Smith, 1991 ; Blain et al., 2001). Durant l'été, la production primaire n'est plus limitée par des paramètres physiques mais principalement par la disponibilité en éléments traces (ou micronutriments) tels que le fer. En effet, de nombreuses études ont montré que le fer jouait un rôle clé dans le contrôle de la croissance des micro-organismes photosynthétiques en particulier au sein de l'ACC (Boyd, 2002a ; de Baar et al., 2005 ; Boyd et al., 2007). Enfin, à la fin de l'été, l'augmentation de la prédation par le zooplancton herbivore contribue également au déclin du bloom phytoplanctonique (Smetacek et al., 2004 ; Safi et al., 2007). L'importance relative de ces différents facteurs dans l'Océan Austral est encore aujourd'hui sujet à débat (Boyd, 2002b), néanmoins, il semble que le fer joue un rôle fondamental. En effet, malgré des concentrations en fer dissous (dFe) généralement très faibles dans les eaux de surface antarctiques (en moyenne de 0.221 à 0.317 nM ; Tagliabue et al., 2012), des blooms importants et récurrents sont observés localement à proximité des sources de fer telles que les marges continentales, les remontées du plancher océanique entourant certaines îles et les régions frontales (Blain et al., 2007 ; Bowie et al., 2009 ; Tagliabue et al., 2012). D'autres types de sources peuvent également favoriser de façon saisonnière la croissance du phytoplancton. Par exemple, ces apports de fer peuvent avoir lieu sous la forme de dépôts de poussières atmosphériques (Tagliabue et al., 2009) ou encore de la fonte de la banquise (e.g. Lannuzel et al., 2007 ; Van der Merwe et al., 2011). Dans la grande majorité des cas, l'apport de fer dans la couche de surface s'effectue par diffusion diapycnale (c'est-à-dire perpendiculaire au gradient de densité), lors des remontées d'eau profondes (par exemple lié à un transport d'Ekman), ou par mélange (ou entrainement) vertical (Tagliabue et al., 2014).

Depuis que le statut de zone HNLC de l'Océan Austral lié aux faibles concentrations en fer mesurées a été établit, de nombreuses études ont été mises en place afin d'étudier les origines et les conséquences d'une telle limitation en fer ainsi que la réponse de la pompe biologique de carbone face à un enrichissement (naturel ou artificiel) en fer (de Baar et al., 2005 ; Boyd et al., 2007). Dans le contexte du changement climatique actuel, l'idée de fertiliser artificiellement en fer les régions HNLC de l'océan afin de stimuler la pompe biologique et d'augmenter la capacité de l'océan à absorber le CO_2 anthropique a progressivement émergé et s'est appuyée principalement sur les processus biogéochimiques qui interviennent au sein de deux hypothèses majeures en paléo-océanographie :

- L' « hypothèse du fer » de John Martin (1990) propose que les cycles glaciaires-interglaciaires du CO_2 atmosphérique pourraient être en partie contrôlés par les variations des apports atmosphériques de fer dans l'Océan Austral, qui favoriseraient localement la production primaire en période glaciaire diminuant significativement la pCO_2 atmosphérique (de l'ordre de 40 % inférieure à la pCO_2 actuelle ; Petit et al., 1999).

- La « Silicic Acid Leakage Hypothesis » (SALH) proposée par Matsumoto et al. (2002), attribue pour partie ces modifications glaciaires-interglaciaires de pCO_2 (environ 50 ppm sur les 100 ppm observés) à une influence plus indirecte des variations des flux de fer, qui dans ce cas, découpleraient les cycles biogéochimiques de l'azote et du silicium dans la couche de mélange de l'ACC. Ceci modifierait la disponibilité des nutriments préformés exportés aux plus faibles latitudes via la circulation thermohaline et augmenterait l'efficacité de la pompe biologique dans ces régions océaniques.

Néanmoins, de nombreuses interrogations demeurent en ce qui concerne l'efficacité réelle de telles fertilisations artificielles, ainsi que sur leurs conséquences sur l'équilibre des systèmes chimiques et biologiques de l'océan (Buesseler & Boyd, 2003). Par exemple, d'après les modèles biogéochimiques couplés aux modèles de circulation océaniques, une diminution de la pCO_2 atmosphérique de 15 ppm à 33 ppm serait possible uniquement dans le cas d'une fertilisation globale et continue de la totalité de l'océan mondial pendant une période d'un siècle, ce qui est techniquement irréalisable (IPCC, 2013).

Certains programmes d'observations et de collecte de données à l'échelle mondiale tels que le programme GEOTRACES, intègrent en partie ces interrogations à leurs objectifs généraux. GEOTRACES est un programme international de recherche ayant pour but de cartographier la distribution des éléments en traces et de certaines compositions isotopiques dans l'océan ainsi que de comprendre les

processus biogéochimiques contrôlant leur distribution. Ce programme comporte de nombreuses campagnes océanographiques, regroupées en « Process Studies » et « Section Cruises ». Les premières ont pour objectif de documenter l'ensemble des processus contrôlant les cycles biogéochimiques des nutriments dans une région d'intérêt. Les campagnes KEOPS (janvier-février 2005) et KEOPS-2 (octobre-novembre 2011) qui se concentrent sur le Plateau de Kerguelen dans le secteur indien de l'Océan Austral font parties de ce type de campagnes océanographiques et seront discutées dans les chapitres 1 et 2 de cette thèse. Les « Section Cruises » telles que le transect SR3 au sud de l'Australie (présenté dans le chapitre 3), sont plutôt dédiées à l'étude de la variabilité saisonnière de la distribution des éléments en étant régulièrement revisitées à différentes périodes de l'année.

3. Le cycle biogéochimique du silicium dans l'Océan Austral

Dans l'Océan Austral, la production primaire est très souvent dominée par des groupes phytoplanctoniques siliceux, dont le succès écologique semble principalement lié à leur capacité à former une paroi cellulaire de silice amorphe. En représentant le principal vecteur de la pompe biologique de carbone dans ces régions de hautes latitudes, ces organismes permettent un lien étroit entre le cycle biogéochimique du silicium et celui du carbone, ainsi que celui d'autres éléments tels que l'azote. L'étude du cycle biogéochimique du silicium (par la quantification des différents réservoirs et flux) présente donc un intérêt scientifique majeur (*Fig. I.4.*), en particulier dans l'ACC dont les eaux de surface se caractérisent par un gradient des concentrations en silicium dissous extrêmement important (Sarmiento et al., 2004) et dont les dépôts sédimentaires sont quasiment exclusivement siliceux.

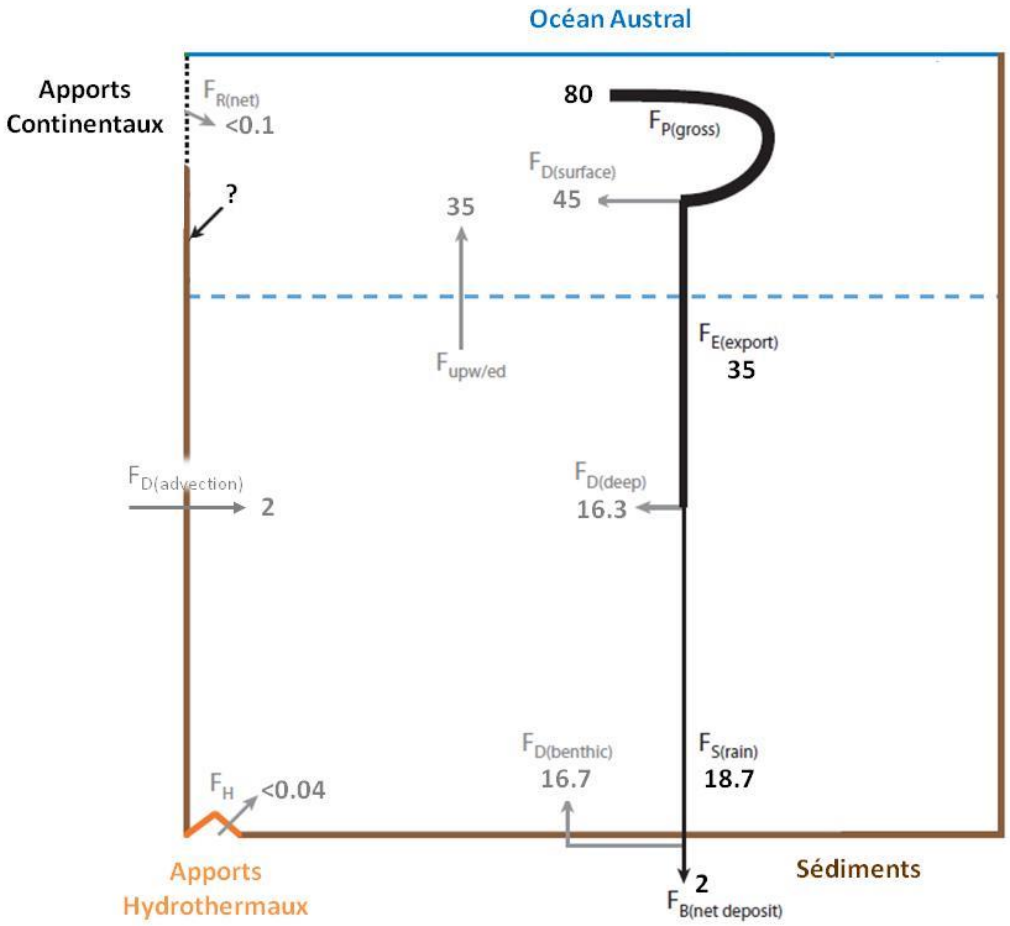

Figure I.4. Représentation schématique du cycle biogéochimique du silicium dans l'Océan Austral (modifié d'après Tréguer & De la Rocha, 2013 et Tréguer, 2014). Les flèches grises représentent les flux (F) de silicium dissous (en Tmoles Si an^{-1}) : $\mathbf{F_{R(net)}}$: apports net des fleuves; $\mathbf{F_{upw/ed}}$: flux de DSi vers la couche de mélange et originaire du réservoir profond ; $\mathbf{F_{D(surface)}}$: Flux de DSi recyclé en surface ; $\mathbf{F_{D(deep)}}$: flux de DSi recyclé en profondeur ; $\mathbf{F_{D(benthic)}}$: flux de DSi recyclé à l'interface eau-sédiment ; $\mathbf{F_H}$: apports hydrothermaux. Les flèches noires représentent les flux de silicium particulaire (en Tmoles Si an^{-1}) : $\mathbf{F_{P(gross)}}$: production de BSi ; $\mathbf{F_{E(export)}}$: flux de BSi exportée en profondeur ; $\mathbf{F_{S(rain)}}$: flux de BSi atteignant l'interface eau-sédiment ; $\mathbf{F_{B(net\ deposit)}}$: dépôt net de BSi dans les sédiments.

Au pH naturel de l'eau de mer (pH ≈ 8), le silicium dissous (ou DSi) se trouve principalement sous la forme d'acide orthosilicique (ou acide silicique) de formule H_4SiO_4. L'océan reçoit des apports d'acide silicique majoritairement depuis la lithosphère via les processus d'érosion des sols et de ruissellement (l'apport par les fleuves représente plus de 80% des flux en direction de l'océan, Tréguer & De La Rocha, 2013). Dans l'Océan Austral, les apports de silicium dans les eaux de surface se font en revanche principalement par mélange vertical : via la convection hivernale, la circulation thermohaline induisant des upwellings, ou la diffusion ($\mathbf{F_{upw/ed}}$ sur la *figure I.4.* ; Tréguer, 2014). Le temps de résidence du silicium dans l'océan étant très long (environ 10 000 ans ; Tréguer & De La Rocha, 2013), les variations

des concentrations de DSi observées en surface sont donc la conséquence des apports et de l'activité biologique, cette dernière résultant de l'équilibre entre les mécanismes d'absorption par les organismes (ou uptake, $\mathbf{F_{P(gross)}}$ sur la *figure I.4.*) et de dissolution des particules siliceuses ($F_{D(surface)}$ sur la *figure I.4.*). En effet, dans la couche euphotique de l'ACC, les organismes siliceux absorbent l'acide silicique et le polymérisent sous la forme de silice amorphe hydratée ($SiO_2.nH_2O$) ou opale, également appelée silice biogénique (BSi). La conséquence principale de cette activité biologique qui consomme le stock de DSi dans les eaux de surface, est la formation d'un gradient latitudinal des concentrations d'acide silicique qui s'étend sur toute la superficie de l'Océan Austral (Ragueneau et al., 2000 ; Sarmiento et al., 2004 ; *Fig. I.5b.*). Ainsi, les concentrations en DSi peuvent atteindre 100 µmoles L^{-1} au sud du PF et diminuent jusqu'à moins de 2 µmoles L^{-1} dans la SAZ en fonction de la saison (e.g. Brzezinski et al., 2001 ; Nelson et al., 2001). Les stocks de DSi ne sont donc jamais épuisés au cours de la saison dans la AZ, alors que la production biologique est limitée par de faibles concentrations d'acide silicique de façon saisonnière dans la PFZ (uniquement à la fin de l'été) et de façon permanente dans la SAZ (Rintoul et al., 2001 ; Trull et al., 2001 ; *Fig. I.5a.*).

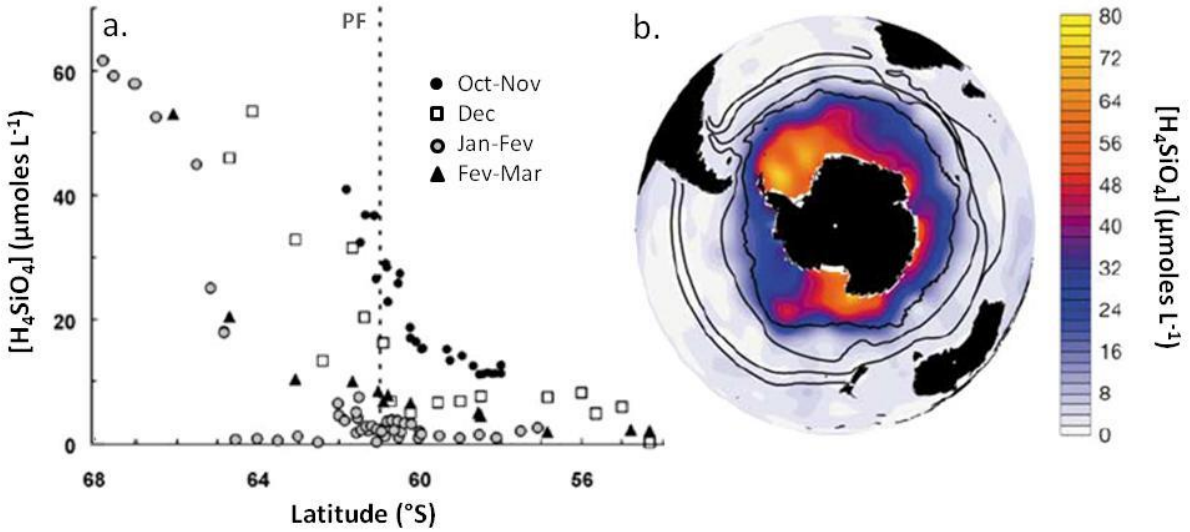

Figure I.5. (a.) Evolution saisonnière des concentrations de surface de DSi (en µmoles L^{-1}) en fonction de la latitude (adapté d'après Nelson et al., 2001 et Sarmiento et al., 2004). (b.) Distribution des concentrations moyennes annuelles de DSi en surface (en µmoles L^{-1}), les lignes noires représentent la position des principaux fronts (du nord au sud les Fronts Sub-Tropicaux Nord et Sud, le Front Sub-Antarctique et le Front Polaire).

La production de silice biogénique moyenne de l'ACC a été estimée à 80 ± 10 Tmoles Si an^{-1} (Pondaven et al., 2000), ce qui représente environ un tiers de la production marine totale de BSi. A

l'échelle globale comme dans l'Océan Austral, environ 50 % de cette production brute est directement recyclée dans les couches superficielles entrainant un apport significatif de DSi dans la ML (Tréguer & De La Rocha, 2013 ; Holzer et al., 2014). On peut donc très certainement envisager que dans certaines zones de l'ACC et/ou à certaines périodes de l'année, la production de silice dans la couche euphotique puisse être basée sur du silicium régénéré plutôt que sur un apport depuis les couches plus profondes de l'océan. Ainsi, seules les particules siliceuses échappant à cette dissolution seront exportées dans l'océan profond puis éventuellement stockées dans les sédiments, cette sédimentation ne représenterait que 3 % de la BSi produite en surface (Tréguer & De La Rocha, 2013). Néanmoins, l'accumulation d'opale dans les sédiments est très importante dans cette région de l'océan, en particulier au sud du PF où elle peut atteindre jusqu'à 90% du poids sec de sédiments, et contribue entre 17 et 37 % de l'opale sédimentaire globale (Ragueneau et al., 2000 ; *Fig. I.6.*).

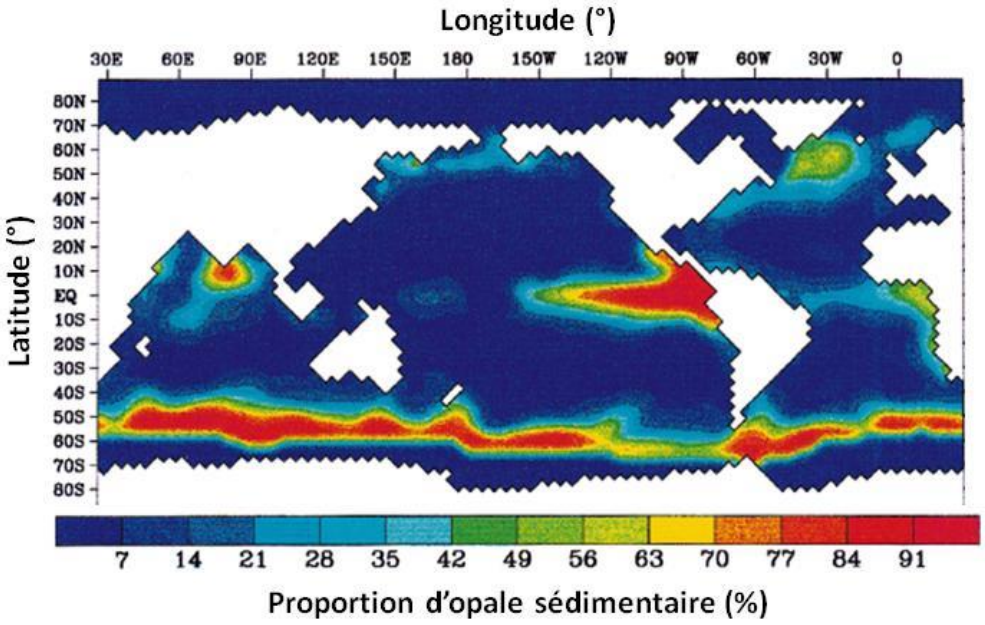

Figure I.6. Distribution des sédiments siliceux dans l'océan global (en % de la masse sèche de sédiments), modélisée pour la période pré-industrielle. D'après Ragueneau et al. (2000).

En résumé, la silice biogénique est produite par les organismes siliceux dans la couche euphotique. Une partie de ce flux est directement recyclée dans l'océan de surface, et l'autre partie est exportée sous la couche de surface. La BSi exportée continue de se dissoudre lorsqu'elle sédimente à travers l'océan profond, régénérant l'acide silicique. Les particules siliceuses qui ne sont pas recyclées sont finalement stockées dans les sédiments. C'est donc dans la couche euphotique que le cycle

biogéochimique du silicium est le plus dynamique et il a été estimé qu'un atome de silicium subit en moyenne 25 cycles d'absorption biologique – dissolution dans l'océan superficiel avant d'être enfoui dans les sédiments (Tréguer & De La Rocha, 2013). De nombreuses incertitudes demeurent quant à la quantification de ces flux, notamment en raison des difficultés analytiques rencontrées dans la mesure de la production et la dissolution de la silice biogénique. En effet, la méthode de marquage radioactif au ^{32}Si (Tréguer et al., 1991) permet d'avoir accès à l'uptake de silicium (ρSi) mais ne donne pas d'information sur la production nette de BSi (i.e. le taux de production moins le taux de dissolution de BSi ; ρNet = ρSi - ρDiss) puisqu'elle ne donne pas accès à la mesure du taux de dissolution de la silice biogénique. Certaines estimations de la production de silice biogénique sont donc biaisées car elles ne tiennent pas compte du recyclage de l'opale dans la ML (e.g. les taux de production en fin de saison sur le plateau de Kerguelen ; Mosseri et al., 2008). Actuellement, en dehors des approches de modélisation (Pondaven et al., 2000 ; Jin et al., 2006 ; Holzer et al., 2014) le taux production nette de BSi ne peut être mesuré avec une précision satisfaisante que grâce à la technique de dilution isotopique du ^{30}Si (Corvaisier et al., 2005), modifiée par Fripiat et al. (2009). Cette méthode permet en effet de déterminer simultanément les taux de production et de dissolution de la BSi à partir du même échantillon. Malheureusement, jusqu'à présent ce procédé ne permet de mesurer que difficilement les taux de dissolution extrêmement faibles rencontrés dans l'ACC (Fripiat et al., 2011c). L'Océan Austral reste donc particulièrement sous-échantillonné en ce qui concerne la mesure des flux de production et de dissolution de la silice biogénique.

Les processus de production et de dissolution du silicium permettent de lier les cycles biogéochimiques du silicium et ceux du carbone et des autres macronutriments (NO_3^- et PO_4^{3-}). Dans l'ACC on observe généralement une plus forte diminution saisonnière des stocks d'acide silicique que des autres nutriments dans les eaux de surface, suggérant un découplage important entre les cycles biogéochimiques de ces différents éléments (e.g. Trull et al., 2001 ; Mosseri et al., 2008). Ce découplage résulte de l'action de la pompe de silicium (Dugdale et al., 1995) impliquant une consommation dans la ML et un export du silicium plus efficace comparé aux autres éléments tels que l'azote ou le phosphore (Holzer et al., 2014). En effet, en raison de son incorporation dans une structure minérale telle que l'opale, le silicium est moins efficacement reminéralisé dans la colonne d'eau que l'azote ou le phosphore organique, favorisant ainsi son export sous la forme de BSi vers l'océan profond et entraînant simultanément un enrichissement des eaux profondes antarctiques en DSi comparé aux eaux de surface. L'azote organique particulaire est quant à lui principalement recyclé dans la ML sous la forme d'ammonium (NH_4^+), représentant une source d'azote régénérée significative pour le développement de nouveaux organismes phytoplanctoniques (Voss et al., 2013). La principale

conséquence de cette pompe de silicium particulièrement active dans l'Océan Austral est l'absence de formation de H_4SiO_4 préformés dans les eaux intermédiaires. Ceux-ci ne seront donc pas transportés vers les basses latitudes via l'export des AAIW et des SAMW comme c'est le cas pour les autres nutriments (NO_3^- et PO_4^{3-} ; Sarmiento et al., 2004 ; 2007 ; *Fig. I.7.*). Le silicium est donc confiné dans les eaux antarctiques par ce processus et une molécule d'acide silicique consommée puis recyclée dans l'ACC n'aurait que 5 % de chance d'être exportée et de nouveau utilisée au nord de 38°S (Holzer et al., 2014). Malgré le développement récent de l'intérêt scientifique et l'avancée des connaissances dans ce domaine, de nombreux efforts sont encore à fournir quant à la compréhension des facteurs contrôlant la pompe de silicium et le découplage saisonnier entre les cycles biogéochimique du silicium et ceux des autres macronutriments ; ainsi que la quantification précise de l'export et du recyclage du silicium dans l'Océan Austral.

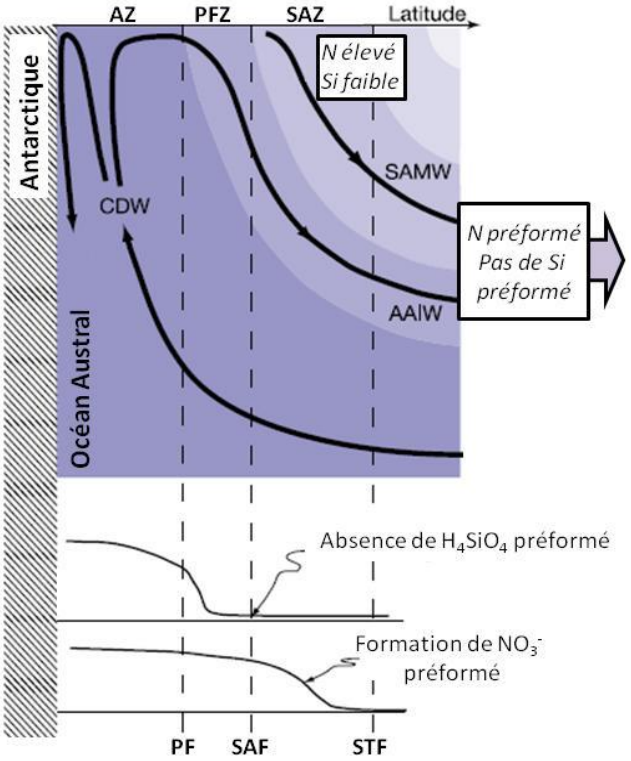

Figure I.7. Représentation schématique des processus biogéochimiques contrôlant la concentration en nutriments (H_4SiO_4 et NO_3^-) en lien avec la circulation océanique de l'Océan Austral (modifié d'après Sarmiento et al., 2004). Les eaux riches en nutriments (Eaux profondes Circumpolaires, CDW) remontent en surface où elles sont appauvries en Si, et exportent du N préformé en plongeant en subsurface (Eaux Antarctiques Intermédiaires, AAIW et Eaux Modales Sub-Antarctiques, SAMW). Les lignes pointillées représentent la position des fronts qui délimitent les zones océaniques. Du sud vers le nord: la Zone Antarctique (AZ), le Front Polaire (PF), la Zone du Front Polaire (PFZ), le Front Sub-Antarctique (SAF), la Zone Sub-Antarctique (SAZ) et le Front Sub-Tropical (STF).

4. Les diatomées : acteurs majeurs de la pompe à silicium dans l'Océan Austral

Dans l'ACC, la production de silice biogénique est attribuée principalement aux diatomées, la contribution précise des autres organismes siliceux (silicoflagellés, radiolaires) est mal connue mais est très probablement beaucoup plus faible que celle des diatomées. Ces organismes ubiquistes sont des

eucaryotes unicellulaires qui dominent généralement la production primaire dans les hautes latitudes de l'hémisphère sud où elles peuvent représenter jusqu'à 75 % de la population phytoplanctonique (Tréguer et al. 1995 ; Ragueneau et al., 2000). Les diatomées ont la particularité d'être entourées d'une paroi externe siliceuse appelée frustule, qui est généralement constitué de deux valves emboîtées, plus ou moins ornementées et entourées d'une ou plusieurs bandes transversales dites cingulaires (*Fig. I.8a.*). Ce frustule leur confère ainsi un avantage écologique non négligeable, notamment en ce qui concerne la protection contre les agressions extérieurs (prédation, etc.). Leur classification spécifique repose ainsi sur la forme et les éléments d'ornementation de leurs frustules qui se caractérisent par une très grande diversité de structures. Parce que ce sont des organismes siliceux, les diatomées nécessitent pour leur croissance et leur division des apports suffisants de DSi. Le métabolisme du silicium constitue ainsi chez ces organismes un métabolisme majeur au même titre que celui du carbone ou de l'azote (Martin-Jézéquel et al., 2000).

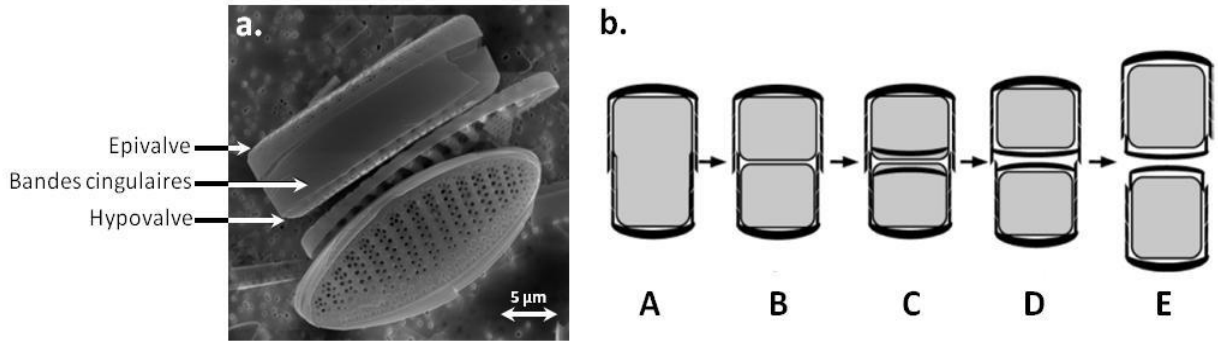

Figure I.8. (a.) Photographie de diatomées (*Fragilariopsis kerguelensis*) en vues cingulaires (en haut) et valvaires (en bas), obtenue en microscopie électronique à balayage et illustrant la morphologie des diatomées (Crédit photo : *I. Closset*, plateforme analytique ALYSES). (b.) Représentation schématique de la division cellulaire d'une diatomée: **A.** Cellule-mère; **B.** 2 cellules-filles dans le frustule de la cellule-mère; **C.** Synthèse des valves; **D.** Exocytose des valves; **E.** Séparation des 2 cellules-filles. Adapté d'après Hildebrand et al. (2008).

Les diatomées peuvent opter pour la reproduction sexuée, mais se développent généralement par division végétative, chaque cellule fille récupérant une des valves de la cellule mère (*Fig. I.8b.*). Lors de la fabrication d'une nouvelle valve, l'assimilation de l'acide silicique se fait par le biais d'un transport actif, lié à la présence protéines transmembranaires (Silicic Acid Transporter, SIT) et suit une cinétique d'absorption de type Michaelis-Menten (Martin-Jézéquel

et al., 2000 ; Thamatrakoln & Hildebrand, 2008), où le taux spécifique d'absorption (V_{Si}, j^{-1}) dépend de la concentration en H_4SiO_4 :

$$V_{Si} = \frac{V_{max} \times [H_4SiO_4]}{K_{Si} + [H_4SiO_4]} \qquad (I.1.)$$

V_{max} représente le taux spécifique d'absorption maximal (j^{-1}) et K_{Si} la constante de demi-saturation (µmole L^{-1}), c'est-à-dire la concentration de DSi pour $V_{max}/2$. Le silicium est transporté dans le cytoplasme de la cellule complexé à des composés intracellulaires pour être ensuite polymérisé sous la forme de silice biogénique dans une vésicule de dépôt (Silica Deposit Vesicle, SDV ; Hildebrand, 2003). Le processus de silicification s'achève par l'expulsion de la SDV hors de la cellule et par le dépôt de la nouvelle valve du frustule. Les diatomées possèdent également des systèmes de régulation du silicium intracellulaire, conduisant à un efflux d'acide silicique hors de la cellule lorsque celui-ci n'est pas utilisé par l'organisme (Martin-Jézéquel et al., 2000 ; *Fig. I.9.*). L'ensemble des processus physiologiques impliqués dans le métabolisme du silicium chez les diatomées est encore malheureusement très mal connu. Ils conditionnent pourtant très probablement la réponse des diatomées face aux variations biogéochimiques de leur environnement (concentration en nutriments, température etc.)

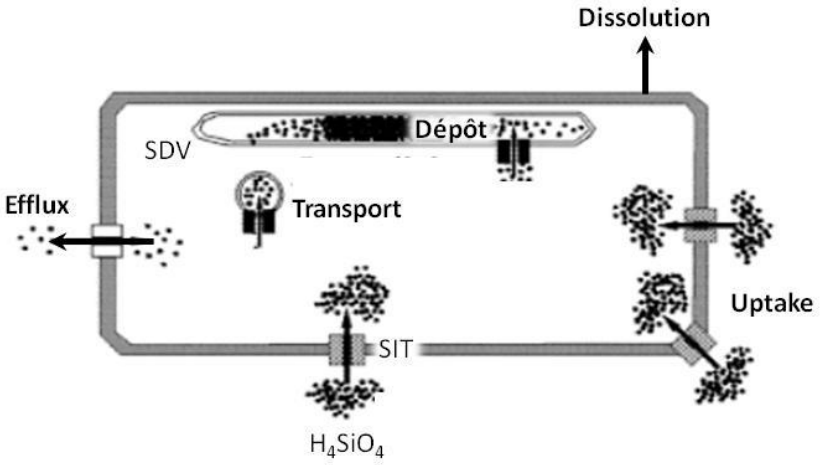

Figure I.9. Représentation schématique des principaux processus impliqués dans le métabolisme du silicium chez les diatomées. Les points représentent le DSi qui pénètre dans la cellule (uptake) par les transporteurs d'acide silicique (SIT). Le DSi est ensuite transporté dans la cellule jusqu'à la vésicule de dépôt (SDV) où il est transformé en BSi. L'opale produite peut retourner au compartiment dissous par simple dissolution dans l'eau de mer ; et la cellule peut réguler sa concentration intracellulaire de DSi en pratiquant de l'efflux. Modifié d'après Martin-Jézéquel et al. (2000).

Contrairement au métabolisme du carbone qui dépend principalement du processus de photosynthèse chez les organismes autotrophes, le métabolisme du silicium semble étroitement lié au cycle cellulaire des organismes (Martin-Jézéquel et al., 2000), et ne dépend pas directement du rythme jour/nuit. Chez les diatomées, ce cycle cellulaire se décompose en plusieurs phases et l'assimilation du silicium et le dépôt de BSi auraient lieu juste avant la phase de division cellulaire (i.e. en phase G2, *Fig. I.10.*). Des conditions défavorables à la croissance des diatomées, telles que la limitation en lumière, en micronutriments ou la température pourraient entrainer un ralentissement du cycle cellulaire et un allongement de certaines phases (e.g. Leynaert et al., 2004 ; Claquin & Martin-Jézéquel, 2005). Dans ces conditions, les diatomées auraient la possibilité d'absorber plus de DSi et donc d'augmenter le degré de silicification. Dans les eaux HNLC limitées en fer de l'Océan Austral, les diatomées prélèveraient donc plus de silicium que d'azote, augmentant ainsi leurs rapports stoechiométriques (Si:C, Si:N et Si:P ; Hutchins & Bruland, 1998 ; Franck et al., 2000), participant en partie au découplage des cycles biogéochimiques de ces différents éléments et à l'appauvrissement préférentiel en silicium des eaux de surface. Ce sont sur ces observations que repose l'hypothèse de la SALH de Matsumoto et al. (2002). En effet, lors des périodes glaciaires, les apports accrus de fer dans l'Océan Austral auraient eut pour conséquence une diminution des rapports d'assimilation Si:N des diatomées entraînant un excès de DSi dans les eaux de surface antarctique comparé à la situation actuelle (Brzezinski et al., 2002). Ce stock de H_4SiO_4 préformé aurait alors été exporté via la circulation thermohaline vers les plus faibles latitudes où il aurait favorisé la croissance des diatomées, augmentant ainsi l'efficacité de la pompe biologique dans ces régions.

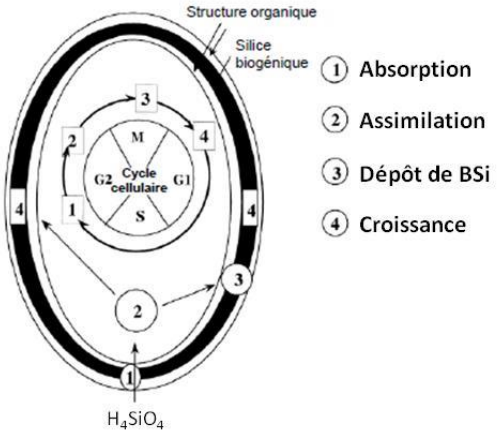

Figure I.10. Représentation schématique des principaux processus de silicification en relation avec le cycle cellulaire chez les diatomées (adapté d'après Ragueneau et al., 2000). Le cycle cellulaire comprend plusieurs phases : Périodes de croissance (G1 et G2), période de réplication de l'ADN (S), période de division cellulaire (M).

L'océan global (en ce inclus l'Océan Austral) est sous-saturé en acide silicique. La silice biogénique constituant le frustule des diatomées est donc constamment soumise à un processus

physico-chimique de dissolution. Afin de le protéger, le frustule est recouvert d'une fine pellicule organique l'isolant de l'environnement sous-saturé. Ainsi, à l'échelle d'un organisme, les processus de production et de dissolution de la BSi sont découplés dans le temps puisque ce n'est qu'après la mort de la cellule et la dégradation de cette matière organique que la BSi commence à se dissoudre (Ragueneau et al., 2000). Différents facteurs physiques, chimiques et biologiques tels que la température, la morphologie du frustule, l'incorporation d'autres éléments dans la BSi, l'activité bactérienne ou le broutage vont influencer l'efficacité de la dissolution des diatomées (e.g. Kamatani, 1982 ; Bidle & Azam, 1999) et vont fortement conditionner les flux de H_4SiO_4 recyclé dans les eaux de surface. Contrairement à l'azote, il n'est pas possible de différentier simplement les sources « régénérées » de DSi de celles dites « nouvelles » puisqu'elles ont toutes deux la même composition chimique. La part de la production de silice liée à ces processus de recyclage ou à l'apport nouveau de DSi est donc actuellement difficile à identifier. Les approches isotopiques, utilisées au cours de ce travail de thèse et présentées dans ce manuscrit, vont nous permettre de progresser sur ces questions.

5. Fonctionnement du système isotopique du silicium

Les isotopes sont des atomes d'un même élément qui diffèrent par leur nombre de neutrons. Ayant le même nombre de protons et d'électrons, ils possèdent des propriétés chimiques similaires mais présentent des vitesses de réaction différentes lors des réactions chimiques ou des processus physiques en raison de leurs différentes masses atomiques. Cette propriété entraine une séparation partielle des isotopes les plus légers et les plus lourds lors d'une réaction qui, en ce qui concerne le silicium, dépend exclusivement de leur masse et est appelée fractionnement isotopique (Fry, 2006). En règle générale, l'isotope le plus léger réagit plus rapidement, entrainant un produit de réaction enrichi en isotope léger alors que les isotopes lourds restent préférentiellement dans le réservoir initial (Hoefs, 2009). Le silicium possède trois isotopes stables de masse atomique ^{28}Si, ^{29}Si et ^{30}Si ayant une abondance relative dans le milieu naturel de 92.23 %, 4.68 % et 3.10 %. Les variations de la composition isotopique d'un échantillon sont généralement estimées en comparant le rapport de l'isotope lourd sur l'isotope léger (e.g. ^{30}Si/^{28}Si) d'un échantillon à celle d'un matériel de référence standard à l'aide de la notation delta (en ‰) :

$$\delta^{30}Si\ (‰) = \left[\frac{(^{30}Si/^{28}Si)echantillon}{(^{30}Si/^{28}Si)standard} - 1\right] \times 1000 \qquad \text{(I.2.)}$$

Dans le cas du silicium, ce matériel de référence est le standard international de Quartz NBS28 (Abraham et al., 2008). Une valeur de $\delta^{30}Si$ positive signifie que l'échantillon est enrichi en isotope lourd (^{30}Si) relativement au standard de référence, alors qu'une valeur négative du delta correspond cette fois à un enrichissement de l'échantillon en isotope léger (^{28}Si). De plus, le fractionnement isotopique du silicium étant dépendant de la masse, la relation $\delta^{30}Si$ vs. $\delta^{29}Si$ d'un échantillon d'eau de mer ou de BSi génère une droite de pente 1.964 (Young et al., 2002) qui peut être utilisée comme un des moyens de contrôle de la fiabilité des analyses (*Fig. I.11.*).

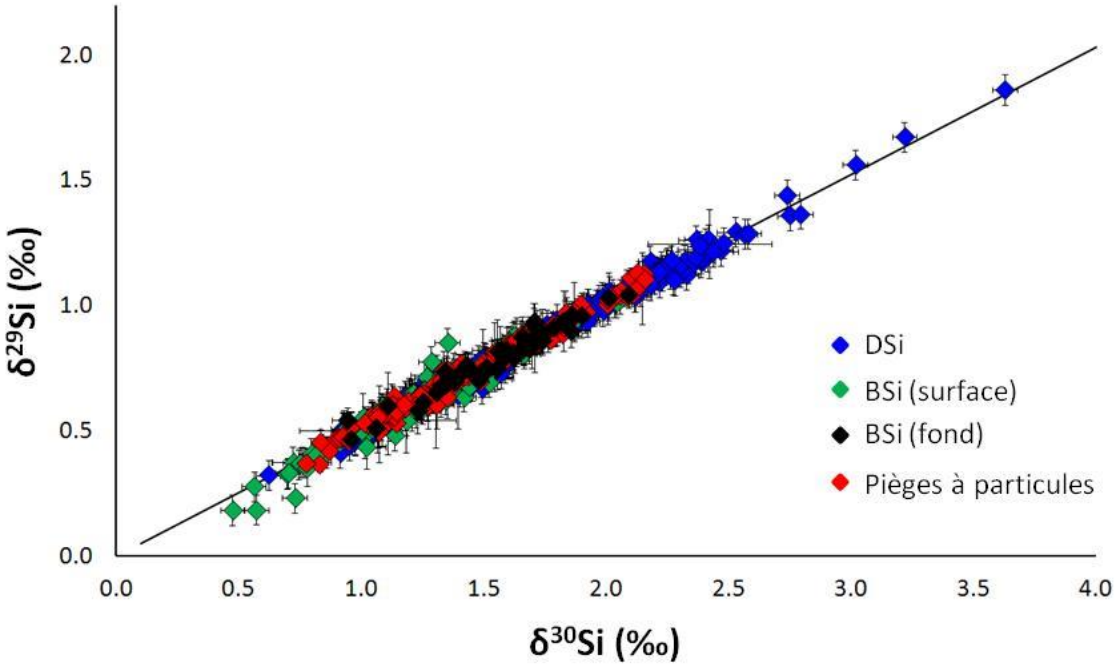

Figure I.11. Illustration du fractionnement dépendant de la masse ($\delta^{29}Si$ vs. $\delta^{30}Si$) de l'ensemble des échantillons analysés dans ce manuscrit. La majorité des points sont situés sur la droite de fractionnement ($\delta^{30}Si = 1.96 \times \delta^{29}Si$, Young et al., 2002).

Lors d'une réaction chimique, l'intensité du fractionnement des isotopes du silicium peut être exprimée par le facteur de fractionnement (α ou ε). Dans le cas d'une réaction unidirectionnelle (telle que la production de silice biogénique par les diatomées par exemple), ce fractionnement est lié aux vitesses de réaction des différents isotopes, on parle alors de fractionnement cinétique (*équation I.3.*) :

$$\alpha = \frac{{}^{L}k}{{}^{H}k} \qquad \text{(I.3.)}$$

Avec *k*, la constante cinétique de la réaction pour l'isotope léger (^{L}k) et pour l'isotope lourd (^{H}k). Dans le cas d'une réaction bidirectionnelle à l'équilibre, on parle de fractionnement à l'équilibre

thermodynamique (*équation I.4.*) et le facteur de fractionnement entre le produit A et le réactif B s'exprime plutôt :

$$\alpha = \frac{R_A}{R_B} \qquad \text{(I.4.)}$$

Avec R, le rapport des isotopes lourds sur les isotopes légers (e.g. dans le cas du δ^{30}Si : ^{30}Si/^{28}Si). Généralement on exprime le facteur de fractionnement sous la forme (en ‰) :

$$\varepsilon = (\alpha - 1) \times 1000 \qquad \text{(I.5.)}$$

Lors d'expériences contrôlées en laboratoire, De la Rocha et al. (1997) ont montré pour la première fois que les diatomées fractionnaient les isotopes du silicium lors de la fabrication de leur frustule opalin (avec $^{30}\varepsilon$ = -1.1 ± 0.4 ‰). Il n'est actuellement pas évident d'identifier avec certitude quelle(s) étape(s) de la formation de BSi chez les diatomées occasionnent un fractionnement des isotopes du silicium. Il semblerait néanmoins que ce dernier ait lieu lors du transport de l'acide silicique par les SIT plutôt que lors des processus de polymérisation de la silice dans la SDV (Milligan et al., 2004). Même si à l'échelle globale, le facteur de fractionnement associé à la production de BSi des diatomées peut varier de -0.54 à -2.09 ‰ (Fripiat et al., 2012 ; Sutton et al., 2013), sa valeur moyenne estimée pour l'ACC n'est pas significativement différent ce celle mesurée *in vitro* ($^{30}\varepsilon$ = -1.2 ± 0.2 ‰ ; Fripiat et al., 2011a). Différents mécanismes peuvent entrainer des variations locales ou saisonnières du facteur de fractionnement lors de la production de silice biogénique. Les premiers travaux visant à estimer le $^{30}\varepsilon$ des diatomées ont suggéré qu'il n'était dépendant ni de la température du milieu, ni de l'espèce considérée (De la Rocha et al., 1997). Cependant la gamme de variation des températures étudiées était limitée (12-22°C) et le nombre d'espèces cultivées très faible (n = 3). En isolant sept espèces de diatomées polaires et sub-polaires, une étude récente a remis en cause cette homogénéité spécifique du $^{30}\varepsilon$ (Sutton et al., 2013). Par exemple, la plus grande différence de $^{30}\varepsilon$ serait observée entre deux espèces dominant régulièrement les blooms phytoplanctoniques antarctiques (*Fragilariopsis kerguelensis,* $^{30}\varepsilon$ = -0.54 ‰ et *Chaetoceros brevis,* $^{30}\varepsilon$ = -2.09 ‰). De la même façon, il a été initialement montré l'absence d'effet de taille sur la composition isotopique des diatomées, et donc sur leur fractionnement isotopique (Cardinal et al., 2007). Pourtant, il a été récemment suggéré que dans les archives sédimentaires, la taille des particules destinées aux analyses isotopique doit être soigneusement sélectionnée afin d'éliminer les autres espèces siliceuses et les débris d'opale des échantillons destinés à l'analyse du δ^{30}Si des communautés de diatomées de surface (Egan et al., 2012). Sans remettre radicalement en cause l'hypothèse d'une composition isotopique homogène des diatomées en dépit de leurs variations de taille, cette étude met en évidence les biais pouvant être

occasionnés lors de l'estimation du facteur de fractionnement des diatomées à partir de la BSi exportée.

D'autres processus liés au métabolisme du silicium chez les diatomées peuvent également entrainer un fractionnement isotopique (*Fig. I.12.*). Par exemple, Demarest et al. (2009) ont montré que lors de leur dissolution, les isotopes les plus légers (^{28}Si) sont préférentiellement dissous avec un $^{30}\varepsilon$ = - 0.55 ‰. Le fractionnement isotopique lié à la dissolution de la BSi est néanmoins fortement discuté en raison des profils homogènes de $\delta^{30}Si$ observés dans la colonne d'eau (e.g. Fripiat et al., 2012), des valeurs de $\delta^{30}Si$ de la BSi exportée fortement similaires à celles de la BSi de surface (Varela et al., 2004 ; Egan et al., 2012), et d'une étude récente sur les processus de dissolution de l'opale sédimentaire (Wetzel et al., 2014). De plus, aucune étude n'a aujourd'hui identifié les mécanismes de transport de l'acide silicique hors de la cellule lorsque celui n'est pas utilisé (i.e. l'efflux). Il semble néanmoins probable qu'ils soient similaires aux mécanismes de transport « entrant » (i.e. l'influx) et donc associés à un fractionnement isotopique lors de l'export par les SIT.

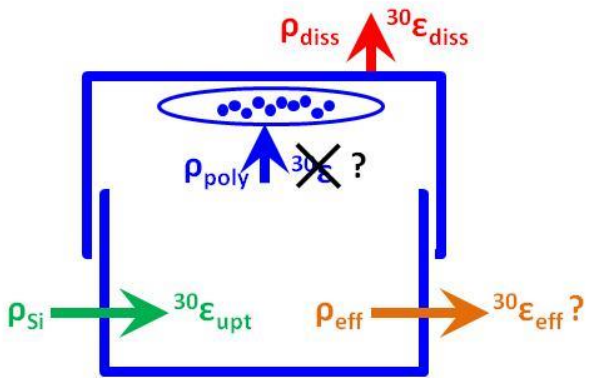

Figure I.12. Représentation schématique des principaux flux (ρ) du métabolisme du silicium chez les diatomées impliquant un fractionnement isotopique potentiel (ε): En vert, l'uptake de DSi ; en orange, l'efflux ; en bleu, le dépôt de BSi et en rouge, la dissolution du frustule.

Les $^{30}\varepsilon$ estimés à partir des données *in situ* représenteraient donc plutôt des facteurs de fractionnement net ($^{30}\varepsilon_{net}$; *Equation I.6.)* qui résulteraient de la combinaison des fractionnements isotopiques associés à chaque étape du métabolisme su silicium chez les diatomées comme proposé par Fripiat et al. (2012) pour expliquer les variations de $\Delta^{30}Si$ ($=\delta^{30}Si_{BSi} - \delta^{30}Si_{DSi}$) observées dans l'Océan Austral.

$$^{30}\varepsilon_{net} = {}^{30}\varepsilon_{upt} + \frac{\rho_{eff}}{\rho_{Si}} \times {}^{30}\varepsilon_{eff} + \frac{\rho_{diss}}{\rho_{Si}} \times {}^{30}\varepsilon_{diss} \qquad \text{(I.6.)}$$

Où $^{30}\varepsilon_{upt}$; $^{30}\varepsilon_{eff}$ et $^{30}\varepsilon_{diss}$ représentent respectivement les facteurs de fractionnement correspondant à l'uptake de Si, l'efflux et la dissolution de la BSi. Les flux d'uptake, de dissolution et d'efflux sont notés ρ_{Si} ; ρ_{diss} et ρ_{eff}.

Ainsi, contrairement à ce qui a été considéré jusqu'à présent, le facteur de fractionnement des diatomées pourrait être beaucoup plus variable que prévu et son estimation à grande échelle beaucoup plus incertaine. Il serait donc intéressant de considérer dans l'avenir des facteurs de fractionnement plutôt régionaux et/ou saisonniers. Par exemple, les variations du Δ^{30}Si observées dans les différentes régions de l'ACC (Fripiat et al., 2012), pourraient être liées à la disponibilité en DSi et à sa cinétique d'absorption par les communautés de diatomées (Cardinal et al., 2007) comme cela a été montré pour les éponges (Hendry et al., 2010 ; Wille et al. 2010). L'impact de ces processus sur la composition isotopique des diatomées n'a encore jamais été étudié. Néanmoins, la cinétique des réactions chimiques étant un processus entraînant un fractionnement isotopique (Young et al., 2002), il est probable que la vitesse d'incorporation de l'acide silicique par les diatomées influence leur $^{30}\varepsilon$.

Deux modèles conceptuels relativement simples, et dont les équations seront présentées dans les différentes études de ce manuscrit, sont généralement utilisés pour estimer le fractionnement des isotopes du Si dans l'océan. Le modèle de Rayleigh (ou modèle fermé) implique que, une fois formés, les produits n'échangent plus avec le réservoir (Mariotti et al., 1981). Dans le cas de la production de silice biogénique, au fur et à mesure que les diatomées consomment l'acide silicique dans les eaux de surface, elles sont retirées (exportées) de la ML qui ne reçoit aucun nouvel apport de DSi. Ces organismes, ainsi que leur environnement, vont donc progressivement s'enrichir en ^{30}Si et la signature isotopique de la BSi produite à un instant *t* sera différente de celle de la BSi accumulée (sous la ML) au cours du temps. Le deuxième modèle est le modèle à l'état stationnaire (dit « steady-state » ou modèle ouvert) qui représente un équilibre isotopique entre le réservoir et le produit (Sigman et al., 1999). Dans ce modèle, la BSi produite serait immédiatement exportée ainsi que le DSi restant qui est remplacé par un apport équivalent d'acide silicique de même composition isotopique. L'accumulation de BSi et l'appauvrissement en DSi de la ML ne sont pas autorisés dans ce système théorique. Connaissant la concentration de H_4SiO_4 et le δ^{30}Si initial, on peut estimer de facteur de fractionnement du système à l'aide des équations de ces modèles. Cependant, Cardinal et al. (2005) ont montré que de nombreux biais peuvent être occasionnés en fonction du choix de la masse d'eau source. En effet,

une faible variation sur la concentration d'acide silicique de cette masse d'eau peu entraîner une variation significative du facteur de fractionnement estimé à partir de cette source.

Ces modèles théoriques sont également difficilement applicables à l'environnement naturel et ne reflètent donc pas fidèlement la réalité des processus se déroulant dans la couche de surface. En effet, dans l'Océan Austral, on ne peut exclure les évènements de mélange vertical ou d'advection latérale apportant des eaux avec des concentrations et des compositions isotopiques différentes de la source. Il est également peu probable que l'apport soit continu et ne provienne que d'une seule masse d'eau source. Les échanges entre le compartiment dissous et particulaire (par exemple la dissolution de la BSi) peuvent également modifier le facteur de fractionnement et faire dévier l'évolution de la composition isotopique de la BSi et DSi des tendances théoriques prédites par ces modèles. Plusieurs interrogations restent donc actuellement ouvertes sur le choix du modèle et des conditions initiales pour les estimations du facteur de fractionnement ainsi que sur le rôle de l'efflux et de la dissolution. Ces questions ont des implications importantes en paléo-océanographie puisque jusqu'à présent, les paléo-variations de la consommation du DSi par les diatomées sont décrites à partir des archives sédimentaires en utilisant soit le modèle de Rayleigh, soit le modèle à l'état stationnaire (e.g. De La Rocha et al., 1998).

En plus de leur utilisation comme traceurs de l'utilisation relative du réservoir d'acide silicique, les distributions du $\delta^{30}Si$ apportent des informations remarquables quant au cycle biogéochimique du silicium dans l'océan moderne. Ce paramètre, couplé ou non à des expériences d'incubations et de dilution isotopique du ^{30}Si, a déjà permis la quantification des flux de silicium dans les eaux de surface (quantification du mélange vertical saisonnier), de son utilisation et de sa régénération dans la couche de mélange (estimation de la production et dissolution de la BSi) mais aussi l'identification des sources d'acide silicique, du devenir des masses d'eau et de leur stock de nutriments dans la colonne d'eau (e.g. Varela et al., 2004 ; Cardinal et al., 2005 ; Fripiat et al., 2011a ; De Souza et al., 2012). Dans l'Océan Austral, il a également été utilisé pour étudier la réponse des diatomées face à la fertilisation artificielle et naturelle en fer (Cavagna et al., 2011 ; Fripiat et al., 2011a). Dans l'océan, les variations naturelles des isotopes du silicium sont faibles comparées aux autres éléments dits « légers » (e.g. C, H, N, O). Ceci explique en partie le développement très récent des applications du $\delta^{30}Si$ dans le domaine de la biogéochimie marine qui est donc étroitement lié aux récentes avancées technologiques, en particulier avec le développement des techniques d'analyses par MC-ICP-MS (e.g. Cardinal et al., 2003 ; Abraham

et al., 2008). Dans l'océan global, les valeurs de $\delta^{30}Si$ varient de +0.5 à +4.4 ‰ pour le compartiment dissous et de -0.7 à +2.8‰ pour le compartiment particulaire (*Fig. I.13.*).

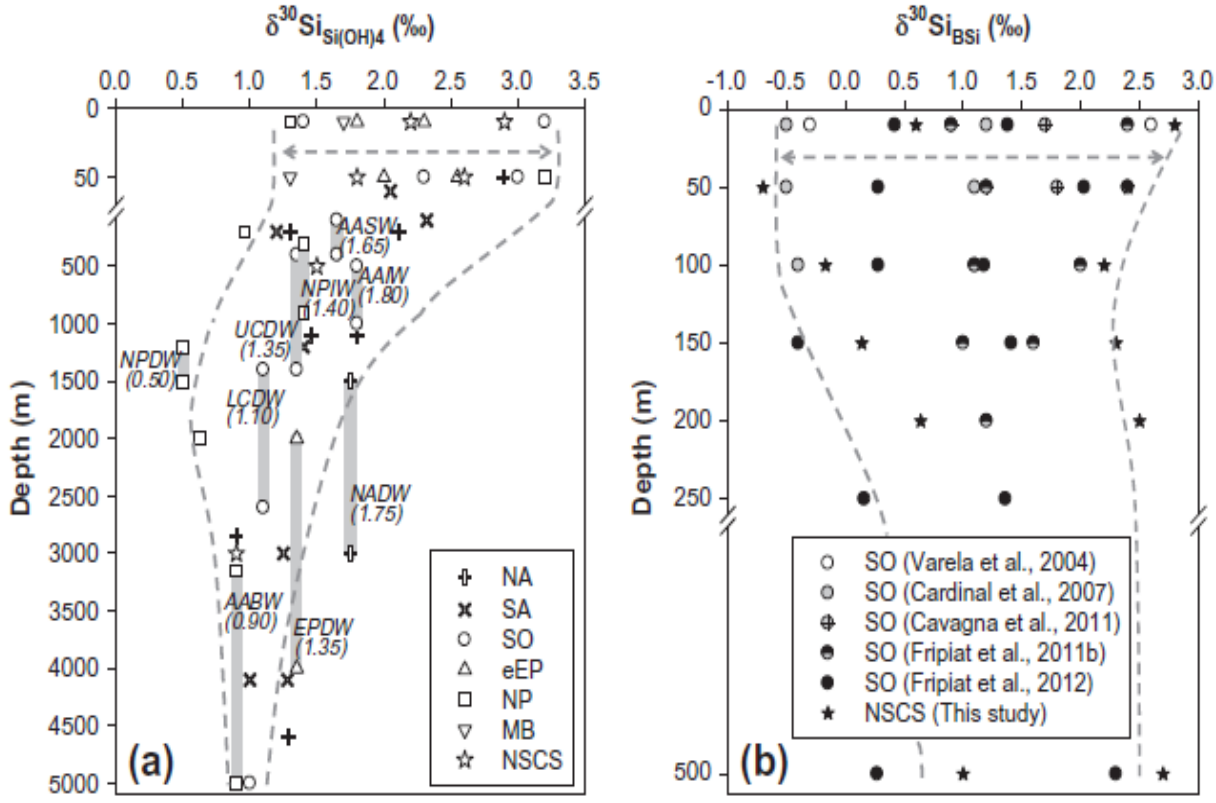

Figure I.13. Distribution des valeurs de $\delta^{30}Si_{DSi}$ (a.) et de $\delta^{30}Si_{BSi}$ (b.) dans l'océan global en fonction de la profondeur et des types de masse d'eau (d'après Cao et al., 2012).

Cependant, ces résultats sont issus de la compilation d'une quinzaine de jeux de données seulement (De la Rocha et al., 2000, 2011 ; Varela et al., 2004 ; Cardinal et al., 2005, 2007 ; Reynolds et al., 2006 ; Beucher et al., 2008, 2011 ; Cavagna et al., 2011 ; Fripiat et al., 2011a, 2011b, 2012 ; Cao et al., 2012 ; De Souza et al., 2012 ; Ehlert et al., 2012 ; Grasse et al., 2013 ; Singh et al., 2015). On se trouve donc encore très loin d'une couverture globale satisfaisante et la plupart des régions étudiées restent encore fortement sous-échantillonnées (*Fig. I.14.*).

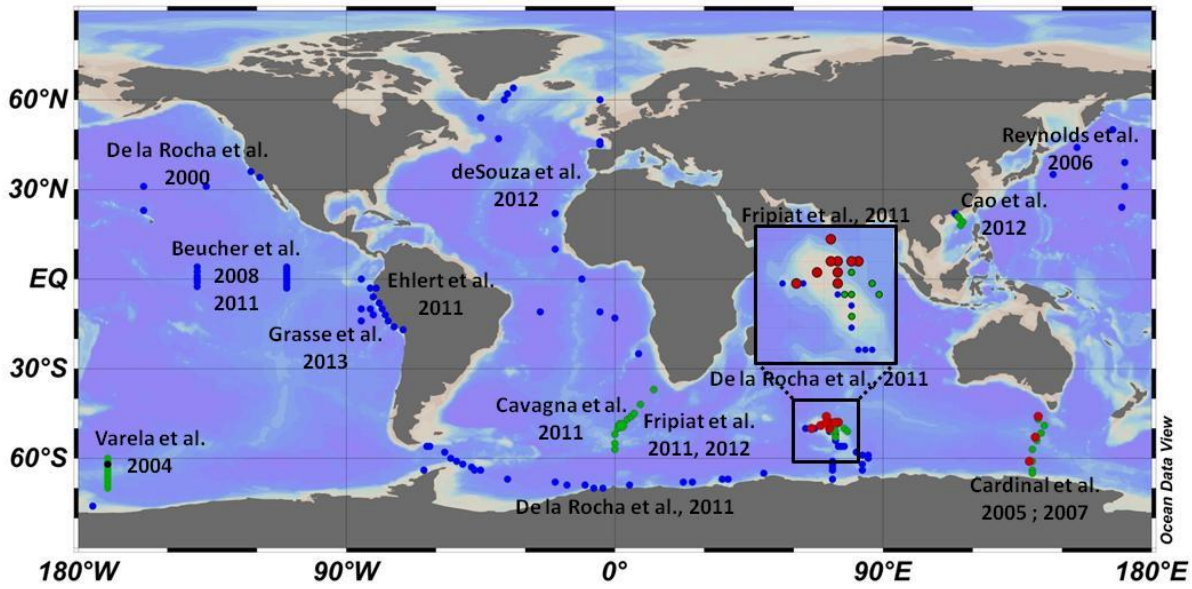

Figure I.14. Répartition géographique des données modernes de $\delta^{30}Si$ dans l'océan global, incluant les résultats présentés dans cette thèse. Les points bleus représentent les données correspondant au DSi, les points verts celles correspondant à la BSi et les points rouges sont les données discutées dans cette thèse. A noter que jusqu'à présent, seule l'étude Varela et al. (2004) a présenté des $\delta^{30}Si$ sur 11 et 7 échantillons de pièges à sédiments (point noir)

6. Objectifs de la thèse

Afin d'apporter des éléments de réponses aux différentes incertitudes qui persistent encore à l'heure actuelle, tant au niveau de la compréhension du cycle biogéochimique du silicium que de l'utilisation de l'outil isotopique, ce travail de thèse s'appuie sur les données de deux programmes internationaux :

- Le **programme KEOPS**, et en particulier la campagne KEOPS-2 (octobre-novembre 2011), est dédié à l'étude de l'impact de la fertilisation naturelle en fer sur les cycles biogéochimiques du carbone et des éléments biogènes associés (Si, N, P) et sur le fonctionnement de la pompe biologique de carbone dans l'Océan Austral. Lors de cette campagne, des échantillons d'eau de mer et de phytoplancton ont été récoltés à différentes stations de la région de Kerguelen ; et des expériences d'incubation ont été menées afin de quantifier les stocks, les flux et les sources de silicium à partir de deux approches isotopiques différentes.

- Le **programme SAZ-Project** inclue trois lignes de mouillages situées dans les principales zones de l'ACC, sur la section SR3 (CLIVAR) entre la Tasmanie et l'Antarctique, ce depuis 1997. L'objectif

principal de ce programme est d'augmenter significativement la couverture géographique et saisonnière d'échantillonnage particulièrement faible au niveau de l'ACC, mais également de mieux comprendre les processus biogéochimiques qui ne sont pas correctement résolus dans les modèles climatiques. Chaque ligne de mouillage comprend au moins deux pièges à particules dont le matériel a été récolté et conservé pour l'analyse de la composition isotopique naturelle des particules en 1999-2000 et en 2001-2002.

Les objectifs spécifiques de la thèse s'articulent donc autour de quatre points principaux :

* De manière générale, un effort a été réalisé afin d'**augmenter les couvertures spatiale et surtout saisonnière** des mesures de la composition isotopique du silicium, ainsi que d'augmenter la résolution des mesures de flux de Si et de δ^{30}Si dans la colonne d'eau et dans la couche euphotique.

* Le cycle biogéochimique du silicium et sa réponse à une fertilisation naturelle en fer avait été étudié à la fin de l'été dans la région du Plateau de Kerguelen (Mosseri et al., 2008 ; Fripiat et al., 2011a ; deBrauwere et al., 2012), mais qu'en est-il dans la même région en début de saison ? Quels sont les facteurs de contrôle de la pompe à silicium dans la région ? Varient-ils au cours de la saison ? Peut-on évaluer la part de la production de BSi liée à un apport nouveau de Si et celle liée à une source de Si régénérée ? Ces questions seront discutées dans le chapitre 1 qui analyse la **variabilité spatiale et temporelle des taux de production et de dissolution de la BSi dans la couche de mélange**.

* De plus, toujours dans ce même contexte, quelles sont les sources de silicium responsables du développement du bloom de diatomées dans la région de Kerguelen ? Varient-elles au cours de la saison ? Peut-on les quantifier ? Ces aspects seront traités dans le chapitre 2 qui s'intéresse aux **processus de contrôle de la distribution spatiale et des variations saisonnières du δ^{30}Si de l'eau de mer et des particules** dans la région.

* Enfin, la signature isotopique des particules sédimentaires (et en particulier des diatomées) est utilisée comme proxy de l'utilisation relative passée du silicium dans l'océan de surface. Quels sont alors les processus qui contrôlent le transfert de ce signal depuis l'océan de surface en profondeur ? Quelles sont les mécanismes qui gouvernent les variations saisonnières du δ^{30}Si des particules qui sédimentent dans la colonne d'eau ? Sont-ils les mêmes dans les différentes zones de l'ACC ? Quelles informations peut-on exploiter de la composition isotopique de ce flux de particules ? L'ensemble de ces interrogations sera examiné dans le chapitre 3 qui présente des données originales sur **la variabilité spatiale et saisonnière de la composition isotopique en silicium du flux de particules dans les principales zones de l'Océan Austral**.

Du point de vue analytique, ce travail de thèse a également pour objectifs d'optimiser la méthode de mesure des flux de dissolution par dilution isotopique afin d'augmenter sa sensibilité ; d'adapter les protocoles de chimie utilisés actuellement pour analyser le $\delta^{30}Si$ des diatomées récoltées sur des filtres à des particules sédimentaires collectées par des pièges à particules ; de mettre en place et d'optimiser les méthodes actuelles de mesure du $\delta^{30}Si$ de l'eau de mer par MC-ICP-MS au laboratoire LOCEAN et au LSCE (IPSL), en contrôlant les biais potentiels liés aux effets de matrice propres aux eaux marines.

7. Références bibliographiques

Abraham K., S. Opfergelt, F. Fripiat, A.-J. Cavagna, J.T.M. de Jong, S.F. Foley, L. André, D. Cardinal (2008) δ30Si and δ29Si Déterminations on USGS BHVO-1 and BHVO-2 Reference Materials with a New Configuration on a Nu Plasma Multi-Collector ICP-MS, Geostandards and Geoanalytical Research, 32(2), 193-202

Achterberg E.P. (2014) Grand challenges in marine biogeochemistry, Frontiers in marine science, 1(7), doi:10.3389/fmars.2014.00007

Arrigo K., D. Worthen, A. Schell, M.P. Lizotte (1998) Primary production in Southern Ocean waters, Journal of Geophysical Research, 103(C8), 15587-15600

Beucher C.P., M.A. Brzezinski, J.L. Jones (2008) Sources and biological fractionation of Silicon isotopes in the Eastern Equatorial Pacific, Geochimica et Cosmochimica Acta, 72, 3063-3073

Beucher C.P., M.A. Brzezinski, J.L. Jones (2011) Mechanisms controlling silicon isotope distribution in the Eastern Equatorial Pacific, Geochimica et Cosmochimica Acta, 75, 4286-4294

Bidle K.D., F. Azam (1999) Accelerated dissolution of diatom silica by marine bacterial assemblages, Nature, 397, 508-512

Blain S., P. Tréguer, S. Belviso, E. Bucciarelli, M. Denis, S. Desabre, M. Fiala, V. Martin-Jézéquel, J. LeFèvre, P. Mayzaud, J.-C. Marty, S. Razouls (2001) A biogeochemical study of the island mass effect in the context of the iron hypothesis: Kerguelen Islands, Southern Ocean, Deep-Sea Research I, 48, 163-187

Blain S., B. Quéguiner, L. Armand, S. Belviso, B. Bombled, L. Bopp, A. Bowie, C. Brunet, C. Brussaard, F. Carlotti, U. Christaki, A. Cordière, I. Durand, F. Ebersbach, J.-L. Fuda, N. Garcia, L. Gerringa, B. Griffiths, C. Guigue, C. Guillerm, S. Jacquet, C. Jeandel, P. Laan, D. Lefèvre, C. Lo Monaco, A. Malits, J. Mosseri, I. Obernosterer, Y..-H. Park, M. Picheral, P. Pondaven, T. Remenyi, V. Sandroni, G. Sarthou, N. Savoye, L. Scouarnec, M. Souhaut, D. Thuiller, K. Timmermans, T. Trull, J. Uitz, P. Van Beek, M. Velhuis, D. Vincent, E. Viollier, L. Vong, T. Wagener (2007): Effect of natural iron fertilization on carbon sequestration in the Southern Ocean. Nature. 446:1070-1075

Bowie A.R., D. Lannuzel, T.A. Remenyi, T. Wagener, P.J. Lam, P.W. Boyd, C. Guieu, A.T. Townsend, T.W. Trull (2009) Biogeochemical iron budgets of the Southern Ocean south of Australia: Decoupling of iron and nutrient cycles in the subantarctic zone by the summertime supply, Global Biogeochemical cycles, 23, GB4034, doi:10.1029/2009GB003500

Boyd P.W. (2002a) The role of iron in the biogeochemistry of the Southern Ocean and equatorial Pacific: a comparison of in situ iron enrichments, Deep-Sea Research II, 49, 1803-1821

Boyd P.W. (2002b) Environmental factors controlling phytoplankton processes in the Southern Ocean, Journal of Phycology, 38, 844-861

Boyd P.W., T.W. Trull (2007) Understanding the export of biogenic particles in oceanic waters: Is there consensus? Progress in Oceanography, 72, 276-312

Boyd P.W., J. LaRoche, M. Gall, R. Frew, R.M.L. McKay (1999) Role of iron, light, and silicate in controlling algal biomass in subantarctic waters SE of New Zealand, Journal of Geophysical Research, 104(C6), 13395-13408

Boyd P.W., A.C. Crossley, G.R. DiTullio, F.B. Griffiths, D.A. Hutchins, B. Quéguiner, P.N. Sedwick, T.W. Trull (2001) Control of phytoplankton growth by iron supply and irradiance in the subantarctic Southern Ocean: Experimental results from the SAZ Project, Journal of Geophysical Research, 106(C12), 31573-31583

Boyd P.W., T. Jickells, C.S. Law, S. Blain, E.A. Boyle, K.O. Buesseler, K.H. Coale, J.J Cullen, H.J.W. de Baar, M. Follows, M. Harvey, C. Lancelot, M. Levasseur, N.P.J. Owens, R. Pollard, R.B. Rivkin, J. Sarmiento, V. Schoemann, V. Smetacek, S. Takeda, A. Tsuda, S. Turner, A.J. Watson (2007) Mesoscale Iron Enrichment Experiments 1993-2004: Synthesis and Future Directions, Science, 315, 612-617, doi:10.1126/science.1131669

Brzezinski M., D.M. Nelson, V.M. Frank, D.E. Sigmon (2001) Silicon dynamics within an intense open-ocean diatom bloom in the Pacific sector of the Southern Ocean, Deep-Sea Research II, 48, 3997-4018

Brzezinski M.A., C.J. Pride, V.M. Franck, D.M. Sigman, J.L. Sarmiento, K. Matsumoto, N. Gruber, G.H. Rau, K.H. Coale (2002) A switch from Si(OH)4 to NO3- depletion in the glacial Southern Ocean, Geophysical Research Letters, 29-12), doi: 10.1029/2001GL014349

Buesseler K.O., P.W. Boyd (2003) Will Ocean Fertilization Work? Science, 300, 67-68

Cao Z., M. Frank, M. Dai, P. Grasse, C. Ehlert (2012) Silicon isotope constraints on sources and utilization od silicic acid in the northern South China Sea, Geochimica et Cosmochimica Acta, 97, 88-104

Cardinal D., L.Y. Alleman, J. de Jong, K. Ziegler, L. André (2003) Isotopic composition of silicon measured by multicollector plasma source mass spectrometry in dry plasma mode, Journal of Analytical Atomic Spectrometry, 18, 213-218

Cardinal D., L.Y. Alleman, F. Dehairs, N. Savoye, T.W. Trull, L. André (2005) Relevance of silicon isotopes to Si-nutrient utilization and Si-source assessment in antarctic waters, Global Biogeochemical cycles, 19, GB2007, doi:10.1029/2004GB002364

Cardinal D., N. Savoye, T.W. Trull, F. Dehairs, E.E. Kopczynska, F. Fripiat, J.-L. Tison, L. André (2007) Silicon isotopes in spring Southern Ocean diatoms: Large zonal changes despite homogeneity among size fractions, Marine Chemistry, 106, 46-62

Cavagna A.-J., F. Fripiat, F. Dehairs, D. Wolf-Gladrow, B. Cisewski, N. Savoye, L. André, D. Cardinal (2011) Silicon uptake and supply during Southern Ocean iron fertilization experiment (EIFEX) tacked by Si isotopes, Limnology and Oceanography, 56(1), 147-160

Chisholm S.W. (2000) Stirring times in the Southern Ocean, Nature, 407, 685-687

Claquin P., V. Martin-Jézéquel (2005) Regulation of the Si and C uptake and of the soluble free-silicon pool in a synchronised culture of Cylindrotheca fusiformis (Bacillariophyceae) : effects on the Si/C ratio, Marine Biology, 146, 877-886, doi: 10.1007/s00227-004-1493-5

Corvaisier R., P. Tréguer, C. Beucher, M. Elskens (2005) Determination of the rate of production and dissolution of biosilica in marine waters by thermal ionisation mass spectrometry, Analytica Chimica Acta, 534, 149-155

De Baar H.J.W., P.W. Boys, K.H. Coale, M.R. Landry, A. Tsuda, P. Assmy, D.C.E. Bakker, Y. Bozec, R.T. Barber, M.A. Brzezinski, K.O. Buesseler, M. Boyé, P.L. Croot, F. Gervais, M.Y. Gorbunov, P.J. Harrison, W.T. Hiscock, P. Laan, C.Lancelot, C.S. Law, M. Levasseur, A. Marchetti, F.J. Millero, J. Nishioka, Y. Nojiri, T. van Oijen, U. Riebesell, M.J.A. Rijkenberg, H. Saito, S. Takeda, K.R. Timmermans, M.J.W. Veldhuis, A.M. Waite C.-S. Wong (2005) Synthesis of iron fertilization experiments: From the Iron Age in the Age of Enlightenment, Journal of Geophysical Research, 110, C09S16, doi:10.1029/2004JC002601

De Brauwere A., F. Fripiat, D. Cardinal, A.-J. Cavagna, F. De Ridder, L. André, M. Elskens (2012) Isotopic model of oceanic silicon cycling: The Kerguelen Plateau case study, Deep-Sea Research I, 70, 42-59

De La Rocha C.L., M.A. Brzezinski, M.J. DeNiro (1997) Fractionation od silicon isotopes by marine diatoms during biogenic silica formation, Geochimica et Cosmochimica Acta, 61(23), 5051-5056

De La Rocha C.L., M.A. Brzezinski, M.J. DeNiro, A. Shemesh (1998) Silicon-isotope composition of diatoms as an indicator of past oceanic change, Nature, 395, 680-683

De La Rocha C.L., M.A. Brzezinski, M.J. DeNiro (2000) A first look at the distribution of the stable isotopes of silicon in natural waters, Geochimica et Cosmochimica Acta, 64(14), 2467-2477

De La Rocha C.L., P. Bescont, A. Croguennoc, E. Ponzevera (2011) The silicon isotopic composition of surface waters in the Atlantic and Indian sectors of the Southern Ocean, Geochimica et Cosmochimica Acta, 75, 5283-5295

De Souza G.F., B.C. Reynolds, J. Rickli, M. Frank, M.A. Saito, L.J.A. Gerringa, B. Bourdon (2012) Southern Ocean control of silicon stable isotope distribution on the deep Atlantic Ocean, Global Biogeochemical Cycles, 26, GB2035, doi:10.1029/2011GB004141

Demarest M.S., M.A. Brzezinski, C.P. Beucher (2009) Fractionation of silicon isotopes during biogenic silica dissolution, Geochimica et Cosmochimica Acta, 73, 5572-5583

Dugdale R.C., F.P. Wilkerson, H.J. Minast (1995) The role of a silicate pump in driving new production, Deep-Sea Research I, 42(5), 697-719

Egan K.E., R.E.M. Rickaby, M.J. Leng, K.R. Hendry; M. Hermoso, H.J. Sloane, H. Bostock, A.N. Halliday (2012) Diatom silicon isotopes as a proxy for silicic acid utilization: A Southern Ocean core top calibration, Geochimica et Cosmochimica Acta, 96, 174-192

Ehlert C., P. Grasse, E. Mollier-Vogel, T. Böschen, J. Franz, G.F. de Souza, B.C. Reynolds, L. Stramma, M. Frank (2012) Factors controlling the silicon isotope distribution in waters and surface sediments of the Peruvian coastal upwelling, Geochimica et Cosmochimica Acta, 99, 128-145

Franck V.M., M.A. Brzezinski, K.H. Coale, D.M. Nelson (2000) Iron and silicic acid concentrations regulate Si uptake north and south of the Polar Frontal Zone in the Pacific Sector of the Southern Ocean, Deep-Sea Research II, 47, 3315-3338

François R., S. Honjo, R. Krishfield, S. Manganini (2002) Factors controlling the flux of organic carbon to the bathypelagic zone of the ocean, Global Biogeochemical Cycles, 16(4), 1087; doi: 10.1029/2001GB001722

Fripiat F., R. Corvaisier, J. Navez, M. Elskens, V. Schoemann, K. Leblanc, L. André, D. Cardinal (2009) Measuring production-dissolution rates of marine biogenic silica by ^{30}Si-isotope dilution using a high-resolution sector field inductively coupled plasma mass spectrometer, Limnology and Oceanography: Methods, 7, 470-478

Fripiat F., A.-J. Cavagna, N. Savoye, F. Dehairs, L. André, D. Cardinal (2011a) Isotopic constraints on the Si-biogeochemical cycle of the Antarctic Zone in the Kerguelen area (KEOPS), Marine Chemistry, 123, 11-22

Fripiat F., A.-J. Cavagna, F. Dehairs, S. Speich, L. André, D. Cardinal (2011b) Silicon pool dynamics and biogenic silica export in the Southern Ocean inferred from Si-isotopes, Ocean Science, 7, 533-547, doi:10.5194/os-7-533-2011

Fripiat F., K. Leblanc, M. Elskens, A.-J. Cavagna, L. Armand, L. André, F. Dehairs, D. Cardinal (2011c) Efficient silicon recycling in summer in both the Polar Frontal and Subantarctic Zones of the Southern Ocean, Marine Ecology Progress Series, 435, 47-61

Fripiat F., A.-J. Cavagna, F. Dehairs, A. deBrauwere, L. André, D. Cardinal (2012) Processes controlling the Si-isotopic composition in the Southern Ocean and application for paleoceanography, Biogeosciences, 9, 2443-2457, doi:10.5194/bg-9-2443-2012

Fry B. (2006) Stable Isotope Ecology, Springer, New York, pp 308

Grasse P., C. Ehlert, M. Frank (2013) The influence of water mass mixing on the dissolved Si isotope composition in the Eastern Equatorial Pacific, Earth and Planetary Science Letters, 380, 60-71

Gruber N., M. Gloor, S.E. Mikaloff Fletcher, S.C. Doney, S. Dutkiewicz, M.J. Follows, M. Gerber, A.R. Jacobson, F. Joos, K. Lindsay, D. Menemenlis, A. Mouchet, S.A. Müller, J.L. Sarmiento, T. Takahashi (2009) Oceanic sources, sinks, and transport of atmospheric CO2, Global Biogeochemical cycles, 23, GB1005, doi: 10.1029/2008GB003349

Hendry K.R., R.B. Georg, R.E.M. Rickaby, L.F. Robinson, A.N. Halliday (2010) Deep ocean nutrients during the Last Glacial Maximum deduced from sponge silicon isotopic compositions, Earth and Planetary Science Letters, 292, 290-300

Hildebrand M. (2003) Biological processing of nanostructured silica in diatoms, Progress in Organic Coatings, 47, 256-266

Hildebrand M. (2008) Diatoms, Biomineralization Processes, and Genomics, Chemical Reviews, 108(11), 4855-4874, doi:10.1021/cr078253z

Hoefs J. (2009) Stable Isotopic geochemistry, SpringerVerlag, New York, pp 241

Holzer M., F.W. Primeau, T. DeVries, R. Matear (2014) The Southern Ocean silicon trap: Data-constrained estimated of regenerated silicic acid, trapping efficiencies, and global transport paths, Journal of Geophysical Research: Oceans, 119, 313-331, doi:10.1002/2013LC009356

Hutchins D.A., K.W. Bruland (1998) Iron-limited diatom growth and Si:N uptake ratios in a coastal upwelling regime, Nature, 393, 561-564

IPCC (2013), Climate Change 2013 : The Physical Science Basis. Contribution of Working Group I to the Fifth Assessment Report of the Intergovernmental Panel on Climate Change, [Stocker T.F., D. Qin, G.-K. Plattner, M. Tignor, S.K. Allen, J. Boschung, A. Nauels, Y. Xia, V. Bex, P.M. Midgley (eds.)], Cambridge University Press, Cambridge, United Kingdom and New York, NY, USA

Jin X., N. Gruber, J.P. Dunne, J.L. Sarmiento, R.A. Armstrong (2006) Diagnosing the contribution of phytoplankton functional groups to the production and export of particulate organic carbon, $CaCO_3$, and opal from global nutrient and alkalinity distributions, Global Biogeochemical cycles, 20, GB2015, doi:10.1029/2005GB002532

Kamatani A. (1982) Dissolution Rates of Silica from Diatoms Decomposing at Various Temperatures, Marine Biology, 68, 91-96

Klaas C., D.E. Archer (2002) Association of sinking organic matter with various types of mineral ballast in the deep sea: Implications for the rain ratio, Global Biogeochemical Cycles, 16(4), 1116, doi:10.1029/2001GB001765

Lannuzel D., V. Schoemann, J. de Jong, J.-L. Tison, L. Chou (2007) Distribution and biogeochemical behavior of iron in the East Antarctic sea ice, Marine Chemistry, 106, 18-32

Lenton A., B. Tilbrook, R.M. Law, D. Bakker, S.C. Doney, N. Gruber, M. Ishii, M. Hoppemas, N.S. Lovenduski, R.J. Matear, B.I. Mc Neil, N. Metzl, S.E. Mikaloff Fletcher, P.M.S. Monteiro, C. Rödenbeck, C. Sweeney, T. Takahashi (2013) Sea-air CO2 fluxes in the Southern Ocean for the period 1990-2009, Biogeosciences, 10, 4037-4054, doi: 10.5194/bg-10-4037-2013

Le Quéré C., G. P. Peters, R.J. Andres, R.M. Andrew, T.A. Boden, P. Ciais, P. Friedlingstein, R.A. Houghton, G. Marland, R. Moriarty, S. Sitch, P. Tans, A. Arneth, A. Arvanitis, D.C.E. Bakker, L. Bopp, J.G. Canadell, L.P. Chini, S.C. Doney, A. Harper, I. Harris, J.I. House, A.K. Jain, S.D. Jones, E. Kato, R.F. Keeling, K. Klein Goldewijk, A. Körtzinger, C. Koven, N., Lefèvre, F. Maignan, A. Omar, T. Ono, G.-H. Park, B. Pfeil, B. Poulter, M.R. Raupach, P. Regnier, C. Rödenbeck, S. Saito, J. Schwinger, J. Segschneider, B.D. Stocker, T. Takahashi, B. Tilbrook, S. van Heuven, N. Viovy, R. Wanninkhof, A. Wiltshire, S. Zaehle (2014) Global Carbon budget 2013, Earth System Science Data, 6, 235-263, doi :10.5194/essd-6-235-2014

Leynaert A., E. Bucciarelli, P. Claquin, R.C. Dugdale, V. Martin-Jézéquel, P. Pondaven, O. Ragueneau (2004) Effect of iron deficiency on diatom cell size and silicic acid uptake kinetics, Limnology and Oceanography, 49(4), 1134-1143

Mariotti A., J.C. Germon, P. Hubert, P. Kaiser, R. Letolle, A. Tardieux, P. Tardieux (1981) Experimental determination of nitrogen kinetic isotope fractionation: some principles; illustration for the denitrification and nitrification processes, Plant and Soil, 32, 413-430

Marshall J., K. Speer (2012) Closure of the meridional overturning circulation through Southern Ocean upwelling, Nature Geoscience, 5, 171-180, doi:10.1038/NGEO1391

Martin J. (1990) Glacial-interglacial CO2 change: the iron hypothesis, Paleoceanography, 5(1), 1-13+

Martin-Jézéquel V., M. Hildebrand, M.A. Brzezinski (2000) Silicon metabolism in diatoms: implications for growth, Journal of Phycology, 36, 821-840

Matsumoto K., J.L. Sarmiento, M.A. Brzezinski (2002) Silicic acid leakage from the Southern Ocean: A possible explanation for glacial atmospheric pCO2, Global Biogeochemical cycles, 16(3), doi: 10.1029/2001GB001442

Metzl N., B. Tilbrook, A. Poisson (1999) The annual fCO2 cycle and the air-sea CO2 flux in the sub-Antarctic Ocean, Tellus, 51B, 849-861

Milligan A.J., D.E. Varela, M.A. Brzezinski, F.M.M. Morel (2004) Dynamics of silicon metabolism and silicon isotopic discrimination in a marine diatom as a function of pCO_2, Limnology and Oceanography, 49(2), 322-329

Moore J.K., M.R. Abbott (2000) Phytoplankton chlorophyll distributions and primary production in the Southern Ocean, Journal of Geophysical Research, 105(C12), 28709-28722

Mosseri J., B. Quéguiner, L. Armand, V. Cornet-Barthaux (2008) Impact of iron on silicon utilization by diatoms in the Southern Ocean: A case study of Si/N cycle decoupling in a naturally iron-enriched area, Deep-Sea Research II, 55, 801-819

Nelson D.M., W.O. Smith Jr (1991) Sverdrup revisited: Critical depths, maximum chlorophyll levels, and the control of Southern Ocean productivity by the irradiance-mixing regime, Limnology and Oceanography, 36(8), 1650-1661

Nelson D.M., M.A. Brzezinski, D.E. Sigmon, V.M. Frank (2001) A seasonal progression of Si limitation in the Pacific sector of the Southern Ocean, Deep-Sea Research II, 48, 3973-3995

Orsi A.H., T. Whitworth III, W.D. Nowlin Jr (1995) On the meridional extent and fronts of the Antarctic Circumpolar Current, Deep-Sea Research I, 42(5), 641-673

Petit J.R., J. Jouzel, D. Raynaud, N.I. Barkov, J.-M. Barnola, I. Basile, J. Chappellaz, M. Davisk, G. Delaygue, M. Delmotte, V.M. Kotlyakov, M. Legrand, V.Y. Lipenkov, C. Lorius, L.Pépin, C. Ritz, E. Saltzmank, M. Stievenard (1999) Climate and atmospheric history of the past 420,000 years from the Vostok ice core, Antarctica, Nature, 399, 429-436

Pondaven P., O. Ragueneau, P. Tréguer, A. Hauvespre, L. Delzileau, J.L. Reyss (2000) Resolving the 'opal paradox' in the Southern Ocean, Nature, 405, 168-172

Quéguiner B. (2013) Iron fertilization and the structure of planktonic communities in high nutrient regions of the Southern Ocean, Deep-Sea Research II, 90, 43-54

Ragueneau O., P. Tréguer, A. Leynaert, R.F. Anderson, M.A. Brzezinski, D.J. DeMaster, R.C. Dugdale, J. Dymont, G. Fisher, R. François, C. Heinze, E. Maier-Reimer, V. Martin-Jézéquel, D.M. Nelson, B. Quéguiner (2000) A review of the Si cycle in the modern ocean: recent progress and missing gaps in the application of biogenic opal as a paleoproductivity proxy, Global and Planetary Change, 26, 317-365

Reynolds B.C., M. Frank, A.N. Halliday (2006) Silicon isotope fractionation during nutrient utilization in the North Pacific, Earth and Planetary Science Letters, 244, 431-443

Rintoul S.R., T.W. Trull (2001) Seasonal evolution of the mixed layer in the Subantarctic Zone south of Australia, Journal of Geophysical Research, 106(C12), 31447-31462

Safi K.A., Griffiths F.B., Hall J.A. (2007) Microzooplankton composition, biomass and grazing rates along the WOCE SR3 line between Tasmania and Antarctica, Deep-Sea Research I, 54, 1025-1041

Sarmiento J.L., N. Gruber, M.A. Brzezinski, J.P. Dunne (2004) High-latitude controls of thermocline nutrients and low latitude biological productivity, Nature, 427, 56-60

Sarmiento J.L., J. Simeon, A. Gnanadesikan, N. Gruber, R.M. Key, R. Schlitzer (2007) Seep ocean biogeochemistry of silicic acid and nitrate, Global Biogeochemical cycles, 21, GB1S90, doi:10.1029/2006GB002720

Sigman D.M., M.A. Altabet, D.C. Mc Corkle, R. François, G. Fischer (1999) The $\delta^{15}N$ of nitrate in the Southern Ocean: Consumption of nitrate in surface waters, Global Biogeochemical Cycles, 13(4), 1149-1166

Singh S.P., S.K. Singh, R. Bhushan, V.K. Rai (2015) dissolved silicon and its isotopes in the water column of the Bay of Bengal: Internal cycling versus lateral transport, Geochimica et Cosmochimica Acta, 151, 172-191

Smetacek V., P. Assmy, J. Henjes (2004) The role of grazing in structuring Southern Ocean pelagic ecosystems and biogeochemical cycles, Antarctic Science, 16(4), 541-558, doi:10.1017/S09544102004002317

Sokolov S., S.R. Rintoul (2007) On the relationship between fronts of the Antarctic Circumpolar Current and surface chlorophyll concentrations in the Southern Ocean, Journal of Geophysical Research, 112, C07030, doi: 10.1029/2006JC004072

Sokolov S., S.R. Rintoul (2009) Circumpolar structure and distribution of the Antarctic Circumpolar Current fronts: 1. Mean circumpolar paths, Journal of Geophysical Research, 114, C11018, doi: 10.1029/2008JC005108

Speer K., S.R. Rintoul, B. Sloyan (2000) The Diabatic Deacon Cell, Journal of Physical Oceanography, 30, 3212-3222

Sutton J.N., D.E. Varela, M.A. Brzezinski, C.P. Beucher (2013) Species-dependent silicon isotope fractionation by marine diatoms, Geochimica et Cosmochimica Acta, 104, 300-309

Tagliabue A., L. Bopp, O. Aumont (2009) Evaluating the importance of atmospheric and sedimentary iron sources to Southern Ocean biogeochemistry, Geophysical Research Letters, 36, L13601, doi:10.29/2009GL038914

Tagliabue A., T. Mtshali, O. Aumont, A.R. Bowie, M.B. Klunder, A.N., Roychoudhury, S. Swart (2012) A global compilation of dissolved iron measurements: focus on distributions and processes in the Southern Ocean, Biogeosciences, 9, 2333-2349, doi:10.5194/bg-9-2333-2012

Tagliabue A., J.-B. Sallée, A.R. Bowie, M. Lévy, S. Swart, P.W. Boyd (2014) Surface-water iron supplies in the Southern Ocean sustained by deep winter mixing, Nature Geoscience, 7, 314-320, doi:10.1038/NGEO2101

Takahashi T., S.C. Sutherland, R. Wanninkhof, C. Sweeney, R.A. Feely, D.W. Chipman, B. Hales, G.Friederich, F. Chavez, C. Sabine, A. Watson, D.C.E. Bakker, U. Schuster, N.Metzl, H.Yoshikawa-Inoue, M. Ishii, T. Midorikawa, Y. Nojiri, A. Körtzinger, T. Steinhoff, M. Hoppema, J. Olafsson, T.S. Arnarson, B. Tilbrook, T. Johannessen, A. Olsen, R. Bellerby, C.S. Wong, B. Belille, N.R. Bates, H.J.W. de Baar (2009) Clomatological mean and decadal change in surface ocean pCO2, and net sea-air CO_2 flux over the global oceans, Deep-Sea Research II, 56, 554-577

Thamatrakoln K., M. Hildebrand (2008) Silicon Uptake in Diatoms Revisited: A Model for Saturable and Nonsaturable Uptake Kinetics and the Role of Silicon Transporters, Plant Physiology, 146, 1397-1407

Tréguer P.J. (2014) The Southern Ocean Silica Cycle, Comptes Rendus Geoscience, 346, 279-286, doi:10.1016/j.crte.2014.07.003

Tréguer P.J., C.L. De La Rocha (2013) The World Ocean Silica Cycle, Annual Review of Marine Science, 5, 477-501, doi:10.1146/annurev-marine-121211-172346

Tréguer P., L. Lindner, A.J. van Bennekom, A. Leynaert, M. Panouse, G. Jacques (1991) Production of biogenic silica in the Weddel-Scotia Seas measured with 32Si, Limnology and Oceanography, 36, 1217-1227

Tréguer P.J., D.M. Nelson, A.J. Van Bennekom, D.J. DeMaster, A. Leynaert, B. Quéguiner (1995) The Silica Balance in the World Ocean: A Reestimate, Science, 268(5209), 375-379

Trull T., S.R. Rintoul, M. Hadfield, E.R. Abraham (2001) Circulation and seasonal evolution of polar waters south of Australia: Implications for iron fertilization of the Southern Ocean, Deep-Sea Research II, 48, 2439-2466

Van der Merwe P., D. Lannuzel, A.R. Bowie, K.M.Meiners (2011) High temporal resolution observations of spring fast ice melt and seawater iron enrichment in East Antarctica, Journal of Geophysical Research, 116, G03017, doi:10.1029/2010JG001628

Varela D.E., C.J. Pride, M.A. Brzezinski (2004) Biological fractionation of silicon isotopes in Southern Ocean surface waters, Global Biogeochemical Cycles, 18, GB1047, doi:10.1029/2003GB002140

Voss M., H.W. Bange, J.W. Dippner, J.J. Middelburg, J.P. Montoya, B. Ward (2015) The marine nitrogen cycle: recent discoveries, uncertainties and the potential relevance of climate change, Philisophical Transactions of the Royal Society B, 368:20130121, doi: 10.1098/rstb.2013.0121

Wetzel F., G.F. de Souza, B.C. Reynolds (2014) What controls silicon isotope fractionation during dissolution of diatom opal?, Geochimica et Cosmochimica Acta, 131, 128-137

Wille M., J. Sutton, M.J. Ellwood, M. Sambridge, W. Maher, S. Eggins, M. Kelly (2010) Silicon isotopic fractionation in marine sponges: A new model for understanding silicon isotopic variations in sponges, Earth and Planetary Science Letters, 292, 281-289

Young E.D., A. Galy, H. Nagahara (2002) Kinetic and equilibrium mass-dependent isotope fractionation laws in nature and their geochemical and cosmochemical significance, Geochimica et Cosmochimica Acta, 66(6), 1095-1104

Chapitre 1

Evolution Saisonnière de la Production de Silice Biogénique dans l'Océan de Surface

PREAMBULE

Contexte de l'étude

Il a été évoqué précédemment que le cycle biogéochimique du silicium est le plus dynamique dans la couche éclairée de l'océan (zone euphotique) et qu'un atome de silicium subit en moyenne 25 cycles d'absorption biologique – dissolution dans l'océan superficiel avant d'être enfoui dans les sédiments (Tréguer & De La Rocha, 2013). Cependant, de nombreuses incertitudes demeurent quant à la quantification de ces flux, notamment en raison des difficultés analytiques rencontrées dans la mesure de la production et la dissolution de la silice biogénique.

La méthode de dilution isotopique du ^{30}Si (Fripiat et al., 2009) permet de déterminer simultanément les taux de production et de dissolution de la BSi à partir du même échantillon. Après avoir enrichi artificiellement le stock de DSi en isotope lourd (^{30}Si), le taux de production est estimé en mesurant l'augmentation de la proportion de ^{30}Si dans le réservoir particulaire. Le taux de dissolution, quant à lui, est estimé en mesurant la diminution (ou dilution) de la proportion de ^{30}Si dans le réservoir dissous liée à la dissolution de la BSi naturellement riche en ^{28}Si (*Fig. 1.1.*).

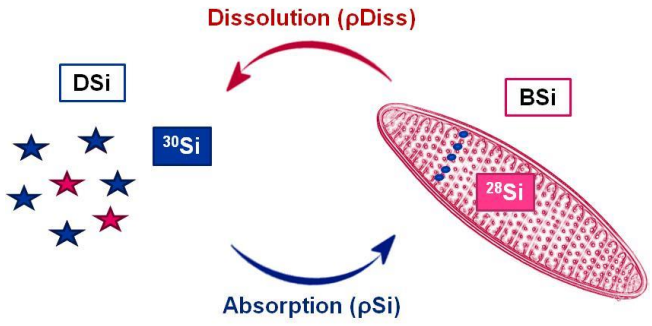

Figure 1.1 Schéma conceptuel illustrant le principe de la mesure des taux de production et de dissolution de silice biogénique par la méthode de dilution isotopique du ^{30}Si. Les couleurs représentent les flux et les stocks dominés par le ^{30}Si (en bleu) ou par le ^{28}Si (en rouge).

Dans ce chapitre, nous avons optimisé avec succès cette méthode afin d'augmenter la sensibilité des mesures des taux de dissolution en pratiquant deux types d'incubations : des incubations « standards », avec un enrichissement en ^{30}Si à 10% de la concentration initiale de H_4SiO_4 pour la mesure du taux de production ; et des incubations dites « sensibles », avec un enrichissement en ^{30}Si

à 100% de la concentration initiale de H_4SiO_4 pour la mesure du taux de dissolution (on double la concentration initiale durant l'incubation).

L'interprétation et la quantification de ces flux nous a permis d'établir un budget saisonnier du silicium dans la région naturellement fertilisée en fer du Plateau de Kerguelen. Cette région héberge en effet chaque année un développement important de diatomées et constitue un laboratoire naturel pour l'étude de l'impact du fer sur les cycles biogéochimiques du carbone, de l'azote et du silicium. Ainsi, à travers l'analyse de ces flux, nous nous sommes intéressés aux variations saisonnières de l'efficacité de la pompe de silicium, ainsi qu'aux processus contrôlant le découplage important entre les cycles du silicium et de l'azote observé dans cette région en fin de saison (Mosseri et al., 2008).

Résumé

Un développement massif de diatomées est observé chaque année dans les eaux de surface naturellement fertilisées en fer du Plateau de Kerguelen (Océan Austral). Nous avons mesuré les flux de production et de dissolution de la silice biogénique (respectivement ρSi et ρDiss) dans la couche de mélange à proximité du Plateau de Kerguelen durant la période printannière (campagne océanographique KEOPS-2). L'objectif principal est de comparer les résultats d'une station de référence « High-Nutrient Low-Chlorophyll » (HNLC) avec ceux des stations présentant différents degrés d'enrichissement en fer. Sur le Plateau, les taux de production de silice biogénique mesurés se trouvent parmi les plus élevés jamais reportés dans l'Océan Austral (jusqu'à 47.9 mmoles m^{-2} j^{-1}), alors que même s'ils sont significatifs (en moyenne 10.2 mmoles m^{-2} j^{-1}), les taux de dissolution sont généralement beaucoup plus faibles que les taux de production. Les rapports d'absorption (ρSi:ρC et ρSi:ρN) confirment également que les diatomées dominent fortement la production primaire dans cette région. Au moment de l'initiation de l'efflorescence, les rapports décroissants dissolution sur production (D:P) indiquent que la reminéralisation de la silice peut être responsable d'une grande partie du taux d'absorption de silicium (qui est alors relativement faible) et que le système tend progressivement vers un régime de production qui serait principalement lié à des sources externes d'acide silicique. De plus, en comparant les résultats des 2 campagnes océanographiques KEOPS (printemps 2011 et été 2005), nous pouvons suggérer qu'il existe une évolution saisonnière des processus découplant les cycles du silicium et de l'azote dans la région. En effet, la consommation des stocks d'acide silicique se déroule uniquement durant la phase de croissance de l'efflorescence, lorsqu'une forte production nette de silice est observée, contribuant ainsi à une plus grande consommation d'acide silicique en comparaison des nitrates. Plus tard dans la saison, le découplage

entre le silicium et l'azote est principalement contrôlé par le recyclage plus efficace de ce dernier comparé au silicium. Les rapports d'absorption bruts (Si:N) sont plus élevés dans les régions riches en fer comparé à la zone HNLC, probablement en raison de la présence de communautés de diatomées différentes. Ceci suggère que la réponse des diatomées à la fertilisation naturelle en fer est plus complexe que ce que l'on pensait précédemment, et que les fertilisations naturelles en fer sur de grandes échelles de temps ne diminuent pas nécessairement les rapports d'absorption Si:N comme le suggère la « Silicic Acid Leakage Hypothesis » (SALH). Finalement, nous avons proposé la première estimation du budget biogéochimique du silicium sur le Plateau de Kerguelen, basée sur des mesures directes. Cette étude met en évidence que les régions naturellement fertilisées en fer de l'Océan Austral peuvent soutenir des régimes très importants de production de silice biogénique, comparables à ceux observés dans les systèmes hautement productifs comme les zones d'upwellings.

Ce chapitre a fait l'objet d'un article publié dans l'issue spéciale du projet KEOPS-2 (Biogeosciences) :

Closset I., M. Lasbleiz, K. Leblanc, B. Quéguiner, A.-J. Cavagna, M. Elskens, J. Navez, D. Cardinal (2014), Seasonal evolution of net and regenerated silica production around a natural Fe-fertilized area in the Southern Ocean estimated with Si isotopic approaches, Biogeosciences, 11, 5827-5846, doi:10.5194/bg-11-5827-2014.

TABLE OF CONTENTS

Seasonal evolution of net and regenerated silica production around a natural Fe-fertilized area in the Southern Ocean estimated from Si isotopic approaches

I. Closset[1], M. Lasbleiz[2], K. Leblanc[2], B. Quéguiner[2], A.-J. Cavagna[3], M. Elskens[3], J. Navez[4], D. Cardinal[1,4]

[1] Sorbonne Universités (UPMC, Univ Paris 06)-CNRS-IRD-MNHN, LOCEAN Laboratory, 4 place Jussieu, F-75005 Paris, France

[2] Aix Marseille Université, CNRS, Université de Toulon, IRD, MIO UM 110, 13288, Marseille, France

[3] Earth and System Sciences & Analytical and Environmental Chemistry, Vrije Universiteit Brussel, Pleinlaan 2, B-1050 Brussels, Belgium

[4] Department of Earth Sciences, Royal Museum for Central Africa, Leuvensesteenweg 13, 3080 Tervuren, Belgium

Correspondence to: I. Closset (ivia.closset@locean-ipsl.upmc.fr)

Abstract

A massive diatom-bloom is observed each year in the surface waters of the naturally Fe fertilized Kerguelen Plateau (Southern Ocean). We measured biogenic silica production and dissolution fluxes (ρSi and ρDiss respectively) in the mixed layer in the vicinity of the Kerguelen Plateau during austral spring 2011 (KEOPS-2 cruise). We compare results from a High-Nutrient Low-Chlorophyll reference station and stations with different degrees of iron enrichment and bloom conditions. Above the Plateau biogenic ρSi are among the highest reported so far in the Southern Ocean (up to 47.9 mmol m^{-2} d^{-1}). Although significant (10.2 mmol m^{-2} d^{-1} in average), ρDiss were generally much lower than production rates. Uptake ratios (ρSi:ρC and ρSi:ρN) confirm that diatoms strongly dominate the

primary production in this area. At the bloom onset, decreasing dissolution to production ratios (D:P) indicate that the remineralization of silica could sustained most of the low silicon uptake and that the system progressively shifts toward a silica production regime which must be mainly supported by new source of silicic acid. Moreover, by comparing results from the two KEOPS-expeditions (spring 2011 and summer 2005), we suggest that there is a seasonal evolution on the processes decoupling Si and N cycles in the area. Indeed, the consumption of H_4SiO_4 standing stocks occurs only during the growing stage of the bloom when strong net silica production is observed, contributing to a higher H_4SiO_4 depletion relative to NO_3^-. Then, the decoupling between H_4SiO_4 and NO_3^- is mainly controlled by the more efficient nitrogen recycling relative to Si. Gross-Si:N uptake ratios were higher in the Fe-rich regions compared to the HNLC area, likely due to different diatoms communities. This suggests that the diatom responses to natural Fe fertilization are more complex than previously thought, and that natural iron fertilization over long time scales does not necessarily decrease Si:N uptake ratios as suggested by the Silicic Acid Leakage Hypothesis. Finally, we propose the first seasonal estimate of Si-biogeochemical budget above the Kerguelen Plateau based on direct measurements. This study points out that naturally iron fertilized areas of the Southern Ocean could sustain very high regimes of biogenic silica production, similar to those observed in highly productive upwelling systems.

I.1. Introduction

Covering 20 % of the World Ocean, the Southern Ocean is considered as a crucial component of the climate system since it represents a net sink for atmospheric CO_2 (Takahashi et al., 2009). It also plays a key role in the global silicon (Si) biogeochemical cycle because diatoms, a siliceous phytoplankton group, are one of the major primary producers in this area (Buesseler et al., 2001; Quéguiner and Brzezinski, 2002; Tréguer and De la Rocha, 2013). As their cell wall is composed of biogenic silica (opal, amorphous $SiO_2.nH_2O$, hereafter referred to as BSi), diatoms take up dissolved silicon (hereafter referred to as DSi) in the form of silicic acid (H_4SiO_4), to produce their siliceous frustules. At global scale, 56 % of this gross production is estimated to be directly recycled in the upper 100 m (Tréguer and De La Rocha, 2013) due to the combined effects of both physico-chemical and biological processes (Kamatani, 1982; Bidle and Azam, 1999; Ragueneau et al., 2000). Only the material escaping dissolution is exported toward the deep ocean and eventually buried in sediments. Consequently, the marine Si biogeochemical cycle is dominated by biogenic silica production and dissolution in the surface mixed layer, and one atom of Si undergoes a cycle of biological uptake by

diatom and subsequent dissolution about 25 times before being removed to the seabed (Tréguer and De La Rocha, 2013). Thus, it is essential to estimate the balance between silica production and dissolution in the euphotic zone which is best illustrated by the integrated dissolution to production rate ratio (∫D:∫P; Brzezinski et al., 2003) or by integrated net production rate (∫ρSiNet = production minus dissolution). Globally, the ∫D:∫P values present an annual mean of 0.56 (Tréguer and De La Rocha, 2013) and range from < 0.1 to > 1, with low D:P values associated to diatom bloom events, and D:P values exceeding 0.5 occurring during non-bloom periods (Brzezinski et al., 2001). However, the number of D:P estimates, due to a small number of Si uptake measurements and an even lower number of Si dissolution measurements, is insufficient compared to the high variability observed regionally and seasonally in the ocean which implies high uncertainty in the global D:P estimate and overall on the marine silicon budget.

Diatoms are ecologically widespread and dominate the primary production in the Antarctic Circumpolar Current (ACC), especially south of the Polar Front (PF), where their productivity accounts for 1/3 of the global marine silica production (Pondaven et al. 2000; Buesseler et al. 2001). Consequently, this part of the Southern Ocean represents a key study area to improve our understanding of the global biogeochemical cycles of both carbon and silicon. Biological processes occurring in the Southern Ocean have indeed a significant impact on global biogeochemistry. For example, the large H_4SiO_4 utilization by diatoms in the ACC, combined to the global overturning circulation would determine the functioning of the biological pump of low latitude areas by inducing a strong silicic acid limitation (Sarmiento et al., 2004). In the Southern Ocean, a much larger depletion of silicic acid than nitrate in surface waters occurs (Trull et al., 2001), which results from the action of a silicon pump, i.e. the preferential export of BSi compared to particulate organic nitrogen (PON; Dugdale et al., 1995). This area is also the largest High Nutrient Low Chlorophyll (HNLC) zone of the global ocean where dissolved iron limitation plays a fundamental role in regulating the primary production and the carbon cycle (De Baar et al., 2005; Boyd et al., 2007; Tagliabue et al., 2012). Indeed, phytoplankton community structure and nutrient cycling could be largely controlled by Fe availability, with highest growth rates located close to iron sources such as continental margins, island systems and frontal regions (Blain et al., 2007; Tagliabue et al., 2012).

In this context, the KErguelen Ocean and Plateau compared Study (KEOPS) program, consisting of two expeditions (late summer 2005 and early spring 2011), was conducted to investigate a naturally iron-fertilized area located in the Indian sector of the Southern Ocean, where the iron availability could

potentially favor the carbon and silicon biological pumps (*Fig. 1.2.*; Blain et al., 2007). Two massive and complex blooms, which are clearly constrained by the local bathymetry, are observed annually over the Kerguelen Plateau and contrast with the HNLC character of surrounding waters (Pollard et al., 2002; Mongin et al., 2008). The first KEOPS expedition (KEOPS-1, January-February 2005) has highlighted the impact of natural iron fertilization on primary production and nutrient cycling, as well as the advantages to study natural laboratories in the context of such ocean fertilization (Blain et al., 2008). The general purpose of KEOPS-2 (October-November 2011) was to improve our knowledge about the processes responsible for this iron fertilization and its impact on the seasonal variations of the mechanisms controlling the primary production and carbon export. While the KEOPS-1 cruise was mainly directed towards the study of the bloom in the South-East area of the Plateau, KEOPS-2 focused mainly on the bloom located North-East of the Kerguelen Islands above the Kerguelen abyssal plain.

In this paper, we investigate the spatial and seasonal variability of silica production and dissolution in the surface waters of the Kerguelen area. The specific objectives are the following:

- Compare the Si cycle dynamics in contrasting productive environments such as the southeastern Kerguelen Plateau bloom, the northeastern Kerguelen bloom in a stationary meander southward the PF and the warmer waters located north of this front, relative to the upstream HNLC area south-west of Kerguelen Islands, and identify controlling processes.

- Determine and quantify the seasonal evolution of processes which drive the Si biogeochemical budget in the upper layer of the Kerguelen Plateau, using the 30Si stable isotope method (Nelson and Goering, 1977a; Fripiat et al, 2009) applied during KEOPS-2 and other techniques of mass and isotopic balance used during KEOPS-1 (^{32}Si radiogenic tracer incubations; Mosseri et al., 2008 and natural silicon isotopic composition, δ^{30}Si; Fripiat et al., 2011a), in order to fully characterize the silicon cycle above the Kerguelen Plateau.

- Discuss the potential role of Fe on silica production – dissolution and on Si:N uptake ratios in the context of the Silicic Acid Leakage Hypothesis (Brzezinski et al., 2002; Sarmiento et al., 2004).

- Finally, compare our dataset with previous results in other productive regions of the global ocean and discuss the different types of diatom dominated regimes.

I.2. Material and methods

I.2.1. KEOPS-2 sampling campaign

The KEOPS-2 cruise was conducted in the Indian sector of the Southern Ocean during the austral spring 2011 (from October 10th to November 20th) on board the R/V Marion Dufresne (TAAF/IPEV) and was focused on the iron-fertilized blooms observed around the Kerguelen Plateau region. This plateau is a large area of relatively shallow seafloor that acts as a barrier to the circumpolar flow of the ACC, forcing a large part of the current to pass north of the plateau. The remaining flow passes south of the Kerguelen Islands and forms the jet of the PF, which exhibits strong meandering and eddy activity (Park et al., 1998, 2008, Roquet et al., 2009). As a consequence, the shallow region located south of Kerguelen Island represents a zone of weak north-eastward circulation (Park et al., 2008; Roquet et al, 2009) and bears a capacity of high chlorophyll a and BSi accumulation during phytoplankton blooms (Blain et al., 2001; Mosseri et al., 2008; Mongin et al., 2008). Over the plateau, enhanced vertical mixing associated to internal waves interact with the local bathymetry (Park et al., 2008) and supply iron and macronutrients from depth to surface waters, enabling to fuel phytoplankton bloom (Blain et al., 2007; Fripiat et al., 2011a).

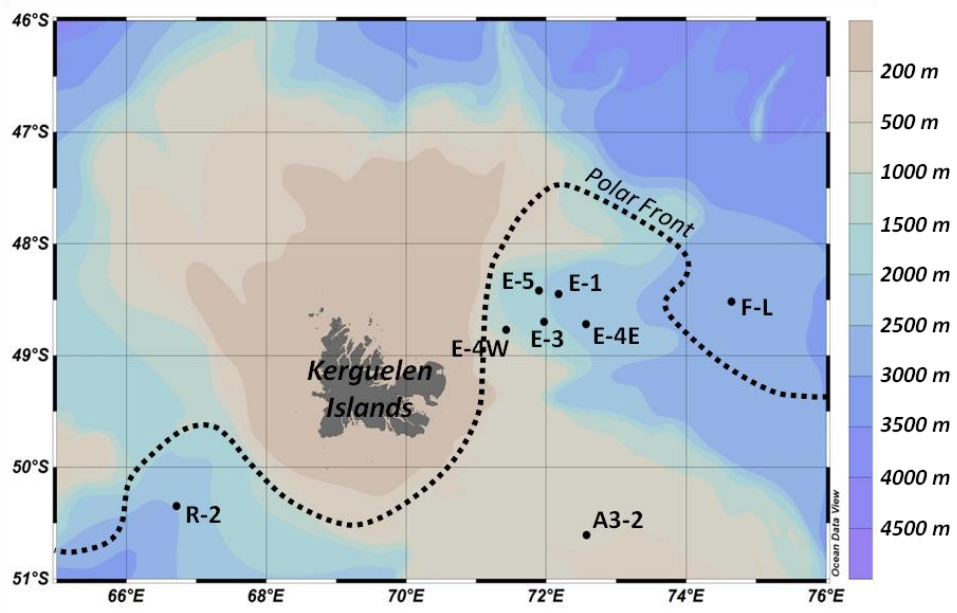

Figure 1.2. Map of the KEOPS-2 cruise area (Indian sector of the Southern Ocean) showing the location of stations discussed in this study. Dotted line represents the position of the Polar Front from Park et al. (in prep.).

The cruise included 8 long-term stations devoted to process studies with incubation experiments (*Fig. 1.2.*). Except for one station (E4E) where we were not able to measure silica dissolution, Si fluxes were investigated in all these process-stations which characteristics are presented in *table 1.1.*:

- A HNLC reference station (R-2) located in deep waters south-west of Kerguelen Islands.

- The Kerguelen Plateau bloom reference station of KEOPS-1 (A3-2).

- A productive open ocean station (F-L) influenced by warmer Sub-Antarctic Surface Water, located north of the Polar Front.

- A productive station (E-4W) located in the plume of chlorophyll observed downstream of the plateau and close to the jet induced by the PF.

- 4 stations (E-1 to E-5) constituting a pseudo-lagrangian survey located in a complex recirculation zone in a stationary meander of the Polar front characterized by strong mesoscale activity (Zhou et al., 2014).

Table 1.1. Characteristics of the stations sampled for Si-fluxes measurements during KEOPS-2. Ze represents the bottom of the euphotic zone (1% of surface Photosynthetically Active Radiation), MLD is the depth of the Mixed Layer (from Park et al., in prep.).

Station	Zone	Position		Date	Ze (m)	MLD (m)
		Latitude	Longitude			
R-2	*HNLC*	50°21.55 S	66°43.0 E	26-Oct	92	124
E-1	*Meander*	48°27.4 S	72°11.3 E	30-Oct	64	69
E-3	*Meander*	48°42.1 S	71°58.0 E	4-Nov	68	35
F-L	*Polar front*	48°31.2 S	74°39.5 E	7-Nov	29	47
E-4W	*Plume*	48°45.9 S	71°25.5 E	12-Nov	31	55
E-4E	*Meander*	48°42.9 S	72°33.8 E	14-Nov	34	80
A3-2	*Plateau*	50°37.5 S	72°34.9 E	17-Nov	38	123
E-5	*Meander*	48°24.7 S	71°54.0 E	19-Nov	54	41

I.2.2 Sample collection, spike and incubation conditions

The isotopic dilution technique adapted by Fripiat et al. (2009) from Corvaisier et al. (2005) aims at simultaneously determining the rates of Si uptake (i.e. silica production) and of biogenic silica dissolution in the same seawater sample. After spiking with a solution enriched in ^{30}Si followed by incubation of the samples, the production rate is estimated from the change in isotopic composition

of the particulate phase (increase in ^{30}Si). Similarly, the isotopic dilution (increase in ^{28}Si) in the ^{30}Si enriched seawater, due to the dissolution of naturally ^{28}Si enriched BSi initially present, is used to estimate the dissolution rate.

Production and dissolution rates were determined at 7 and 5 depths respectively, corresponding to different levels of Photosynthetically Active Radiation (PAR), from 75 % to 0.1 % of surface irradiance. Seawater was collected at defined depths in the euphotic layer using Niskin bottles mounted on a CTD-rosette. For each depth, 5 l of seawater were sampled. 1 l was subsampled to obtain a natural silicon isotopic standard (i.e. not spiked with ^{30}Si) to be processed along with the samples to correct for the matrix effect and mass bias during isotopic analysis (Fripiat et al., 2009). These unspiked samples were immediately filtered on 0.8 µm Nuclepore polycarbonate membranes to separate biogenic silica from silicic acid. The membrane was dried at 50 °C overnight and the filtrate was directly preconcentrated (see section – Sample preparation and isotopic measurements) and stored at room temperature in the dark.

The remaining seawater volume was subsampled in 2 l aliquots spiked with $H_4{}^{30}SiO_4$-enriched solution (99 % ^{30}Si). Aliquots devoted to production measurements were spiked with a spike contribution representing usually less than 10 % of natural concentrations to minimize the perturbation of the natural DSi contents (Nelson & Goering, 1977a). In order to improve the detection limit of the method for dissolution, a second 2 l aliquot was spiked by adding ^{30}Si in the same amount as natural DSi (i.e. DSi spike addition at 100 % of the initial DSi). This provided sufficient sensitivity for the isotopic measurements of dissolution (see section – *Accuracy of the model, detection limit and standard deviation*).

Immediately after spike addition and gentle mixing, 1 l was filtered following the same procedure than for the unspiked standard, to determine the initial conditions (t_0). The second half of the sample was poured into polycarbonate incubation-bottles and incubated under light conditions simulating those prevailing in situ for 24 h (10 % spiked samples) and for 48 h (100 % spiked samples). Deck-incubators were fitted with blue plastic optical filters to simulate the light attenuation of the corresponding sampling depths, and temperature was regulated by circulating surface seawater. At the end of the incubation period, samples were filtered and treated as described above to characterize the final conditions of the incubation (t_{24} or t_{48}).

I.2.3. Sample preparation and isotopic measurements

Preconcentration of H_4SiO_4 in the seawater samples (for both production and dissolution measurements) was applied on-board to increase the Si:salinity ratio, because the maximum salinity of the solution that can be introduced in the mass spectrometer is about 2 ‰ (Fripiat et al., 2009). This step was achieved using a protocol adapted from the MAGIC method (Karl & Tien, 1992; Reynolds et al., 2006). The H_4SiO_4 in seawater was scavenged by the brucite precipitate ($Mg(OH)_2$) obtained by adding 1 ml of 14 N NaOH to the 1 l of seawater sample and strong stirring. The precipitate was recovered by decantation and centrifugation, and was then dissolved in 3 ml of 3 N HCl.

In the shore based laboratory, polycarbonate membranes (t_0, t_{24} and t_{48} for both production and dissolution measurements) were digested in one step using a protocol adapted from Ragueneau et al. (2005) with 4 ml of 0.2 N NaOH during 40 min at 100 °C to hydrolyse BSi. Samples were then neutralized with 1 ml of 1 N HCl to stop the reaction.

An aliquot of the solutions obtained after preconcentration and digestion was used to determine colorimetrically the DSi and BSi concentrations, following the method of Strickland and Parsons (1972). The remaining sample was diluted to 100 ppb Si in a 2 % HNO_3 solution to determine the initial and final Si isotopic composition of the dissolved and particulate phases using a Element 2 (Thermo-Fischer) HR-SF-ICP-MS (High Resolution – Sector Field – Inductively Coupled Plasma – Mass Spectrometer) with the same configuration used by Fripiat et al. (2009). The sequence of analysis consists in: blank – natural standard – spiked sample 1 – natural standard – spiked sample 2 – natural standard – spiked sample 3 – natural standard – blank. The average of the two blanks were subtracted to each standard and sample. To test whether our dissolution measurements were biased by a ^{30}Si contamination linked to a possible memory effect in the HR-SF-ICP-MS, we compared the average composition of the first natural standards (i.e., without contamination from memory effect, n = 55) with the composition of natural standards analyzed after a spiked sample (n = 102). There was no significant difference between natural standards passed before and after a 100 % DSi spiked sample (T-test, p-value <0.001). We can thus exclude significant memory effect when applying the analytical sequence described above.

I.3. Results

I.3.1 Accuracy of the model, detection limit and standard deviation

To estimate the production and dissolution of biogenic silica (ρSi and ρDiss, respectively), two different models are available: the linear one-compartmental model described by Nelson and Goering (1977a, b) and the non-linear two-compartmental model described in de Brauwere et al. (2005) and Elskens et al. (2007). In the latter, both isotopic composition and concentration changes occurring during the incubation time are taken into account to estimate production and dissolution rates simultaneously. Lack of consideration of these changes could induce significant biases in the estimated fluxes (Elskens et al., 2007). In this model the fluxes are calculated by resolving a system of 4 equations given by:

$$[\mathrm{DSi}]_t = [\mathrm{DSi}]_{t0} + (\rho\mathrm{Diss} - \rho\mathrm{Si}) \times t \qquad (1.1.)$$

$$[\mathrm{BSi}]_t = [\mathrm{BSi}]_{t0} + (\rho\mathrm{Si} - \rho\mathrm{Diss}) \times t \qquad (1.2.)$$

$$æ\mathrm{DSi}_t = æ\mathrm{DSi}_{t0} \times \left(1 + \frac{\rho\mathrm{Diss} - \rho\mathrm{Si}}{[\mathrm{DSi}]_{t0}} \times t\right)^{\frac{\rho\mathrm{Diss}}{\rho\mathrm{Si} - \rho\mathrm{Diss}}} \qquad (1.3.)$$

$$æ\mathrm{BSi}_t = \frac{æ\mathrm{DSi}_{t0} \times [\mathrm{DSi}]_{t0}}{[\mathrm{BSi}]_{t0} + (\rho\mathrm{Si} - \rho\mathrm{Diss}) \times t} \times \left(1 - \left(1 + \frac{\rho\mathrm{Diss} - \rho\mathrm{Si}}{[\mathrm{DSi}]_{t0}} \times t\right)^{\frac{\rho\mathrm{Si}}{\rho\mathrm{Si} - \rho\mathrm{Diss}}}\right) \qquad (1.4.)$$

where [BSi] and [DSi] are the dissolved silicon and biogenic silica concentrations (in µmol l^{-1}); æBSi and æDSi are the abundance in excess of ^{30}Si (measured minus natural abundances) in the particulate and dissolved phase respectively; the subscribes t_0 and t refer to the initial and final incubation values.

The best solution is found numerically by optimizing parameter values (ρSi and ρDiss) and minimizing the cost function (weighted sum of squared differences between calculated and measured variables, [BSi], [H_4SiO_4], æBSi and æDSi for the four equations simultaneously; de Brauwere et al., 2005; Elskens et al., 2007).

The relevance of the 2 models against a given data set has already been discussed by Elskens et al. (2007) and Fripiat et al. (2011b). Taking into account these considerations, and after testing the accuracy and the sensitivity of each model, we use preferentially the non-linear 2 compartmental

model to estimate the biogenic silica production and dissolution during KEOPS-2. This model was tested according to the four criteria and the residual of the cost function was checked to follow a Chi² distribution as detailed in Elskens et al. (2007). Due to unexpected sampling problems on-board, we were not able to measure $[DSi]_t$. Thus, in addition to the biogenic silica production and dissolution rates, this variable was also estimated by the model (*Eqs. 1.1.* to *1.4.*). Under these conditions, one degree of freedom is lost but the system remains identifiable with 3 unknowns and 4 equations.

KEOPS-2 took place during the onset of the blooms, the biogenic silica production rates were quite high and far above the detection limit, except for 3 depths of the HNLC reference station (R-2) and for the deepest value at each station (0.01 % PAR attenuation depth, 8 samples). However, since biogenic silica dissolution rates were expected to be low in early spring, it is essential to determine the limit of detection for the ^{30}Si isotopic dilution.

In most cases, final æDSi were significantly different from initial æDSi (paired T-test, p-value < 0.001). The detection limit for isotopic dilution was then estimated as being the lowest difference between initial and final 30Si isotopic abundances (ΔæDSi) measurable by the instrument. Every æDSi solutions have been analyzed in duplicates with a pooled standard deviation of 0.32 % (n = 35). In addition, we analyzed the same in-house standard several times during every analytical session. This solution was a 10 % spiked seawater from Southern Ocean analyzed since several years with a æDSi at 11.83 ± 0.43 % (n = 40). The relative standard deviation (RSD) on æDSi of this standard solution is 0.43 % (n = 40) and represents the long-term reproducibility of HR-SF-ICP-MS measurements. Therefore, each KEOPS-2 incubation with a ΔæDSi between t_0 and t_{48} higher than this RSD was considered to be significantly different from zero, and hence above the detection limit. This was the case for almost all the KEOPS-2 dataset (see e.g. *Fig. 1.3.*), except for 7 values showing a change in ^{30}Si abundance below the detection limit. This included 4 samples from the HNLC reference station R-2 where biological activity was extremely low.

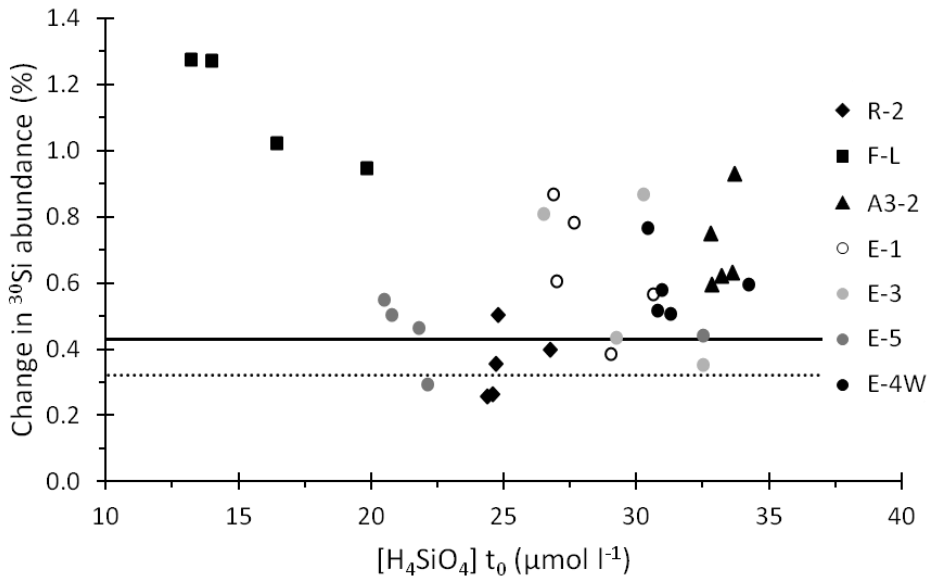

Figure 1.3. Comparison of changes in ^{30}Si-abundance of seawater for each incubation (symbols) with detection limit of the ^{30}Si-isotopic dilution method (plain line) estimated from the reproductibility of an internal standard (0.43%, n = 40). The dotted line represents the detection limit obtained from the average reproductibility of all dissolution duplicates (0.32%, n = 35).

Due to time and sampled water volume constraints, the sampling strategy adopted for KEOPS-2 gave the priority to highest vertical resolution instead of replicate incubations. Since only the analytical reproducibility was taken into account in the model, the standard deviations on Si uptake and dissolution rates were likely to be underestimated. Therefore we will use a theoretical relative precision for the whole incubation experiments of 10 %, as estimated for Si uptake rates by Fripiat et al. (2009).

I.3.2. Physical, chemical and biological parameters

The vertical structure of upper layer waters in the area was characteristic of the Antarctic Surface Water in the vicinity of the Polar Front (Park et al., 1998, 2008). The Winter Water (WW), identified by the minimum of temperature centered around 200 m, was capped by a homogeneous mixed layer (ML) induced by seasonal stratification. The boundary between the surface ML and the WW is usually marked by a strong seasonal pycnocline. However, at some stations, the stratification of the surface layer was relatively complex and showed two successive discontinuities evidenced by two different density gradients as indicated in *figure 1.4*.

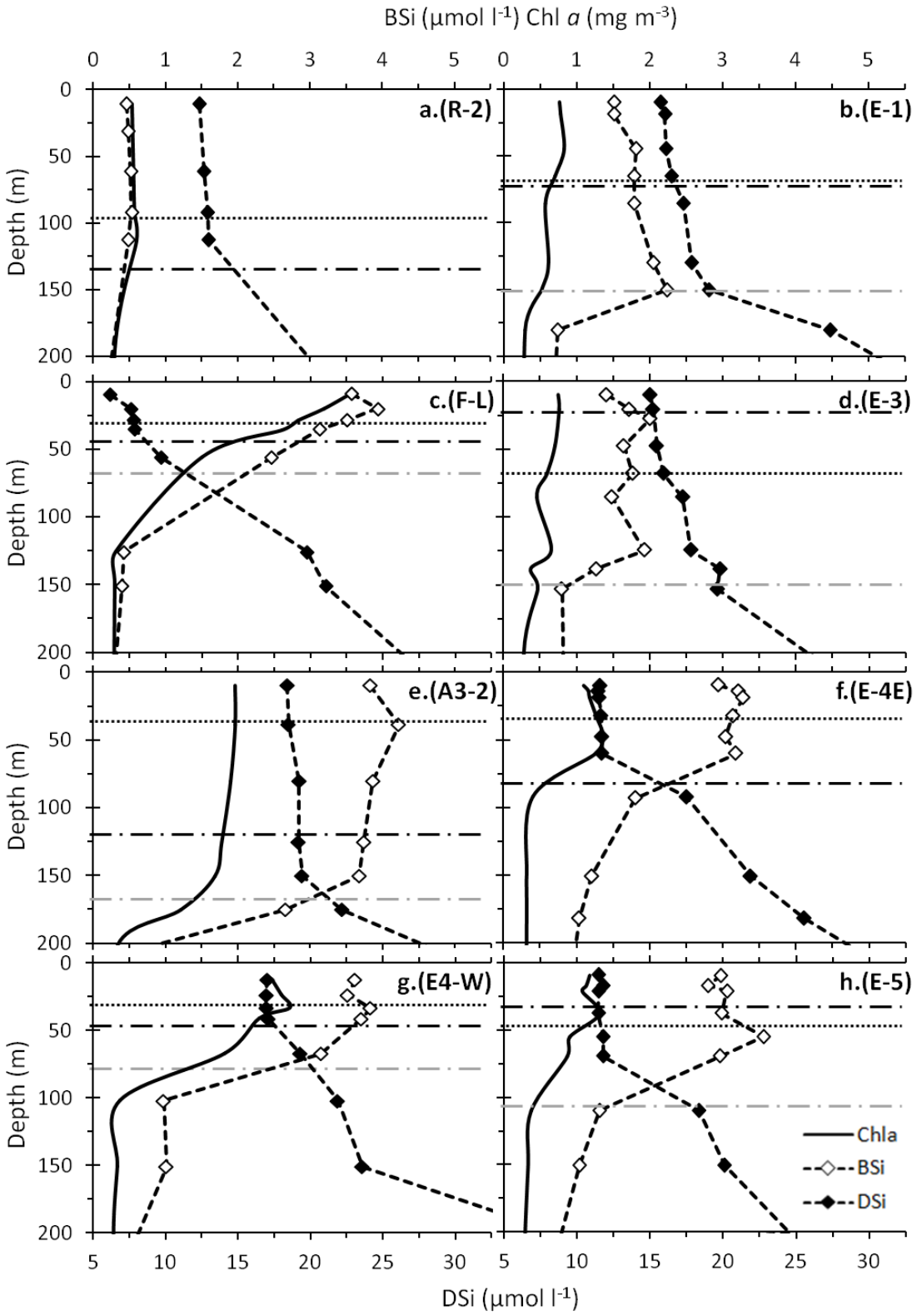

Figure 1.4. Vertical distribution of chlorophyll *a* (continuous-black line; estimated from CTD fluorescence), biogenic silica concentration ([BSi], light dots) and H_4SiO_4 concentration ([DSi], dark dots). Dotted lines show the bottom of the euphotic layer (1% of Photosynthetically Active Radiation, Ze) for each station. Dark dashed lines represent the Mixed Layer Depth (MLD; estimated by Park et al., in prep.) and grey dashed lines correspond to a 2nd density gradient identify from the density CTD-profile.

During KEOPS-2, the surface ML depth, defined by the density difference of 0.02 from the surface (Park et al, in prep.), showed a large variability between stations (*Fig. 1.4.*). A strong and shallow stratification was measured north of the polar front, while wind events induced weak stratification and deep ML in the stations above the plateau and in the HNLC area. Stations in the recirculation zone (E-1 to E-5) supported a complex stratification due to their highly spatial and temporal dynamic and were characterized by 2 distinct density discontinuities.

All the stations located south of the Polar Front had quite homogeneous Chl-*a*, BSi and DSi stocks from the surface to the deepest density discontinuity (below the so-called ML; *Fig. 1.4.*). North of the Polar Front, these stocks were higher at the surface and decreased with depth (*Fig. 1.4c.*). Stations A3-2 and E-4W present similar BSi and DSi surface concentrations (*Fig. 1.4e., 1.4g.*). At these 2 stations, DSi concentrations increase gradually while Chl-*a* and BSi decrease drastically below the deepest density discontinuity. Station R-2 contrasted from the latter stations by its low BSi, low Chl-*a* content and relatively high DSi concentrations, confirming its HNLC character (*Fig. 1.4a.*). During the lagrangian survey (stations E-1, E-3, E-4E and E-5), we observed a DSi depletion from ≈15 to ≈10 µmol l^{-1} in surface waters, an increase of Chl-*a* concentrations from < 1 to > 1 mg m^{-3} and a doubling of the BSi content from ≈1.5 to > 3 µmol l^{-1} (*Fig. 1.4b., 1.4d., 1.4f., 1.4h.*). Such temporal variations were mainly driven by diatom production as described below.

I.3.3. Biogenic silica production and dissolution rates

Silica production rates were quite homogeneously distributed in the euphotic layer with an exception for the station F-L located north of the Polar Front where it decreases progressively with depth (*Fig. 1.5a.*). Surface ρSi varied from 0.036 ± 0.003 µmol l^{-1} d^{-1} (R-2 in the HNLC area) to 1.28 ± 0.12 µmol l^{-1} d^{-1} (A3-2, above the Plateau). All over the study area, Si uptake rates reached very low values at the base of the euphotic layer. Note that the same decreasing trend was also observed in primary production experiments performed in parallel (see e.g. Cavagna et al., in prep.).

BSi dissolution rates were considerably lower than Si uptake rates except in the HNLC area (R-2) and at station E-3 where ρSi was in the lower range of the KEOPS-2 dataset. Vertical profiles of ρDiss (*Fig. 1.5b.*) were quite homogeneous from the surface to the base of the euphotic layer and did not increase at depth. This indicates that, the physical and biogeochemical processes affecting BSi

dissolution did not vary significantly over the water column. This is also consistent with the low accumulation of biogenic silica observed at depth in spring (Lasbleiz et al., 2014) which contrasts with the occurrence of deep BSi maxima at the end of summer (Mosseri et al., 2008). Moreover, silica dissolution rates were not significantly different between bloom stations, and were comparable to those measured by Brzezinski et al. (2001) for the same season in the Pacific sector and by Beucher et al. (2004) and Fripiat et al. (2011b) for the end of summer in the Australian sector.

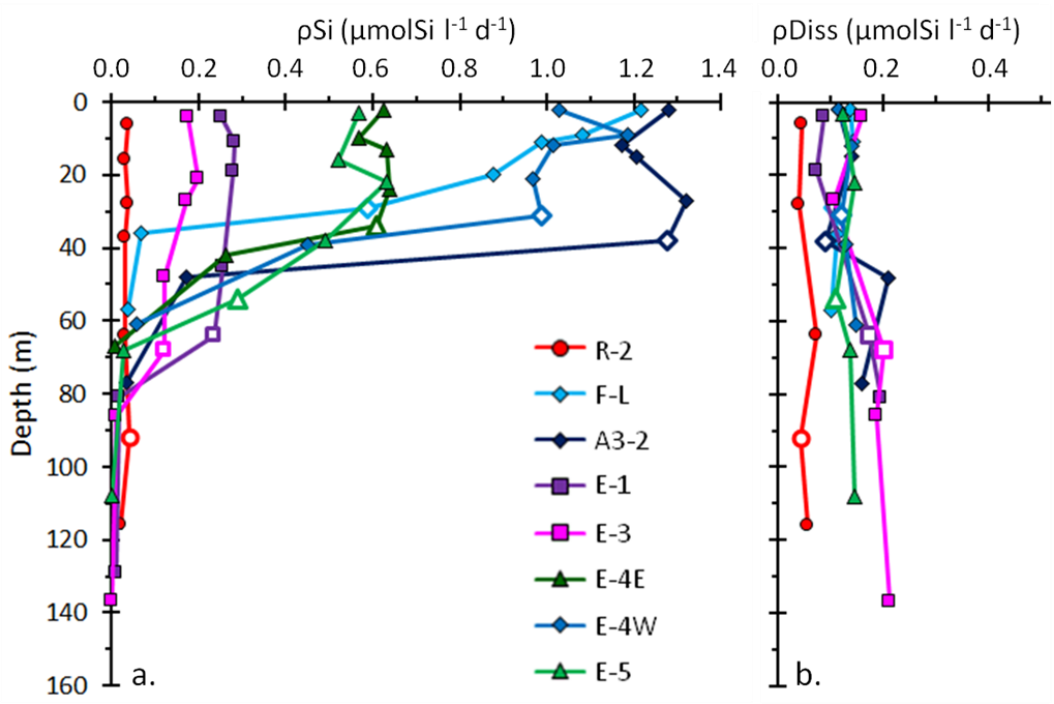

Figure 1.5. Vertical distribution of Si-uptake (ρSi, panel a.) and biogenic silica dissolution (ρDiss, panel b.) in KEOPS-2 stations. Open symbols represent the depth at the bottom of the euphotic layer (1% of Photosynthetically Active Radiation) for each station.

As silica production was close to zero below the euphotic layer, all the vertically integrated values presented in table 2 were calculated from 100 % to 1 % of the surface PAR. The integrated Si uptake rates (∫ρSi) varied from 3.09 ± 0.01 mmol m^{-2} d^{-1} (R-2, in the HNLC area) to 47.9 ± 0.4 mmol m^{-2} d^{-1} (A3-2, above the Plateau), and were among the highest reported so far in the Southern Ocean (see review in Fripiat, 2010). Integrated BSi dissolution rates (∫ρDiss) were generally much lower than integrated production rates with values ranging from 3.79 ± 0.03 mmol m^{-2} d^{-1} north of the Polar Front (F-L) to 9.99 ± 0.03 mmol m^{-2} d^{-1} at E-3. Because ρDiss did not vary over depth, or between stations,

integrated dissolution estimates were correlated with the depth of the euphotic layer (Ze), with higher values in stations with deeper Ze, e.g. E-1 and E-3 (R^2 = 0.83, *not shown*).

Net production rate of BSi in the euphotic layer (∫ρNet) represents the difference between gross silica production and dissolution rates (*Fig. 1.6.*) and could be associated to an uptake of "new-H_4SiO_4" i.e. uptake that does not come from remineralisation processes within the ML. As for the net primary production, the net silica production could be defined as the part of the BSi that accumulates in the surface layer during the productive period, which would then be potentially available later for export to the mesopelagic layer (Brzezinski et al., 2001; Quéguiner, 2013). During the pseudo-lagrangian survey, net silica production was quite low during the first 2 visits (E-1 and E-3 with respectively 9.6 ± 0.1 and 0.5 ± 0.1 mmol m^{-2} d^{-1}) and reached the maximal value at the last visit (E-5, 20.5 ± 0.2 mmol m^{-2} d^{-1}). The highest net production rate was observed above the Kerguelen Plateau (A3-2, 43.4 ± 0.4 mmol m^{-2} d^{-1}). In the HNLC area (Station R-2), silica dissolution was higher than silica production, leading to a negative ∫ρNet (-1.78 ± 0.02 mmol m^{-2} d^{-1}).

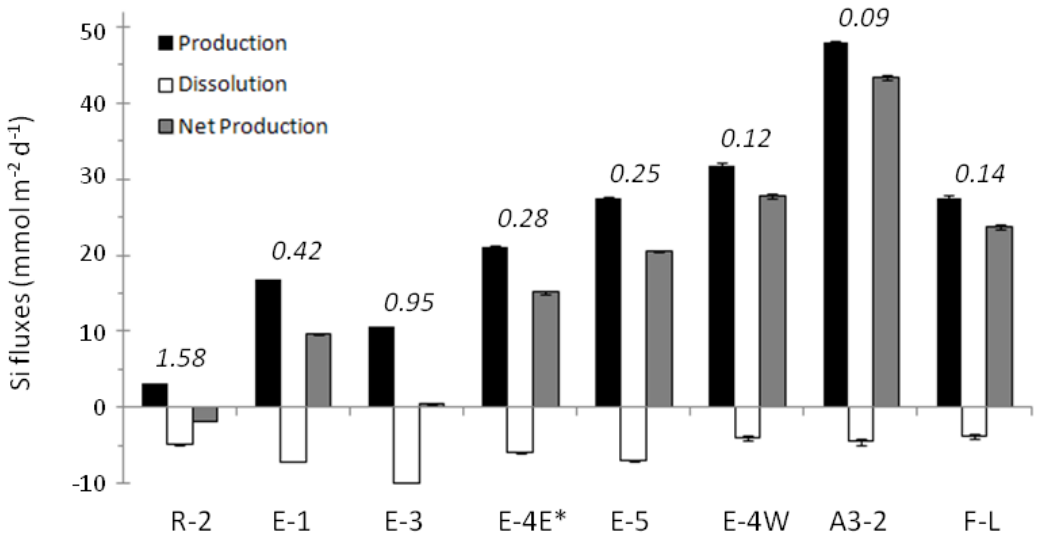

* Since no dissolution rates were measured at E4E, dissolution and net production do not correspond to calculations from direct measurements but only to estimations. Dissolution was calculated as the average of all KEOPS-2 integrated dissolution rates.

Figure 1.6. Si-uptake (black), biogenic silica dissolution (white) and net silica production (grey) integrated over the euphotic layer (1% of Photosynthetically Active Radiation). Italic values correspond to the integrated dissolution to production ratio (∫D:∫P).

I.3.4. Specific rates of production and dissolution

The specific Si uptake rate (VSi, d^{-1}) and dissolution rate (VDiss, d^{-1}) give the fraction of the BSi pool produced or dissolved in one day as follows:

$$\mathrm{VSi} = \frac{\rho\mathrm{Si}}{[\mathrm{BSi}]} \qquad (1.5.)$$

$$\text{and } \mathrm{VDiss} = \frac{\rho\mathrm{Diss}}{[\mathrm{BSi}]} \qquad (1.6.)$$

VSi is mainly impacted by nutrient and/or light limitation (Frank et al., 2000; Claquin et al., 2002) and by the diatom community composition (Leynaert et al., 2004). During KEOPS-2, VSi values (*profiles not shown*) presented the same decreasing trends with depth as Si uptake, which is consistent with an impact of light limitation on silica production. Globally, relatively high "integrated specific Si-uptake rates" (∫VSi, calculated by the averaged integrated ρ divided by the integrated BSi) prevailed for KEOPS-2 (≈0.1 to ≈0.3 d^{-1}; *Table 1.2.*). Such values are not different from those of nutrient-replete diatoms growing in the open ocean zone of the Southern Ocean (Brzezinski et al., 2001). By contrast, the HNLC area showed a ∫VSi value below 0.1 d^{-1}, suggesting non-optimal conditions for the growth of diatoms and/or artifact of siliceous detritus, which is important in other HNLC regions (e.g. Krause et al., 2010; Fripiat et al., 2011b). ∫VDiss varied around one order of magnitude during KEOPS-2 with low specific rates in productive stations (e.g. 0.03 d^{-1} above the Plateau), and higher values in the HNLC area (up to 0.15 d^{-1}). Interestingly, E-3 showed unexpected high ∫VDiss (0.12 d^{-1}; *Table 1.2.*).

Table 1.2. Biogenic silica concentration (∫[BSi]), Si-uptake (∫ρSi), biogenic silica dissolution (∫ρDiss), silica net production (∫ρNet) integrated over the euphotic layer (1% of surface Photosynthetically Active Radiation), and integrated specific rates of Si-uptake and silica dissolution (calculated as ∫VSi = ∫ρSi/[BSi] and ∫Diss = ∫ρDiss/[BSi] respectively).

Station	Zone	∫[BSi] mmol m^{-2}	∫ρSi mmol m^{-2} d^{-1}	∫ρDiss mmol m^{-2} d^{-1}	∫ρNet mmol m^{-2} d^{-1}	Specific rates ∫VSi (d^{-1})	∫VDiss (d^{-1})
R-2	*HNLC*	33.28 ± *0.1*	3.09 ± *0.01*	4.88 ± *0.01*	-1.78 ± *0.02*	0.09	0.15
E-1	*Meander*	96.1 ± *0.2*	16.8 ± *0.1*	7.11 ± *0.02*	9.6 ± *0.1*	0.17	0.07
E-3	*Meander*	83.6 ± *0.2*	10.5 ± *0.1*	9.99 ± *0.03*	0.5 ± *0.1*	0.13	0.12
F-L	*Polar front*	97.8 ± *0.5*	27.5 ± *0.3*	3.79 ± *0.03*	23.8 ± *0.3*	0.28	0.04
E-4W	*Plume*	142.0 ± *0.7*	31.8 ± *0.3*	3.97 ± *0.03*	27.9 ± *0.3*	0.22	0.03
E-4E	*Meander*	104.3 ± *0.5*	21.0 ± *0.2*	5.89 ± *0.03**	15.1 ± *0.2**	0.20	0.06*
A3-2	*Plateau*	173.6 ± *0.7*	47.9 ± *0.4*	4.50 ± *0.03*	43.4 ± *0.4*	0.28	0.03
E-5	*Meander*	159.5 ± *0.4*	27.5 ± *0.2*	6.97 ± *0.03*	20.5 ± *0.2*	0.17	0.04

* Since no dissolution rates were measured at E4E, these values do not correspond to calculations from direct measurements but only to estimations. Dissolution was calculated as the average of all KEOPS-2 integrated dissolution rates.

I.4 Discussion

I.4.1. Seasonality of the balance between silica production and dissolution

The D:P ratios integrated between the surface and the 1 % PAR attenuation depth (∫D:∫P; also summarized in *table 1.3.*) are presented in *figure 1.6.*

Table 1.3. Dissolution to production ratio (∫D:∫P), fraction of the silica production supported by new silicic acid (1-∫D:∫P), silicon to carbon (C) and nitrogen (N) uptake ratios (C and N assimilation were measured by Cavagna et al., in prep.). ρN represents both nitrate and ammonium uptake. All these values are integrated over the euphotic layer (1% of surface Photosynthetically Active Radiation).

Station	Zone	∫D:∫P	1-∫D:∫P	gross-∫ρSi:∫ρC	gross-∫ρSi:∫ρN
R-2	*HNLC*	1.58	-0.58	0.28	0.44
E-1	*Meander*	0.42	0.58	0.38	1.27
E-3	*Meander*	0.95	0.05	0.18	0.74
F-L	*Polar front*	0.14	0.86	0.10	0.32
E-4W	*Plume*	0.12	0.88	0.15	0.93
E-4E	*Meander*	0.28	0.72	0.27	1.26
A3-2	*Plateau*	0.09	0.91	0.30	1.51
E-5	*Meander*	0.25	0.75	0.35	1.41

* Since no dissolution rates were measured at E4E, these values do not correspond to calculations from direct measurements but only to estimations. Dissolution was calculated as the average of all KEOPS-2 integrated dissolution rates.

At the HNLC reference station R-2, the ∫D:∫P value >1 indicates that the integrated dissolution rate exceeds the measured integrated production rate (note that both fluxes were very low at R-2). This situation leads to a net loss of biogenic silica by dissolution in the euphotic zone and suggests that a short development of diatoms could have occurred before our sampling. This observation is in accordance with the high barium excess measured between 200 and 400 m at R-2 (Jacquet et al, 2014), indicating a high carbon mineralization activity in the mesopelagic zone which could be likely associated to a surface production event prior sampling. High ∫D:∫P values have already been measured occasionally in the Southern Ocean during the summer bloom (review in Tréguer and De La Rocha, 2013).

In the Kerguelen bloom area, ∫D:∫P ratios ranged from 0.09 (station A3-2) to 0.95 (station E-3) and depended on the stage of the blooms. The ∫D:∫P ratios were relatively high at stations visited in the beginning of the cruise, indicating that a significant fraction of silica was recycled in the surface waters in early spring, and then decreased as the bloom took place. The highest ∫D:∫P ratio occurred at station E-3. This station was characterized by a low BSi stock (83.6 mmol Si m^{-2}), a low integrated BSi production rate (10.5 mmol Si m^{-2} d^{-1} integrated over the euphotic layer; *Table 1.2.*), a dissolution rate close to the mean for all stations, and high specific dissolution rate. This may evidence a higher relative proportion of detrital silica free of organic matter at this station which could be due to stronger bacterial and/or grazing activities inducing a top-down control on diatom growth. Without considering E-3, ∫D:∫P ratios decreased progressively from E-1 to E-5 and showed low values at the most productive stations E-4W, A3-2 and F-L. Here, ∫D:∫P ratios were similar to those measured in nutrient-replete conditions such as productive upwelling regions (Brzezinski et al., 2003).

High ∫D:∫P ratios in winter and in early spring indicate that silica dissolution is sufficient to sustain a large fraction of the low Si uptake rates observed during non-bloom conditions and during the bloom onset, i.e. when primary production is still low. Indeed there is a temporal decoupling between silica production and dissolution since the dissolution kinetic is slow. It is only after diatom death and removal of their protecting organic coating by micro-organisms that the silica frustules can dissolve (Kamatani, 1982; Bidle and Azam, 1999; Bidle et al., 2003). By contrast, the progressive decrease of the ∫D:∫P values implies that the majority of gross silica production is sustained by the silicic acid pool supplied from below (winter water) as the bloom develops. This pool can be regarded as the “new” Si reservoir, similar to nitrate for N. Thus, we observe a seasonal shift from Si uptake behaving mainly as a regenerated production before the bloom onset, when silica production is still very low, and then behaving more like a new production during bloom, when we observe higher Si uptake rates.

An opposite shift at the end of the productive period was suggested by Brzezinski et al. (2001) in the upwelling system of the Monterey Bay with ∫D:∫P ratios increasing following the bloom development. In this case, higher ∫D:∫P values were associated to an increase of the relative proportion of detrital BSi in the water column. Similarly, the occurrence of an accumulation of dissolving BSi in subsurface following productive periods inducing a net loss of BSi in late summer (∫D:∫P = 1.7) was already identified in the Australian sector of the Southern Ocean (Fripiat et al., 2011b). Since KEOPS-2 took place at the start of the bloom and since there was no silica dissolution rate measured from

KEOPS-1, such increase of ∫D:∫P ratio in the Kerguelen area at the end of the blooming season has not been observed but will be discussed in *section I.4.3*.

Because silica dissolution profiles were not significantly different from each other between all the KEOPS-2 bloom stations (*Fig. 1.5b.*), it can be ruled out as a process explaining the variability in ∫D:∫P ratios. The observed decreasing trend of ∫D:∫P ratios was actually mainly driven by the increase of BSi production rates (from 3.09 ± 0.01 to 47.9 ± 0.4 mmol Si m^{-2} d^{-1}) and by the accumulation of living diatoms with high specific Si uptake rates in the euphotic layer (*Table 1.2.*).

The fraction of silica production supported by new silicic acid is estimated by 1-∫D:∫P. During KEOPS-2 it ranged from -0.58 in the HNLC station, where we observed a net loss of biogenic silica, to a maximum of 0.91 above the plateau, where maximum production rates were recorded (A3-2, *Table 1.3.*). When plotting 1-∫D:∫P vs. gross silica production rate, Brzezinski et al. (2003) found that 8 regional estimates of this parameter representing a large range of ocean environments, fall along an hyperbolic curve and thus it might be possible to predict the strength of the silicon pump in a system based on its mean silica production. To obtain a zero-intercept of the curve satisfying the assumption that when the fraction of silica production supported by new silicic acid approaches 0, the production must also be 0, we have plotted the 1-∫D:∫P as a function of the net silica production (instead of the gross production in Brzezinski et al., 2003). Since these two variables are not fully independent, the equation of the model matching all the data follows a rectangular hyperbola (*Fig. 1.7.*). This fitting has been obtained on KEOPS-2, Brzezinski et al. (2003) and Fripiat et al. (2011b) data.

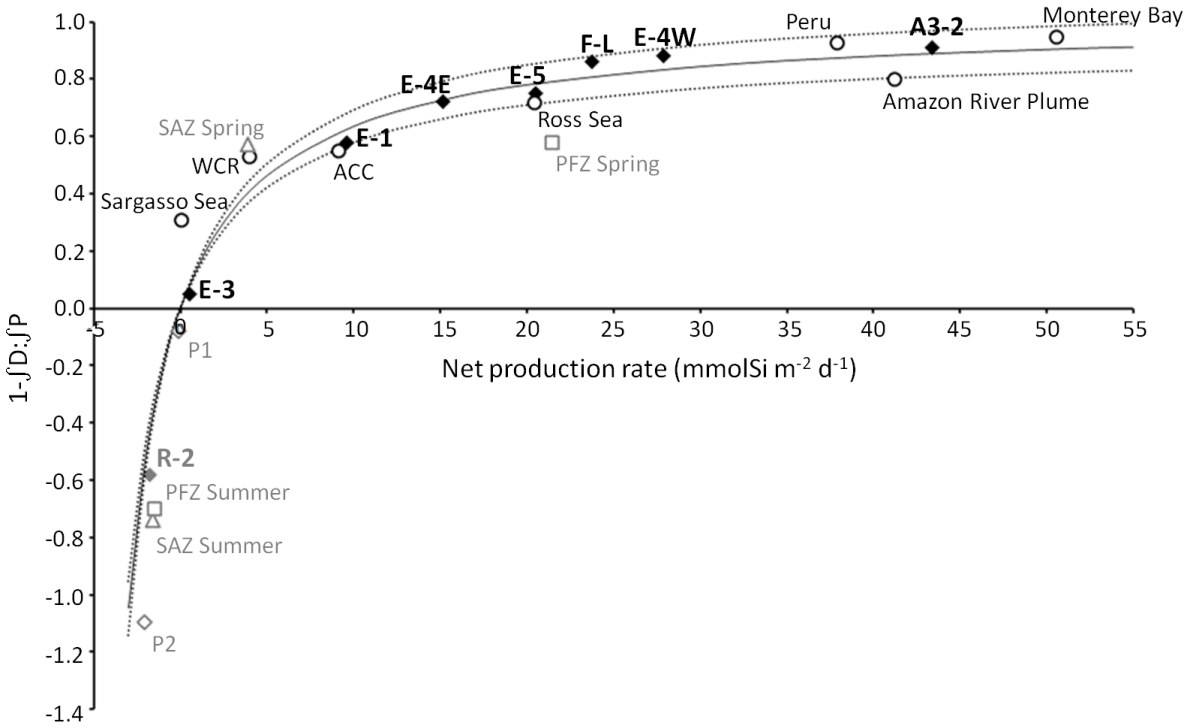

Figure 1.7. Fraction of biogenic silica production supported by new silicic acid (1-∫D:∫P) as a function of the integrated net silica production rate ($\int\rho_{net}$) during KEOPS-2 (filled black diamonds) compared with different regions of the global ocean (Open circles; Brzezinski et al., 2003 and references therein; and open diamonds; Fripiat et al., 2011b). Triangles and squares show the mean values for different growth seasons for SAZ and PFZ, respectively (Fripiat et al., 2011b). The plain line is a rectangular hyperbola to fit all data points (grey symbols were excluded from the model since they represent either negative 1-∫D:∫P value which are not allowed by the model, or average while all other symbols refer to single stations). The equation of the curve is $1\text{-}\int D:\int P = 1.01 \times \int\rho_{net}/(5.89 + \int\rho_{net})$. Dotted lines correspond to ± 1sd of the $1\text{-}\int D:\int P_{max}$.

Using *figure 1.7.*, we can identify several parameters characterizing the distribution of both KEOPS-2 stations and other oceanic regions. The 1-∫D:∫Pmax is centered around 1 as it is not possible to have more than 100 % of silica production supported by new-H_4SiO_4. The KρNet (5.89 ± 2.24 mmol m^{-2} d^{-1}) represents the value of net silica production at which the system shifts from a regenerated to a new biogenic silica production (i.e., 1-∫D:∫P = 0.5). In KEOPS-2 stations showing a net silica production below KρNet, the development of diatoms is mainly controlled by recycled sources of silicon, while above this value, the supply of new H_4SiO_4 is the main source of nutrients for biogenic silica production. It is important to keep in mind that this model is mainly governed by the dependency of its two variables and thus, we cannot use it to make predictions about the silicon cycle functioning of stations where only one of the two parameters was estimated (e.g. net silica production estimated from the change in BSi concentrations). It however allows us to sort KEOPS-2 stations into specific groups and to compare them with other oceanic regions. For example, *figure 1.7.* is remarkably helpful to

differentiate stations with low net production rates (x-axis) that have very variable fraction of new Si production (y-axis).

KEOPS-2 stations follow the same trend as that of Brzezinski et al. (2003) and encompass almost the full range of variability observed in very contrasting oceanic regions (e.g. HNLC, oligotrophic, coastal upwelling, river plume). They can be sorted in 3 functional groups:

- The "low activity stations" group includes the HNLC reference station R-2 and station E-3 that showed a net loss of BSi with negative values of ∫ρSiNet or close to 0 (*Fig. 1.6.*; *Table 1.2.*). In *Fig. 1.7.*, the HNLC station falls in the negative part of the hyperbolic curve, close to stations mainly characterized by detrital BSi dominance and where a release of silicon from dissolving BSi takes place following a productive period (e.g. the late summer SAZ-Sense station P2 located in the Polar Front Zone; Fripiat et al., 2011b). Despite its low iron concentration, the high ∫D:∫P ratio observed at R-2 suggests that a short development of diatoms could have occurred before our sampling in agreement with Jacquet et al. (2014) and Dehairs et al. (in prep.). This kind of low diatom production in the HNLC area surrounding the Kerguelen Plateau has already been suggested at the end of summer by Mosseri et al (2008). Since net silica dissolution is not sustainable, the values measured at R-2 should necessarily represent conditions that prevail on a short period of time. Production and dissolution rates are indeed snapshot measurements over 24 h or 48 h. Although H_4SiO_4 concentrations were not limiting in surface waters, E-3 was characterized by very low silica production that could be exclusively sustained by recycled silicic acid (1-∫D:∫P = 0.05) and seemed to have approached steady state conditions as siliceous biomass cannot increase in a system supported solely by regenerated silicic acid (Brzezinski and Nelson, 1989). This situation could be the result of a previous attempt to bloom that would have aborted due to the destabilization of the ML.

- The "starting-bloom" group is represented by station E-1 that has been visited in the beginning of the KEOPS-2 cruise (early November). Although carbon incubation experiments reveal that the bloom began to grow at this station (Cavagna et al., in prep.), low Si uptake (*Fig. 1.5a.*) and low net-silica production (*Fig. 1.6.*) were still observed. A moderate 1-∫D:∫P ratio (0.58) indicates that BSi production at E-1 is controlled both by new and regenerated sources of H_4SiO_4.

- The “spring-bloom” group includes stations holding a strong capacity for BSi accumulation, i.e. with low dissolution rates and high net silica production rates. *Figure 1.5a.* allows us to distinguish between stations from the lagrangian study E-4E and E-5, with only moderate surface ρSi values (respectively 0.62 ± 0.06 µmol l^{-1} d^{-1} and 0.57 ± 0.06 µmol l^{-1} d^{-1}) and ∫D:∫P ratio close to 0.3 (*Table 1.3.*); and stations A3-2, F-L and E-4W showing particularly high surface production rates (> 1 µmol l^{-1} d^{-1}) and ∫D:∫P ratio close to 0.1 (*Table 1.3.*). Blooms with such a low ∫D:∫P ratio have the potential to accumulate a large fraction of BSi production and/or export a large amount of BSi into the deep ocean (Quéguiner, 2013; Tréguer and De La Rocha, 2013). Despite their location on both sides of the Polar Front and in different part of the Kerguelen bloom, stations E-4W and F-L fall close to each other along the hyperbolic curve (*Fig. 1.7.*). Consequently, they should operate in a comparable way in term of silica production dynamic which is quite similar to the average value of PFZ spring bloom conditions measured by Brzezinski et al. (2001). So, even though complex physical settings (Park et al., in prep.) are very different between E-4W (which is not part of PF with high surface DSi concentration of 17 µmol l^{-1}) and F-L (with lower surface DSi concentration of 6 µmol l^{-1}) diatom production regime behave as typical PFZ stations. This was also observed with carbon export and mesopelagic remineralization by Jacquet et al. (2014). Compared to F-L and E-4W, A3-2 is highly active in term of silica production and can be compared to the Amazon river plume and coastal upwelling systems such as Monterey Bay or Peru. This highlights once again the exceptional character of diatoms-dominated ecosystems sustained by natural iron fertilization in the Southern Ocean.

I.4.2. Decoupling between Si, C and N cycles in the Kerguelen area

In the Kerguelen area, the high NO_3^- concentrations in surface waters compared to H_4SiO_4 depletion observed annually at the end of the bloom period suggest a strong decoupling between the seasonal consumption of these two nutrients (Mosseri et al., 2008). This situation could be partly induced by differential recycling processes between Si and N strengthening the silicon pump. Si is thus primarily exported to deeper water through sinking of biogenic silica while PON is mostly recycled in the ML and used as nitrogen source for the development of new phytoplankton organisms including diatoms. Since organic matter is more quickly and efficiently remineralized compared to silica, this decoupling also occurs between Si and C.

The strength of the silicon pump could be investigated by comparing the Si:C and Si:N uptake-ratios. In this study, we use only the gross uptake ratios (∫ρSi:∫ρN and ∫ρSi:∫ρC), calculated respectively as:

$$\int \rho Si : \int \rho N = \frac{\rho Si}{\rho(NO_3^- + NH_4^+)} \qquad (1.7.)$$

$$\text{and } \int \rho Si : \int \rho C = \frac{\rho Si}{\text{gross } \rho C} \qquad (1.8.)$$

which reflect only the stoichiometry of phytoplankton nutrient uptake. We will not consider net uptake ratios that could be calculated but would be biased by the significant rates of nitrification estimated at all KEOPS-2 stations (see Cavagna et al., in prep. and Dehairs et al., in prep.). Note that both ∫ρSi:∫ρC and ∫ρSi:∫ρN uptake ratios are underestimates of actual diatom uptake ratios because of the simultaneous C and N uptake by non-siliceous organisms. Diatoms growing in nutrient replete conditions present Si:C and Si:N elemental ratios around 0.13 (from 0.09 to 0.15) and 1 (from 0.8 to 1.2) respectively, with the variability of these ratios depending on diatom species, size classes and growth rates (Brzezinski, 1985; Martin-Jézéquel et al., 2000).

Si:C and Si:N uptake ratios are strongly impacted by co-limitations which alter growth rates and in most cases increase silicification processes, and thus lead to higher uptake ratios (Claquin et al., 2002; Leynaert et al., 2004; Bucciarelli et al., 2010). During the KEOPS-2 study, ∫ρSi:∫ρC and ∫ρSi:∫ρN uptake ratios vary from 0.10 to 0.38 and from 0.32 to 1.51 respectively (*Table 1.3.*).

In our study, these variations could not be explained by limitation from macronutrient (such as silicic acid) as already proposed by Nelson and Tréguer, (1992) and Quéguiner, (2001). Indeed, KEOPS-2 took place at the beginning of the growth period (October-November) and a bloom onset was observed above the Plateau (Blain et al., in prep.). It is thus not surprising that macronutrient concentrations in the surface layer were not limiting for diatom growth (cf. Cavagna et al., in prep. for N uptake). For silicic acid, kinetic experiments conducted during the cruise at all sites demonstrated the lack of response of phytoplankton to H_4SiO_4 enrichment (*data not shown*). Indeed, at all stations, mixed layer silicic acid concentrations were high (from 6.2 to 18.5 µmol.l^{-1}; *Fig. 1.4.*) preventing limitation of biogenic silica production by H_4SiO_4 availability as VSi at ambient DSi were always similar to Vmax, the maximum uptake rate achievable when Si is not limiting (*data not shown*).

Results from a previous cruise in the same area (austral spring 1995) already highlighted the crucial role played by the light-mixing regime on the control of diatom growth in the nutrient replete waters (Blain et al., 2001). Light-limitation also takes part in the decoupling between Si, N and C cycles by decreasing the growth rate and consequently increasing Si:N and Si:C uptake-ratios (Claquin et al., 2002). At all stations the ρSi:ρC uptake ratios increase slightly with depth and reach a maximum at the bottom of the euphotic layer (*data not shown*), in agreement with the fact that C assimilation is light-dependent through photosynthesis while silicification processes mainly involves energy coming from respiration (Martin-Jézéquel et al., 2000; Claquin et al., 2002). However, because Si uptakes reach very low values at the base of the euphotic layer (*Fig. 1.5a.*), our data suggest that BSi production rates were not fully independent of light levels and that there was a close coupling between C and Si assimilation processes (see Cavagna et al., in prep. for carbon uptake). This coupling of ρSi with light was also observed in other regions as the Equatorial Pacific and the North Pacific Subtropical gyre by Krause et al. (2011). Note however that this is not in contradiction with Claquin et al. (2002) given the different time scales of the two studies.

Limitation by trace metals (especially iron) also alters the stoichiometry of phytoplankton nutrient uptake and its elemental composition and, eventually, contributes to the decoupling between Si, N and C cycles. From bottle enrichment experiments, it has been argued that diatoms have higher Si:N uptake ratios under Fe stress (Takeda 1998; Hutchins and Bruland 1998; Franck et al., 2000). Interestingly, relatively high ∫ρSi:∫ρN ratios were measured for the Kerguelen spring bloom (*Table 1.3.*), with the highest value above the Plateau (1.5, station A3-2) although this area was naturally Fe-enriched (Sarthou et al., in prep.; Queroue et al., in prep.). In the KEOPS-2 productive stations, diatoms can take up more H_4SiO_4 compared to nitrogen and carbon. Indeed, these organisms are known to store silicic acid in their vacuoles or linked to other intracellular components (Martin-Jézéquel et al., 2000, Hildebrand, 2008), or could be more silicified. By contrast, 3 stations showed low ∫ρSi:∫ρN uptake ratios (0.44, 0.74 and 0.32 for R-2, E-3 and F-L respectively). Lower Si:N and Si:C integrated uptake ratios in these areas might be partly due to changes in phytoplankton composition. By measuring phytoplankton pigment composition in the HNLC station, Lasbleiz et al. (2014) estimated a lower contribution of microphytoplankton due to a higher proportion of nanophytoplankton organisms such as nanoflagellates. Thus, since the phytoplankton community at R may contain a significant fraction of non-siliceous organisms, the C and N uptake ratios were not solely prescribed by diatoms and thus could explain the low ∫ρSi:∫ρN uptake ratios observed. However, the higher concentrations in fucoxanthin over the other pigments at all other stations clearly evidence the dominance of large diatoms in the Kerguelen blooms (Lasbleiz et al., 2014). The very low ∫ρSi:∫ρN uptake ratios estimated

at F-L could not result from a dominance of non-siliceous phytoplanktonic organisms but likely from different diatom communities showing contrasted degree of silicification and adapted to the specific hydrological and biogeochemical conditions occurring north of the Polar Front. Indeed, previous studies in the Southern Ocean have already shown that diatom community composition could explain more differences in silicification than physiological responses to environmental factors such as iron concentration (Baines et al., 2010; Assmy et al., 2013).

Thus, at a seasonal scale and above the plateau, the combination of this increased Si uptake and nitrogen regeneration processes including nitrification (see e.g. in Cavagna et al., in prep.; Dehairs et al., in prep.) in the beginning of the bloom, and preferential recycling of organic matter at the bloom offset helps to explain the depletion of most of the Si from surface layer observed between early spring (18.7 µmol l^{-1}, averaged in the upper 80 m at station A3-2, KEOPS-2) and the end of summer (1.9 µmol l^{-1}, averaged in the upper 80 m at station A3, KEOPS-1; Mosseri et al., 2008), while nitrate remains abundant (23 µmol l^{-1}, averaged in the upper 80 m at station A3, KEOPS-1; Mosseri et al., 2008). Fe-replete diatom assemblages, such as those found at A3-2 (Sarthou et al., in prep.), will deplete silicic acid from the water column before nitrate. Such silicon pump above Kerguelen Plateau would then not be driven solely by Fe-limitation contrary to incubation experiments from coastal upwelling systems (Hutchins and Bruland, 1998). Indeed, Fe enrichments in bottle experiments fertilise on short time scale (days) a diatom community that is not adapted to higher Fe levels. Here, by comparing ∫ρSi:∫ρN uptake ratios on different natural communities adapted to their specific ambient Fe levels, our results suggest that natural Fe fertilisation might favour diatoms with higher Si:N ratios. Above the Kerguelen Plateau, diatoms seem to maintain a relatively higher degree of silicification until the demise of the bloom, since Mosseri et al. (2008) observed the same range of ∫ρSi:∫ρN at A3 (1.6 ± 0.5, n=3).

If confirmed in other naturally fertilized regions, these observations may have great implications in our understanding of the past and future functioning of the Southern Ocean and its role in the regulation of climate. Indeed, the silicon pump occurring in the ACC results in an Antarctic Surface Water (AASW) relatively replete in NO_3^- but strongly depleted in H_4SiO_4 as observed by Blain et al. (2007) and Mosseri et al. (2008) in the Kerguelen region. This property is then exported toward lower latitudes by the Antarctic Intermediate Water (AAIW) and Subantarctic Mode Water (SAMW) (Sarmiento et al., 2004), currently favouring non siliceous organisms production in these regions. Thus, any change in Si:N uptake ratios south of the region of AAIW and SAMW formation might in turn modify diatom productivity at low latitude. Matsumoto et al. (2002) proposed that a Silicic Acid Leakage

Hypothesis (SALH) could explain the drop of atmospheric pCO_2 during glacial times and would be mainly driven by changes in Si:N ratios of diatoms induced by an increase in iron supply to the Southern Ocean. This hypothesis is based on in vitro and artificial Fe-enrichment experiments showing lower Si:N uptake ratios for diatoms in non Fe-stressed conditions (Takeda, 1998; Hutchins & Bruland, 1998), so that the increase of Fe-deposition in the Southern Ocean during glacial times would drive AASW towards NO3- depletion instead of the actual H_4SiO_4 depletion (Brzezinski et al., 2002).

Our results could indicate that glacial Fe fertilization may not have necessarily resulted in a decrease in Si:N uptake ratios in AASW contrary to what has been proposed as an explanation for the SALH (Brzezinski et al. 2002). Other processes leading to SALH could be invoked, such as shifts in AAIW and SAMW formation rates (Crosta et al., 2007), variations in phytoplankton assemblages (including relative contribution of non-siliceous organisms) or changes in NO_3^- remineralization efficiency. Since this interpretation is based on several incubations for several samplings (during spring and summer) in a single Fe-enriched station (A3, n = 4) and only one station in the HNLC region (R-2), further investigations concerning the seasonality of net silica production and Si:N uptake ratios in both naturally Fe-fertilized and HNLC areas of the Southern Ocean are clearly needed to validate this observation.

I.4.3. Seasonality and budget of the silicon cycle above the Kerguelen Plateau

In order to investigate the seasonal evolution of Si biogeochemical cycle in the Kerguelen iron-fertilized bloom (station A3), we combined in *figure 1.8.* the KEOPS-1 and KEOPS-2 silicon fluxes measured using different isotopic approaches (stable and radiogenic isotope tracer incubations: ^{30}Si and ^{32}Si respectively, and, natural silicon isotopic composition, $\delta^{30}Si$, of both diatoms and seawater). Assuming that the whole water mass above the Kerguelen Plateau may have been significantly ventilated with surface waters from the HNLC area at the annual scale, Fripiat et al. (2011a) used the HNLC winter water (WW) characteristics to represent the initial conditions of the winter H_4SiO_4 stock in the fertilized area surface layer (0-100 m). Because the biological activity (Si and C assimilation) took place only in the upper 80 m during KEOPS-2, Si fluxes, stocks and values estimated by Fripiat et al (2011a) discussed in this section were recalculated from the surface to 80 m (instead of 100 m in Fripiat et al. 2011a).

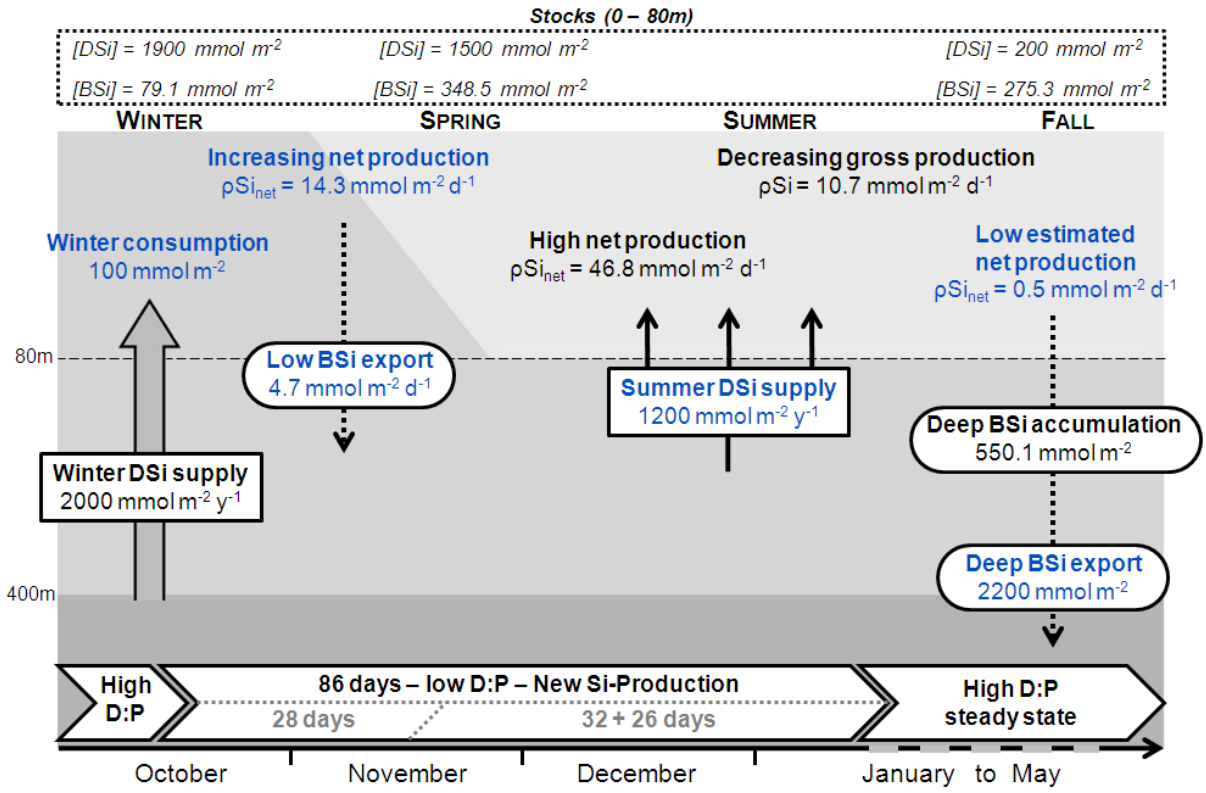

Figure 1.8. Schematic view of the seasonal silicon cycle in the mixed layer above the Kerguelen Plateau as estimated from natural and enriched Si isotopic measurements. Blue silicon fluxes correspond to estimated values while dark fluxes correspond to direct measurements. The 3 main water masses are represented by dark-grey for Upper Circumpolar Deep Water (UCDW), medium-grey for the Winter Water (WW) and light-grey for the Mixed Layer (ML). Variation of biogenic silica and H_4SiO_4 standing stocks integrated over 80m (respectively [BSi] and [DSi]) are shown in the upper panel. Vertical continuous arrows represent DSi supplies from deep water to the ML, and dotted arrows correspond to particulate silica fluxes. Integrated silica production rates are calculated from the surface to 80m. Horizontal white arrows represent the state of the bloom (indicated by the D:P ratio) through time. Winter consumption has been estimated from the difference of winter mixing supply (Fripiat et al., 2011a) and the standing stock measured at the first A3 visit (KEOPS-2). The difference in standing stocks between the two visits at A3 (28 days, KEOPS-2) yields to the net silica production of 14.3 $mmol.m^{-2}.d^{-1}$. The DSi standing stock at the second visit of A3 can sustain the net silica production measured for 32 days (this study) while the summer DSi supply estimated by Fripiat et al. (2011a) can sustain the same net production by an extra 26 days. The fall production measurements and standing stocks are from Mosseri et al. (2008, KEOPS-1). Since no silica dissolution is available from KEOPS-1, fall net production has been estimated from the difference between average gross silica production during KEOPS-1 (Mosseri et al., 2008) and average silica dissolution measured at all stations south of the Polar Front (KEOPS-2, this study). Deep BSi accumulation is calculated by integrating over the 100-200m depth layer data from Mosseri et al. 2008 (see text for further details).

The winter supply of DSi estimated from the seasonal H_4SiO_4 depletion during KEOPS-1 from the Upper Deep Circumpolar Water (UDCW) to the WW is around 2 mol m^{-2}, which is not significantly different from the 1.9 mol m^{-2} DSi stock we measured by mid-October during KEOPS-2 (A3-1). This

confirms that, as suggested by Fripiat et al (2011a), the HNLC winter water is representative of the Si source with initial Si pool conditions prevailing before the bloom onset in the fertilized area. At this time, silica production (which was not measured during this 1st visit) should be very low since only little BSi accumulation was observed in the ML (79.1 mmol m^{-2}), and only 2 - 1.9 = 0.1 mol m^{-2} of H_4SiO_4 was consumed in the surface water before our sampling compared to the estimated WW initial stock. The system was likely exclusively driven by regenerated silica production inducing a potentially high ∫D:∫P ratio (close to 1). Irradiance and mixed layer regime should be the more likely dominant factors controlling the bloom development for eukaryotes in winter and in early spring (Boyd et al., 2001; Blain et al., 2013). Models have previously reported that the interannual variability of mixed layer depth significantly affects both the date of the bloom onset and the maximum chlorophyll concentration in the region (Pondaven et al., 1998). Then, because H_4SiO_4 and Fe were not at limiting concentrations in the surface layer (Sarthou et al., in prep.), the light-mixing regime that occurred above the Plateau by mid-October, should have been still unfavourable to diatom growth.

As the surface irradiance becomes more favourable with time, biogenic silica production progressively increases and reaches the highest net production value (46.8 mmol m^{-2} d^{-1}) measured during our 2nd visit to A3 (mid-November). Between these 2 samplings (i.e. during 28 days), the H_4SiO_4 depletion in the ML (1.9 - 1.5 = 0.4 mol m^{-2}) yields to an average ∫ρNet of 14.3 mmol m^{-2} d^{-1}. Although it was located in different blooms of the Kerguelen region with different diatom communities, this value is in good agreement with the net silica production measured at station E-1 which we characterized as a “starting-bloom” dynamic. Consequently, we can predict that simultaneously to the rise of silica production above the Plateau, the ∫D:∫P ratio should decrease toward values around 0.5 as measured at E-1, and that the silica production could be controlled by both new and regenerated sources of H_4SiO_4. In this situation, almost all the net BSi production is accumulated in the surface water: 348.5 mmol m^{-2} (BSi stock integrated over 80 m, this study) and very low export of biogenic silica is allowed from the ML to the bottom layer: 4.7 mmol m^{-2} d^{-1} (estimated from the difference between net production calculated with DSi standing stocks and that calculated using BSi standing stocks, 14.3 and 9.6 mmol m^{-2} d^{-1} respectively). These observations are in good agreement with the low carbon export (4 % of the surface primary production) estimated during the first visit at A3 by Jacquet et al. (2014). Indeed, such early spring bloom generally starts by the development of lightly silicified diatoms with potentially low sedimentation rates (Quéguiner, 2013).

The H_4SiO_4 stock measured during the second visit at A3 (1.5 mol m^{-2}) can sustain the strong net silica production rates measured there for 32 days. Using natural Si isotopic approach, Fripiat et al. (2011a) suggested that diatoms could receive in addition, at least 1.2 mol m^{-2} of DSi coming from the WW during the productive period in the upper 80 m of the fertilized area, allowing 26 supplementary days of growth for diatoms with the same high Si uptake rate. Taking into account the sum of such winter and summer vertical Si supply, the high productive period as measured in A3-2 can be maintained during 86 days. Remarkably, this is almost similar to the estimation by Mongin et al. (2008) based on satellite products of 85 days of blooming over the Kerguelen plateau. Using a box-model approach, De Brauwere et al. (2012) suggested that the bloom could also persist over the same duration without considering this summer Si supply from deep-waters. This appears unlikely because the high net silica production we measured at A3-2 could not be sustained for more than 32 days. Even if such high net silica production should probably not be representative of the Si uptake by diatoms over the Plateau during the rest of bloom period, an additional source of Si is needed. The very good accordance of our results with the bloom duration from Mongin et al. (2008) suggests that this summer H_4SiO_4 input in the ML is realistic and could sustain a significant part of the phytoplankton growth above the Kerguelen Plateau. Indeed, high internal wave activity above the plateau is assumed to be a major process for vertical dissolved iron (and other nutrients) supply on the upper waters (Park et al., 2008; Blain et al., 2008).

These vertical fluxes allow a 2-month period of highly active blooming, with a system controlled exclusively by new sources of H4SiO4 (∫D:∫P = 0.09, A3-2, *Table 1.3.*), inducing the strong DSi depletion observed in January (DSi stocks at 0.2 mol m^{-2}, KEOPS-1; Mosseri et al., 2008) and the high BSi accumulation in the ML (348.5 mmol m^{-2}, KEOPS-2; this study) which could be exported at the end of summer when the water column stratification becomes weaker. The gross-∫ρSi measured here is in the upper range of published values in the Southern Ocean and the specific Si uptake rate was relatively high (respectively 47.9 mmol m^{-2} d^{-1} and 0.28 d^{-1} in the euphotic layer; *Table 1.2.*). This could indicate that diatoms have already reached their maximum BSi production rate, and that our second visit to A3 could represent the maximum of the bloom dynamic above the Plateau. This is quite consistent with the date of the bloom peak estimated in early December both by modeling and satellite approaches (Mongin et al., 2008 and de Brauwere et al., 2012). The H_4SiO_4 standing stock in the ML would then be depleted by mid-January (0.2 mol m^{-2}, KEOPS-1; Mosseri et al., 2008). Then the bloom would shift toward a steady state dynamic, almost entirely controlled by regenerated Si with decreasing gross silica production down to 10.7 mmol m^{-2} d^{-1}, KEOPS-1 (Mosseri et al., 2008) and where H_4SiO_4 concentration in the ML becomes limiting for diatom growth.

This progression of Si limitation could be associated to a change in the phytoplankton community as observed between the different visits at A3 during KEOPS-1 (Mosseri et al., 2008; Armand et al., 2008), and could be related to the selection of species with higher affinities with silicic acid resulting in a better ability to grow at low H_4SiO_4 concentrations. Such change in the community structure in response to physical and biological forcing was also proposed in a conceptual scheme by Quéguiner (2013). In spring, diatoms presenting high growth rates and low degree of silicification dominate the bloom which development is mainly controlled by new nutrients sources. This diatom assemblage will be soon affected by the availability of both silicic acid and iron, and will change for a population showing lower growth rates exclusively sustained by regenerated sources of H_4SiO_4. This second assemblage, beginning to dominate in January, could thus persist at steady state until May, when PAR decreases below the threshold of 1 mol photon m^{-2} d^{-1} (Blain et al., 2013) in waters that are quite depleted in H_4SiO_4, as it is composed by small diatoms with high affinities for silicic acid (Mosseri et al., 2008) and a deep silica maximum (DSM) characterized by strongly silicified large–sized diatoms growing at the base of the ML in the nutrient gradient (Quéguiner, 2013). Under such conditions, a very low net silica production and a ∫D:∫P ratio close to 1 are expected. Unfortunately no silica dissolution measurements are available from KEOPS-1. However, we can try to estimate the net production from the difference between the KEOPS-1 average gross silica production (10.7 mmol m^{-2} d^{-1}; Mosseri et al., 2008) and average silica dissolution measured at all stations south of the Polar Front during KEOPS-2 (10.2 mmol m^{-2} d^{-1}). The choice of a constant silica dissolution rate throughout the productive season may seem surprising at first sight. However, there are several reasons to support this hypothesis: (i) Brzezinski et al. (2001) show that the seasonal variability of silica dissolution rates in the Southern Ocean is very low (6.7 mmol m^{-2} d^{-1} in October/November to 6.6 mmol m^{-2} d^{-1} in February/March); (ii) ∫ρDiss measured close to the Polar Front by Fripiat et al. (2011b) in late summer were very close to our spring dissolution values (4.9 to 6.6 mmol m^{-2} d^{-1}) (iii) As best seen on *figure 1.5b.*, all KEOPS-2 stations except the HNLC one (R-2) have similar silica dissolution profiles. Thus it is reasonable to assume that the net silica production estimated above the plateau in late summer should be around 0.5 mmol m^{-2} d^{-1}.

The BSi standing stock observed in the upper layer in late summer (275.3 mmol m^{-2}, KEOPS-1; Mosseri et al., 2008) is lower than that measured in spring (348.5 mmol m^{-2}). This could indicate that a part of the BSi that was produced before reaching a silica production in steady state (i.e. sustained almost entirely by regenerating production) was not accumulated in the surface ML at the end of the

productive period. In fact, a part of the summer production can be stocked in the form a DSM as measured in late summer above the plateau (550.1 mmol m^{-2} between 100 and 200 m; Mosseri et al., 2008) which was not yet present at KEOPS-2. This subsurface biogenic silica accumulation mainly results from the combination of sedimentation of living but inactive cells and the occurrence of phytoplankton populations living at depth (Uitz et al., 2009; Fripiat et al., 2011a). The part of the summer net silica production which is not accumulated below the ML should thus be exported to deeper waters as the seasonal stratification breaks down with the intensification of vertical mixing. In term of carbon export, this flux could represent 14 to 31 % of the surface primary production (KEOPS-1, station A3; Jacquet et al., 2008). As proposed by Quéguiner (2013), a massive export of biogenic silica and organic matter (58 days x 46.8 mmol m^{-2} d^{-1} - (275.3 + 550 mmol m^{-2}) = 2.2 mol Si m^{-2}) should occur and could then represent the major annual event of the silicon and biological carbon pumps.

Although our budget of the silicon biogeochemical cycle above the Kerguelen Plateau is based on different silicon isotopic approaches and is sustained by silicon stocks and fluxes coming from different years, it matches very well with all the previous individual findings. The seasonal variations of ∫D:∫P ratio are in accordance with those observed by Brzezinski et al. (2001) across the Polar Front Zone and are quite well represented by the recent model of Coffineau et al. (2013), who estimate a ∫D:P ratio ranging from 0.64 in winter to 0.19 during the spring bloom. The good accordance of our approach with outcomes from different studies also highlights that, to fully characterize the silicon cycle in a region of interest, we need to measure both silica production and dissolution rates. Indeed, taking only into account the gross silica production in such a synthesis exercise (i.e. without measuring silica dissolution as it is the case in most studies) could lead to misinterpretations of the silicon pump functioning. For instance, we would not be able to identify shifts between “new” and “regenerated” silica production neither to accurately calculate the real bloom duration without considering silica recycling. Without taking into account dissolution, silica production would have been overestimated by 21 % in the mixed layer (58.2 mmol m^{-2} d^{-1} compared to the 47.9 mmol m^{-2} d^{-1} of real net silica production), and the bloom duration computation would have yielded 74 days, which is not consistent with the 85 days of KEOPS-1 bloom duration observed by Mongin et al. (2008).

I.5. Conclusions

Our study addressed the seasonal evolution of the efficiency of the silicon pump and of the biogenic silica fluxes in the mixed layer under different naturally iron-fertilized bloom conditions

around the Kerguelen region. Integrated Si uptake rates were among the highest reported so far in the Southern Ocean. They varied from 3.09 ± 0.01 mmol m^{-2} d^{-1} in the HNLC area (R-2) to 47.9 ± 0.4 mmol m^{-2} d^{-1} above the plateau (A3-2) and seemed to be strongly coupled with C uptake over depth. Indeed, C and Si assimilation were very low below the euphotic layer indicating the occurrence of a subsurface accumulation of living but inactive diatoms. Although significant, silica dissolution rates were generally much lower than production rates and did not vary between bloom stations nor over depth.

We observed a shift from a BSi production regime based on the regeneration of H_4SiO_4 during the early stages of bloom onset (with an averaged ∫D:∫P ratio of 0.98) to a regime based on new production during the bloom development (with an averaged ∫D:∫P ratio of 0.18). This change switched on an active silicon pump which led to the decoupling between Si and N cycles as well as a strong H_4SiO_4 depletion of surface water by late summer, with significant implications for global biogeochemical properties. Indeed, the system progressively shifted toward a stronger silicon pump as Si uptake rates increased and nitrogen became preferentially remineralized when the bloom was well established. This led ultimately to a strong Si limitation and drove the system toward a regenerated silica production regime which allowed the persistence of the bloom in a steady state despite the low concentrations of silicic acid concentrations. Our results confirm and complete the concept of a seasonal transition from a diatom new production to a diatom regenerated production already proposed in the Antarctic Zone by Brzezinski et al. (2003).

Moreover, in opposition to previous artificial Fe-enrichment bottle experiments outcomes, Si:N and Si:C uptake ratios during KEOPS-2 were not higher in the HNLC area compared to the fertilized region. This observation could have great implications on our understanding on processes involved in setting atmospheric pCO_2 during glacial-interglacial transitions. Our results suggest that the increase of low latitude diatom production observed during glacial periods should not be controlled primarily by a shift in the nutrient uptake stoichiometry of Antarctic diatoms induced by an enhanced iron supply, as proposed in the silicic acid leakage hypothesis (Matsumoto et al., 2002; Brzezinski et al., 2002), but further investigations are clearly needed to validate this idea.

The combination of the results from the two KEOPS cruises (early spring and late summer) and of different isotopic approaches, allowed the first seasonal estimate of a closed silicon biogeochemical budget in the iron-fertilized area above the Kerguelen Plateau based on direct measurements. Our

estimates emphasize the interest of combining different tracers and methods with different sensitivities to physical and biological processes to better constrain and quantify all the processes simultaneously. The major outcome of this seasonal budget is that the winter and summer silicon supplies to the mixed layer (3.2 mol m^{-2} y^{-1}) seem to be well balanced by the combination of biogenic silica accumulation (both in the upper layer and in the winter waters) and late summer BSi export (respectively 0.3 + 0.6 + 2.2 = 3.1 mol m^{-2} y^{-1}). This confirms the occurrence of a significant summer Si supply from Winter Water as suggested by Fripiat et al. (2011a) sustaining the diatom bloom over the Kerguelen Plateau.

Finally, a striking feature of this study is that naturally iron fertilized areas of the Southern Ocean, like the Kerguelen Plateau, could sustain a biogenic silica production regime similar to those observed in coastal upwelling systems or in large river plume. This highlights the exceptional character of diatoms-dominated ecosystems associated to natural iron fertilization in the Southern Ocean, and their significant role in the global Si biogeochemical cycle. Even if the outcomes of this budget are consistent with previous measurements, large uncertainties remain about the seasonal evolution of dissolution rates at the end of the productive period. Indeed, in order to fully characterize the Si-biogeochemical cycle in a region of interest, it is recommended to measure both BSi production and dissolution rates. In combination, the natural silicon isotopic composition ($\delta^{30}Si$) of diatoms and seawater represents a powerful tool for identifying silicon sources and silica production over larger temporal and spatial scales (Fripiat et al., 2011a; Tréguer and De la Rocha, 2013), and will be also examined during KEOPS-2. The combination of several isotopic approaches, as well as modeling exercises (such as in Pondaven et al., 1998; De Brauwere et al., 2012; Coffineau et al., 2013), by allowing to better constrain and quantify different physical and biogeochemical processes simultaneously, would strongly improve our understanding of the regional Si biogeochemical cycle and its implications in the global ocean biogeochemistry.

Acknowledgements

Authors would like to thank Pr. Stéphane Blain as the KEOPS-2 project coordinator, the captain and the crew of the R/V Marion-Dufresne II for assistance on board. We are also especially grateful to Luc André who has allowed the access to the HR-SF-ICP-MS at the Royal Museum of Central Africa. We

thank the two anonymous reviewers for their constructive and helpful comments. This work was supported by the French Research program of INSU-CNRS LEFE-CYBER ('Les enveloppes fluides et l'environnement' – 'Cycles biogéochimiques, environnement et ressources'), the French ANR ('Agence Nationale de la Recherche', SIMI-6 program), the French CNES ('Centre National d'Etudes Spatiales') and the French Polar Institute IPEV (Institut Polaire Paul-Emile Victor). The research leading to these results has also received funding from the European Union Seventh Framework Programme under grant agreement n°294146 (MuSiCC Marie Curie CIG).

I.6. References

Assmy P., Smetacek V., Montresor M., Klaas C., Henjes J., Strass V., Arrieta J., Bathmann U., Berg G., Breitbarth E., Cisewski B., Friedrichs L., Fuchs N., Herndl G., Jansen S., Krägefsky S., Latasa M., Peeken I., Röttgers R., Scharek R., Schüller S., Steigenberger S., Webb A., Wolf-Gladrow D. (2013) Thick-shelled, grazer-protected diatoms decouple ocean carbon and silicon cycles in the iron-limited Antarctic Circumpolar Current. Proceedings of the National Academy of Sciences of the United States of America. 110(51):20633–20638

Armand L., Cornet-Barthaux V., Mosseri J., Quéguiner B. (2008) Late summer diatom biomass and community structure on and around the naturally iron-fertilised Kerguelen Plateau in the Southern Ocean. Deep-Sea Research II. 55:653-676

Baines S., Twining B., Brzezinski M., Nelson D., Fisher N. (2010) Causes and biogeochemical implications of regional differences in silicification of marine diatoms. Global Biogeochemical Cycles. 24:GB4031. Doi10.1029/2010GB003856

Beucher C., Tréguer P., Hapette A. M., Corvaisier R. (2004) Intense summer Si-recycling in the surface Southern Ocean. Geophysical research letters. 31:L09305. doi:10.1029/2003GL018998

Bidle K. D., Azam F. (1999) Accelerated dissolution of diatom silica by marine bacterial assemblages. Nature. 397:508-512

Bidle K. D., Brzezinski M., Long R., Jones J., Azam F. (2003) Diminished efficiency in the oceanic silica pump caused by bacteria-mediated silica dissolution. Limnology and Oceanography. 48(5):1855-1868

Blain S., Tréguer P., Belviso S., Bucciarelli E., Denis M., Desabre S., Fiala M., Martin-Jézéquel V., Le Fèvre J., Mayzaud P., Marty J.-C., Razouls S. (2001) A biogeochemical study of the island mass effect in the context of the iron hypothesis: Kerguelen Islands, Southern Ocean. Deep-Sea Research I. 48:163-187

Blain S., Quéguiner B., Armand L., Belviso S., Bombled B., Bopp L., Bowie A., Brunet C., Brussaard C., Carlotti F., Christaki U., Cordière A., Durand I., Ebersbach F., Fuda J.-L., Garcia N., Gerringa L., Griffiths B., Guigue C., Guillerm C., Jacquet S., Jeandel C., Laan P., Lefèvre D., Lo Monaco C., Malits A., Mosseri J., Obernosterer I., Park Y.-H., Picheral M., Pondaven P., Remenyi T., Sandroni V., Sarthou G., Savoye N., Scouarnec L., Souhaut M., Thuiller D., Timmermans K., Trull T., Uitz J., Van Beek P., Velhuis M., Vincent D., Viollier E., Vong L., Wagener T. (2007) Effect of natural iron fertilization on carbon sequestration in the Southern Ocean. Nature. 446:1070-1075

Boyd P., Crossley A., diTullio G., Friffiths F., Hutchins D., Queguiner B., Sedwick P., Trull T. (2007) Control of phytoplankton growth by iron supply and irradiance in the subantarctic Southern Ocean: Experimental results from the SAZ Project. Journal of Geaophysical Research. 106:31573-31583

Blain S., Quéguiner B., Trull T. (2008) The natural iron fertilization experiment KEOPS (KErguelen Ocean and Plateau compared Study): An overview. Deep-Sea Research II. 55:559-565

Blain S., Renaut S., Xing X., Claustre H., Guinet C. (2013) Instrumented elephant seals reveal the seasonality in chloropyll and light-mixing regime in the iron fertilized Southern Ocean. Geophysical Research Letters. 40:1-5

Blain S. KEOPS2: implementation and overview. In preparation for Biogeosciences.

Boyd P., Crossley A., DiTullio G., Griffiths F., Hutchins D., Quéguiner B., Sedwick ., Trull T. (2001) Control of phytoplankton growth by iron supply and irradiance in the subantarctic Southern Ocean: Experimental results from the SAZ Project. Journal of Geophysical Research. 106(C12):31573-31583

Boyd P., Jickells T., Law C., Blain S., Boyle E., Buesseler K., Coale K., Kullen J., De Baar H., Follows M., Harvey M., Lancelot C., Levasseur M., Owens N., Pollard R., Rivkin R., Sarmiento J., Schoemann V., Smetacek V., Takeda S., Tsuda A., Turner S., Watson A. (2007) Mesoscale Iron Enrichment Experiments 1993-2005: Synthesis and Future Directions. Science. 315:612-617

Brzezinski M. (1985) The Si:C:N ratio of marine diatoms: interspecific variability and the effect of some environmental variables. Journal of Phycology. 21:347-357

Brzezinski M., Nelson D. (1989) Seasonal changes in the silicon cycle within a Gulf Stream warm-core ring. Deep-Sea Research. 36(7):1009-1030

Brzezinski M., Nelson D., Franck V., Sigmon D. (2001) Silicon dynamics within an intense open-ocean diatom bloom in the Pacific sector of the Southern Ocean. Deep-Sea Research II. 48:3997-4018

Brzezinski M. A., Pride C. J., Frank V. M., Sigman D. M., Sarmiento J. L., Matsumoto K., Gruber N., Rau G. H., Coale K. H. (2002) A switch from Si(OH)4 to NO3- depletion on the glacial Southern Ocean. Geophysical Research Letters. 29(12), doi:10.1029/2001GL014349

Brzezinski M., Jones J., Bidle K., Azam F. (2003) The balance between silica production and silica dissolution in the sea: Insights from Monterey Bay, California, applied to the global data set. Limnology and Oceanography. 48(5):1846-1854

Bucciarelli E., Pondaven P., Sarthou G. (2010) Effects of an iron-light co-limitation on the elemental composition (Si, C, N) of the marine diatoms Thalassiosira oceanica and Ditylum brightwellii. Biogeosciences. 7:657-669

Buesseler K., Ball L., Andrews J., Cochran J., Hirschberg D., Bacon M., Fleer A., Brzezinski M. (2001) Upper ocean export of particulate organic carbon and biogenic silica in the Southern Ocean along 170°W. Deep-Sea Research II. 48:4275-4297

Cavagna A. J. Blain S., Cardinal D., Closset I., Dehairs F., Fernandez C., Flores-Leive L., Lasbleiz M., Lefèvre D., Leblanc K., Quéguiner B., Biological productivity regime and in-situ methods comparison around the Kerguelen Island in the Southern Ocean. KEOPS 2 primary and community producers regime using various uptake rates and their stoichiometric ratios. In preparation for Biogeosciences.

Claquin P., Martin-Jézéquel V., Kromkamp J. C., Veldhuis M. J. W., Kraay G. W. (2002) Uncoupling of silicon compared to carbon and nitrogen metabolisms, and role of the cell cycle, in continuous cultures of Thalassiosira pseudonana (Bacillariophyceae) under light, nitrogen and phosphorus control. Journal of Phycology. 38:922-930

Coffineau N., De La Rocha C., Pondaven P. (2013) Exploring interacting influences on the silicon isotopic composition of the surface ocean: a case study from the Kerguelen Plateau. Biogeosciences Discussion. 10:11405-11446

Corvaisier R., Tréguer P., Beucher C., Elskens M. (2005) Determination of the rate of production and dissolution of biosilica in marine waters by thermal ionisation mass spectrometry. Analytica Chimica Acta. 534:149-155

Crosta X., Beucher C., Pahnke K., Brzezinski M. (2007) Silicic acid leakage from the Southern Ocean: Opposing effects of nutrient uptake and oceanic circulation. Geophysical Research Letters. 34, L13601, doi:10.1029/2006GL029083

De Baar H., Boyd P., Coale K., Landry M., Tsuda A., Assmy P., Bakker D., Bozec Y., Barber R., Brzezinski M., Buesseler K., Boye M., Croot P., Gervais F., Gorbunov M., Harrison P., Hiscock W., LaanP., Lancelot C., Law C., Levasseur M., Marchetti A., Millero F., Nishioka J., Nojiri Y., van Oijen T., Riebesell U., Rikenberg M., Saito H., Takeda S., Timmermans K., Veldhuis M., Waite A., Wong C.-S. (2005) Synthesis of iron fertilization experiments: From the Iron Age in the Age of Enlightenment. Journal of Geophysical Research. 110:C09S16, doi:10.1029/2004JC002601

De Brauwere A., De Ridder F., Elskens M., Schoukens J., Pintelon R., Baeyens W. (2005) Refined parameter and uncertainty estimation when both variables are subject to error. Case study: estimation of Si consumption and regeneration rates in a marine environment. Journal of Marine Systems. 55:205-221

De Brauwere A., Fripiat F., Cardinal D., Cavagna A.-J., De Ridder F., André L., Elskens M. (2012) Isotopic model of oceanic silicon cycling: the Kerguelen Plateau case study. Deep-Sea Research I. 70:42-59

Dehairs F., Trull T., Fernandez C., Davies D., Cavagna A. J., Planchon F., Fripiat F., Nitrate isotopic composition in the Kerguelen area (Southern Ocean) during KEOPS 2. In preparation for Biogeosciences.

Dugdale R., Wilkerson F., Minas H. (1995) The role of a silicate pump in driving new production. Deep-Sea Research I. 5(42):697-719

Elskens M., de Brauwere A., Beucher C., Corvaisier R., Savoye N., Tréguer P., Baeyens W. (2007) Statistical process control in assessing production and dissolution rates of biogenic silica in marine environments. Marine Chemistry. 106:272-286

Franck V., Brzezinski M., Coale K., Nelson D. (2000) Iron and silicic acid concentrations regulate Si uptake north and south of the Polar Frontal Zone in the Pacific Sector of the Southern Ocean. Deep-Sea Research II. 47:3315-3338

Fripiat F., Corvaisier R., Navez J., Elskens M., Schoemann V., Leblanc K., André L., Cardinal D. (2009) Measuring production-dissolution rates of marine biogenic silica by 30Si-isotope dilution using a high-resolution sector field inductively coupled plasma mass spectrometer. Limnology and Oceanography: Methods. 7:470-478

Fripiat F. (2010) Isotopic approaches of the silicon cycle: The Southern Ocean case study (Ph. D. dissertation). Université Libre de Bruxelles, Brussels. 266p

Fripiat F., Cavagna A. J., Savoye N., Dehairs F., André L., Cardinal D. (2011a) Isotopic constraints on the Si-biogeochemical cycle of the Antarctic Zone in the Kerguelen area (KEOPS). Marine Chemistry. 123:11-22

Fripiat F., Leblanc K., Elskens M., Cavagna A. J., Armand L., André L., Dehairs F., Cardinal D. (2011b) Efficient silicon recycling in summer in both the Polar Frontal and Subantarctic Zones of the Southern Ocean. Marine Ecology Progress Series. 435:47-61

Hildebrand M. (2008) Diatoms, Biomineralization Processes, and Genomics. Chemical Review. 108(11):4855-4874

Hutchins D., Bruland K. (1998) Iron-limited diatom growth and Si:N uptake ratios in a coastal upwelling regime. Nature. 393:561-564

Jacquet S. H. M., Dehairs F., Savoye N., Obernosterer I., Christaki U., Monnin C., Cardinal D. (2008) Mesopelagic organic carbon remineralization in the Kerguelen Plateau region tracked by biogenic particulate Ba. Deep-Sea Research II. 55:868-879

Jacquet S. H. M., Dehairs F., Cavagna A. J., Planchon F., Monin L., André L., Closset I., Cardinal D. (2014) Early season mesopelagic carbon remineralization and transfer efficiency in the naturally iron-fertilized Kerguenlen area. Biogeosciences Discussion. 11:9035-9069

Kamatani A. (1982) Dissolution rates of silica from diatoms decomposing at various temperatures. Marine Biology. 68:91-96

Karl D., Tien G. (1992) MAGIC: A sensitive and precise method for measuring dissolved phosphorus in aquatic environment. Limnology and Oceanography. 37(1):105-116

Krause J. W., Nelson D. M., Brzezinski M. A. (2011) Biogenic silica production and the diatom contribution to primary production and nitrate uptake in the eastern equatorial Pacific Ocean. Deep-Sea Research II. 58:434-448

Lasbleiz M., Leblanc K., Blain S., Ras J., Cornet-Barthaux V., Hélias Nunige S., Quéguiner B. (2014) Pigments, elemental composition (C, N, P, Si) and stoichiometry of particulate matter, in the naturally iron fertilized region of Kerguelen in the Southern Ocean. Biogeosciences Discussion. 11:8259-8324.

Leynaert A., Bucciarelli E., Claquin P., Dugdale R. C., Martin-Jézéquel V., Pondaven P., Ragueneau O. (2004) Effect of iron deficiency on diatom cell size and silicic acid uptake kinetics. Limnology and Oceanography. 49(4):1134-1143

Matsumoto K., Sarmiento J. L., Brzezinski M. A. (2002) Silicic acid leakage from the Southern Ocean: A possible explanation for glacial atmospheric pCO2. Global Biogeochemical Cycles. 16(3), doi:10.1029/2001GB001442

Martin-Jézéquel V., Hildebrand M., Brzezinski M. (2000) Silicon metabolism in diatoms: implications for growth. Journal of Phycology. 36:821-840

Mongin M., Molina E., Trull T. (2008) Seasonality and scale of the Kerguelen plateau phytoplankton bloom: A remote sensing and modeling analysis of the influence of natural iron fertilization in the Southern Ocean. Deep-Sea Research II. 55:880-892

Mosseri J., Quéguiner B., Armand L., Cornet-Barthaux V. (2008) Impact of iron on silicon utilization by diatoms in the Southern Ocean: A case study of Si/N cycle decoupling in a naturally iron-enriched area. Deep-Sea Research II. 55:810-819

Nelson D. and Goering J. J. (1977a) A Stable Isotope Tracer Method to Measure Silicic Acid Uptake by Marine Phytoplankton. Analytical Biogeochemistry. 78:139-147

Nelson D. and Goering J. J. (1977b) Near-surface silica dissolution in the upwelling region off northwest Africa. Deep –Sea Research. 24:65-73

Nelson D., Tréguer P. (1992) Role of silicon as a limiting nutrient to Antarctic diatoms: evidence from kinetic studies in the Ross Sea ice-edge zone. Marine ecology progress series. 80:255-264

Park Y.-H., Charriaud E., Ruiz Pino D., Jeandel C. (1998) Seasonal and interannual variability of the mixed layer properties and steric height at station KERFIX, southwest of Kerguelen. Journal of Marine Systems. 17:571-586

Park Y.-H., Roquet F., Durand I., Fuda J.-L. (2008) Large-scale circulation over and around the Northern Kerguelen Plateau. Deep-Sea Research II. 55:566-581

Park Y.-H., Water masses and circulation in the Polar Front region east of the Kerguelen Islands. In preparation for Biogeosciences.

Pollard R., Lucas M., Read J. (2002) Physical controls on biogeochemical zonation in the Southern Ocean. Deep-Sea Research II. 49:3289-3305

Pondaven P., Fravalo C., Ruiz-PinoD., Tréguer P., Quéguiner B., Jeandel C. (1998) Modelling the silica pump in the Permanently Open Ocean Zone of the Southern Ocean. Journal of Marine Systems. 17:587-619

Pondaven P., Ragueneau O., Tréguer P., Hauvespre A., Dézileau L., Reyss J.L. (2000) Resolving the "opal paradox" in the Southern Ocean. Nature. 405(6783):168-172

Quéguiner B. (2001) Biogenic silica production in the Australian sector of the Subantarctic Zone of the Southern Ocean in late summer 1998. Journal of Geophysical Research. 106(C12):31627-31636

Quéguiner B. (2013) Iron fertilization and the structure of planktonic communities in high nutrient regions of the Southern Ocean. Deep-Sea Research II. 90:43-54

Quéguiner B., Brzezinski M. (2002) Biogenic silica production rates and particulate organic matter distribution in the Atlantic sector of the Southern Ocean during austral spring 1992. Deep-Sea Research II. 49:1765-1786

Quéroué F., Dissolved iron in the vicinity of the Kerguelen plateau (KEOPS-2 experiment). In preparation for Biogeosciences.

Ragueneau O., Treguer P., Leynaert A., Anderson R. F., Brzezinski M. A., DeMaster D. J., Dugdale R. C., Dymont J., Fisher G., François R., Heinze C., Maier-Reimer E., Martin-Jézéquel V., Nelson D. M., Quéguiner B. (2000) A review of the Si cycle in the modern ocean: recent progress and missing gaps in the application of biogenic opal as a paleoproductivity proxy. Global Planet Change. 26:317-365

Ragueneau O., Savoye N., Del Amo Y., Cotten J., Tardiveau B., Leynaert A. (2005) A new method for the measurement of biogenic silica in suspended matter of coastal waters: using Si:Al ratios to correct for the mineral interference. Continental Shelf Research. 25:697-710

Reynolds B., Frank M., Halliday A. (2006) Silicon isotope fractionation during nutrient utilization in the North Pacific. Earth and Planetary Science Letters. 244:431-443

Roquet F., Park Y.-H. Guinet C., Bailleul F., Charrassin J.-B. (2009) Observations of the Fawn Trough Current over the Kerguelen Plateau from instrumented elephant seals. Journal of Marine Systems. 78:377-393

Sarmiento J., Gruber N., Brzezinski M., Dunne J. (2004) High-latitude controls of thermocline nutrients and now latitude biological productivity. Nature. 427:56-60

Sarthou G., Chever F., Quéroué F., Bowie A., Van der Merwe P., Cheize M., Sirois M., Bucciarelli E., Fe-Cu impact in incubation experiments of natural plankton communities and Fe- and Cu-binding ligand production at the vicinity of the Kerguelen Island, Southern Ocean. In preparation for Biogeosciences.

Strickland J., Parsons T. (1972) A pratical handbook of sea water analysis. Fisheries research board of Canada. 167:65-70

Tagliabue A., Mtshali T., Aumont O., Bowie A., Klunder M., Roychoudhury A., Swart S. (2012) A global compilation of dissolved iron measurements: focus on distributions and processes in the Southern Ocean. Biogeosciences. 9:2333-2349

Takahashi T. ,Sutherland S., Wanninkhof R., Sweeney C., Feely R., Chipman D., Hales B., Friederich G., Chavez F., Sabine C., Watson A., Bakker E., Schuster U., Metzl N., Yoshikawa-Inoue H., Ishii M., Midorikawa T., Nojiri Y., Körtzinger A., Steinhoff T., Hoppema M., Olafsson J., Arnarson T., Tilbrook B., Johannessen T., Olsen A., Bellerby R., Wong C.S., Delille B., Bates N.R., debar H. (2009) Climatological mean and decadal change in surface ocean pCO2, and net sea-air CO2 flux over the global oceans. Deep-sea Research II. 56:554-577

Takeda S. (1998) Influence of iron availability on nutrient consumption ratio of diatoms in oceanic waters. Nature. 393:774-777

Tréguer P., De La Rocha C. (2013) The World Ocean Silica Cycle. Annual Review of Marine Science. 5:477-501

Trull T., Rintoul S., Hadfield M., Abraham E. (2001) Circulation and seasonal evolution of polar waters south of Australia: Implications for iron fertilization of the Southern Ocean. Deep-Sea Research II. 48:2439-2466

Uitz J., Claustre H., Griffiths B., Ras J., Garcia N., Sandroni V. (2009) A phytoplankton class-specific primary production model applied to the Kerguelen Islands region (Southern Ocean). Deep-Sea Research I. 56:541-560

Zhou M., Zhu Y., d'Ovidio F., Park Y.-H., Durand I., Kestenare E., Sanial V., Van-Beek P., Quéguiner B., Carlotti F., Blain S. (2014) Surface currents and upwelling in Kerguelen Plateau regions. Biogeosciences Discussion. 11:68-6876

Chapitre 2

Facteurs de Contrôle des Variations Saisonnières des Isotopes du Silicium

PREAMBULE

Contexte de l'étude

Dans la grande majorité des études impliquant les isotopes du silicium dans l'océan, les variations de la composition isotopique du compartiment dissous et/ou particulaire sont expliquées à l'aide de l'un des 2 modèles simples dont les principes ont été présentés précédemment (cf. *Introduction générale*) et sont résumés dans la *figure 2.1.*

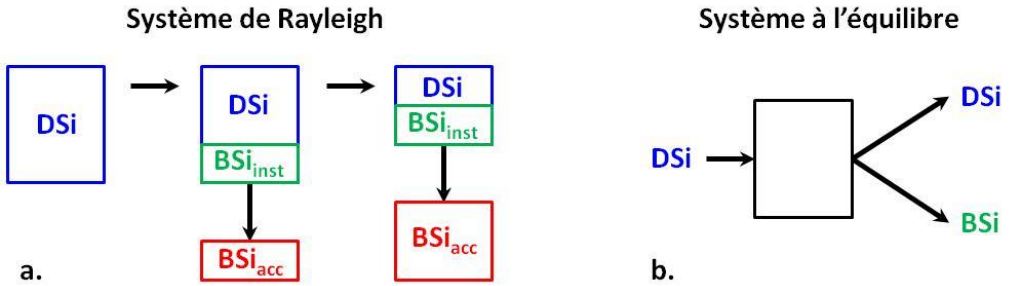

Figure 2.1. Schéma du fonctionnement du modèle de Rayleigh (ou fermé, a.) et du modèle à l'équilibre (ou ouvert, b.). Le substrat considéré ici est l'acide silicique (DSi, en bleu), le produit est la silice biogénique (BSi, en vert dans le modèle à l'équilibre) et qui peut être instantanée (BSi_{inst}, en vert) ou accumulée (BSi_{acc}, en rouge) dans le modèle de Rayleigh. Le modèle de Rayleigh implique une diminution du stock de DSi et une augmentation du stock de BSi accumulée, alors qu'il ny a pas de variation de stock dans le modèle à l'équilibre.

Conceptuellement, l'application de ces modèles aux variations du $\delta^{30}Si$ dans l'Océan Austral reste délicate. En effet, Le modèle de Rayleigh implique que la ML ne reçoit aucun nouvel apport de DSi et que la BSi, une fois produite n'interagit plus avec le réservoir dissous. Les conditions hydrodynamiques particulièrement dynamiques rencontrées dans l'ACC, avec par exemple des ML extrêmement profondes en hiver, et les taux de dissolution significatifs de la BSi dans l'océan de surface (notamment à la fin de la période de production), nous éloignent des conditions optimales d'application de ce modèle. A l'inverse, l'accumulation de BSi et l'appauvrissement en DSi de la ML observés lors des campagnes océanographiques telles que KEOPS ne sont pas autorisés dans le modèle à l'équilibre. De plus, de nombreuses incertitudes sont généralement associées au choix des conditions initiales utilisées dans ces modèles et peuvent occasionner des biais significatifs lors de l'estimation de certains paramètres à l'aide de ces modèles (e.g. Cardinal et al., 2005). Afin de mieux comprendre les processus contrôlant les variations saisonnières de la distribution des isotopes du silicium dans l'Océan

Austral, il est donc nécessaire d'obtenir des informations précises sur les masses d'eau sources utilisées dans ces modèles.

L'objectif principal de ce chapitre est donc de déterminer les conditions biogéochimiques précédant le développement du phytoplancton dans la zone naturellement fertilisée en fer du Plateau de Kerguelen et de les confronter aux modèles existants dans la région (De Brauwere et al., 2012 ; Coffineau et al., 2014). En identifiant la masse d'eau source, nous avons rectifié les estimations de production annuelle nette de BSi et confirmé la présence d'apports estivaux de Si dans la ML. De plus, la comparaison des résultats des 2 campagnes KEOPS nous a permis de mettre en évidence un découplage entre la dynamique isotopique du compartiment dissous et celle du compartiment particulaire. L'ensemble de ces résultats nous permettra d'améliorer significativement les modèles biogéochimique du cycle du silicium dans l'Océan Austral (et en particulier dans la région du Plateau de Kerguelen).

Résumé

Les processus biogéochimiques se déroulant dans les eaux de l'Océan Austral jouent un rôle crucial dans le contrôle de la production primaire marine globale en influençant la disponibilité des nutriments dans les eaux de surface des basses latitudes. En raison des faibles concentrations en fer mesurées dans la couche de mélange (ML), cet océan représente la plus grande région « High Nutrient-Low Chlorophyll » (HNLC) de l'océan global. Il peut néanmoins supporter localement des développements importants de phytoplancton, généralement associés à de larges discontinuités bathymétriques et combinés à des forçages hydrodynamiques importants qui contribuent à apporter naturellement du fer dans la ML. Durant la campagne océanographique KEOPS-2 (printemps 2011), les signatures isotopiques de l'acide silicique (DSi) et de la silice biogénique (BSi) en suspension ont été étudiées sur toute la colonne d'eau avec une résolution spatiale encore jamais atteinte dans ce genre de régions (le Plateau de Kerguelen). Dans cette étude, nous utilisons les mesures de $\delta^{30}Si$ pour identifier et suivre les sources de silicium qui alimentent le bloom, et pour étudier l'évolution saisonnière du cycle biogéochimique du silicium dans la zone fertilisée en fer. L'objectif principal est de comparer les résultats d'une station HNLC de référence avec ceux de stations présentant différents degrés d'enrichissement en fer. Les signatures isotopiques des réservoirs dissous et particulaire sont généralement fortement variables dans les 500 premiers mètres, reflétant ainsi l'action d'une pompe de silicium efficace et qui a été rapidement initiée au printemps. Elles sont en revanche relativement homogènes dans les eaux plus profondes. L'étude de l'équilibre massique et isotopique du silicium a

permis d'identifier, pour la zone fertilisée en fer, une source unique de Si située dans les eaux hivernales (WW) originaires du sud-est du Plateau de Kerguelen et qui se dispersent vers le nord. Cependant, lorsqu'elles atteignent une rétroflexion du Front Polaire (PF), la composition isotopique de l'acide silicique des WW s'alourdit progressivement. Ceci pourrait provenir d'une succession de mélanges isopycnaux entre ces WW initiales et différentes masses d'eau de la ML, illustrant ainsi la ventilation significative des eaux de surface associée à l'activité à méso-échelle importante qui définit cette zone. En comparant les résultats issus des deux campagnes KEOPS, la relation entre la consommation de DSi, la production de BSi et leurs compositions isotopiques respectives apparait découplée dans la zone fertilisée en fer. Le réservoir de DSi évolue suivant un système ouvert lié à la forte ventilation de la ML alors que la BSi se comporte plus comme un système fermé montrant une augmentation exponentielle des valeurs de delta qui sembleraient principalement dépendantes des rapports « Si-supply:Si-uptake » et de l'efficacité d'export du système. Ce découplage saisonnier peut aider à expliquer le faible facteur de fractionnement observé dans la ML à la fin de l'été. En prenant en compte ces considérations, nous avons ré-évalué la production nette de BSi dans la zone fertilisée en fer à 3.0 ± 0.3 moles Si m^{-2} an^{-1}. Ce taux de production correspond mieux aux précédentes estimations de la production de BSi dans la zone Antarctique, et serait exclusivement associé à des populations de phytoplancton de la ML. Ces notions confirment que la composition isotopique du silicium dissous et particulaire est un outil prometteur pour améliorer notre compréhension du cycle biogéochimique du silicium étant donné qu'il permet d'identifier et quantifier les processus impliqués dans ce cycle tels que l'absorption de Si, la dissolution de la BSi ou le mélange des masses d'eau. Ces notions apporteront de nouveaux éléments pour mieux contraindre les modèles biogéochimiques se concentrant sur le contrôle saisonnier de la consommation de DSi, de la production de BSi et de leurs variations au cours du temps, en particulier dans la région naturellement fertilisée en fer du Plateau de Kerguelen.

Ce chapitre fera l'objet d'un article finalisé et soumis courant 2015 :

Closset I., D. Cardinal, F. Thil, Controls on seasonal variations of Si isotopic composition of diatoms and seawater related to iron supply and mesoscale activity in the naturally Fe-fertilized Kerguelen area (Southern Ocean).

TABLE OF CONTENTS

Controls on seasonal variations of Si isotopic composition of diatoms and seawater related to iron supply and mesoscale activity in the naturally Fe-fertilized Kerguelen area (Southern Ocean)

Closset Ivia[1], Cardinal Damien[1], François Thil[2]

[1] Sorbonne Universités (UPMC, Univ Paris 06)-CNRS-IRD-MNHN, LOCEAN Laboratory, 4 place Jussieu, F-75005 Paris, France

[2] Laboratoire des Sciences du Climat et de l'Environnement, CNRS 91190 Gif-sur-Yvette, France

Correspondence to: I. Closset (ivia.closset@locean-ipsl.upmc.fr)

Abstract

Southern Ocean biogeochemical processes have a crucial role on global marine primary production and elemental cycling by influencing the nutrient availability in low latitude surface water. Because of its low iron concentration, it represents the highest High Nutrient-Low Chlorophyll (HNLC) area of the global ocean but can sustain locally strong phytoplankton blooms associated to large bathymetric discontinuities combined to strong hydrodynamic forcing which naturally bring iron in the Mixed Layer (ML). Silicon isotopic signatures ($\delta^{30}Si$) of seawater silicic acid (DSi) and suspended biogenic silica (BSi) were investigates for the whole water column with an unprecedented spatial resolution in such a region (the Kerguelen Plateau), during the KEOPS-2 experiment (spring 2011). In this study, we use $\delta^{30}Si$ measurements to track the silicon sources that fuel the bloom, and to investigate the seasonal evolution of Si biogeochemical cycle in the iron fertilized area. We compare results from a HNLC reference station and stations with different degrees of iron enrichment and bloom conditions. Dissolved and particulate $\delta^{30}Si$ signatures were generally highly variable in the upper 500m, reflecting the effect of a strong silicon pump that was quickly initiated in spring, while they were quite homogeneous in deeper waters. The Si-isotopic and mass balance identified a unique WW Si-source for the iron-fertilized area originating from the southeastern Kerguelen Plateau and that spread northward. However, when reaching a retroflection of the Polar Front (PF), the $\delta^{30}Si$ composition of

WW silicic acid pool was getting progressively heavier. This would result from sequential isopycnal mixings between these initial WW and ML water masses, highlighting the significant ventilation of surface waters associated to the strong mesoscale activity that defined this zone. When comparing the results from the two KEOPS-expeditions, the relationship between DSi depletion, BSi production and their isotopic composition appears decoupled in the iron fertilized area. The DSi reservoir evolved as an open system due to the high ML ventilation while the BSi pool behaved more as a closed system showing an exponential increasing of delta values that seemed to depend mainly on the Si-supply:Si-uptake ratio and the export efficiency of the system. This seasonal decoupling could help to explain the low apparent fractionation factor observed here in the ML at the end of summer. Taking into account these considerations, we refined the seasonal net BSi production of the iron-fertilized area to 3.0 ± 0.3 mol Si m^{-2} y^{-1}, that was exclusively sustained by ML phytoplankton population, and which was well consistent with previous estimates of BSi production for the Antarctic Zone. These insights confirm that the isotopic composition of dissolved and particulate silicon is a promising tool to improve our understanding on the Si-biogeochemical cycle since the isotopic and mass balance allows to resolve the processes involved i.e. uptake, dissolution, mixing. They will provide new constraints for application to biogeochemical models of seasonal controls on DSi consumption and BSi production and their variations over time in the naturally iron-fertilized Kerguelen area.

II.1. Introduction

The Southern Ocean plays a crucial role in the regulation of the global climate as it contributes significantly to the world's ocean primary production and represents a major carbon sink (Takahashi et al., 2009). In the Southern Ocean, diatoms, a phytoplankton group that produce an opaline cell wall or frustule (amorphous $SiO_2.nH_2O$), are responsible for more than 75% of the annual primary production in this ocean, in particular in the area south of the Antarctic Polar Front (PF) where they form massive blooms (e.g. Brzezinski et al., 2001). These latter are often associated with high carbon export events as diatoms could be easily removed from the mixed layer (ML) via aggregation, settling or grazing processes (Boyd & Trull, 2007; Buesseler 1998) and thus contribute to the extensive biogenic silica (hereafter referred to as BSi) deposition that characterize the sediments of this region (Tréguer & De la Rocha, 2013; Ragueneau et al., 2000). Since diatoms preferentially take up light ^{28}Si isotopes, their biological activity leaves a clear imprint on the isotopic composition of both silicic acid (H4SiO4, hereafter referred to as DSi) and BSi, enriching the DSi pool with heavy ^{30}Si isotope (De la Rocha et al.,

1997). While a recent study has point out that this preferential uptake may vary among diatom's species (Sutton et al., 2013), field studies have reported constant Si isotopic fractionation factor ($^{30}\varepsilon$) for the Antarctic Circumpolar Current, ACC (De la Rocha et al., 2000; Varela et al., 2004 ; Cardinal et al., 2005), estimated to -1.2 ± 0.2 ‰ on average (Fripiat et al., 2011a). On the opposite, it is not clear whether BSi dissolution fractionate silicon isotopes. The two only studies of this process based on controlled laboratory experiments give contradictory results. The most recent reported no preferential release of a given Si isotope when sediment core diatom opal enduring strong alkaline digestion (Wetzel et al., 2014), while Demarest et al. (2009) estimated a fractionation factor of -0.55 ‰ between relatively fresh siliceous particles and produced H_4SiO_4 reacting in an undersaturated seawater. This fractionation is opposite to the one occurring during Si uptake (BSi dissolution preferentially releases 28Si) which would reduce the overall (or net) fractionation factor. Thus, information on the silicon isotopic composition ($\delta^{30}Si$) potentially enables to identify DSi sources and discriminate and quantify different processes such as Si-uptake, BSi dissolution or physical (e.g. Fripiat et al., 2011a). Since they have absolute requirement for silicic acid, diatoms generate the largest latitudinal gradient of DSi from replete conditions south of the PF, in the Antarctic Zone (AZ), to depleted conditions in the Sub-Antarctic Zone (SAZ) (Pondaven et al., 2000; Brzezinski et al., 2001; Sarmiento et al., 2004). This contrasts strongly with the High Nutrient Low Chlorophyll (HNLC) characteristics of the Southern Ocean which could be more specifically defined as a High Nitrate Low Silicon Low Chlorophyll area (HNLSiLC). Indeed, the distribution of DSi is very different from those of the other macronutrients (e.g. phosphates and nitrate) (Trull et al., 2001; Sarmiento et al., 2004). The greater net depletion of silicic acid relative to nitrate in the ACC implies a strong silicon pump, i.e. the more efficient recycling of organic matter in surface water and the preferential export of BSi compared to particulate organic nitrogen (PON; Dugdale et al., 1995). Thus, during their northward transport, the nutrient-rich Antarctic Surface Waters (AASW) undergo a stronger decoupling between Si and N cycles that will impact lower latitudes via intermediate water mass formation in the northern ACC (Sarmiento et al., 2004). Overall, this induces a strong silicic acid limitation in low-latitude basins that could determine the efficiency of the global ocean carbon sink (Sarmiento et al., 2004; Matsumoto & Sarmiento, 2008).

Several studies based on in vitro and artificial Fe-enrichments showed that Fe stress is partly responsible for the HNLSiLC status of the SO (see review in De Baar et al., 2005; Boyd et al., 2007). The decoupling between Si and N in the Southern Ocean may be not exclusively due to difference in remineralisation rate of Si relative to N but also to the availability in micronutrient (and especially iron; Takeda, 1998; Hutchins & Bruland, 1998; Frank et al., 2000). It has been reported that under Fe stress, diatoms increase their Si:N uptake ratio, changing their degree of silicification and depleting surface

DSi stock well before nitrates (Leynaert et al., 2004; Bucciarelli et al., 2010). This has great implications in paleo-oceanography as it has been proposed that a silicic acid leakage hypothesis (SALH) driven by an increase of Fe-deposition in the Southern Ocean that have changed the Si:N ratios of diatoms could explain a significant part of the drop of atmospheric pCO_2 during glacial times by shifting AASW from the actual H_4SiO_4 seasonal drawdown toward NO_3^- depletion (Brzezinski et al., 2002; Mastumoto et al., 2002). Thus, understanding the processes that control this decoupling and the nutrient distribution in the Southern Ocean is of critical importance to improve our knowledge about the role of the Southern Ocean in regulating global biogeochemical cycles of nutrients. In this context, several studies has been performed on the role of iron in nutrient biogeochemical cycles, in regions characterized by natural (or artificial) Fe-fertilization such as the Kerguelen Plateau (e.g. KEOPS program; Blain et al., 2007).

The KEOPS program consisted of two expeditions (late-summer 2005 and early-spring 2011) conducted in a naturally iron-fertilized area located in the Indian sector of the Southern Ocean where a massive diatom bloom is observed annually in the vicinity of the Kerguelen Plateau, contrasting with the HNLC character of nearby environment (Pollard et al., 2002; Mongin et al., 2008). The first KEOPS expedition (January-February 2005) has highlighted that this bloom is sustained by continuous iron supply originated from iron-rich deep waters to the Mixed Layer (ML), through enhanced vertical inputs associated to internal waves that interact with the local bathymetry (Blain et al., 2007; Park et al., 2008b). A strong decoupling between NO_3^- and H_4SiO_4 was observed above the Plateau in February with concentrations > 20 µmol L^{-1} and close to 0, respectively (Mosseri et al., 2008). These authors have suggested that the decline of the bloom was strongly controlled by silicic acid and iron co-limitations. Results from KEOPS-2 (October-November 2011) show that the Kerguelen's bloom was characterized by a complex and heterogeneous distribution of phytoplankton communities and dynamics (e.g. Cavagna et al., 2014; Closset et al., 2014; Lasbleiz et al., 2014), in response to a mosaic of biogeochemical conditions that originate from the strong mesoscale activity prevailing in the vicinity of the Kerguelen Islands (Park et al., 2014). Silicon isotopes were studied during this first cruise and highlighted important aspects of the Si biogeochemical cycle in both the HNLC and the fertilized area (Fripiat et al., 2011a). Using the HNLC WW Si properties, they estimated a seasonal net BSi production of 10.5 ± 1.3 mol Si m^{-2} y^{-1} in the iron-fertilized waters with a significant contribution from diatom silicification in the deep BSi maximum. The net BSi production in the ML (5.0 ± 0.3 mol Si m^{-2} y^{-1}) was slightly higher than published values for the AZ (2.4 to 3.3 mol Si m^{-2} y^{-1}; Pondaven et al., 2000; Nelson et al., 2002; Pollard et al., 2006), probably because they did not have access to the appropriate initial conditions that prevail before diatom development. By comparing this net BSi production and the seasonal H_4SiO_4 depletion, and by considering the Si isotopic dynamics above the Kerguelen Plateau,

they evidenced that the ML received at least an additional 1.5 mol Si m^{-2} during the growth period, providing firm evidence of the significant ventilation of the Plateau waters. Combining the Si-properties of KEOPS-1 HNLC waters and those of previous studies in the ACC, they refined the ACC fractionation factor estimate to - 0.2 ± 0.2 ‰ and demonstrated the usefulness of the Si isotopic tool to quantitatively investigate the Si-biogeochemical cycle and to discriminate between the different processes involved (e.g. BSi production and dissolution, water mixing).

In this paper, we investigate the spatial and seasonal variability of silicon isotopic composition of both seawater ($\delta^{30}Si_{DSi}$) and siliceous particles ($\delta^{30}Si_{BSi}$) in deep and surface waters of the Kerguelen area during the spring period. Our specific objectives are the following:

- Describe the early spring spatial distribution of silicon isotopes in contrasting productive (and non productive) environments off Kerguelen Islands.

- Discuss the potential role of iron in regulating the Si biogeochemical cycle and isotope dynamic in the Southern Ocean surface and subsurface waters.

- Finally, identify and track the Si sources that fuel the phytoplankton bloom above the Plateau and characterize the temporal evolution of silicon biogeochemical cycle by combining our results KEOPS-2 with KEOPS-1 data which correspond to the bloom decline.

II.2. Material and Methods

II.2.1 Cruise settings, KEOPS-2 sampling strategy

The KEOPS-2 expedition was conducted in the Kerguelen Plateau region (Indian sector of the Southern Ocean) from 10 October to 20 November 2011 (austral spring) on board of the R/V Marion Dufresne (TAAF/IPEV). This shallow Plateau acts as a barrier to the ACC whose 60% of the total flux passes north of the Kerguelen Islands, mostly associated with the SAF, while 40% is transported across the southern part of the Plateau and forms the jet of the PF (Park et al., 2008a, 2014; Roquet et al., 2009). This strong current is then deflected to the north following the eastern escarpment of the Plateau and forms a permanent cyclonic meandering associated to strong mesoscale activity (Park et al., 2014; Zhou et al., 2014). As a consequence, the circulation in the northern Kerguelen Plateau south of this PF is relatively weak (Park et al., 2008a; Roquet et al., 2009) and has great potential for

sustaining elevated primary production (Blain et al., 2001; Mongin et al., 2008). There, the biological activity is fuelled by iron and macronutrients originated from deep layers, which are supplied to the ML via enhanced vertical mixing associated with internal waves (Park et al., 2008b). These particular hydrographic features generate contrasted biogeochemical and physical environments where phytoplankton communities will respond differently to iron availability. During KEOPS-2, the vertical structure of water masses was characteristic of the Antarctic zone (AZ) in the vicinity of the PF (Park et al., 2008a). Except for the first visit at over the Plateau (A3) where they reached the surface, the remnant Winter Water (WW, generally from 100 to 400m), where capped by a homogeneous, warm and fresh mixed layer (ML or AASW) induced by seasonal stratification. Below these subsurface waters, a subsurface temperature maximum between 400 and 1400 m associated to the Upper Circumpolar Deep Waters (UCDW), followed by an oxygen minimum between 1400 and 2600 m that correspond to the Lower Circumpolar Deep Water (LCDW) in all the out-Plateau stations. The deeper Antarctic Bottom Waters (AABW) were found only at station F-L, north of the PF.

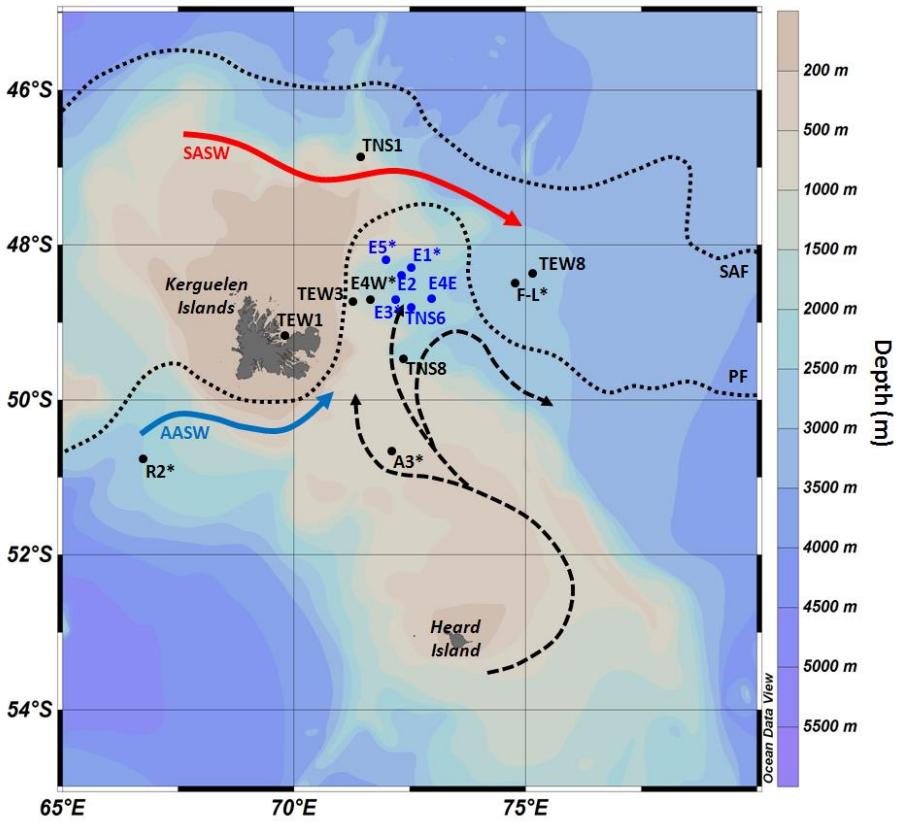

Figure 2.2. Map of the KEOPS-2 cruise area (Indian sector of the Southern Ocean) showing the location of stations discussed in this study and the general surface circulation (black arrows: above the Plateau; blue arrow: the Antarctic Surface Waters; red arrow: the Sub-Antarctic Surface Water; from Park et al., 2014). Dotted line represents the position of the Polar Front (PF) and the Sub-Antarctic Front (SAF) defined by Park et al. (2014).

The cruise consisted in two transects north to south (TNS stations) and east to west (TEW stations) aiming at documenting the spatial extension of the bloom and its coastal-offshore gradient; and 9 long-term stations devoted to process studies (*Fig. 2.2.*):

- A HNLC reference station (R-2) located upstream of the eastward ACC flow, south of the Kerguelen Islands.

- 2 visits at the KEOPS-1 Plateau bloom reference station (A3-1 and A3-2).

- A productive station (E-4W) located in the plume of chlorophyll north of A3 and close to the jet induced by the PF.

- An open ocean station (F-L) influenced by warmer Subantarctic Surface Water, located north of the PF.

- 5 stations (E-1 to E-5) constituting a pseudo-Lagrangian survey and located in the area of PF retroflection characterized by strong mesoscale activity (Zhou et al., 2014) and hereafter referred to as the Meander.

II.2.2. Sample collection and preparation

Si isotopic compositions from a total of 236 seawater samples and 138 particulate samples are presented in this study (*Table B2.*). These latter included 80 samples collected in the ML using Niskin bottles and 58 samples coming from *in situ* pumps (ISP). At all stations, seawater and particles were collected using a CTD (Conductivity-Temperature-Depth) rosette equipped with 12 L Niskin bottles. Seawater (approximately 5 L) was immediately filtered through polycarbonate membranes (Nuclepore, 0.4 µm) using large volume filtration units. Filtered water samples were stored in the dark in acid cleaned polypropylene bottles and membranes were dried overnight at 50 °C and stored in polycarbonate Petri dishes at room temperature. Since particle concentration decreases with depth, deep-water particles were collected using in-situ pumps at 7 stations (see *figure 2.2.*) by filtering 70 to 1800 L of seawater through hydrophilic polyestersulphone membranes (SUPOR, 0.8 µm). Approximately 1/8 of the SUPOR membranes were dedicated to silicon isotopic analysis and were dried overnight at 50 °C and stored in Petri dishes at room temperature.

a) Particles digestion and BSi analyses

The membranes (Nuclepore and SUPOR) were subjected to a wet-alkaline digestion (adapted from Ragueneau et al., 2005). BSi was dissolved in Teflon tubes using a 0.2 µmol L^{-1} NaOH solution (pH 13.3) at 100°C for 40 min followed by neutralization with HCl (1 mol L^{-1}). As this digestion can also solubilize some lithogenic silica (mainly clay minerals), a second and identical digestion was applied to the membranes, and aluminum (Al, a tracer of lithogenic source) was analyzed in the two leachates using an Inductively Coupled Plasma Mass Spectrometer (ICP-MS; detection limit = 3.18 ppb). Using the Si:Al ratio measured in the 2nd digestion, potential lithogenic silicon dissolved in the first digestion can be estimated (Ragueneau et al., 2005). Unfortunately, polycarbonate membranes used for silicon isotopic analysis were contaminated by Al during filtrations onboard. However, SUPOR filters as well as Al concentrations estimated on other filters (Lasbleiz et al., 2014) revealed negligible lithogenic silicon in the first leachate (on average 1.26 % for SUPOR filters). Such a lithogenic contribution should not bias significantly our $\delta^{30}Si$ value except in station TEW3 where $\delta^{30}Si_{BSi}$ were unusually light (0.57 ± 0.16 ‰, *not shown*), and that will not be taken into account in the following discussion. Indeed, using a light end-member $\delta^{30}Si_{LSi}$ of -2.3 ‰ reported in clays (Opfergelt & Delmelle, 2012) and our maximum $\delta^{30}Si_{BSi}$ (2.06 ‰ station R2, 2400m) as extreme end-members, we calculated a maximum interference in the isotopic signal of 0.05 ‰ which is similar to our analytical precision for $\delta^{30}Si$ (0.05 ‰, cf below). BSi concentrations were determined with a colorimetric method according to Grasshoff et al. (1999) and by ICP-MS on the same samples as for Si-isotopic composition. Every ISP samples has been analyzed in duplicates with a pooled standard deviation of 5.0 ± 4.6 % (n = 58), which corresponds to our average reproducibility of BSi measurements, and which is slightly better than the uncertainty estimated for this method (10 %, Ragueneau et al., 2005). Moreover, independent measurements of BSi concentration from the surface to 900 m performed during KEOPS-2 by Lasbleiz et al. (2014) on other filters from same stations were similar to our results and indicated that no significant bias occurred regardless to the method used.

b) Seawater preconcentration and DSi analyses

A two-step preconcentration procedure adapted from the MAGIC method (Karl & Tien, 1992; Reynolds et al., 2006) was performed on seawater samples to increase H_4SiO_4 concentration and reduce the anionic matrix that could interfere with Si during isotopic analysis (e.g. sulfates, SO_4^{2-}; Hughes et al., 2011). DSi was co-precipitated in two steps with brucite ($Mg(OH)_2$) by adding 2% (v/v), following by 1% (v/v) of 1M NaOH to the seawater sample. This solution was shaken and left for 1h and the precipitate was recovered by centrifugation and redissolved with 1M HCl. The supernatant

was removed and analyzed for Si concentration using colorimetric method according to Grasshoff et al. (1999). Complete Si recovery was monitored by checking systematically that no detectable amount of silicic acid remained in the supernatant after coprecipitation and centrifugation. DSi concentrations in seawater samples were determined with a colorimetric method (Grasshoff et al., 1999) on the same samples as for Si-isotopic composition. Average reproducibility of DSi measurements is 6.7 % (calculated from 98 in-house silicon solution analyses at the ± 1 sd level).

II.2.3. Purification

Separation of Si from other ions in the sample was achieved by passing the solution through a cation-exchange column (BioRad cation exchange resin DOWEX 50W-X12, 200 to 400 mesh, in H^+ form) using a protocol described in Georg et al. (2006). After purification systematic analysis of major elements (such as Mg, Ca, Na, Al) were performed by ICP-MS to ensure the sample purity prior to isotopic analyses (Si/X weight ratio usually > 50). Si concentrations were also measured in the purified solutions to check for complete recovery. This purification step did not allow the complete removal of the anionic matrix, which consists primarily of Cl^-, SO_4^{2-} and to a lesser extent PO_4^{3-} and NO_3^-. Cl- originating from seawater can be neglected compared to Cl- added as HCl to dissolve the brucite. Therefore the solutions dedicated to DSi isotopic measurements were analyzed by anionic chromatography to control the concentration of sulfates. Indeed, in these samples, SO_4^{2-} concentrations could induce a significant shift in isotopic measurements (*see supplementary method 2* and Van den Boorn et al. (2009) for rock digestion solutions). Thus, as proposed by Hughes et al. (2011), samples and standards used for DSi isotopic analyses were doped with sulfuric acid in large excess compared to the natural SO_4^{2-} concentrations in order to control this sulfate matrix effect

II.2.4. Isotopic measurements

The purified and sulfates doped Si solutions were analyzed for isotopic measurements on a Thermo Neptune$^+$ Multicollector Inductively Coupled Plasma Mass Spectrometer (MC-ICP-MS; LSCE, Gif-sur-Yvette) in dry plasma mode using Mg external doping to correct for the mass bias (Cardinal et al., 2003; Abraham et at., 2008). Samples were injected into the plasma with an Apex desolvating nebulization system connected with a PFA nebulizer (100 µL min^{-1} uptake rate) and without additional gaz. Silicon isotopic compositions ($\delta^{30}Si$) were calculated as the permil deviation from the quartz standard NBS28 (RM8546). They were measured relative to an in-house standard Quartz Merck, which

was not significantly different from NBS28 (Abraham et al., 2008), analyzed immediately after and before the sample and expressed as:

$$\delta^{30}Si\ (‰) = \left[\frac{(^{30}Si/^{28}Si)sample}{(^{30}Si/^{28}Si)standard} - 1\right] \times 1000 \qquad (2.1.)$$

Blanks levels were below 1% of the main signal and were subtracted from each sample and standard analyses. Measurements were carried out in medium resolution mode (M/ΔM > 6000) to optimize the separation of ^{30}Si peak and $^{14}N^{16}O$ interference (< 0.5 % of the ^{30}Si peak) and were performed on the interference free left side of the peak (Abraham et al., 2008). δ^{29}Si and δ^{30}Si were compared to the mass dependent fractionation line (*Fig. B2.*) and samples falling outside of its analytical error were excluded from final dataset. Typical analytical conditions are provided in *Table 2.1*.

Table 1: Neptune^{+} MC-ICP-MS operating conditions

Resolution	Medium
Foward Power	1200 W
Accelerating Voltage	10 kV
Plasma Mode	Dry Plasma
Cool Gas Flow Rate	16 L min^{-1}
Auxiliary Gas Flow Rate	1.1-1.4 L min^{-1}
Sample Gas Flow Rate	0.9-1 L min^{-1}
Cones Type	Nickel X-Skimmer cone + Standard Ni-Sample cone
Desolvator	Apex (ESI)
Nebulizer	PFA microcentric nebuliser 100 µL min^{-1}
Running Concentrations	Si = 2-2.5 ppm, Mg = 2-2.5 ppm
Sensitivity	3-4 V ppm^{-1}
Blank Level	< 1% signal
^{30}Si Interference	< 30 mV (usually 10-15 mV)

Numerous analyses of a secondary reference material such as Diatomite (δ^{30}Si = 1.26 ‰ and δ^{29}Si = 0.64 ‰, Reynolds et al., 2007) generated over the entire procedure indicated an average precision and a long-term analytical reproducibility (24 months) on δ^{30}Si values of 1.28 ± 0.05 ‰ and 0.66 ± 0.06 ‰ for δ^{29}Si (1 sd, n = 128) and confirmed that no uncorrected isotopic bias occurred. All BSi samples and some DSi samples have been fully replicated and measured on separate days (chemical preparation plus isotopic measurements). In these cases, the average global reproducibility on full duplicates δ^{30}Si is 0.06 ‰ (1 sd, n= 108) and 0.04 ‰ (n= 78) for $\delta^{30}Si_{BSi}$ and $\delta^{30}Si_{DSi}$ respectively.

Error bars shown in all figures correspond to the analytical reproducibility or to the global reproducibility if greater than 0.05 ‰.

II.3. Results

II.3.1. General considerations

During KEOPS-2, $\delta^{30}Si_{DSi}$ displayed a clear inverse relation with silicic acid concentration as commonly observed in the Southern Ocean (*Fig. B3.*; De la Rocha et al., 2000; Cardinal et al., 2005; Fripiat et al., 2011a, 2011b, 2012; Cavagna et al., 2011; De Souza et al. 2012). The water column profiles showed a general increase in H_4SiO_4 concentrations while isotopic composition of silicic acid became gradually lighter with depth. In the upper 500m, $\delta^{30}Si_{BSi}$ values were systematically lighter than $\delta^{30}Si_{DSi}$ values in agreement with the preferential uptake of ^{28}Si by diatoms (De La Rocha et al., 1997). Below 500 m there was still a slight increase of $\delta^{30}Si_{BSi}$ and a decrease of $\delta^{30}Si_{DSi}$ values coincident with increasing H_4SiO_4 concentrations. In contrast to the ML, $\delta^{30}Si_{BSi}$ were there systematically higher than $\delta^{30}Si_{DSi}$ (on average 1.74 ± 0.13 and 1.20 ± 0.17 ‰, respectively). This situation differs significantly from the one observed in the Atlantic sector in summer by Fripiat et al. (2012) where the isotopic signature of BSi exported to depth was directly comparable to the $\delta^{30}Si_{BSi}$ values of particles in the ML. The surface KEOPS-2 $\delta^{30}Si_{BSi}$ (ranging from 0.47 ‰ to 2.04 ‰) and $\delta^{30}Si_{DSi}$ (ranging from 1.96 ‰ to 2.79 ‰) encompass nearly the full range of delta results reported from previous Southern Ocean studies (-0.7 ‰ to 2.8 ‰ for BSi and 0.5 ‰ to 4.4 ‰ for DSi, e.g. Cao et al., 2012; De Souza et al., 2012; Fripiat et al., 2012). *Figure 2.3.* shows the central values and dispersion of $\delta^{30}Si_{DSi}$ calculated as the median value and interquartile range respectively, for each water mass present in the main KEOPS-2 stations.

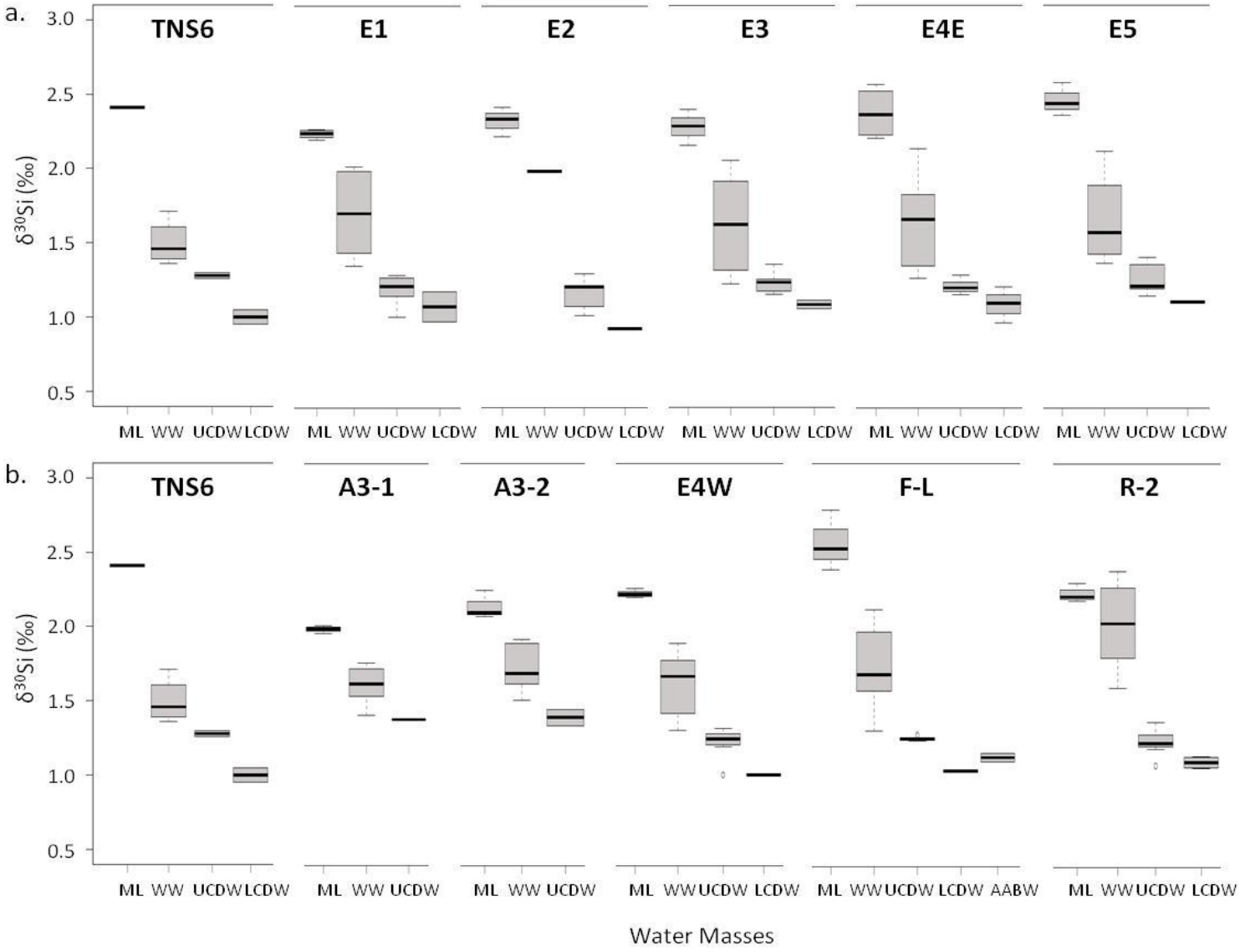

Figure 2.3. Central value and dispersion of silicic acid $\delta^{30}Si$ of the main water masses for stations of (a.) the Meander and (b.) contrasted KEOPS-2 stations (note that transect stations are not shown). The boxes, whiskers and symbols cover the 25th to 75th, the 10th to 90th and the 5th to 95th percentiles, respectively. Strait lines represent the median and dots are outliers. Water masses are the Mixed Layer (ML), Winter Waters (WW), Upper circumpolar Deep Waters (UCDW), Lower Circumpolar Deep Waters (LCDW), and Antarctic Bottom Waters (AABW).

In general, $\delta^{30}Si_{DSi}$ signatures in KEOPS-2 deep waters were homogeneous and did not show large changes with depth or between stations (on average 1.28 ± 0.08 ‰ and 1.05 ± 0.06 ‰ for UCDW and LCDW respectively). There is a much higher variability in Si-isotopic composition between stations, with central values ranging from 1.99 ‰ to 2.53 ‰ and 1.46 ‰ to 2.03 ‰ in the ML and WW respectively. Note that the WW exhibited systematically the largest dispersion of delta values and were systematically associated to a strong isotopic gradient toward light $\delta^{30}Si_{DSi}$ with depth (*not shown*). Consequently, the mean and median values were probably not representative of the real WW Si-properties. Usually, the depth displaying a temperature minimum (T-min between 1.5 and 2°C in the Kerguelen area; Park et al., 2014) is chosen as the most traditional definition of the remnant surface winter water. However, in some stations, it was not possible to clearly determine T-min (e.g. R2 and E2) and/or there was a significant salinity gradient above the T-min depth (e.g. TNS01, F-L). Trull et al. (2014) have proposed that a shallower depth based on a threshold increase in salinity of 0.05 (S-threshold depth) could better represent the WW characteristics. They ascribed this situation to a weaker winter mixing compared to previous year and thus, the nutrient depletion between the T-min and S-threshold depths could not be associated to recent consumption. In the following we will use the S-threshold approach since it would be the most appropriate to reflect the pre-bloom biogeochemical conditions (see *Table 2.2*).

Table 2: Central values of H_4SiO_4 concentrations (µmol L^{-1}) and $\delta^{30}Si_{DSi}$ signatures (‰) for different water masses across the Kerguelen Plateau region (ML: Mixed Layer; WW: Winter Water; UCDW: Upper Circumpolar Deep Water; LCDW: Lower Circumpolar Deep Water; AABW: Anatarctic Bottom Water). Except for the WW, median and interquatile range 2/3 represent the "central values" and dispersion for the water masses. Since they displayed the strongest gradient of values, the WW Si-properties were defined using the threshold salinity method (see text for further details).

		ML		WW		UCDW		LCDW		AABW	
Station	**CTD #**	**$[H_4SiO_4]$ (µmol L^{-1})**	**$\delta^{30}Si_{DSi}$ (‰)**	**$[H_4SiO_4]$ (µmol L^{-1})**	**$\delta^{30}Si_{DSi}$ (‰)**	**$[H_4SiO_4]$ (µmol L^{-1})**	**$\delta^{30}Si_{DSi}$ (‰)**	**$[H_4SiO_4]$ (µmol L^{-1})**	**$\delta^{30}Si_{DSi}$ (‰)**	**$[H_4SiO_4]$ (µmol L^{-1})**	**$\delta^{30}Si_{DSi}$ (‰)**
A3-1	4	22,89 ± *0,53*	1,99 ± *0,03*	31,55 ± *2,21*	1,76 ± *0,03*	70,39 ± *0,00*	1,38 ± *0,00*				
TNS08	8	18,41 ± *0,84*	2,30 ± *0,06*	26,80 ± *1,88*	1,93 ± *0,03*	72,46 ± *4,61*	1,22 ± *0,05*				
TNS06	10	16,56 ± *3,93*	2,41 ± *0,00*	31,31 ± *2,19*	1,71 ± *0,02*	73,26 ± *5,39*	1,28 ± *0,02*	92,17 ± *3,79*	1,00 ± *0,05*		
TNS01	15	8,96 ± *0,50*	2,26 ± *0,07*	13,40 ± *0,94*	2,23 ± *0,11*	57,49 ± *8,23*	1,35 ± *0,04*	89,20 ± *8,39*	1,01 ± *0,01*		
R2	17	12,94 ± *0,49*	2,21 ± *0,06*	21,74 ± *1,52*	1,92 ± *0,04*	66,18 ± *15,18*	1,23 ± *0,08*	90,91 ± *16,85*	1,10 ± *0,07*		
E1	27	15,92 ± *1,97*	2,24 ± *0,04*	28,88 ± *2,02*	1,84 ± *0,06*	76,46 ± *5,24*	1,22 ± *0,11*	94,72 ± *6,34*	1,08 ± *0,10*		
TEW1	35	13,93 ± *3,73*	2,19 ± *0,22*								
TEW3	38	15,93 ± *8,76*	2,31 ± *0,16*	24,74 ± *1,73*	1,86 ± *0,03*	75,14 ± *0,00*	1,41 ± *0,02*				
E2	43	17,65 ± *3,23*	2,34 ± *0,10*	20,32 ± *1,42*	1,99 ± *0,02*	73,80 ± *2,30*	1,21 ± *0,14*	75,24 ± *0,00*	0,93 ± *0,04*		
TEW8	47	9,20 ± *2,24*	2,47 ± *0,03*	20,62 ± *1,44*	2,08 ± *0,03*	66,67 ± *9,20*	1,40 ± *0,06*	133,84 ± *0,00*	1,07 ± *0,00*		
E3	50	16,67 ± *3,72*	2,23 ± *0,16*	28,88 ± *2,02*	1,92 ± *0,01*	78,85 ± *4,75*	1,24 ± *0,06*	82,52 ± *0,00*	1,09 ± *0,03*		
FL	63	8,70 ± *1,17*	2,53 ± *0,20*	14,42 ± *1,01*	2,12 ± *0,07*	70,70 ± *7,11*	1,26 ± *0,01*	101,94 ± *0,00*	1,04 ± *0,04*	135,36 ± *0,00*	1,13 ± *0,03*
E4W	81	19,90 ± *4,66*	2,21 ± *0,11*	36,71 ± *2,57*	1,67 ± *0,03*	76,46 ± *5,00*	1,25 ± *0,07*	101,94 ± *0,00*	1,01 ± *0,03*		
E4E	94	15,42 ± *7,46*	2,36 ± *0,26*	20,62 ± *1,44*	2,21 ± *0,02*	78,28 ± *3,58*	1,20 ± *0,05*	90,61 ± *2,72*	1,10 ± *0,08*		
A3-2	107	19,56 ± *0,48*	2,10 ± *0,05*	31,90 ± *2,23*	1,69 ± *0,03*	71,66 ± *8,56*	1,39 ± *0,05*				
E5	114	12,94 ± *0,00*	2,44 ± *0,11*	22,75 ± *1,59*	2,12 ± *0,04*	86,31 ± *13,67*	1,21 ± *0,13*	112,72 ± *0,00*	1,11 ± *0,04*		

II.3.2. Spatial distribution of Si isotopes in the Kerguelen area

The spatial variability of Si-isotopic signatures was studied along a west to east (TEW) and a south to north sections (TNS) covering the Plateau and the basin east of Kerguelen Islands (*Fig. 2.4.*).

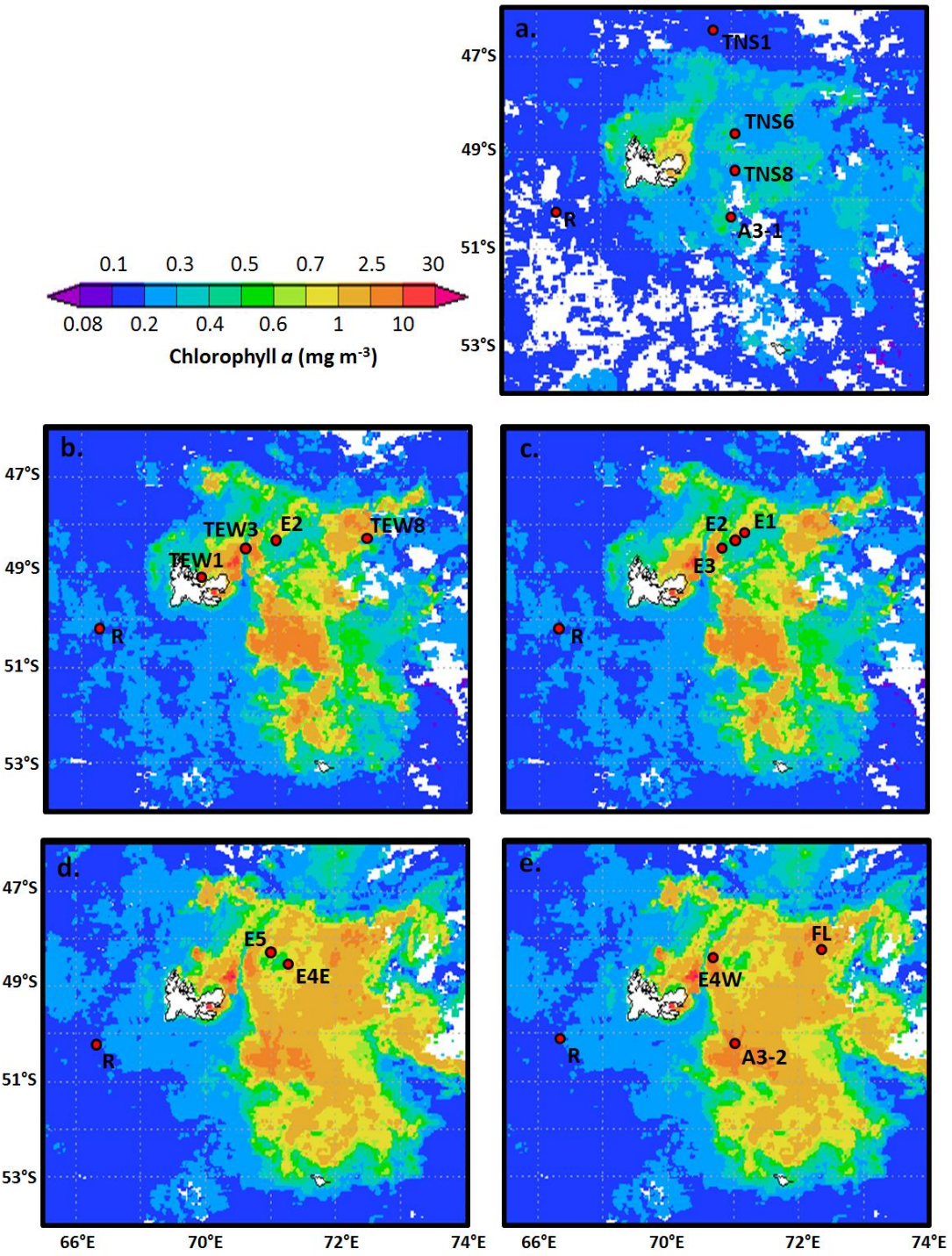

Figure 2.4. SeaWiFS composite satellite images (generated by Nasa's Giovanni, giovanni.gsf.nasa.gov) of the chlorophyll *a* distribution in KEOPS-2 surface waters around the date of the differents operations, along with the corresponding sampled stations. Note that the HNLC reference station (R) was sampled at the beginning of the cruise but appears in all panels as a reference.

The TNS transect was characterized by very low chlorophyll *a* and biogenic silica biomasses (*Fig. 2.4.*) and a decreasing gradient of surface H_4SiO_4 concentrations northward from 22.89 ± 0.53 µmol L^{-1} above the plateau (A3-1) to 8.96 ± 0.5 µmol L^{-1} north of the PF (TNS1, *Fig. 2.5.*). Accordingly, the $\delta^{30}Si_{DSi}$ displayed lighter values above the plateau (A3-1, 1.99 ± 0.03 ‰) compared to north of the PF (TNS1, 2.26 ± 0.07 ‰), but higher $\delta^{30}Si_{DSi}$ signatures were found in the middle zone of this transect which corresponds to the station located in the PF meander (TNS6, 2.41 ± 0.00 ‰). The $\delta^{30}Si_{BSi}$ displayed a similar trend with the lightest Si-isotopic composition above the plateau (A3-1, 0.77 ± 0.5 ‰) and increasing values northward (up to 1.31 ± 0.04 ‰ at station TNS1), in accordance with increasing production (and increasing BSi stock) as the spring season progresses. Note that TNS1 was distinct from other stations by its typical PFZ characteristics, i.e. low chlorophyll *a* biomass with greater proportion of nano-phytoplankton (Lasbleiz et al., 2014), warmer and fresher surface water and the influence of AAIW between 200 and 600 m (*Fig. 2.6.*, Park et al., 2014). Thus, its low DSi and BSi content and quite heavy Si-isotopic composition of both seawater and particles can likely be explained by its off-plateau location north of the PF which acts as a boundary isolating northern, warm and poor waters from southern, cold and productive waters of the Kerguelen region.

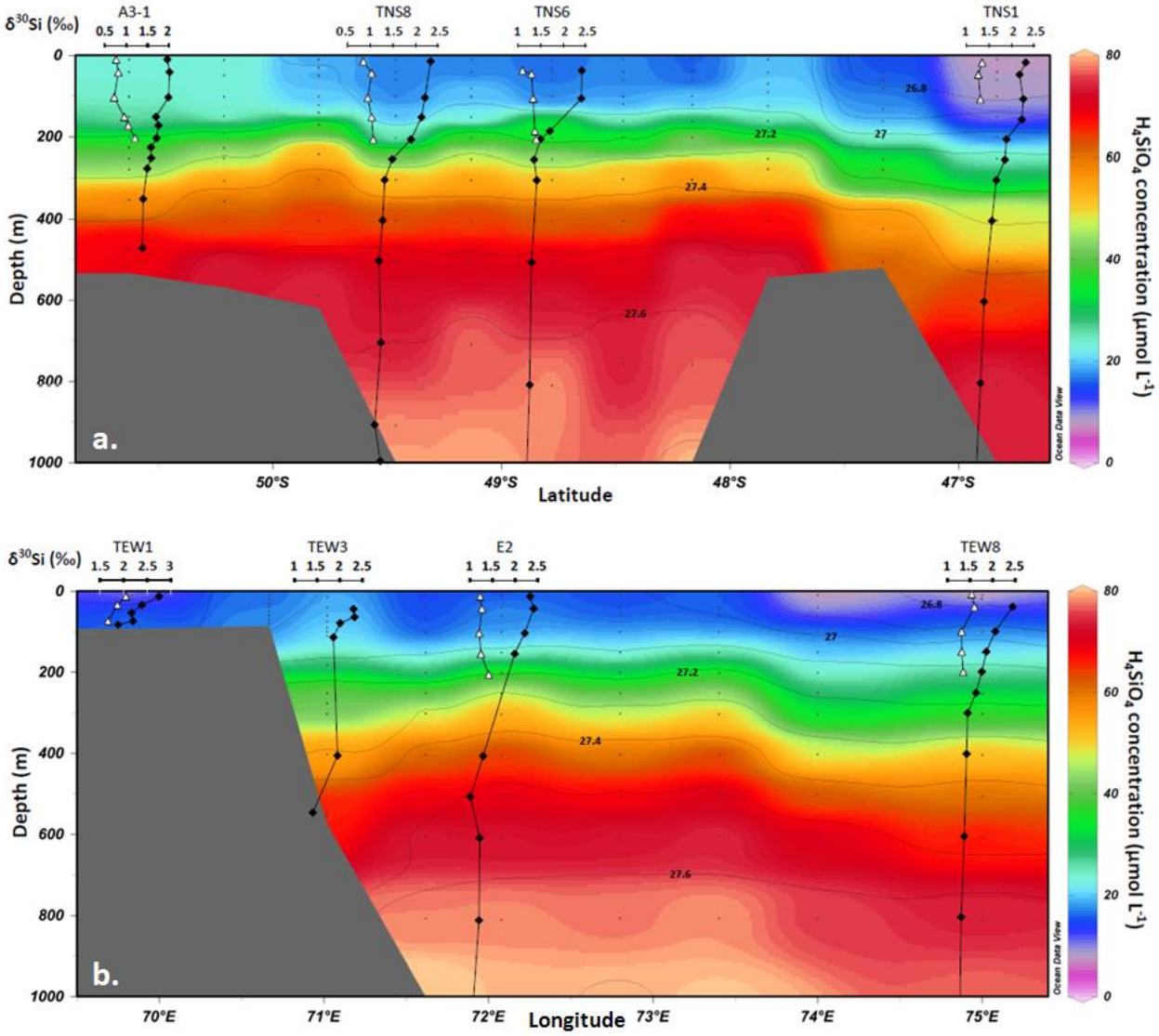

Figure 2.5. Relationship between density (thin black lines) and silicic acid concentration (color shade, µmol L^{-1}), with depth profiles of silicon isotopic composition of seawater (black diamonds) and biogenic silica (white triangles) for (a.) the North-South transect (TNS) and (b.) the East-West transect (TEW).

The TEW transect is composed by 4 stations representing very distinct features across the Kerguelen area. TEW1 exhibited very heavy values of $\delta^{30}Si_{DSi}$ and $\delta^{30}Si_{BSi}$ (2.19 ± 0.22 ‰ and 1.86 ± 0.19 ‰, respectively; *Fig. 2.3.*) in accordance with its coastal situation holding chlorophyll *a* and biogenic silica concentrations (Lasbleiz et al., 2014). The strong phytoplankton growth observed at this shallow station located north of the Kerguelen Islands was likely impacted freshwater discharge from the numerous rivers along the east coast of Kerguelen Islands (*Fig. 2.6.*). TEW3 is located in the vicinity of the western branch of the PF that flow northward along the shelf-edge (Park et al., 2014) and is

associated to a narrow band of low chlorophyll *a* and low BSi water displaying relatively heavy $\delta^{30}Si_{DSi}$ signature (2.32 ± 0.01 ‰, *Fig. 2.4.*). This very low production regime was likely associated to a concentrated strong flow originated from the southwest where phytoplankton growth was limited by unfavorable light-mixing conditions. E2 was sampled in the deep middle zone of this transect and displayed intermediate $\delta^{30}Si_{DSi}$ and $\delta^{30}Si_{BSi}$ signatures in accordance with its moderate production and nutrient standing stock characteristics (*Fig. 2.4.*). TEW8 was located north of the PF in the plume that extend northeastward of the island in relatively warm surface waters with low DSi content (*Fig. 2.4.* and *Fig. 2.5.*). During KEOPS-2, this station exhibit high biomass (Chlorophyll *a* and BSi) thanks to its moderate iron enrichment originated from the northern Kerguelen Plateau (Bowie et al., 2014; Sanial et al., 2014). These biogeochemical conditions yielded the heavy $\delta^{30}Si_{DSi}$ and $\delta^{30}Si_{BSi}$ signatures measured in the ML (2.47 ± 0.03 ‰ and 1.59 ± 0.03 ‰, respectively; *Fig. 2.3.*) and will be discussed in details along with F-L in *section II.4.2*.

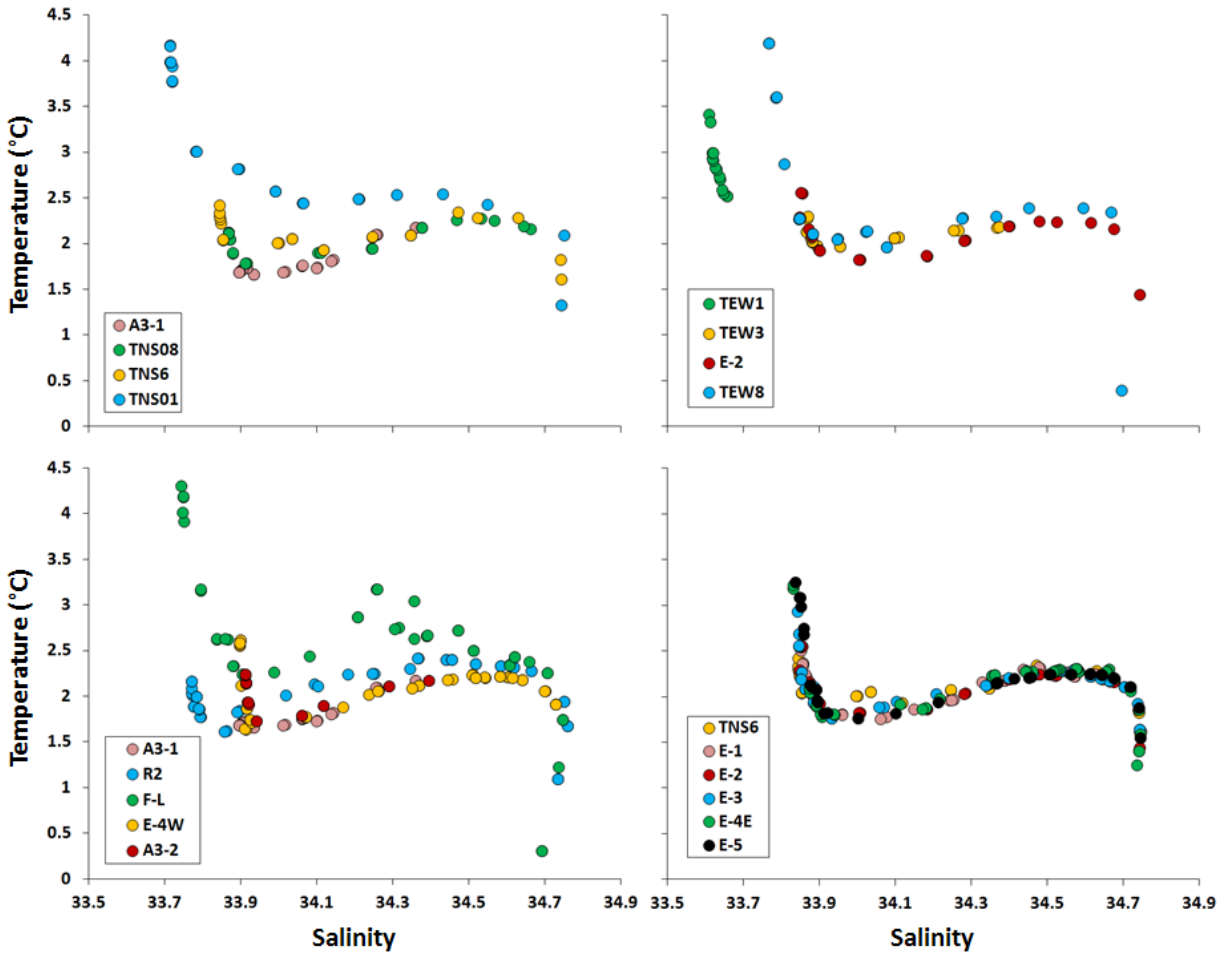

Figure 2.6. Potential temperature – salinity (θ-S) diagram for all KEOPS-2 stations

II.4 Discussion

II.4.1. General models on isotopic fractionation accompanying nutrient consumption

Isotopic variations induced by biological Si-utilization in the Southern Ocean ML could be described in a first approximation using 2 different models, for closed and open systems. In the closed system (also referred to as Rayleigh model) the surface ocean is considered to have a finite pool of DSi and nutrient consumption is not replenished by any external sources. In this case, the reaction progresses in a sequential mode over time, consuming substrate (here silicic acid) that was initially present in the ML, and increasing exponentially its $\delta^{30}Si$ (*equation 2.2.*). The isotopic composition of the short-term or instantaneous product (here exported BSi, *equation 2.3.*) differs from the long-term product that accumulates (here in the ML) and finally hold the same signature than the initial substrate when everything is consumed in the system (*equation 2.4.*):

$$\delta^{30}Si_{sub} = \delta^{30}Si_{init} - {}^{30}\varepsilon \ln(1-f) \qquad (2.2.)$$

$$\delta^{30}Si_{inst} = \delta^{30}Si_{sub} + {}^{30}\varepsilon \qquad (2.3.)$$

$$\delta^{30}Si_{acc} = \delta^{30}Si_{init} + {}^{30}\varepsilon \left(\frac{f \times \ln f}{1-f}\right) \qquad (2.4.)$$

where $^{30}\varepsilon$ is the isotopic fractionation factor of the reaction, *f* the fraction of the remaining substrate and the subscripts “sub”, “init”, “acc” and “inst” refer to the remaining substrate, the initial substrate, the accumulated product and the instantaneous product respectively.

The contrasting system is an open flow-through system (also referred to as steady-state model) where continuous supplies of substrate balance the export of product. In this model, the DSi supply equals the sum of the BSi produced and immediately exported and the residual H_4SiO_4 stock leaving the system. Only one product forms from substrate and both $\delta^{30}Si_{DSi}$ and $\delta^{30}Si_{BSi}$ signatures display linear changes (*equations 2.5.* and *2.6.*):

$$\delta^{30}Si_{sub} = \delta^{30}Si_{init} - {}^{30}\varepsilon(1-f) \qquad (2.5.)$$

$$\delta^{30}Si_{prod} = \delta^{30}Si_{init} + {}^{30}\varepsilon \times f \qquad (2.6.)$$

In these ideal situations, the $\Delta^{30}Si$, i.e. the difference between $\delta^{30}Si_{DSi}$ and $\delta^{30}Si_{BSi}$, is considered as constant and homogeneous. In the ocean, it could actually be altered by other processes such as water mixing or BSi dissolution that would affect the isotopic and mass balance (e.g. Demarest et al., 2009). Moreover, it is likely that natural environments rather proceed in a mixed way between these ideal closed and open systems, with real fractionation trend lying between the 2 curves depending on

the Si-uptake:Si-supply ratio occurring in the system (Fry 2006). This could be particularly the case in the Southern Ocean where large nutrient consumption was observed in regions characterized by intense mixing events that strongly deepen the ML and bring H_4SiO_4 in surface waters (e.g. Brzezinski et al., 2001; Nelson et al., 2001).

II.4.2. Distribution of Si isotopes vs. source and supply of iron

a) The HNLC reference station

In the ML the productive high biomass and HNLC areas exhibited significant different silicon isotopic composition of both seawater and particles, reflecting the different degrees of Si-utilization by diatoms throughout KEOPS-2 expedition.

The HNLC reference station (R-2) supported low chlorophyll *a* and BSi biomass and very low Si-uptake rates, consistent with its iron-depleted condition and the dominance of non-siliceous organisms (see details in Lasbleiz et al., 2014 and Closset et al., 2014). In surface waters, the concentration of biogenic silica was the lowest measured in surface during KEOPS-2 (0.30 ± 0.03 µmol L^{-1}) and its silicon isotopic composition was low (0.73 ± 0.04 ‰) and similar to E4-W and A3-1, *Fig. 2.7.*). This is typical of non-bloom conditions and in the same range as those measured in HNLC waters of the Southern Ocean (e.g. Fripiat et al., 2011a, 2011b; Mosseri et al., 2008). However, this station displayed unexpected low silicic acid concentration and heavy $\delta^{30}Si_{DSi}$ in the ML (12.94 ± 0.49 µmol L^{-1} and 2.21 ± 0.06 ‰, respectively; *Fig. 2.3.*). This latter is significantly heavier than the Si-isotopic composition of the fertilized area measured few days before (1.99 ± 0.03 ‰, A3-1). As already proposed by Closset et al. (2014) and Lasbleiz et al. (2014), this suggests that a short development of diatoms could have occurred just before our sampling, consuming a fraction of the H_4SiO_4 standing stock and increasing the $\delta^{30}Si_{DSi}$ of surface waters. The same evidence of surface production has also been deduced by Dehairs et al. (2014), who observed a slight nitrate depletion and enrichment of $\delta^{15}N\text{-}NO_3^-$. Indeed, in early spring, the low iron concentration that prevails at this station might be sufficient to trigger a short phytoplankton growth (dominated by nanophytoplankton; Lasbleiz et al., 2014) as soon as light conditions became favorable. Then, the bloom quickly stops as iron is completely depleted from surface waters. Both the high silica dissolution to production ratio (D:P > 1) observed in the ML (Closset et al., 2014) and the high barium excess measured between 200 and 400 m (Jacquet et al., 2014) suggest that this material was exported and remineralized when we visited the station. This could be confirmed by the clear $\delta^{30}Si_{BSi}$ maximum observed between 100 and 200 m (*Fig. 2.7.*) and

that could result from the Si isotopic fractionation during opal dissolution (Demarest et al., 2009) or more likely by the preferential dissolution of isotopically light diatoms that was initially produced from lighter H_4SiO_4.

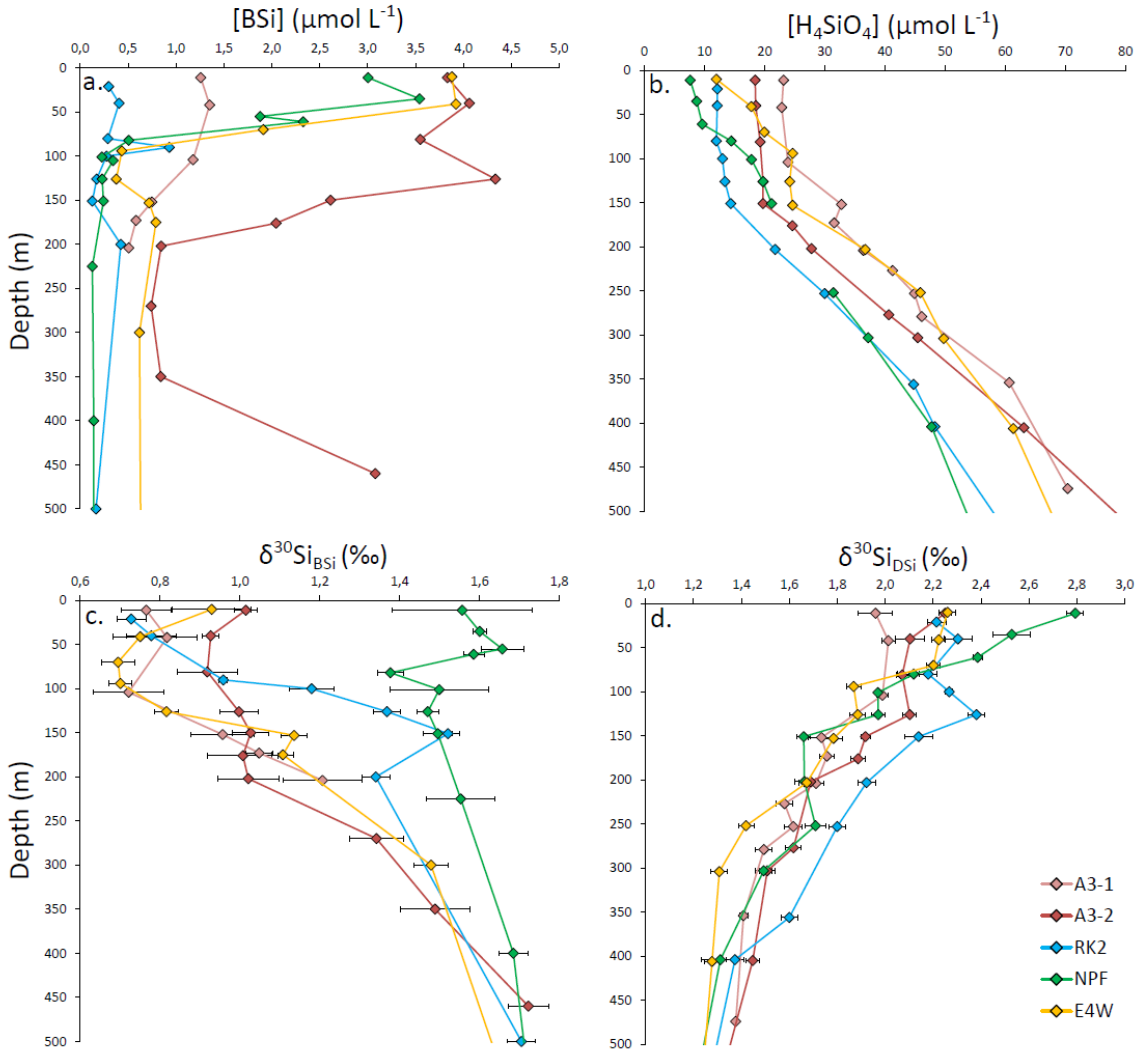

Figure 2.7. Vertical profiles of biogenic silica and silicic acic concentration (a. and b.; µmol L^{-1}) and isotopic composition of dissolved and particulate silicon (c. and d.; ‰) for the main contrasted KEOPS-2 stations (A3, R-2, E4W and F-L)

By contrast, all other KEOPS-2 stations (except TNS1 and TEW3) were characterized by the development of large spring blooms that were not homogeneous in time and space depending on the degree, the mode and the timing of their iron fertilization (Bowie et al., 2014; Trull et al., 2014). These blooms were organized in 3 main features related to their different iron supplies and are discussed separately in the following.

b) The Kerguelen Plateau zone

This area was characterized by large and recurrent blooms located southeast of the islands, mainly above the Kerguelen Plateau and delimited northward by the Polar Front (Blain et al., 2001, 2007)

During our first visit to A3 (A3-1), low $\delta^{30}Si_{DSi}$ and $\delta^{30}Si_{BSi}$ (1.99 ± 0.03 ‰ and 0.77 ± 0.05 ‰, respectively, *Fig. 2.3.*) were measured in the ML compared to those observed in the HNLC reference station (R-2) where, as discussed previously, a short production event could have occurred just before our sampling. This could indicate that biogeochemical conditions prevailing at A3-1 were characteristics of a pre-bloom or early-bloom period. Indeed, low chlorophyll *a* and biogenic silica concentrations were observed despite high nutrients standing stocks (H_4SiO_4 and NO_3^-, *Fig. 2.7.*, see Blain et al., 2014 for NO_3^-) and relatively high iron concentrations (Bowie et al., 2014). This situation may likely be due to a non-optimal light-mixing regime at this station since WW (i.e. subsurface waters colder than 2°C, Park et al., 2014) still reached the surface (*Fig. 2.6.*). Comparable silicon isotopic properties at stations A3-1 and E4W located at the edge of the Kerguelen Plateau (*Fig. 2.7.*) in ML and WW emphasized that the northward circulation above the Plateau could also lead to a northward advection of part of the southeast production. This observation is supported by similar populations of diatoms observed by Lasbleiz et al. (2014) at these 2 stations (mainly represented by the genus *Chaetoceros* and *Thalassiosira*) and by radium isotopes (Sanial et al., 2014) which suggested that the transit time of surface water between Heard Island and A3 range from 1 week to 2 months.

The largest phytoplankton development was observed during the 2nd visit at A3, where chlorophyll *a* and BSi concentrations increased more than 2 fold over 1 month. This growth was also observed in the Si-isotopic signature of both seawater and particles which increased significantly (from 1.99 ± 0.03 ‰ to 2.10 ± 0.05 ‰ and from 0.77 ± 0.05 ‰ to 0.96 ± 0.08, respectively, *Fig. 2.3.*) as a result of the preferential uptake of ^{28}Si of diatoms (De la Rocha et al., 1997). There, the continuous supply of nutrients and iron to the ML coming from the WW both in winter and during the productive period allowed a spring biogenic silica production comparable to the highest productive regions, such as upwelling systems or river plumes (up to 43.4 ± 0.4 mmol m^{-2} d^{-1} for net opal-production integrated over the euphotic zone, Fripiat et al., 2011a; Closset et al., 2014).

Moreover, during the 2nd visit at A3, an intense mixing event strongly deepened the ML and exported diatoms with heavy Si-isotopic composition and increased the $\delta^{30}Si_{DSi}$ of seawater up to 200 m, explaining the 2 different profiles we observed between these 2 stations (*Fig. 2.7.*). This is consistent with a bloom started in the southeast part of the Plateau and spread northward following the main surface circulation pattern of the region (Park et al., 2014).

c) The recirculation zone in the Polar Front meander

A zone of retroflexion of the PF northeast of the Kerguelen Islands (also referred to as "meander") was investigated through several visits constituting a pseudo-lagrangian time-series (station TNS6 and E1 to E5, *Fig. 2.4.*). The central part of this meander was characterized by a complex standing or gently flowing water circulation associated with low to moderate dissolved iron concentrations (Bowie et al., 2014; Blain et al., 2014). Here, surface waters displayed generally higher $\delta^{30}Si_{DSi}$ signatures and lower H_4SiO_4 concentrations compare to above the Plateau (*Fig. 2.8.*) supporting the idea of a northward surface circulation with a progressive consumption and enrichment in ^{30}Si of the dissolved pool. Indeed, according Park et al. (2014), this zone could correspond to the latest arrival of water originated from the shallow Plateau, explaining partly the delay observed between the initiation of production here and the southernmost bloom located above the Plateau and in the PF plume (*Fig. 2.4.*). Moreover, radium isotopes (Sanial et al., 2014) suggested that the passage of chemical elements (such as iron) across the PF could also occur and significantly fuel the phytoplankton bloom in this area, and would mix Si-poor SASW with heavy $\delta^{30}Si_{DSi}$ and Si-rich AASW with light $\delta^{30}Si_{DSi}$.

The moderate iron fertilization occurring in the meander increased both the BSi production rate and biomass, with larger increase at the 2 last visits (E4E and E5, Closset et al., 2014; Lasbleiz et al. 2014). However, no clear trend was identified in the ML central values of $\delta^{30}Si_{DSi}$ and $\delta^{30}Si_{BSi}$ since both these parameters were not significantly different from TNS6 to E4E (*Fig. 2.3.*). This observation is strengthened by the homogeneous $\delta^{30}Si_{DSi}$ profiles in all the meander's stations (*Fig. 2.8.*).

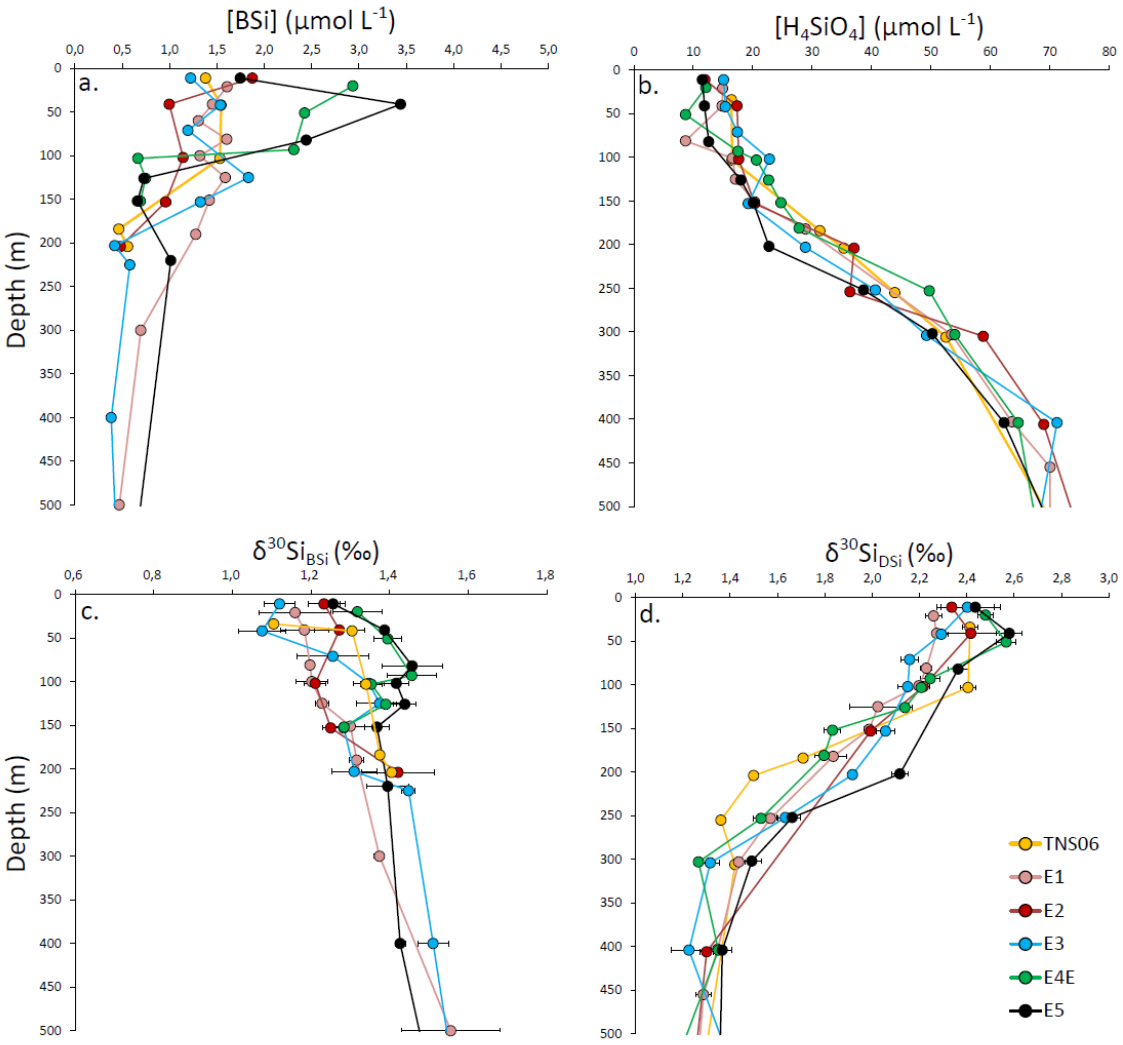

Figure 2.8. Vertical profiles of biogenic silica and silicic acic concentration (a. and b.; µmol L^{-1}) and isotopic composition of dissolved and particulate silicon (c. and d.; ‰) for the KEOPS-2 Meander stations (TNS6, E1, E2, E3, E4E and E5)

However, depending on their surface $\delta^{30}Si_{BSi}$ signatures and the general shape of this parameter's profile in the water column, we can sort these stations in 3 main functional clusters:

(i) TNS6 and E3 displayed the lightest isotopic composition of biogenic silica in surface waters (1.11 ± 0.02 ‰ and 1.12 ± 0.04 ‰, respectively) and correspond to "non-active stations". The high variability of $\delta^{30}Si_{BSi}$ with depth at E3 and its relatively high BSi dissolution rate (Closset et al., 2014) could be the result of a previous attempt to bloom.

(ii) E1 and E2 correspond to the "bloom-initiation stations" and displayed very similar profiles except in the upper 50 m where the $\delta^{30}Si_{BSi}$ of surface diatoms seemed to be heavier at E2 (*Fig. 2.8.*). This could suggest that the low net BSi production measured here (Closset et al., 2014) could be sufficient to initiate the accumulation of siliceous biomass in the upper layer of the ML.

(iii) E4E and E5 were representative of "spring-bloom stations" with high net silica production rates and low dissolution to production ratios (Closset et al., 2014) and thus displayed a high potential for BSi accumulation in the ML. Interestingly, the $\delta^{30}Si_{BSi}$ profiles suggest that this accumulation was confined in the lower part or just below the ML since we observe a significant $\delta^{30}Si_{BSi}$ maximum between 50-150 m (up to 1.46 ‰, *Fig. 2.8.*). Such a subsurface increase of diatom's $\delta^{30}Si$ signature could result either from the dissolution of biogenic silica, from a significant BSi accumulation in the deeper layers. It has been reported that biogenic silica dissolution preferentially releases ^{28}Si with a fractionation factor of -0.55 ± 0.05 ‰ (Demarest et al., 2009). This fractionation is opposite to that occurring during Si uptake and could affect the vertical distribution of $\delta^{30}Si_{BSi}$ by shifting the remaining particles toward more positive delta values. While the isotopic composition of subsurface suspended biogenic silica generally reflects the one of the ML (Varela et al., 2004; Fripiat et al., 2012; Closset et al., in prep) some significant effect of progressive opal dissolution has been already alledged in the Southern Ocean (Fripiat et al., 2011a, b). However, since KEOPS-2 was conducted in early spring (October-November), accumulation and dissolution of detrital diatoms were quite unlikely at the beginning of the growth period. Lasbleiz et al. (2014), associated the low biomass in the meander surface layer to the occurrence of a deep silica maximum, and suggested that the high mesoscale activity in this area may have favored the transfer and the accumulation of particles at depth. Indeed, using ^{234}Th, Planchon et al. (2014) measured the highest export efficiencies at stations E but suggested that relatively low carbon export occurred inside the meander during the onset of the bloom. Thus, the heavy Si-isotopic composition of particles observed at depth at station E4E and E5 might result from exported surface layer diatoms that will accumulate at the base of the ML, as already proposed in a conceptual scheme by Quéguiner (2013)

d) The Polar Front Zone

A plume of chlorophyll *a* was present in the Polar Front Zone (stations F-L and TEW8, *Fig. 2.4.*), extending eastward of the Kerguelen Plateau and showing strong mesoscale activity associated to the temporal and spatial variability of the Polar Front (Park et al., 2014). There, the productive waters were

characterized by a shallow and warm ML (Sub-Antarctic Surface Waters > 4°C), providing favorable conditions for phytoplankton development. Moderate to high iron enrichments were measured at this station (Blain et al., 2014; Bowie et al., 2014) and could explain the high biomass composed by communities distinct than those found above the Plateau (mostly small diatoms and nanoflagellates, Lasbleiz et al., 2014).

The Si-isotopic composition of ML seawater and particles measured at F-L were the heaviest of KEOPS-2 stations (*Table 2.2.*) coinciding with a strong Si-depletion in surface water (*Fig. 2.4.*). These $\delta^{30}Si_{DSi}$ signatures fall in the range of previous reported values in the PFZ ML, from 2.05 ± 0.03 ‰ in spring (Cardinal et al., 2005) to 2.77 ± 0.23 ‰ in late summer (Fripiat et al., 2011a) in the Australian and Atlantic sector of the Southern Ocean respectively. Similarly $\delta^{30}Si_{BSi}$ as reported in Closset et al. (in prep) show that the seasonal variations of isotopic composition of settling opal ranged from 1.14 ± 0.03 ‰ to 2.15 ± 0.07 ‰ in the Australian sector of the Southern Ocean. In the PFZ, heavier $\delta^{30}Si$ signatures can be attributed to a higher relative utilization of silicic acid by diatoms since the net BSi production could be relatively high in these Si-poor surface waters and exclusively based on "new" sources of H_4SiO_4 (Closset et al., 2014). Note that higher $\delta^{30}Si_{DSi}$ values were also measured in the PFZ WW (on average 2.14 ± 0.08 ‰ for all stations located north of the PF, *Table 2.2.*). This confirms that Si source is different in the PFZ, i.e. could be advected from coastal water from the northern Kerguelen shelf across the PF jet as reported for Fe supply and circulation (Bowie et al., 2014; Park et al., 2014). Since the distance between PF and SAF here was particularly reduced promoting cross-frontal advection and exchanges (Park et al., 2014), this WW signal would then be exported northward as subsurface layer in the PFZ is a precursor of the AAIW and will become the main Si-suppliers to the surface waters at lower latitudes (Sarmiento et al., 2004). Indeed, in the Atlantic sector of the Southern Ocean, Fripiat et al. (2011b) has estimated that almost all the Si in the AAIW originated from the PFZ WW.

II.4.2. Spatio-temporal variability of Si mass and isotopic balance in the iron fertilized area

By comparing with KEOPS-1 conducted during summer 2005 in the iron fertilized area, the Si isotopic signature dataset should encompass now the full range of the seasonality of the Si isotopic composition and allow refining the Si biogeochemical cycle in this area (Fripiat et al., 2011a; De Brauwere et al., 2012). To this purpose, the short term temporal evolution of the bloom development

was investigated through the several visits in the Meander that constituted a pseudo-lagrangian time-series conducted over 27 days during the bloom-initiation.

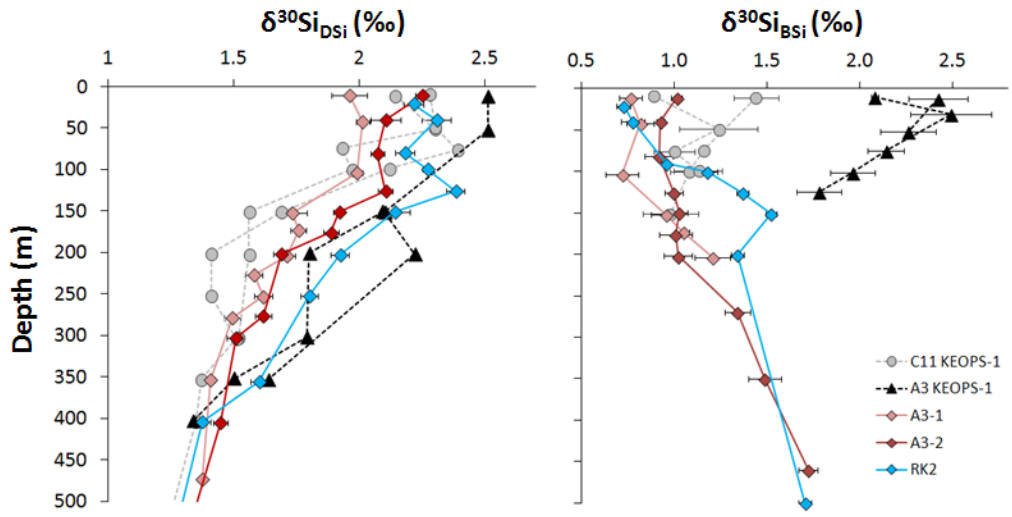

Figure 2.9. Seasonal evolution of the isotopic composition of dissolved (a.) and particulate silicon (b.) in the upper 500 m of the iron-fertilized and HNLC reference stations. Summer isotopic signatures (KEOPS-1, Fripiat et al., 2011a) are in grey and black colors; results from the spring period (this study) are in red and blue color.

As expected, the silicon isotopic properties measured in the ML during the austral spring (KEOPS-2) were significantly lighter than those measured by Fripiat et al. (2011a) at the end of summer (*Fig. 2.9.*).

This is consistent with the seasonal progression of Si consumption in surface waters that would lead to a ^{30}Si enrichment in both the dissolved and particulate Si-phases (De la Rocha et al., 1997). Indeed, both the heavy $\delta^{30}Si$ values and the maximal H_4SiO_4 depletion observed during KEOPS-1 indicated that the bloom was already decaying, while all the biogeochemical conditions during KEOPS-2 were representative of bloom initiation (this study and Closset et al., 2014). Temporally, the bloom above the plateau usually peaks in late November and declines gradually until January as nutrients (mainly iron and silicic acid) became limited (Blain et al., 2007; Mongin et al., 2008). Then, a second and less important bloom could persist at steady state until May when light level started to be insufficient to maintain photosynthetic activity (Blain et al., 2013). The 1st visit to A3 revealed relatively high H_4SiO_4 concentrations and low BSi and chlorophyll *a* stocks in the ML and WW can be associated

to the initial conditions prevailing before the summer stratification (Park et al., 2014; Blain et al. 2014). WW for A3-1, A3-2 and E4W averaged silicic acid concentration and isotopic signature (33.4 ± 2.9 µmol L^{-1} and 1.71 ± 0.05 respectively), whereas concentrations and $\delta^{30}Si$ measured at A3 during KEOPS-1 represent the conditions at the end of the season (*Fig. 2.10.*). These initial conditions differ from the HNLC WW chosen by Fripiat et al. (2011a) as ultimate Si-source fuelling the bloom above the Plateau (52.5 ± 3.3 µmol L^{-1} and 1.5 ± 0.0 ‰ for H_4SiO_4 concentration and $\delta^{30}Si_{DSi}$, respectively), but were not significantly different from the A3 WW reported by Fripiat et al. (2011a). Indeed, ML $\delta^{30}Si_{DSi}$ in the early spring were clearly off the steady state fractionation trend when using the same initial Si-pool conditions as in Fripiat et al. (2011a). Several features suggested that the Plateau ML was largely ventilated with AASW originated from the surrounding areas (Park et al., 2008a, 2014; Sanial et al., 2014), making the HNLC WW a relevant source of Si for the diatoms that develop at station A3. Although this assumption likely reflects reality, it appears that the WW Si-pool isotopic and contents properties of HNLC KEOPS-2 reference station R-2 could be ascribed as a common Si-source (cf. section above).

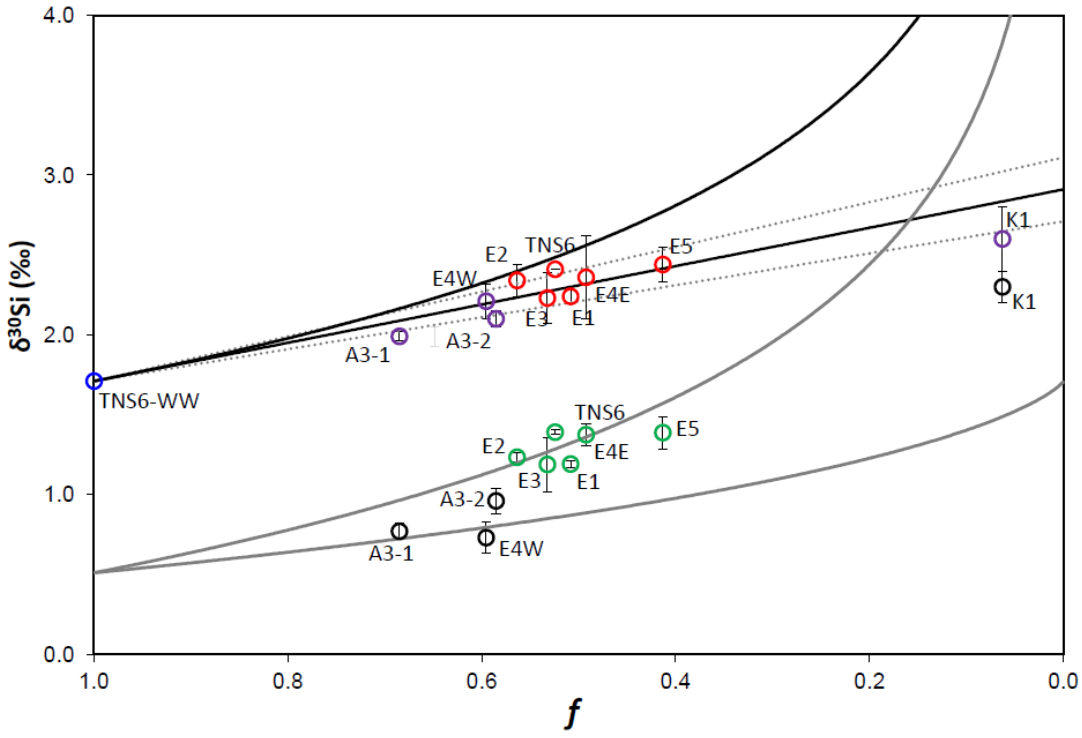

Figure 2.10. Silicon isotopic composition vs. silicic acid concentration for the different ML Si-reservoir in the iron-fertilized area of the Kerguelen Plateau. A unique source (TNS6-WW, blue dot) was used for all Plateau and Meander stations. ML dissolved Si-pools above the Plateau (purple dots) and in the Meander (red dots), fit well with a steady state fractionation law (straighted black line) but not with a Rayleigh distillation law (curved black line). ML particulate Si-pools above the Plateau (black dots) and in the Meander (green dots) lie between the instantaneous and the accumulated products predicted by a Rayleigh distillation model (grey lines). Summer isotopic signatures (K1) are from Fripiat et al. (2011a).

In the meander, the initial conditions were represented by the Si-properties of TNS6 WW (31.3 µmol L^{-1} and 1.71 ± 0.02 ‰ for H_4SiO_4 concentration and $\delta^{30}Si_{DSi}$, respectively) which were similar to those used for the Plateau. This strengthens the idea of a unique Si-source originated from the south and that flow northward above the shallow Kerguelen Plateau to reach finally the PF retroflection area. Thus, using the mean ACC $^{30}\varepsilon$ value of -1.2 ± 0.2 ‰ compiled by Fripiat et al. (2011a) and the averaged Plateau-WW as initial conditions, we will attempt to describe the seasonal dynamic of the Si-biogeochemical cycle in the fertilized area off Kerguelen Islands.

a) Mixed layer dissolved Si-pool

Using KEOPS-1 HNLC WW characteristics (52.5 ± 3.3 µmol Si L^{-1} and 1.5 ± 0.0 ‰) to represent the initial conditions of WW in the fertilized area, Fripiat et al. (2011a) estimated a seasonal depletion in the ML at 5.0 ± 0.3 mol Si m^{-2} y^{-1}. By identifying a more appropriate Si-source for the Plateau ML, we can refine this calculation and reduce the seasonal net BSi production in the upper 100 m to 3.0 ± 0.3 mol Si m^{-2} y^{-1}. This flux is 40 % lower than the previous estimate but corresponds well to the range of published net BSi production values for the AZ (2.4 to 3.3 mol Si m^{-2} y^{-1}; Pondaven et al., 2000; Nelson et al., 2002; Pollard et al., 2006) and still balance the total Si supply estimated for the Plateau ML (4.0 ± 0.7 mol Si m^{-2} y^{-1}, Fripiat et al. (2011a).

As previously reported by Fripiat et al. (2011a), the seasonal evolution of $\delta^{30}Si_{DSi}$ in the fertilized area seems to follow a steady state fractionation law (*Fig. 2.10.*). Even if this model does not reflect any temporal evolution because it implies a constant H_4SiO_4 relative consumption (*f*) and BSi accumulation with time (Fry, 2009), it appears appropriate to describe the Si-utilization that occurred above the Kerguelen Plateau where deep and regular mixing events are expected to supply nutrients in surface waters (Park et al., 2008b). Indeed, in *figure 2.10.*, most the Plateau and Meander ML $\delta^{30}Si_{DSi}$ stations were clearly off the Rayleigh fractionation trend. It seems that ML aligns along a steady state trend, with the following decreasing *f* (i.e. increasing Si utilization) A3-1, A3-2, E1 to E4E Meander stations, E5 and A3 KEOPS-1. Surprisingly, in this model, Meander stations exhibit higher isotopic signatures and higher H_4SiO_4 depletion compared to the productive Plateau stations A3-2 and E4W while they were sampled several days before these two stations (see *figure 2.4.*). This situation was not due to a higher Si-uptake in the Meander ML as the net BSi production at A3-2 was twice the one measured at E5 (Closset et al., 2014), but could be explained by a strong mixing event that occurred just before our 2nd visit to A3. This vertical mixing was induced by strong temporary winds and supplied

water with high silicic acid content and light $\delta^{30}Si$ in the euphotic zone. This would thus increase the apparent Si utilization (*f*) and lighten the isotopic signature of seawater. Note that, as previously mentioned, no clear temporal evolution can be shown in the Meander ML $\delta^{30}Si_{DSi}$ signatures. The strong mesoscale activity that lead to ML instabilities and regularly mix the water masses were likely the reason of this situation.

b) Winter Waters dissolved Si-pool

By comparing WW Si-properties from KEOPS-1 HNLC and fertilized area (52.5 ± 3.3 µmol Si L^{-1} and 34.2 ± 1.9 µmol Si L^{-1}), Fripiat et al. (2011a) estimated a seasonal depletion in the 100 to 400 m layer of 5.5 ± 0.3 mol Si m^{-2} y^{-1} and ascribe it to a net BSi production of a subsurface diatom population since a deep BSi and chlorophyll maximum was observed here in January (Mosseri et al., 2008; Uitz et al., 2009). The WW characteristics measured during our first visit at A3 (31.55 ± 2.2 µmol Si L^{-1} ; 1.76 ± 0.1 ‰) were similar to the one observed at the end of the productive season by Fripiat et al. (2011a) suggesting that, contrary to what was previously proposed, WW did not have undergone seasonal Si uptake above the Plateau. This conclusion is not contradictory with the development of a subsurface diatom community that could partly explain the deep BSi accumulation observed here during KEOPS-1. Indeed, in such communities, the BSi production may likely be sustain by regenerated source of Si (high D:P ratio, Closset et al., 2014) and would not finally consume the DSi standing stock.

In contrast to the ML, the WW $\delta^{30}Si_{DSi}$ signatures of the fertilized area (*figure 2.3.*; *Table 2.2.*) display significant temporal variations (from 1.71 ± 0.02 ‰ at TNS6 to 2.21 ± 0.02 ‰ at E4E). It seems unlikely that such shift of WW toward higher $\delta^{30}Si$ values are explained by the progressive consumption of silicic acid by a secondary diatom community just below the ML. Indeed, although deep silica maximum are common features in the Southern Ocean (Parslow et al., 2001), we did not measure any Si uptake below the euphotic layer during KEOPS-2 (Closset et al., 2014). Since this area hold strong mesoscale activity (Zhou et al., 2014; Park et al., 2014), an alternative process that could have decreased the WW DSi pool and enriched the WW $\delta^{30}Si_{DSi}$ may likely be the isopycnal mixing between initial WW and several sequential surface ML water masses (*Fig. 2.11.*). In this case, the resulting water mass should lie on a theoretical mixing curve involving the TNS6 WW and different ML water masses with Si-properties located between the initial and final ML end-members (TNS6 ML and E5 ML).

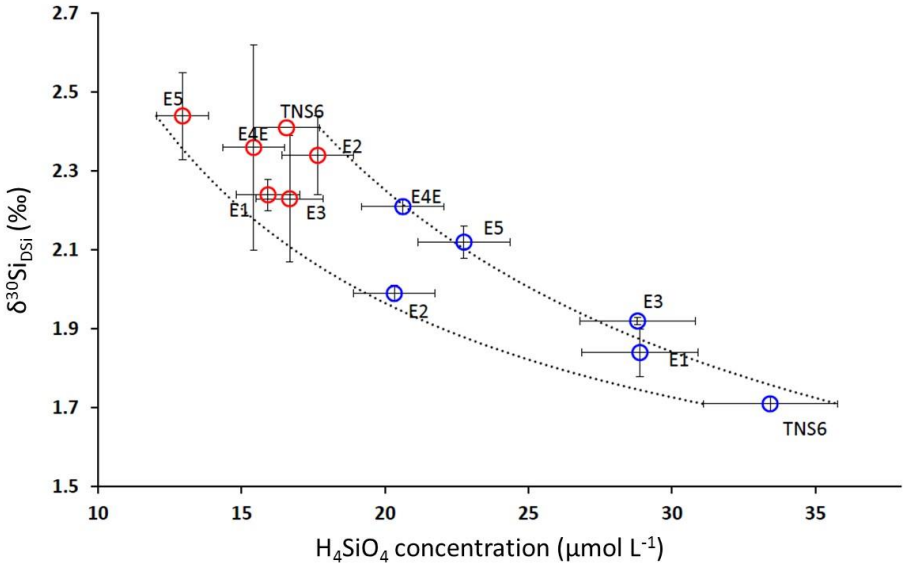

Figure 2.11. Potential mixing curves between TNS6-WW and the different Meander ML water masses, WW are in blue and ML are in red. The two end-members were identified by dotted lines. The ML averages and error bars were calcultated based on the median values and interquatile range 2/3 for each station while they were the « central value » defined using the salinity threshold method for WW (see *Table 2.2.*).

For example E1 WW might results from the mixing between TNS6 WW and TNS6 ML, E2 WW from the mixing between TNS6 WW and E1 ML etc. Although it works very well for these 2 examples, the strong uncertainties associated with the definition of Si-properties that were representative of WW water masses prevent us to define correctly the exact end-members of these mixings. Consequently, only a range of potential mixing curves can be identify in *figure 2.11.*, but all the Meander WW fall between two extreme situations. In any case, and contrary to the subsurface Si-uptake observed in summer during KEOPS-1 (Fripiat et al., 2011a), our results indicate that the Si-properties of the WW source remained unaltered in the southern part of the Plateau. Then, when the water masses joined the meander, the mesoscale activity occurring into this hydrological structure induced a mixing between WW and ML that lead to an enrichment of the Si isotopic signature and a dilution of the DSi pool of this source.

c) Mixed layer particulate Si-pool

While the open model equations seem appropriate to describe the evolution of seawater Si-isotopic composition, it is arguable when considering the $\delta^{30}Si_{BSi}$, since it conceptually assumes the lack of BSi accumulation (Fry, 2009). As shown in *figure 2.10.*, the signatures of opal during the 2 KEOPS expeditions were clearly off the steady-state fractionation trend for BSi and lied between the 2

products involved in the closed-model. Indeed, the Rayleigh fractionation equations describe 2 extreme ideal situations: all the BSi produced in the ML is immediately exported from the system (the so-called instantaneous BSi, *equation 2.3.*), or all BSi accumulates in the ML (the so-called accumulated BSi, *equation 2.4.*). During diatom development, and all along the season in the Kerguelen fertilized area, the system shifted from one situation to another or remained between these 2 extremes depending on the bloom maturity and/or the hydrodynamical conditions of the surface waters. The instabilities of the ML depth at TNS6, "bloom-initiation" stations (E1, E2 and E3) and at E4E reduced the phytoplankton growth as discussed previously, but also prevent any biomass retention in surface waters. In these systems, diatoms did not accumulate in the ML but settled toward deeper layers, exporting carbon and biogenic silica (Laurenceau et al., 2014; Planchon et al., 2014). Their Si-isotopic properties felt close to the instantaneous product curve of the Rayleigh fractionation law (*Fig. 2.10.*). Considering the early stage of the season during KEOPS-2 expedition, and since Si-uptake rates above the Plateau were among the highest reported so far for the Southern Ocean, it appears that BSi and C export did not occurred yet at station A3 and E4W (Jacquet et al., 2014; Planchon et al., 2014; Rembauville et al., 2014). There, BSi was accumulating in the ML, resulting in Si-isotopic properties that seemed to be switched toward the accumulated product curve of the Rayleigh model. The last 2 stations lied between these 2 ideal curves since they combined the 2 biogeochemical processes (BSi accumulation and export). Indeed, the high Si-uptake rates observed at E5 (20.5 ± 0.2 mmol m^{-2} d^{-1}; Closset et al., 2014) associated to the strengthening of the summer stratification would progressively reduce vertical Si supply and allow a better phytoplankton retention in the ML. KEOPS-1 expedition occurred during the decaying phase of the bloom. Thus, the biological material present in the ML at the end of summer was likely composed of old and detrital diatoms that was partly exported in December (Rembauville et al., 2014) and living cells that were just produced from regenerated Si-sources (Closset et al., 2014). The $\delta^{30}Si_{BSi}$ observed in these surface waters would result from the combination of a partial export of old particles which was remaining in the ML, lightening the isotopic signature, and of the addition of new and heavier diatoms that would increase the delta value. This situation was well consistent with the strong seasonality of primary and export production that characterized the Southern Ocean and that lead to a temporal decoupling between these 2 processes in the ML (see e.g. in Buesseler et al., 2001).

The contrasted seasonal evolutions of $\delta^{30}Si_{DSi}$ and $\delta^{30}Si_{BSi}$ (following an open or a closed system respectively) is consistent with BSi and DSi isotopic offsets previously reported (Varela et al. 2004; Cardinal et al. 2007; Fripiat et al., 2012) leading to temporal variations of the ML $\Delta^{30}Si$ ($\Delta^{30}Si = \delta^{30}Si_{BSi} - \delta^{30}Si_{DSi}$), with low $\Delta^{30}Si$ at the end of summer when the ML silicic acid pool was highly depleted. Fripiat

et al. (2012) attributed such offsets to modifications of the Si-uptake to Si-supply ratio in surface waters due to spatial variability of the biogeochemical conditions among the different zones of the ACC (AZ vs. PFZ). They suggested that in regions (or period of the season) where the Si-uptake to supply ratio was low, i.e. that display limited diatom growth and significant vertical mixing, the ML is supplied with isotopically light H_4SiO_4 that would lighten the $\delta^{30}Si_{DSi}$ signature of surface waters without impacting the isotopic composition of biogenic silica, therefore reducing their $\Delta^{30}Si$. Our results point out that an alternative approach to change the $\Delta^{30}Si$ could be obtained when the system behaves in a mixed way between open and closed systems with a decoupling between the dissolved and particulate pools. In this case, opal accumulation in the ML will increase the $\Delta^{30}Si$ while when biogenic silica is exported in deeper layer, the $\Delta^{30}Si$ will be dampened and will differ significantly from $^{30}\varepsilon$. The export of BSi outside of a closed system is also the only situation that could explain $\delta^{30}Si_{BSi}$ values exceeding Si-source $\delta^{30}Si_{DSi}$ as observed at the end of summer above the Plateau (*Fig. 2.10.*, Fripiat et al., 2011a). In this case, diatoms that remain in the ML would represent an instantaneous product strongly enriched in heavy Si-isotope while when surface waters are strongly stratified, they could be retained in the ML and would correspond to an accumulated product.

II.5 Conclusions

The present study addressed the spatial distribution and seasonal evolution both for concentration and isotopic composition of dissolved and biogenic Si in the naturally iron-fertilized region of the Kerguelen Plateau. The spatial distribution of $\delta^{30}Si$ signatures of seawater and particulate matter in the ML was strongly impacted by the complex mesoscale structure of water masses generated by the interaction between the location of the PF and the bathymetry. In contrast, in deep layer (> 500 m), $\delta^{30}Si_{DSi}$ were remarkably homogeneous (on average 1.28 ± 0.08 ‰ and 1.05 ± 0.06 ‰ for UCDW and LCDW respectively) and deep $\delta^{30}Si_{BSi}$ exhibit similar values in all out-plateau KEOPS-2 stations (on average 1.74 ± 0.13 ‰), suggesting that dissolution of opal did not have any significant isotopic effect during this early season.

This work from KEOPS-2 in the early spring adds significantly to the existing database on Si isotopic composition in the Southern Ocean. Indeed, the measured silicon properties of the ML can then be then considered as representative of the bloom initiation as also supported by companion

studies from the same cruise (Blain et al., 2014; Cavagna et al., 2014; Closset et al., 2014; Lasbleiz et al., 2014). During this period, the Kerguelen area was characterized by a mosaic of biogeochemical environments displaying different modes and intensities of iron enrichment (Bowie et al., 2014; Trull et al., 2014). The HNLC area, strongly iron-limited (station R-2), exhibited very low biomass, low BSi-production and isotopically light BSi. However, a short winter production event in agreement with other proxies (Closset et al., 2014; Dehairs et al., 2014; Jacquet et al., 2014) could explain the relatively high $\delta^{30}Si_{DSi}$ values measured at this station precluding its application as non-productive reference station in the context of silicon biogeochemical cycle. The iron flux in the ML above the Plateau (Park et al., 2014; Sanial et al., 2014) strongly stimulated phytoplankton production increasing significantly its $\delta^{30}Si_{BSi}$ (from 0.77 ± 0.05 ‰ to 0.96 ± 0.08 ‰ over 27 days during KEOPS-2) and simultaneously enriching the ML in ^{30}Si (up to 2.10 ± 0.05 ‰). North of the PF, the ML the iron supply originated mostly from the northern part of the Kerguelen Plateau (Sanial et al., 2014). There, stocks and Si-isotopic composition of seawater and particles were respectively lower and heavier than above the Plateau in accordance with its PFZ characteristics as already reported by Cardinal et al. (2007, 2005), Varela et al. (2004) and Fripiat et al. (2011b) in the Australian and the Atlantic sector of the Southern Ocean. The situation was different in the Meander since these stations received only moderate and sporadic iron supplies, mainly via cross-front exchanges induced by a complex and elevated mesoscale activity that occur in this zone (Park et al., 2014; Sanial et al., 2014). There, non-optimal light-mixing regime and nutrients availability (including iron) delayed the bloom development and lead the system to behave at steady-state. Indeed, although the biomass was clearly accumulated in November, and probably after several aborted attempts to bloom in October (Closset et al., 2014; Lasbleiz et al., 2014), both Si isotopic signatures and mass balance did not evolve significantly in the Meander ML.

Our Si-isotopic data allow a better constraining of the silicon biogeochemical cycle above the Kerguelen Plateau, by determining the initial conditions before diatom growth and identifying the Si sources, the connections between different water masses involved and their circulation throughout the area. The same source can be applied for both Plateau and Meander stations suggesting that water masses and the ML bloom originated from the southeast part of the Kerguelen Plateau and spread northward. The Si-properties of this source (31.5 ± 2.2 µmol Si L^{-1} and 1.76 ± 0.03 ‰) allow us to refine the seasonal net BSi production at 3.0 ± 0.3 mol Si m^{-2} y^{-1} above the Plateau (instead of 10.5 ± 1.3 mol Si m^{-2} y^{-1} estimated by Fripiat et al., 2011a), which is more consistent with the published values for the AZ (2.4 to 3.3 mol Si m^{-2} y^{-1}; Pondaven et al., 2000; Nelson et al., 2002; Pollard et al., 2006). This also suggest that, even if some subsurface diatom communities can develop below the ML at the end of summer, the WW did not have undergone any net BSi production above the plateau since their

characteristics were similar over the whole season. Indeed, such diatom communities growing at the end of the productive period likely displayed high D:P ratio and were mostly sustained by regenerated sources of Si, preventing any alteration of the isotopic composition and/or consumption of the DSi pool above the Kerguelen Plateau. However, a significant mixing between WW and ML in the Meander would have decreased the WW H_4SiO_4 concentrations and increased the WW $\delta^{30}Si_{DSi}$ values.

The major outcome of this study is that, in the naturally Fe-fertilized area of Kerguelen, the dissolved and particulate Si-pools were decoupled. Indeed, by combining results from the 2 KEOPS expeditions, we have observed that $\delta^{30}Si$ of seawater and diatoms were not directly linked together with a simple Rayleigh or steady-state isotopic fractionation model. It seems that, in this high productive area, the strong mesoscale activity, promoting vertical and lateral nutrient exchanges, drove the evolution of $\delta^{30}Si_{DSi}$ as an open system, while $\delta^{30}Si_{BSi}$ behave more as a closed system. Depending on the regime of BSi export that operate (e.g. BSi accumulation in the ML in early spring vs. massive export event at the end of the productive season), the ML $\delta^{30}Si_{BSi}$ can be alternatively described by the accumulation or instantaneous product, or could lie between these 2 ideal situations. The intensity of decoupling between the 2 models will then depend essentially on the variability of Si-supply to Si-uptake ratio and on the export efficiency of the system as already suggested by Fripiat et al. (2012). If confirmed in other productive regions of the Southern Ocean, this observation could have great implications for paleoceanographic studies. Indeed, the $\delta^{30}Si_{BSi}$ is currently used as a proxy for past reconstructions of surface Si-utilization (De la Rocha et al., 1998; Brzezinski et al., 2002; Etourneau et al., 2012; Ehlert et al., 2013). In their approaches, they relate the isotopic signature of sedimentary opal with the $\delta^{30}Si_{DSi}$ and the extent of DSi consumption in surface waters by using either the Rayleigh's or steady state's equations without taking into account this possible decoupling between $\delta^{30}Si_{DSi}$ and $\delta^{30}Si_{BSi}$ and its seasonal variability. This study emphasizes the necessity to further monitor seasonal variations of the Si isotopic signatures in surface waters by developing time-series analysis of $\delta^{30}Si_{DSi}$ in the ML and of exported biogenic silica to calibrate this proxy. The production of such a dataset would also greatly help to refine existing models involving Si isotopic and mass balance in the Southern Ocean (De Brauwere et al., 2012; Fripiat et al., 2012; Coffineau et al., 2014).

Acknowledgements

Authors would like to thank Pr. Stéphane Blain as the KEOPS-2 project coordinator, the captain and the crew of the R/V Marion-Dufresne II for assistance on board. This work was supported by the French Research program of INSU-CNRS LEFE-CYBER ('Les enveloppes fluides et l'environnement' – 'Cycles biogéochimiques, environnement et ressources'), the French ANR ('Agence Nationale de la Recherche', SIMI-6 program), the French CNES ('Centre National d'Etudes Spatiales') and the French Polar Institute IPEV (Institut Polaire Paul-Emile Victor). The research leading to these results has also received funding from the European Union Seventh Framework Programme under grant agreement n°294146 (MuSiCC Marie Curie CIG).

II.6 References

Abraham K., S. Opfergelt, F. Fripiat, A-J. Cavagna, J.T.M. de Jong, S.F. Foley, L. André, D. Cardinal (2008), δ30Si and δ29Si Determination on USGS BHVO-1 and BHVO-2 Reference Materails with a New Configuration on a Nu Plasma Multi-Collector ICP-MS, Geostandards and Geoanalytical Research, 32(2), 193-202.

Blain S., P., Tréguer, S. Belviso, E. Bucciarelli, M. Denis, S. Desabre, M. Fiala, V. Martin Jézéquel, J. Le Fèvre, P. Mayzaud, J.-C. Marty, S. Razouls (2001), A biogeochemical study of the island mass effect in the context of the iron hypothesis: Kerguelen Islands, Southern Ocean, Deep-Sea Research I, 48, 163-187.

Blain S., B. Quéguiner, L. Armand, S. Belviso, B. Bombled, L. Bopp, A. Bowie, C. Brunet, C. Brussaard, F. Carlotti, U. Christaki, A. Corbière, I. Durand, F. Ebersbach, J.-L. Fuda, N. Garcia, L. Gerringa, B. Griffiths, C. Guigue, C. Guillerm, S. Jacquet, C. Jeandel, P. Laan, D. Lefèvre, C. Lo Monaco, A. Malits, J. Mosseri, I. Obernosterer, Y.-H. Park, M. Picheral, P. Pondaven, T. Remenyi, V. Sandroni, G. Sarthou, N. Savoye, L. Scouarnec, M. Souhaut, D. Thuiller, K. Timmermans, T. Trull, J. Uitz, P. van Beek, M. Veldhuis, D. Vincent, E. Viollier, L. Vong, T. Wagener (2007), Effect of natural iron fertilization on carbon sequestration in the Southern Ocean, Nature, 446, 1070-1075, doi:10.1038/nature05700.

Blain S., S. Renaut, X. Xing, H. Claustre, C. Guinet (2013), Instrumented elephant seals reveal the seasonality in chlorophyll and light-mixing regime in the iron-fertilized Southern Ocean, Geophysical Research Letters, 40, doi:10.1002/2013GL058065.

Blain S., J. Capparos, A Guéneuguès, I Obernosterer, L. Oriol (2014), Distributions and stoichiometry of dissolved nitrogen and phosphorus in the iron fertilized region near Kerguelen (Southern Ocean), Biogeosciences Discussion, 11, 9949-9977.

Bowie, A.R., P. Van der Merwe, F. Quéroué, T. Trull, M. Fourquez, F. Planchon, G. Sarthou, F. Chever, A. T. Townsend, I. Obernosterer, J.-B. Sallée, S. Blain (2014). Iron budgets for three distinct biogeochemical sites around the Kerguelen archipelago (Southern Ocean) during the natural fertilization experiment KEOPS-2. Biogeosciences discussion. 11, 17861-17923.

Boyd P.W and T.W. Trull (2007), Understanding the export of biogenic particles in oceanic waters: Is there concensus?, Progress in Oceanography, 72, 276-312.

Brzezinski M.A., D.M. Nelson, V.M. Franck, D.E. Sigmon (2001), Silicon dynamics within an intense open-ocean diatom bloom in the Pacific sector of the Southern Ocean, Deep-sea research II, 48, 3997-4018.

Brzezinski M.A., C.J. Pride, V.M. Frank (2002), A switch from $Si(OH)_4$ to NO_3^- depletion in the glacial Southern Ocean, Geophysical research letters, 29(12), doi:10.1029/2001GL014349.

Bucciarelli E., P. Pondaven, G. Sarthou (2010) Effects of an iron-light co-limitation on the elemental composistion (Si, C, N) of the marine diatoms *Thalassiosira oceanica* and *Ditylum brightwellii*, Biogeosciences, 7, 657-669.

Buesseler K.O. (1998), The decoupling of production and particulate export in the surface ocean, Global Biogeochemical Cycles, 12(2), 297-310.

Buesseler K.O., L. Ball, J. Andrews, J. K. Cochran, D. J. Hirschberg, M. P. Bacon, A. Fleer, M. Brzezinski (2001), Upper ocean export of particulate organic carbon and biogenic silica in the Southern Ocean along 170°W, Deep-Sea Research II, 48, 4275-4297.

Cao Z., M. Frank, M. Dai, P. Grasse, C. Ehlert (2012) Silicon isotope constraints on sources and utilization od silicic acid in the northern South China Sea, Geochimica et Cosmochimica Acta, 97, 88-104

Cardinal D., L.Y. Alleman, J. De Jong, K. Ziegler, L. André (2003), Isotopic composition of silicon measured by multicollector plasma source mass spectrometry in dry plasma mode, Journal of Analytical Atomic Spectrometry, 18, 213-218.

Cardinal D., L.Y. Alleman, F. Dehairs, N. Savoye, T.W. Trull, L. André (2005), Relevance of silicon isotopes to Si-nutrient utilization and Si-source assessment in Antarctic waters, Global biogeochemical cycles, 19(GB2007), doi:10.1029/2004GB002364.

Cardinal D., N. Savoye, T.W. Trull, F. Dehairs, E.E. Kopczynska, F. Fripiat, J.-L. Tison, L. André (2007) Silicon isotopes in spring Southern Ocean diatoms: Large zonal changes despite homogeneity among size fractions, Marine Chemistry, 106, 46-62

Cavagna A-J., F. Fripiat, F. Dehairs, D. Wolf-Gladrow, B. Cisewski, N. Savoye, L. André, D. Cardinal (2011), Silicon uptake and supply during a Southern Ocean iron fertilization experiment (EIFEX) tracked by Si isotopes, Limnology and Oceanography, 56(1), 147-160, doi:10.4319/lo.2011.56.1.0147.

Cavagna A-J., F. Fripiat, M. Elskens, F. Dehairs, P. Mangion, L. Chirurgien, I. Closset, M. Lasleiz, L. Flores-Leiva, D. Cardinal, K. Leblanc, C. Fernadez, D. Lefèvre, L. Oriol, S. Blain, B. Quéguiner (2014), Biological productivity regime and associated N cycling in the vicinity of Kerguelen Island area, Southern Ocean, Biogeosciences Discussion, 11, 18073-18104.

Closset I., M. Lasbleiz, K. Leblanc, B. Quéguine, A.-J. Cavagna, M. Elskens, J. Navez, D. Cardinal (2014), Seasonal evolution of net and regenerated silica production around a natural Fe-fertilized area in the Southern Ocean estimated with Si isotopic approaches, Biogeosciences, 11, 5827-5846, doi:10.5194/bg-11-5827-2014.

Closset I., D. Cardinal, S. Bray, F. Thil, I. Djouraev, A. S. Rigual-Hernandez, T. Trull, Seasonal variations, origin and fate of settling diatoms in the Southern Ocean tracked by silicon isotope records in deep sediment traps, in preparation for Global Biogeochemical Cycles.

Coffineau N., C. L. De la Rocha, P. Pondaven (2014), Exploring interacting influences on the silicon isotopic composition of the surface ocean: a case study from the Kerguelen Plateau, Biogeosciences, 11, 1371-1391.

De Baar H.J.W., P.W. Boys, K.H. Coale, M.R. Landry, A. Tsuda, P. Assmy, D.C.E. Bakker, Y. Bozec, R.T. Barber, M.A. Brzezinski, K.O. Buesseler, M. Boyé, P.L. Croot, F. Gervais, M.Y. Gorbunov, P.J. Harrison, W.T. Hiscock, P. Laan, C.Lancelot, C.S. Law, M. Levasseur, A. Marchetti, F.J. Millero, J. Nishioka, Y. Nojiri, T. van Oijen, U. Riebesell, M.J.A. Rijkenberg, H. Saito, S. Takeda, K.R. Timmermans, M.J.W. Veldhuis, A.M. Waite C.-S. Wong (2005) Synthesis of iron fertilization experiments: From the Iron Age in the Age of Enlightenment, Journal of Geophysical Research, 110, C09S16, doi:10.1029/2004JC002601

De Brauwere A., F. Fripiat, D. Cardinal, A.-J. Cavagna, F. De Ridder, L. André, M. Elskens (2012), Isotopic model of oceanic silicon cycling: The Kerguelen Plateau case study, Deep-Sea Research I, 70, 42-59.

Dehairs F., F. Fripiat, A.-J. Cavagna, T. W. Trull, C. Fernandez, D. Davies, A. Roukaerts, D. Fonseca Batista, F. Planchon, M. Elskens (2014), Nitrogen cycling in the Southern Ocean Kerguelen Plateau area: evidence for significant surface nitrification from nitrate isotopic compositions, Biogeosciences Discussion, 11, 13905-13955.

De La Rocha C.L., M.A. Brzezinski, M.J. DeNiro (1997), Fractionation of silicon isotopes by marine diatoms during biogenic silica formation, Geochimica et Cosmochimica Acta, 61(23), 5051-5056.

De La Rocha C.L., M.A. Brzezinski, M.J. DeNiro, A. Shemesh (1998), Silicon-isotope composition of diatoms as an indicator of past oceanic change, Nature, 395, 680-683.

De La Rocha C.L., D.A. Hutchins, M.A. Brzezinski, Y. Zhang (2000), Effects of iron and zinc deficiency on elemental composition and silica production by diatoms, Marine Ecology Progress Series, 195,71-79.

De Souza G. F., B. C. Reynolds, J. Rickli, M. Frank, M. A. Saito, L. J. A. Gerringa, B. Bourdon (2012), Southern Ocean control of silicon stable isotope distribution in the deep Atlantic Ocean, Global Biogeochemical Cycles, 26, GB2035, doi:10.1029/2011GB004141.

Demarest M.S., M.A. Brzezinski, C.P. Beucher (2009), Fractionation of silicon isotopes during biogenic silica dissolution, Geochimica et Cosmochimica Acta, 73, 5572-5583, doi:10.1016/j.gca.2009.06.019.

Dugdale R.C., F.P. Wilkerson, H.J. Minas (1995), The role of a silicate pump in driving new production, Deep-Sea Research I, 42(5), 697-719.

Ehlert C., P.grasse, M. Frank (2013), Changes in silicate utilization and upwelling intensity off Peru since the Last Glacial Maximum – insights from silicon and neodymium isotopes, Quaternary Science Reviews, 72, 18-35.

Etourneau J., C. Ehlert, M. Frank, P. Martinez, R. Scheider (2012), Contribution of changes in opal productivity and nutrient distribution in the coastal upwelling systems to Late Pliocene/Early Pleistocene climate cooling, Climate of the Past, 8, 1435-1445.

Frank V.M., M.A. Brzezinski, K.H. Coale, D.M. Nelson (2000) Iron and silicic acid concentrations regulate Si uptake north and south of the Polar Frontal Zone in the Pacific Sector of the Southern Ocean, Deep-Sea Research II, 47,3315-3338.

Fripiat F., A-J. Cavagna, N. Savoye, F. Dehairs, L. André, D. Cardinal (2011a), Isotopic constraints on the Si-biogeochemical cycle of the Antarctic Zone in the Kerguelen area (KEOPS), Marine Chemistry, 123, 11-22, doi:10.1016/j.marchem.2010.08.005.

Fripiat F., A-J. Cavagna, F. Dehairs, S. Speich, L. André, D. Cardinal (2011b), Silicon pool dynamics and biogenic silica export in the Southern Ocean inferred from Si-isotopes, Ocean Science, 7, 533-547, doi:10.5194/os-7-533-2011.

Fripiat F., A-J. Cavagna, F. Dehairs, A. de Brauwere, L. André, D. Cardinal (2012), Processes controlling the Si-isotopic composition in the Southern Ocean and application for paleoceanography, Biogeosciences, 9, 2443-2457, doi:10.5194/bg-9-2443-2012.

Fry B. (2006) Stable Isotope Ecology, Springer, New York, pp 308

Georg R.B., B.C. Reynolds, M. Frank, A. N. Halliday (2006), New sample preparation techniques for the determination of Si isotopic compositions using MC-ICPMS, Chemical Geology, 235, 95-104.

Grasshoff K., K. Kremling, M. Ehrhardt (1999), Methods of Seawater Analysis 3rd edition completely Revised and Extended edition. Wiley-VCH. ISBN 3-527-29589-5.

Hughes H.J., C. Delvigne, M. Korntheuer, J. De Jong, L. André, D. Cardinal (2011), Controlling the mass bias introduced by anionic and organic matrices in silicon isotopic measurements, Journal of Analytical Atomic Spectrometry, 26, 1892-1896.

Hutchins D.A., K.W. Bruland (1998), Iron-limited diatom growth and Si:N uptake ratios in a coastal upwelling regime, Nature, 393, 561-564.

Jacquet S. H. M., F. Dehairs, A.-J. Cavagna, F. Planchon, L. Monin, L. André, I. Closset, D. Cardinal (2014), Early season mesopelagic carbon remineralization and transfer efficiency in the naturally iron-fertilized Kerguelen area, Biogeosciences Discussion, 11, 9035-9069.

Karl D. M., G. Tien (1992), MAGIC: A sensitive and precise method for measuring dissolved phosphorus in aquatic environments, Limnology and Oceanography, 37(1), 105-116.

Laurenceau E.C., T.W. Trull, D.M. Davies, S.G. Bray, J. Doran, F. Planchon, F. Carlotti, M-P. Jouandet, A-J. Cavagna, A.M. Waite, S. Blain (2014), The relative importance phytoplankton aggregates and zooplankton fecal pellets to carbon export: insights from free-drifting sediment trap deployments in naturally iron-fertilised waters near the Kerguelen plateau, Biogeosciences Discussion, 11, 13623-13673.

Lasbleiz M., K. Leblanc, S. Blain, J. Ras, V. Cornet-Barthaux, S. Hélias Nunige, B. Quéguiner (2014), Pigments, elemental composition (C, N, P and Si), and stoichiometry of particulate matter in the naturally iron fertilized region of Kerguelen in the Southern Ocean, Biogeosciences, 11, 5931-5955, doi:10.5194/bg-11-5931-2014.

Leynaert A., E. Bucciarelli, P. Claquin, R.C. Dugdale, V. Martin-Jézéquel, P. Pondaven, O. Raguegeau (2004), Effect of iron deficiency on diatom cell size and silicic acid uptake kinetics, Limnology and Oceanography, 49(4), 1134-1143.

Matsumoto K., J.L. Sarmiento (2008), A corollary to the silicic acid leakage hypothesis, Paleoceanography, 23, PA2203, doi:10.1029/2007PA001515.

Matsumoto K., J.L. Sarmiento, M.A. Brzezinski (2002), Silicic acid leakage from the Southern Ocean: A possible explanation for glacial atmospheric pCO_2, Global Biogeochemical Cycles, 16(3), doi:10.1029/2001GB001442.

Mongin M., E. Molina, T.W. Trull (2008), Seasonality and scale of the Kerguelen plateau phytoplankton bloom: A remote sensing and modeling analysis of the influence of natural iron fertilization in the Southern Ocean, Deep-Sea Research II, 55, 880-892.

Mosseri J., B. Quéguiner, L. Armand, V. Cornet-Barthaux (2008), Impact of iron on silicon utilization by diatoms in the Southern Ocean: A case study of Si/N cycle decoupling in a naturally iron-enriched area, Deep-sea research II, 55, 801-819.

Nelson D.M., M.A. Brzezinski, D.E. Sigmon, V.M. Franck (2001), A seasonal progression of Si limitation in the Pacific sector of the Southern Ocean, Deep-sea research II, 48, 3973-3995.

Nelson D.M., R.F. Anderson, R.T. Barber, M.A. Brzezinski, K.O. Buesseler, Z. Chase, R.W. Collier, M.-L. Dickson, R. François, M.R. Hiscock, S. Honjo, J. Marra, W.R. Martin, R.N. Sambrotto, F.L. Sayles, D.E. Sigmon (2002) Vartical budgets for organic carbon and biogenic silica in the Pacific sector of the Southern Ocean, 1996-1998, Deep-Sea Research II, 49, 1645-1674

Opfergelt S., P. Delmelle (2012), silicon isotopes and continental weathering processes: Assessing controls on Si transfer to the ocean, Comptes Rendus Geoscience, 344, 723-738, doi:10.1016/j.crte.2012.09.006.

Park Y.-H., F. Roquet, I. Durand, J.-L. Fuda (2008a), Large-scale circulation over and around the Northern Kerguelen Plateau, Deep-Sea Research II, 55, 566-581.

Park Y.-H., F. J.-L Fuda, I. Durand, A.C. Naveira Garabato (2008b), Internal tides and vertical mixing over the Kerguelen Plateau, Deep-Sea Research II, 55, 582-593.

Park Y.-H., I. Durand, E. Kestenare, G. Rougier, M. Zhou, F. d'Ovidio, C. Cotté, J.-H. Lee (2014), Polar Front around the Kerguelen Islands: An up-to-date determination and associated circulation of surface/subsurface waterJournal of Geophysical Research: Oceans, 119, doi:10.1002/2014JC010061.

Parslow J.S., P.W. Boyd, S.R. Rintoul, F.B. Griffiths (2001), A persistent subsurface chlorophyll maximum in the Interpolar Frontal Zone south of Australia: Seasonal progression and implications for phytoplankton-light-nutrient interactions, Journal of geophysical research, 106(C12), 31543-31557.

Planchon F., D. Ballas, A.-J. Cavagna, A. R. Bowie, D. Davies, T. Trull, E. Laurenceau, P. Van der Merwe, F. Dehairs (2014), Carbon export in the naturally iron-fertilized Kerguelen area of the Southern Ocean based on the 234^{Th} approach, Biogeosciences Discussion, 11, 15991-16032.

Pollard R.T., M.I. Lucas, J.F. Read (2002), Physical controls on biogeochemical zonation in the Southern Ocean, Deep-Sea Research II, 49, 3289-3305.

Pollard R., P. Tréguer, J. Read (2006), Quantifying nutrient supply to the Southern Ocean, Journal of Geophysical Research, 111, C05011, doi:10.1029/2005JC003076

Pondaven P., O. Ragueneau, P. Tréguer, A. Hauvespre, L. Dezileau, J.L. Reyss (2000), Resolving the 'opal paradox' in the Southern Ocean, Nature, 405, 168-172.

Quéguiner B. (2013), Iron fertilization and the structure of planktonic communities in high nutrient regions of the Southern Ocean, Deep-Sea Research II, 90, 43-54.

Ragueneau O., P. Tréguer, A. Leynaert, R.F. Anderson, M.A. Brzezinski, D.J. DeMaster, R.C. Dugdale, J. Dymond, G. Fischer, R. François, C. Heinze, E. Maier-Reimer, V. Martin-Jézéquel, D.M. Nelson, B. Quéguiner (2000), A review of the Si cycle in the modern ocean: recent progress and missing gaps in the application of biogenic opal as a paleoproductivity proxy, Global and Planetary Change, 26, 317-365.

Ragueneau O., N. Savoye, Y. Del Amo, J. Cotten, B. Tardiveau, A. Leynaert (2005), A new method for the measurement of biogenic silica in suspended matter of coastal waters: using Si:Al ratios to correct for the mineral interference, Continental Shelf Research, 25, 697-710.

Rembauville M., S. Blain, I. Salter (2014), Export fluxes in a naturally fertilized area of the Southern Ocean, the Kerguelen plateau: ecological vectors of carbon and biogenic silica to depth (part 2), Biogeosciences Discussion, 11, 17089-17150.

Reynolds B.C., M. Frank, A. N. Halliday (2006), Silicon isotope fractionation during nutrient utilization in the North Pacific, Earth and Planetary Science Letters, 244, 431-443.

Reynolds B.C., J. Aggarwal, L. André, D. Baxter, C. Beucher, M.A. Brzezinski, E. Engström, R.B. Georg, M. Land, M.J. Leng, S. Opfergelt, I. Rodushkin, H.J. Sloane, S.H.J.M. van den Boorn, P.Z. Vroon, D. Cardinal (2007), An inter-laboratory comparison of Si isotope reference materials, Journal of Analytical Atomic Spectrometry,22, 561-568, doi:10.1039/b616755a.

Roquet F., Y.-H. Park, C. Guinet, F. Bailleul., J.-B. Charrassin (2009), Obervations of the Fawn Trough Current over the Kerguelen Plateau from instrumented elephant seals, Journal of Marine Systems, 78, 377-393.

Sabine C.L., R.A. Feely, N. Gruber, R.M. Key, K. Lee, J.L. Bullister, R. Wanninkhof, C.S. Wong, D.W.R. Wallace, B. Tilbrook, F.J. Millero, T.-H. Peng, A. Kozyr, T. Ono, A.F. Rios (2004), The Ocean Sink for Anthropogenic CO_2, Science, 305 , 367-371.

Sanial V., P. van Beek, B. Lansard, M. Souhaut, E. Kestenare, F. d'Ovidio, M. Zhou, S. Blain (2014), Use of Ra isotopes to deduce rapid transfer of sediment-derived inputs off Kerguelen, Biogeosciences Discussion, 11, 14023-14061.

Sarmiento J.L., N. Gurber, M.A. Brzezinski, J.P. Dunne (2004), High-latitude controls of thermocline nutrients and low latitude biological productivity, Nature, 427, 56-60.

Sutton J.N., D.E. Varela, M.A. Brzezinski, C.P. Beucher (2013), Species-dependent silicon isotope fractionation by marine diatoms, Geochimica et Cosmochimica Acta, 104, 300-309.

Takahashi T., S.C. Sutherland, R. Wanninkhof, C. Sweeney, R.A. Feely, D.W. Chipman, B. Hales, G. Friederich, F. Chavez, C. Sabine, A. Watson, D.C.E. Bakker, U. Schuster, N. Metzl, H. Yoshikawa-Inoue, M. Ishii, T. Midorikawa, Y. Nojiri, A. Körtzinger, T. Steinhoff, M. Hoppema, J. Olafsson, T.S. Arnarson, B. Tilbrook, T. Johannessen, A. Olsen, R. Bellerby, C.S. Wong, B. Delille, N.R. Bates, H.J.W. de Baar (2009), Climatological mean and decadal change in surface ocean pCO2, and net sea-air CO2 flux over the global oceans, Deep-Sea Research II, 56, 554-577, doi: 10.1016/j.dsr2.2008.12.009.

Takeda S. (1998), Influence of iron availability on nutrient consumption ratio of diatoms in oceanic waters, Nature, 393, 774-777.

Tréguer P.J., C.L. De La Rocha (2013), The World Ocean Silica Cycle, Annual Review of Marine Science, 5, 477-501.

Trull T., S.R. Rintoul, M. Hadfield, E.R. Abraham (2001), Circulation and seasonal evolution of polar waters south of Australia: Implications for iron fertilization of the Southern Ocean, Deep-Sea Research II, 48, 2439-2466.

Trull T., D. M. Davies, F. Dehairs, A.-J. Cavagna, M. Lasbleiz, E. C. Laurenceau, F. d'Ovidio, F. Planchon, K. Leblanc, B. Quéguiner, S. Blain (2014), Chemometric perspectives on plankton community responses to natural iron fertilization over and downstream of the Kerguelen Plateau in the Southern Ocean, Biogeosciences Discussion, 11, 13841-13903.

Uitz J., H. Claustre, F.B. Griffiths, J. Ras, N. Garcia, V. Sandroni (2009) A phytoplankton class-specific primary production model applied to the Kerguelen Islands region (Southern Ocean), Deep-Sea Research I, 56, 541-560

Varela D.E., C.J., Pride, M.A. Brzezinski (2004), Biological fractionation of silicon isotopes in Southern Ocean surface waters, Global biogeochemical cycles, 18(GB1047), doi:10.1029/2003GB002140.

Van den Boorn S.H.J.M., P.Z. Vroon, M.J. Van Bergen (2009), Sulfur-induced offsets in MC-ICP-MS silicon-isotope measurements, Journal of Analytical Atomic Spectrometry, 24, 1111-1114.

Wetzel F., G.F. de Souza, B.C. Reynolds (2014), What controls silicon isotope fractionation during dissolution of diatom opal?, Geochimica et Cosmochimica Acta, 131, 128-137, doi:10.1016/j.gca.2014.01.028.

Zhou M., Y. Zhu, F. d'Ovidio, Y.-H. Park, I. Durand, E. Kestenare, V. Sanial, P. Van-Beek, B. Quéguiner, F. Carlotti, S. Blain (2014), Surface currents and upwelling in Kerguelen Plateau regions, Biogeosciences Discussion, 11, 6845-6876.

Chapitre 3

Variations Saisonnières, Origine et Devenir du Flux de Diatomées dans la Colonne d'eau

PREAMBULE

Contexte de l'étude

Les deux premiers chapitres de ce travail de thèse montrent que la notion de saisonnalité est très importante dans la compréhension de la distribution et des variations du $\delta^{30}Si$ de l'eau de mer et des particules siliceuses. Or jusqu'à présent, aucune étude ne s'est concentrée sur un suivi annuel complet de l'évolution de la composition isotopique de la BSi et encore moins du DSi. Les deux campagnes océanographiques impliquées dans le programme KEOPS n'ont permis d'échantillonner que deux phases du développement phytoplanctonique (l'initiation de l'efflorescence au printemps – KEOPS-2 – et le déclin du bloom à la fin de l'été – KEOPS-1). La production de nouveaux jeux de données issues de séries temporelles à haute fréquence, tels que présentés dans ce chapitre, permet de s'intéresser plus particulièrement à cette notion de saisonnalité des variations de la composition isotopique du réservoir particulaire de silicium, ainsi qu'au transfert de ce signal depuis la surface vers l'océan profond. En effet, à ce jour une seule étude incluant uniquement 18 points issus de pièges à particules placés dans la Zone Antarctique de l'Océan Austral s'est intéressée à cette notion de transfert du $\delta^{30}Si$ dans la colonne d'eau (*Fig. 3.1.* ; Varela et al., 2004).

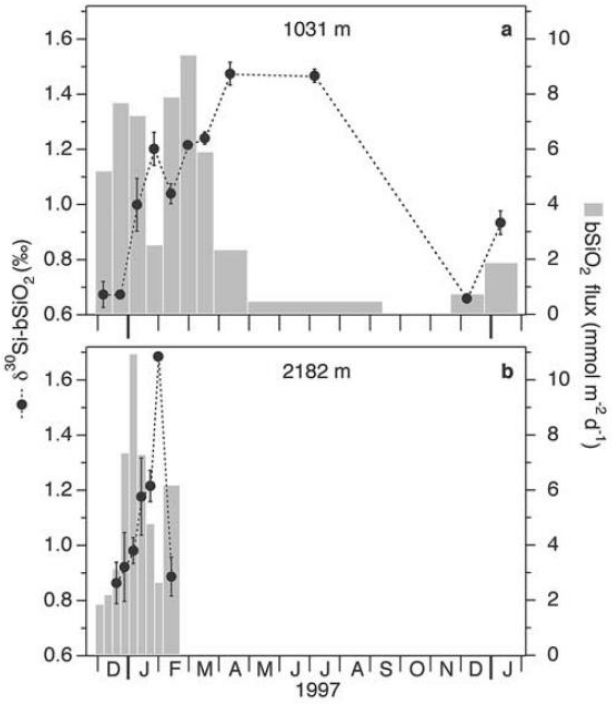

Figure 3.1. L'unique enregistrement actuel de l'évolution saisonnière de la composition isotopique ($\delta^{30}Si$-$bSiO_2$) et du flux de BSi ($bSiO_2$ flux) mesuré par Varela et al. (2004) dans des pièges à particules de la Zone Antarctique lors du programme AESOPS.

Les résultats discutés dans ce chapitre représentent donc le plus grand jeu de données issues de pièges à particules actuellement produit et nous permettent de confirmer que le signal isotopique de surface est bien conservé tout au long de la sédimentation des particules vers le fond. En étudiant les variations du $\delta^{30}Si$ du flux de ces particules nous avons apporté des informations qualitatives et/ou quantitatives concernant la consommation d'acide silicique par les organismes siliceux dans les eaux de surface des différentes régions de l'Océan Austral ainsi que sur l'apport de DSi dans la couche de mélange (ML) lors d'évènements de mélange vertical de la colonne d'eau. De plus, la comparaison des signatures isotopiques du flux de particules à différentes profondeurs nous donne également accès à des informations complémentaires telles que l'estimation de la vitesse de sédimentation des particules siliceuses et de ses variations saisonnières, paramètres particulièrement délicats à mesurer in-situ.

Résumé

L'Océan Austral joue un rôle important dans le contrôle des niveaux de CO_2 atmosphérique. Le transfert biologique du carbone dans l'océan interne est couplé à la disponibilité en silicium dissous (DSi) dans la couche de mélange (ML), qui forme un substrat minéral permettant aux diatomées de dominer la production primaire. Dans cet océan, les variations du cycle du silicium sont nombreuses mais ne sont pas encore totalement comprises. Dans cette étude, Nous utilisons les mesures de $\delta^{30}Si$ pour retracer les flux de silice vers l'océan profond dans les 3 zones majeures de l'Océan Austral (La Zone Antarctique, AZ ; la Zone du Front Polaire, PFZ et la Zone Sub-Antactique, SAZ). Les variations du flux de silice biogénique exportée (BSi) ainsi que celles de sa composition isotopique révèlent un éventail de notions importantes telles que :

i) Les taux de sédimentation de la BSi peuvent être supérieurs à 200 m j^{-1} en été dans l'AZ. Ils diminuent vers de très faibles valeurs en hiver, permettant ainsi aux particules de se maintenir dans la colonne d'eau jusqu'au printemps suivant.

ii) Des mélanges verticaux occasionnels affectent le $\delta^{30}Si$ de la BSi exportée à la fois dans la SAZ et dans l'AZ, mais la relation entre la consommation de DSi, les flux de BSi et leur composition isotopique restent raisonnablement bien décrits par un mélange entre les modèles ouvert et fermé.

Ces résultats, ainsi que les suivis des flux de BSi et de leur composition isotopique apportent de nouveaux éléments pour l'application des modèles biogéochimiques se concentrant sur le contrôle saisonnier de la production et de l'export de BSi, de leurs variations au cours du temps, et sur la façon dont ces signaux sont actuellement archivés dans les sédiments.

Ce chapitre a été soumis dans Global Biogeochemical Cycles et est en cours de révision :

Closset I., D. Cardinal, S. Bray, F. Thil, I. Djouraev, A. Rigual-Hernandez, T. Trull (2015), Seasonal variations, origin and fate of settling diatoms in the Southern Ocean tracked by silicon isotope records in deep sediments traps, in prep. for Global Biogeochemical cycles.

TABLE OF CONTENTS

Seasonal variations, origin and fate of settling diatoms in the Southern Ocean tracked by silicon isotope records in deep sediment traps

Closset Ivia[1], Damien Cardinal[1], Stephen Bray[2], François Thil[3], Irina Djouraev[4], Andrés S. Rigual-Hernandez[5], Thomas Trull[2]

[1] Sorbonne Universités (UPMC, Univ Paris 06)-CNRS-IRD-MNHN, LOCEAN Laboratory, 4 place Jussieu, F-75005 Paris, France

[2] Antarctic Climate and Ecosystems Cooperative Research Center, ACE CRC Private Bag 80, Hobart 7001, Tasmania

[3] Laboratoire des Sciences du Climat et de l'Environnement, CNRS 91190 Gif-sur-Yvette, France

[4] IRD-Sorbonne Universités (UPMC, Univ Paris 06)-CNRS-MNHN, LOCEAN Laboratory, IRD France Nord, 32, avenue Henry Varagnat, F-93143 Bondy, France

[5] Department of Biological Sciences, Macquarie University, North Ryde NSW 2109, Australia

Correspondence to: I. Closset (ivia.closset@locean-ipsl.upmc.fr)

Abstract

The Southern Ocean plays a pivotal role in the control of atmospheric CO_2 levels. The biological carbon transfer to the ocean interior is coupled to the availability of dissolved silicon (DSi) as the mineral substrate that allows diatoms to dominate primary production. Importantly, variations in the silicon cycling are large but not well understood. We use $\delta^{30}Si$ measurements to track seasonal flows

of silica to the deep sea for the three major zones (Antarctic, AZ; Polar Frontal, PFZ and Subantarctic, SAZ) of the open Southern Ocean. Variations in the exported flux of biogenic silica (BSi) and its $\delta^{30}Si$ composition reveal a range of insights, including that i) the sinking rate of BSi exceeds 200 m d^{-1} in summer in the AZ, yet decreases to very low values in winter that allow particles to remain in the water column through to the following spring, ii) occasional vertical mixing events affect the $\delta^{30}Si$ composition of exported BSi in both the SAZ and AZ, but the relationship between DSi depletion, BSi fluxes and its composition remains reasonably described by a mix of open- and closed-system models. These insights and the records of BSi fluxes and compositions provide new constraints for application to biogeochemical models of seasonal controls on production and export, and their variations over time as recorded by sediments.

III.1 Introduction

The Southern Ocean is a crucial component of the climate system. In this region, the oceanic biogeochemical cycles of carbon and silicon are closely connected through diatoms that dominate the primary production in the Antarctic Circumpolar Current (ACC, Ragueneau et al., 2000; Assmy et al., 2013; Tréguer & De la Rocha, 2013). As siliceous phytoplankton they have an absolute requirement for silicic acid (H_4SiO_4, hereafter referred to as DSi) to build their biogenic silica cell wall or frustule (amorphous $SiO_2.nH_2O$, hereafter referred to as BSi). Diatoms are also the major exporters of organic matter and silica in the polar Southern Ocean where they dominate the modern BSi deposition (Ragueneau et al., 2000). Several processes occurring in the Southern Ocean impact on the biogeochemical properties of the low-latitude surface waters and on their biological productivity. Currently, the large DSi utilization by diatoms in the ACC, combined to the global overturning circulation would determine the functioning of the biological pump of low latitude areas by feeding the mixed layer (ML) in nutrients such as nitrate and by maintaining a strong silicon limitation (Sarmiento et al., 2004). Indeed, the seasonality of both irradiance and mixing regimes of surface waters, combined to the lack of micronutrients such as iron, prevent the complete consumption of macronutrients in the ML with the notable exception of DSi, so that the Southern Ocean represents the largest High Nutrient Low Chlorophyll (HNLC) area in the global ocean (Martin 1990).

The physical and biogeochemical properties of surface waters in the ACC vary from north to south and the Southern Ocean is divided into several oceanographic zones by different circumpolar fronts (Orsi et al., 1995 and *Fig. 3.2.*). The southern region is the Antarctic Zone (AZ) where biological production is not limited by macronutrient availability but mainly controlled by irradiance and iron concentrations (Trull et al., 2001b). To its north, the Polar Front Zone (PFZ) lies between the Polar Front (PF) and the Sub-Antarctic Front (SAF). Here, silicic acid concentrations remain high in the ML until at least mid-summer (Rintoul & Trull, 2001; Trull et al., 2001b). Although the physical and biogeochemical properties of these two zones differ in many ways, the dynamics of the primary production reveals some similarities such as strong seasonality and the predominance of diatoms (Honjo et al., 2000). On the northern end, the Sub-Antarctic Zone (SAZ) is located north of the SAF and is a region of transition from the cold nutrient rich polar conditions to the warm nutrient poor conditions of the subtropical waters to the north. In this zone, nitrate and phosphate concentrations remain moderately high, but DSi concentrations are low throughout the year and drop to nearly undetectable levels in summer (Rintoul & Trull, 2001; Trull et al., 2001b), limiting diatoms and favoring non-siliceous autotrophic organisms such as coccolithophorids (Kopczynka et al., 2001; De Salas et al., 2011).

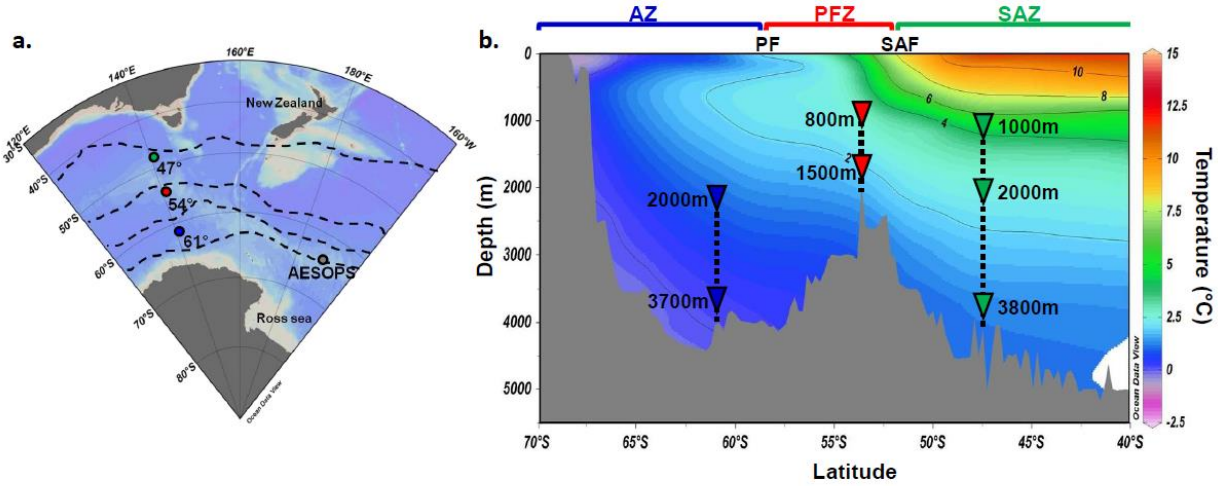

Figure 3.2. (a) Map showing the location of stations discussed in this study. From south to north, dotted lines represent the position of the Southern Antarctic Circumpolar Current Front (SACCF), Polar Front (PF), Sub-Antarctic Front (SAF) and Sub-Tropical Front (STF) respectively. (b) Schematic view of the mooring configuration in relation to the bathymetry and the mean seawater temperature compiled from Electronic Atlas of WOCE Data.

In order to study the marine silicon cycle, which is still marked by major uncertainties (Tréguer & De La Rocha, 2013), silicon isotopes have been shown particularly useful because during silicification diatoms preferentially incorporate the lightest Si-isotope (^{28}Si) into their cell wall (De la Rocha et al., 1997) leaving the stable isotope composition of DSi (expressed as $\delta^{30}Si$, *see section 3.4*) enriched in the heaviest Si-isotope (^{30}Si). This leads to a progressive increase in $\delta^{30}Si$ of both substrate ($\delta^{30}Si_{DSi}$) and product ($\delta^{30}Si_{BSi}$) as the nutrient pool is consumed, and results in the occurrence of a general inverse relationship between silicic acid concentration and $\delta^{30}Si$ of both silicic acid and diatom opal (e.g. Varela et al., 2004; Cardinal et al., 2005, 2007; Fripiat et al., 2011a). Consequently, $\delta^{30}Si$ signatures can be used to trace the processes affecting both modern and past oceanic biogeochemical Si cycles (e.g. De Souza et al. 2014). Several works have used the $\delta^{30}Si$ signature preserved in diatom opal as a proxy for their Si-utilization over geologic time in the Southern Ocean (e.g. De la Rocha et al., 1998; Brzezinski et al., 2002; Beucher et al., 2008; Panizzo et al., 2014), but only one study has investigated the variations of exported opal $\delta^{30}Si$ using time series sediment traps located in the Antarctic Zone of the Southern Ocean (Varela et al., 2004). Thus, the mechanisms governing the seasonal variations of diatom $\delta^{30}Si$ signature and its transfer to depth must be better constrained before they can be used as a tracer for present and past changes in Si utilization.

In this paper, we investigate the spatial and seasonal variability of silicon isotopic composition of sinking particles collected in deep sediment traps at three sites in the Southern Ocean in the Antarctic, Polar Frontal, and Subantarctic Zones. Our specific objectives are the following:

(1) Identify the processes that control the transfer of $\delta^{30}Si_{BSi}$ to depth in order to fully validate its use in paleoceanographic records as a proxy of the relative silicic acid utilization and diatom production in surface water.

(2) Analyze the seasonality of $\delta^{30}Si_{BSi}$ flux in different zones of the ACC to infer information about the mechanisms and processes that govern surface Si dynamics and fate of diatoms in these regions.

(3) Explore the latitudinal variations of isotopic composition of siliceous particles in deep Southern Ocean to determine whether the distribution and seasonal variations of $\delta^{30}Si$ may be modelled as a single simple system.

III.2. Material & Methods

III.2.1. Sample collection and processing

Samples were collected from 7 sediment traps deployed on 3 open-ocean moorings along a north-south transect at 140°E in the Australian Sector. Stations were located in the AZ, PFZ and SAZ at 61°S, 54°S and 47°S respectively. The shallowest traps were deployed at approximately 1 km below surface to minimize advection or swimmer problems, and deepest traps approximately 700m from the bottom to avoid resuspended material. Both moorings in the SAZ and PFZ operated from 21/07/1999 to 29/08/2000 while it ran from 26/11/2001 to 29/09/2002 in the AZ. For each mooring, cup rotation intervals were synchronized between traps and are given in *Table C1*. These intervals were defined depending on anticipated mass fluxes to allow a high sampling resolution in austral summer while lower time-resolution was chosen during winter. Just before their deployment, sampling cups were filled with unfiltered seawater from the region mixed with a buffered solution of sodium tetraborate (1 g L^{-1}), sodium chloride (5 g L^{-1}) and mercury chloride (3 g L^{-1}). The moorings were designed to remain reasonably vertical. Thus large hydrodynamic artifacts in the particles collections were not expected (Buesseler et al., 2007). Following Trull et al. (2001a), who found little difference among similar traps using $^{230}Th_{xs}$ we did not estimate trap efficiencies because of the large uncertainties associated to this method (Yu et al., 2001). Upon recovery, samples were sieved through 1mm sieve cloth to remove swimmers and were split into 10 equal aliquots. One of these latter was filtrated on 0.45 µm polycarbonate membrane, dried at 60°C, grounded and homogenized. This aliquot was then subsampled for BSi concentration and Si isotopic measurements and stored in 6 mL glass vials for later analysis.

III.2.2. Digestion and BSi analyses

The material collected in the trap was solubilized using a 2-step alkaline digestion adapted from Ragueneau et al. (2005). Briefly, between 0.5 and 10 mg of sediments was dissolved in Teflon tubes with a 0.2 mol L^{-1} NaOH (pH 13.3) at 100°C for 40 min followed by neutralization with HCl (1 mol L^{-1}) to stop the reaction. A second and identical digestion was applied to estimate potential lithogenic contamination in the first leaching. Indeed, total SiO_2 of particles is composed of biogenic and lithogenic components (mainly clay minerals) and the alkaline digestion can also solubilize a significant proportion of these aluminosilicates (Ragueneau et al., 2005). If not controlled, this could bias the biogenic Si fluxes and their Si isotopic signatures (*see Supplementary Method 3*). Aluminium, a tracer

of lithogenic source, was analysed in the two leachates using an Inductively Coupled Plasma Mass Spectrometer (ICP-MS; detection limit = 3.18 ppb) to quantify lithogenic Si contribution. Si concentrations were measured with a colorimetric method according to Grasshoff et al. (1999) and by ICP-MS on the same leachates as for Si-isotopic composition. For each sediment trap sample, at least two full chemical replicates were processed. Average reproducibility of these replicates on BSi concentration is 9.0 ± 6.7 % (1 sd, n = 129) which is well in agreement with the uncertainty estimated for this method (10 %, Ragueneau et al., 2005).

III.2.3. Purification

To avoid matrix effects during isotopic analyses, we purified the samples by cation-exchange chromatography (BioRad cation exchange resin DOWEX 50W-X12, 200 to 400 mesh, in H+ form) using a protocol described in Georg et al. (2006). After purification systematic analysis of major elements (such as Mg, Ca, Na, Al) were performed by ICP-MS in order to ensure the sample purity prior to isotopic analyses. Si concentrations were also measured in the purified solutions to check for complete recovery. Moreover five samples were analyzed in anionic chromatography to control the concentration of sulfate in the matrix since it has been shown to induce a significant shift in isotopic measurements for SO_4^{2-}:Si weight ratio above 0.02 (Van den Boorn et al., 2009). In these samples, sulfate concentration was systematically below the detection limit (< 100 ppb) and lead to a SO_4^{2-}:Si ratio < 0.02 that does not require any correction for anionic matrix as proposed by Hughes et al. (2011) for rock digestion solutions.

III.2.4. Isotopic measurements

Isotopic measurements were carried out on a Thermo Neptune$^+$ Multicollector Inductively Coupled Plasma Mass Spectrometer (MC-ICP-MS; LSCE, Gif-sur-Yvette) in dry plasma mode using Mg external doping to correct for the mass bias (Cardinal et al., 2003; Abraham et al., 2008). Si solutions were introduced into the plasma via an Apex desolvating nebulization system equipped with a PFA nebulizer (100 µL min^{-1} uptake rate) without additional gaz. Solutions were analyzed in medium resolution mode (M/ΔM> 6000) to find the optimum conditions to minimize the interference on ^{30}Si peak. δ^{30}Si obtained from the samples were calculated relative to the quartz standard NBS28 (RM8546). They were measured relative to a in-house standard Quartz Merck, which was not

significantly different from NBS28 (Abraham et al., 2008), using a standard-sample-standard bracketing technique, and expressed as follows:

$$\delta^{30}Si\ (‰) = \left[\frac{(^{30}Si/^{28}Si)sample}{(^{30}Si/^{28}Si)standard} - 1\right] \times 1000 \qquad (3.1.)$$

Interference-free measurement was ensured by checking that $\delta^{29}Si$ and $\delta^{30}Si$ for all the samples was consistent with the mass dependent fractionation line (*Fig. C4.*). The signal was optimized to reduce the $^{14}N^{16}O$ interference on m/z 30 below 0.5 % of the ^{30}Si peak. Measurements were performed on the left side of the peak where interference is minimal. Blanks were maintained below 1 % of the main signal and were subtracted for each sample and standard. Typical analytical conditions are provided in *table 3.1.* Long-term reproducibility and accuracy on $\delta^{30}Si$ values over the analytical procedure was calculated using the standard deviation of 109 analyzes generated over 2.5 years of a secondary reference material (Diatomite, $\delta^{30}Si$ = 1.28 ± 0.05 ‰, $\delta^{29}Si$ = 0.65 ± 0.04 ‰, 1 sd). This value is similar to the 1.26 ‰ $\delta^{30}Si$ signature of diatomite estimated during an inter-laboratory comparison exercise by Reynolds et al. (2007). Reproducibility of full chemical procedure has been estimated by at least one replicate of each sample (chemical preparation plus isotopic measurements) and average of reproducibility on duplicates $\delta^{30}Si$ is 0.05 ± 0.03 ‰ (1 sd, n= 129). Noteworthy, this indicates that the BSi leaching procedure does not induce an additional bias and that uncertainty mostly originates from analytical measurements.

Table 3.1 Neptune^{+} MC-ICP-MS operating conditions

Resolution	Medium
Foward Power	1200 W
Accelerating Voltage	10 kV
Plasma Mode	Dry Plasma
Cool Gas Flow Rate	16 L min^{-1}
Auxiliary Gas Flow Rate	1.1-1.4 L min^{-1}
Sample Gas Flow Rate	0.9-1 L min^{-1}
Cones Type	Nickel X-Skimmer cone + Standard Ni-Sample cone
Desolvator	Apex (ESI)
Nebulizer	PFA microcentric nebuliser 100 µL min^{-1}
Running Concentrations	Si = 2-2.5 ppm, Mg = 2-2.5 ppm
Sensitivity	3-4 V ppm^{-1}
Blank Level	< 1% signal
^{30}Si Interference	< 30 mV (usually 10-15 mV)

Since the alkaline digestion also dissolves LSi, and because it has a silicon isotopic signature significantly different from BSi (-2.3 to +0.1 ‰ compared to -0.3 to +2.6 ‰ for living diatoms; Opfergelt & Delmelle, 2012), it is essential to estimate accurately the amount of LSi that contributes to the Si in each leachate used for isotopic measurement. In the case where this fraction is significant, the δ^{30}Si value should be corrected from lithogenic contamination (*see Supplementary Method 3*). Though significant such corrections do not impact shape of seasonal profile and interpretation of the data.

III.2.5. Isotopic fractionation models describing nutrient consumption

Isotopic variations accompanying nutrient uptake are generally described using two different fractionation models, for closed and open systems. In the closed system (also referred to as Rayleigh model) the surface ocean is considered to have a limited pool of DSi that is progressively consumed by diatoms and exported to the deep ocean. The reaction progresses in a sequential mode, consuming substrate (here silicic acid) that was supplied at the beginning, and increasing exponentially its δ^{30}Si over time (*equation 3.2.*; Fry, 2006). There are two products in the closed system, the instantaneous product (here exported BSi, *equation 3.3.*) and the accumulated product that finally hold the same δ^{30}Si than the initial substrate when everything is consumed in the system (*equation 3.4.*):

$$\delta^{30}Si_{sub} = \delta^{30}Si_{init} - {}^{30}\varepsilon \ln(1-f) \qquad (3.2.)$$

$$\delta^{30}Si_{inst} = \delta^{30}Si_{sub} + {}^{30}\varepsilon \qquad (3.3.)$$

$$\delta^{30}Si_{acc} = \delta^{30}Si_{init} + {}^{30}\varepsilon \left(\frac{f \times \ln f}{1-f}\right) \qquad (3.4.)$$

where $^{30}\varepsilon$ is the isotopic fractionation factor of the reaction, *f* the fraction of the remaining substrate and the subscripts “sub”, “init”, “acc” and “inst” refer to the remaining substrate, the initial substrate, the accumulated product and the instantaneous product respectively. In the open system (also referred to as steady-state model), a continuous supply of substrate balances the export of product. Only one product forms from substrate and both isotopic compositions of DSi and BSi display linear changes (*equations 3.5.* and *3.6.*; Fry, 2006):

$$\delta^{30}Si_{sub} = \delta^{30}Si_{init} - {}^{30}\varepsilon(1-f) \qquad (3.5.)$$

$$\delta^{30}Si_{prod} = \delta^{30}Si_{init} + {}^{30}\varepsilon \times f \qquad (3.6.)$$

These ideal relations could be altered by other processes such as water mixing or BSi dissolution that would affect the isotopic and mass balance (e.g. Demarest et al., 2009).

III.3. Results and Discussion

III.3.1. Latitudinal and seasonal variability of exported fluxes along 140°W

SAZ and PFZ moorings were programmed to sample over more than one year (405 days), while traps in the AZ collected particles for a shorter period (317 days). Considering the low particle fluxes registered at the onset and at the end of the experiment in this zone, we can assume that fluxes in the non-sampled winter period were close to 0 (Trull et al., 2001a). Consequently, the total deep mass flux integrated over the sampling period varied by almost one order of magnitude from 12 mg m^{-2} yr^{-1} in the SAZ (1000 m) to 95 mg m^{-2} yr^{-1} in the AZ (2000 m), with PFZ values being intermediate (*Table 3.2.*). The deep annual flux of biogenic silica follows a pattern much more contrasted with the highest flux in the AZ (1408 mmol m^{-2} yr^{-1} at 2000 m) and the lowest in the SAZ (14 mmol m^{-2} yr^{-1} at 3800 m), i.e. two orders of magnitude range. These fluxes are consistent with those measured by Honjo et al. (2000) in different stations from the same zones of the Southern Ocean in the Pacific sector (along 170°W). Note that since the largest flux attenuation is often found shallower in the water column, these estimations reflected only the deep fluxes and differ considerably from particles exported out of the euphotic zone (Boyd and Trull, 2007; Holzer et al., 2014).

Table 3.2. Mass flux, biogenic silica flux and silicon isotopic composition of particles ($\delta^{30}Si$) integrated over the sampling period.

Station	Depth (m)	Sampling period	Mass flux g m^{-2} yr^{-1}	BSi flux mmol m^{-2} yr^{-1}	$\delta^{30}Si$ (‰)
AZ	2000	26-Nov-01	95	1409	1,29
	3700	to 09-Oct-02	79	1240	1,35
PFZ	800	21-Jul-99	52	661	1,59
	1500	to 29-Aug-00	33	477	1,43
SAZ	1000	21-Jul-99	12	15	1,58
	2000	to 29-Aug-00	18	25	1,65
	3800		15	14	1,52

Globally, the total flux decreased with depth at all stations, except for the shallowest SAZ trap at 1000 m that displayed a lower flux than the 2 deeper traps. Indeed, since particles produced in the ML do not sink vertically, shallower traps may under-sample at current velocities that do not affect

deeper traps (Siegel et al., 1990). Moreover, some evidence for horizontal advection of particles at mesopelagic depths has already been highlighted in this area (Cardinal et al., 2001).

Biogenic silica and mass fluxes were highly correlated in all the AZ and PFZ traps ($R^2 > 0.9$, *Fig. 3.3.*), as already reported in previous studies (e.g. Honjo et al., 2000; Trull et al., 2001a). This results from the dominance of opal in the settling particles south of the SAF: the relative contribution of biogenic silica to the bulk flux ranged from 89 % to 94 % in the AZ and from 76 % to 87 % in the PFZ, and could be mainly attributable to the occurrence of diverse assemblage of diatoms as counted in the same sediment traps (Rigual-Hernandez et al., 2015; Rigual-Hernandez pers. comm.). In the SAZ however, biogenic silica fluxes corresponded to 5,6 to 8.3 % of the bulk fluxes. The correlations between BSi and mass flux were weaker (*Fig. 3.3.*) since, in these warmer waters, dissolution of diatom frustules can be particularly high already in the ML (Boyd et al., 2004; Fripiat et al., 2011b). These observations highlight once again the crucial role of diatoms in export controls south of the SAF, while they should be less important in the SAZ, where non-siliceous material dominated biogenic fluxes (Trull et al., 2001a; Ebersbach et al., 2011).

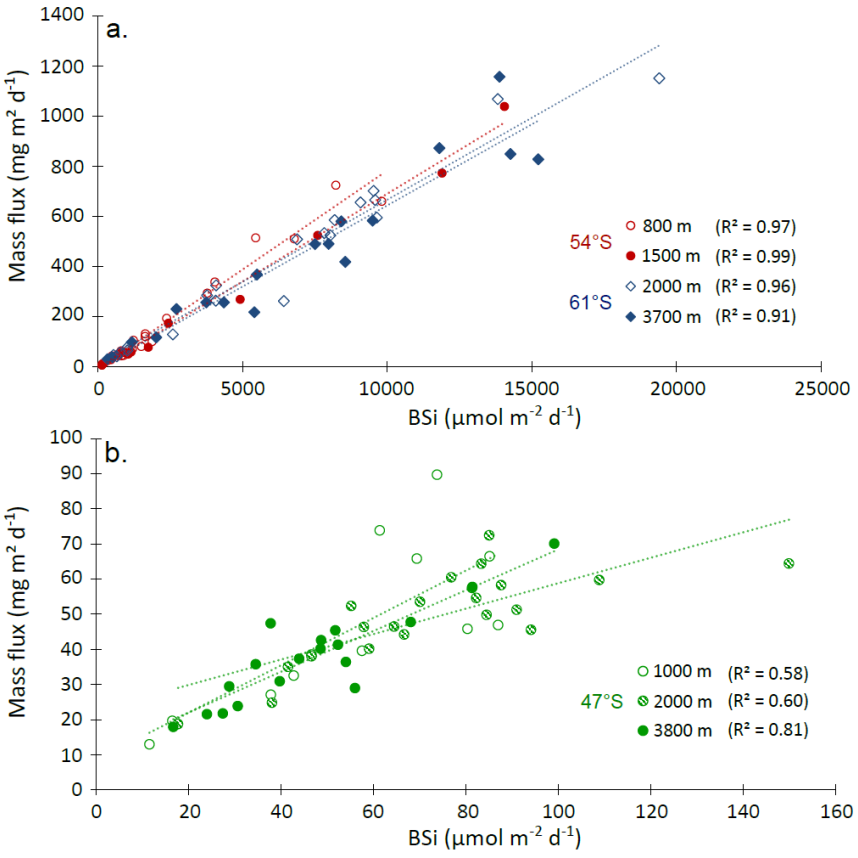

Figure 3.3. Correlations between the mass flux (mg m^{-2} d^{-1}) and biogenic silica flux (BSi in µmol m^{-2} d^{-1}) (a) in the Antarctic Zone (blue diamonds) and the Polar Front Zone (red dots) and (b) in the Sub-Antarctic Zone (green dots).

All the traps collected low total mass and BSi fluxes in early spring (*Fig. 3.4.*). Then, as already observed by Honjo et al. (2000) in the Pacific sector, the onset of export was progressively delayed towards the south (from early-September in the SAZ to mid-December in the AZ).

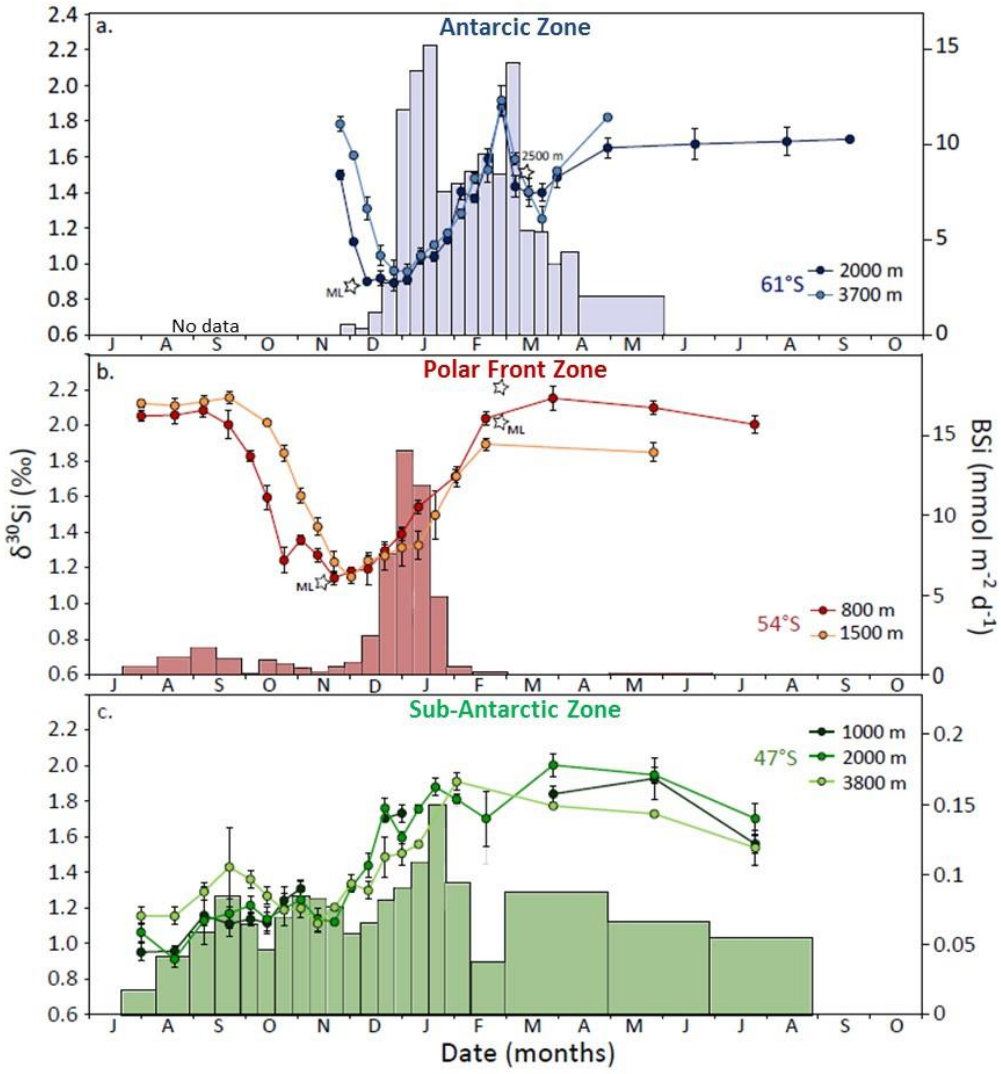

Figure 3.4. Seasonal variations of silicon isotopic composition ($\delta^{30}Si$ in ‰) of settling biogenic silica in comparison to the opal flux (BSi in mmol m^{-2} d^{-1}) in (a) the Antarctic Zone, (b) the Polar Front Zone and (c) the Sub-Antarctic Zone. The BSi fluxes correspond to the sediment traps located at 2000 m in the AZ, 1500 m in the PFZ and 2000 m in the SAZ. Stars correspond to $\delta^{30}Si$ measured in the mixed layer (ML) or at depth by Cardinal et al. (2007) in the same transect and Fripiat et al. (2012) in the Atlantic sector.

Export fluxes showed contrasted seasonal variations depending on the sampling zone. Indeed, south of the SAF, fluxes reached a sharp maximum occurring during austral summer. Particle fluxes in the AZ seem to reveal two summer maxima separated by a period of reduced fluxes (*Fig. 3.4a.*). There, the fluxes collected by the deeper trap and shallower traps displayed similar seasonal patterns and

magnitudes, suggesting little dissolution of opal between 2000 and 3700 m. In the PFZ, the period of enhanced export occurred 15 days later at 1500 m compared to 800 m. In contrast, export during austral winter exhibited a long period of very low particle flux from June to November and from March to October in the AZ and PFZ respectively (*Fig. 3.4a., 3.4b.*). North of the SAF in the SAZ, particle and BSi fluxes were much lower and displayed a larger variability than those recorded in the 2 other zones (*Fig. 3.4c.*) and those observed by Trull et al. (2001a) in 1997-1998 for the same SAZ and PFZ stations).

III.3.2. Biogeochemical dynamics of Si in regions dominated by diatoms south of the SAF

a) Seasonal variations of Si isotopic composition of sinking diatoms

- *Spring*

The seasonality of silicon isotopic composition of settling particles in the two stations south of the SAF is similar in many respects (*Fig. 3.4a., 3.4b.*). The lowest $\delta^{30}Si_{BSi}$ occurred at the onset of particles export. In the AZ, this light silicon isotopic composition (0.90 ± 0.01 ‰, n = 2, at 2000 m in December) is directly comparable to the $\delta^{30}Si$ of surface diatoms (0.85 ± 0.29 ‰) sampled above the sediment traps few weeks before (Cardinal et al., 2007). For PFZ, although not from the same year, the $\delta^{30}Si$ of surface diatoms above the PFZ mooring measured in mid-November 2001 (1.1 ± 0.02 ‰, Cardinal et al. 2007), was also highly consistent with the sediment trap $\delta^{30}Si$ we measured for late November 1999 at 54°S (1.14 ± 0.04‰). These light $\delta^{30}Si$ could then be considered as spring values for diatoms blooming south of the SAF. Since, for each mooring, this signature is not significantly different among the depths or from surface waters, we can furthermore assume that dissolution processes occurring during settling did not affect the $\delta^{30}Si$ of BSi. The constancy of Si isotopic signature of BSi through depth has been already observed for suspended particles of the Atlantic Sector (Fripiat et al., 2012) as well as for the AESOPS sediment traps in the Southern Ocean south of New Zealand (Varela et al., 2004).

- *Summer*

After these initial low values, the $\delta^{30}Si$ signatures became gradually heavier as the flux of BSi collected in the cups evidenced enhanced production and export of particles from the surface waters (*Fig. 3.4a., 3.4b.*). This reflects the response to the BSi production and export of diatoms through the ML, because $\delta^{30}Si$ signatures of both the remaining seawater and newly formed diatoms will increase concomitant with the progressive increase of nutrient consumption and Si limitation in surface waters

(see *section III.3.3.* for quantitative descriptions). The seasonal development of the diatom bloom in the Pacific Sector of the Southern Ocean was followed in 1998 by Nelson et al. (2001) and showed a silicic acid depletion of more than 40 µmol L^{-1} in the AZ surface waters. In the PFZ, the high $\delta^{30}Si$ signature (2.04 ± 0.04 ‰ in February) was in the same range than those measured in the Atlantic Sector in the end of summer (2.00 ± 0.02 ‰ in the ML and 2.29 ± 0.06 ‰ at 1068 m, Fripiat et al., 2012) suggesting that the spatial scale of the summertime DSi depletion and potential Si limitation in the PFZ may be nearly circumpolar. Here, both the lower silicic acid concentrations and the occurrence of some degree of Si limitation north of the PF explain heavier $\delta^{30}Si$ signal at 54°S when compared to AZ (*Fig. 3.4b.*).

- *Fall*

In March, the settling particles became suddenly lighter by -0.8 to -1.0 ‰ in the AZ (*Fig. 3.4a.*). Such a huge shift was also observed in sediment traps in the AZ along 170°W (Varela et al., 2004) and suggests the occurrence of vertical mixing events supplying waters with high silicic acid content and light $\delta^{30}Si$ into the euphotic zone. Indeed, during the AESOPS-program Brzezinski et al. (2001) and Nelson et al. (2001) measured relatively elevated DSi concentrations during February and March between 60.5°S and 65°S. They proposed that these mixing events ultimately led to the collapse of the bloom in the AZ (Brzezinski et al., 2001). The $\delta^{30}Si_{BSi}$ collected in our shallower trap during this period (1.43 ± 0.05 ‰) was also highly consistent with the $\delta^{30}Si$ of suspended particles measured at 2500 m in the Atlantic Sector by Fripiat et al. (2012) (1.42 ± 0.2 ‰ in March 2008), suggesting that the influence of mixing events may be widespread in the AZ and recurrent over years. By contrast, no $\delta^{30}Si$ decline was observed at the end of summer in the PFZ suggesting that the demise of the bloom here may not be associated with mixing events or variations in the MLD as in the AZ but might more probably be controlled by iron and/or silicic acid limitation in the surface water (Boyd et al., 1999).

- *Winter*

The silicon isotopic composition of settling particles remains strikingly heavy and constant between May and October (1.7 ± 0.02 ‰ averaged) in the AZ and between February and October (2.1 ± 0.05 ‰ averaged) in the PFZ, at a time when winter deep convection takes place (*Fig. 3.4a., 3.4b.*). It only starts to decrease at the beginning of spring when the BSi flux increases as a result of the initiation of export production from surface water. Indeed, the same heavy signature was observed in the single cup that collected particles during winter in the AZ along 170°W (Varela et al., 2004). The

authors proposed that the material has arrived in this cup early during the sampling time interval, and corresponded likely to frustules sinking before the occurrence of winter night. Since we recorded this high $\delta^{30}Si$ in several cups throughout the winter period (4 cups at 2000m from mid-April to October 2002), this cannot be the case in our samples. So, these high $\delta^{30}Si$ signatures are representative of the low flux of diatoms reaching the traps during the non-productive period. Diatoms bearing an isotopic signature typical of late summer that continue to settle in deep traps several months after the end of the growing season might explain such heavy $\delta^{30}Si$. These diatoms might be empty, broken and/or partly dissolved due to the influence of trophic interactions that could be important during the post-bloom period and that could help to retain particles in the ML. Indeed, both mesozooplankton and microzooplankton communities (such as copepods and heteroflagellates respectively) are likely to control significantly the fate of diatoms. In his conceptual scheme of the bloom dynamics in the Southern Ocean, Quéguiner (2013) suggests that zooplankton can in turn transform their fecal pellets into smaller particles that are easily retained in the ML where bacteria could progressively degrade the organic matter associated to this material. Then, while no study was conducted on the particle size spectra in our samples, we can reasonably assume that winter fluxes were composed of small particles and diatom fragments that have a heavier $\delta^{30}Si$ signature compared to "fresh" diatoms (on average 0.5 ‰ higher than normal range for diatoms, Egan et al., 2012).

All these processes would contribute to generate a weak flux of isotopically heavy diatoms as observed in the trap. By summing all the BSi fluxes collected in the traps during winter, we can estimate this BSi stock to 0.24 mol m^{-2} and 0.28 mol m^{-2} in the AZ and PFZ respectively. These values in both zones are consistent with the BSi stock measured in the euphotic zone at the end of summer along the AESOPS transect (170°W in the Pacific Sector): from 0.17 to 0.22 mol m^{-2} in the AZ in March 1998 (Brzezinski et al., 2001; Sigmon et al., 2002). BSi standing stock in the PFZ (from 0.05 to 0.08 mol m^{-2}) was however lower than those required to maintain the flux of siliceous material we measured during the whole winter at 54°S. Since AESOPS values were integrated over the euphotic layer (from 100 % to 1 % of the surface Photosynthetically Active Radiation – PAR), they did not take into account the occurrence of biogenic material (usually dominated by diatoms) just below the ML as already observed in summer and autumn at our PFZ mooring station (Boyd et al., 2001; Parslow et al., 2001). In March, this subsurface opal accumulation could be located at depths greater than 100m. In the Indian Sector HNLC waters, Mosseri et al. (2008) measured during the bloom offset BSi concentrations (from 0.2 to 0.5 mol m^{-2} integrated over 200 m) that were comparable to our estimations (note that this range of values is also similar in the iron-fertilized stations located over the Kerguelen Plateau – 0.2 to 0.8 mol m^{-2}). Thus we can reasonably assume that the BSi stock estimated from the sum of opal fluxes collected

in winter cups can be explained by the BSi stock that can be found in the ML after the demise of the summer bloom in both the AZ and PFZ.

- *Winter – spring transition*

Early spring, the $\delta^{30}Si$ signal started to decrease progressively from 1.50 ± 0.04 ‰ to 0.89 ± 0.04 ‰ in the AZ and from 2.1 ± 0.04 ‰ to 1.14 ± 0.04 ‰ in the PFZ. The progressive lightening of silicon isotopic composition of settling particles implies that a mix between old and isotopically heavy diatom fragments and recent particles with light $\delta^{30}Si$ signature formed during the spring bloom with an increasing contribution of fresh particles to this mixing. The combination of elevated lights levels and shallower MLDs allow the development of a diatom-dominated bloom with maximum biomass and productivity centered between the southern edge of the PF and 66°S (Nelson et al., 2001; Grigorov et al., 2014). Note that the $\delta^{30}Si$ decreased 2 months earlier at 54°S than at 61°S and in the same way, started to increase one month earlier in spring (*Fig. 3.4b.*). These two observations reflect the seasonal progression of bloom development and then Si-consumption that starts first in the Subantarctic waters located north of the PFZ and spread southward during summer as already revealed by Brzezinski et al. (2001) and Nelson et al. (2001) in the Pacific sector of the Southern Ocean.

b) Settling rates

The progressive consumption of H_4SiO_4 which should control as first order the observed silicon isotopic seasonal variations, is likely associated to a succession of different phytoplankton (and zooplankton) populations in the ML (Quéguiner, 2013) that produce finally a succession of different type of particles sinking with distinct velocities. Settling rate is a key parameter regarding the fate of organic matter produced in the ML which is highly variable and difficult to assess (Boyd and Trull, 2007). Since biological and physical degradation processes (e.g. bacterial respiration, grazing) will affect more efficiently slow sinking particles (Ragueneau 2000, Goutx et al., 2007), the rate at which a particle will sink through the water column will strongly affect its transfer efficiency to depth and thus the efficiency of the biological carbon pump (Trull et al., 2008; Iversen and Ploug, 2013).

The settling velocity of particles is commonly expressed using Stokes law where it mainly depends on size and excess density of particles (partly controlled by porosity and particle composition). However, recent studies have revealed that no simple physical formulation seems to be able to explain

the wide range of sinking rates observed in the ocean (from less than 1 m d^{-1} to more than several hundred m d^{-1}; Turner et al., 2002; Stemmann et al., 2004; Trull et al., 2008; Mc Donnell and Buesseler, 2010). Direct measurements of this crucial parameter could be performed in situ using specific sediment traps (e.g. Trull et al., 2008) or optical cameras (e.g. Asper and Smith, 2003) but they remain very scarce for the open ocean. In this study we propose to estimate the diatom settling rates using time-series analysis of $\delta^{30}Si$ of particles in sediment traps located at different depths.

Since the isotopic composition of BSi transferred to depth was comparable to the one leaving the ML (*Fig. 3.4a.*) and integrated $\delta^{30}Si$ are not related to depth (*Table 3.2.*) we can assume that the $\delta^{30}Si$ signature of settling particles was not affected by any significant dissolution processes during their export through the water column. Then, each pool of diatoms produced at one time in the ML should have the same $\delta^{30}Si$ in both the shallowest and deepest trap. By comparing the time lag between the occurrence of particles with the same $\delta^{30}Si$ at different trap depths, we can calculate the sinking velocity of this pool of diatoms between the 2 targeted depths. Note that, the values estimated using this approach represent only deep settling speeds since they were not estimated from the ML but in the water layer between two deep sediment traps. Moreover, it is important to keep in mind that because of the time length of the sampling for each cup (at least 8 days), the rates calculated in this study correspond to a lower limit estimate of sinking velocities.

In the AZ, the $\delta^{30}Si$ values were similar in the shallowest and deepest traps from January to April suggesting that particles sank quickly through the water column, coinciding with the maximum of BSi flux. Such rapid sedimentation during the summer bloom period (W_{bloom}) may be expressed by dividing the distance between the traps with the cup sampling time interval, i.e. at least 213 m d^{-1} between 2000 and 3700 m (*Fig. 3.5.*). In the PFZ, we observed a small time lag between the isotopic signatures of material collected in both traps from December to mid-February. Indeed, the $\delta^{30}Si$ started to decrease between cup 3 and 4 in the shallowest trap while it did not show any significant drop before cup 4 at 1500 m. Similarly, it reached its minimum value one cup later in the deepest trap in spring (*Fig. 3.4b.*). This time lag in particles fluxes could be also observed in *figure C6.* where BSi fluxes reach their maximum one cup earlier at 800 m. Taking into account this 10 days offset in the sampling time interval, sinking rates of particles may be estimated using the same relation than in the AZ and were at least 35 m d^{-1} between 800 and 1500 m (*Fig. 3.5.*). Both values (213 m d^{-1} and 35 m d^{-1} at 61°S and 54°S respectively) were in the range of published values for marine snow composed by diatom flocs (10 to several hundreds m d^{-1}; Turner, 2002; Trull et al., 2008; Laurenceau et al., 2014). While the

sinking velocity of single diatom cells or chains is in the range of 1 to 10 m d^{-1} (Turner, 2002), this speed could be increased by several orders of magnitude in the case of diatom aggregates. Indeed, during austral summers (1999, 2001 and 2007), the flux of particles and diatom composition in the ML at these two latitudes were mainly composed by the highly silicified diatom *Fragilariopsis kerguelensis* (De Salas et al., 2011; Rigual Hernandez et al., 2015) that are known to form chains and may reach rapidly the traps as fast-sinking phyto-detrital and/or fecal aggregates as already proposed by Ebersbach et al. (2011), Grigorov et al. (2014) and Laurenceau et al. (2014) for the PFZ site, the AESOPS transect and the Kerguelen Plateau respectively.

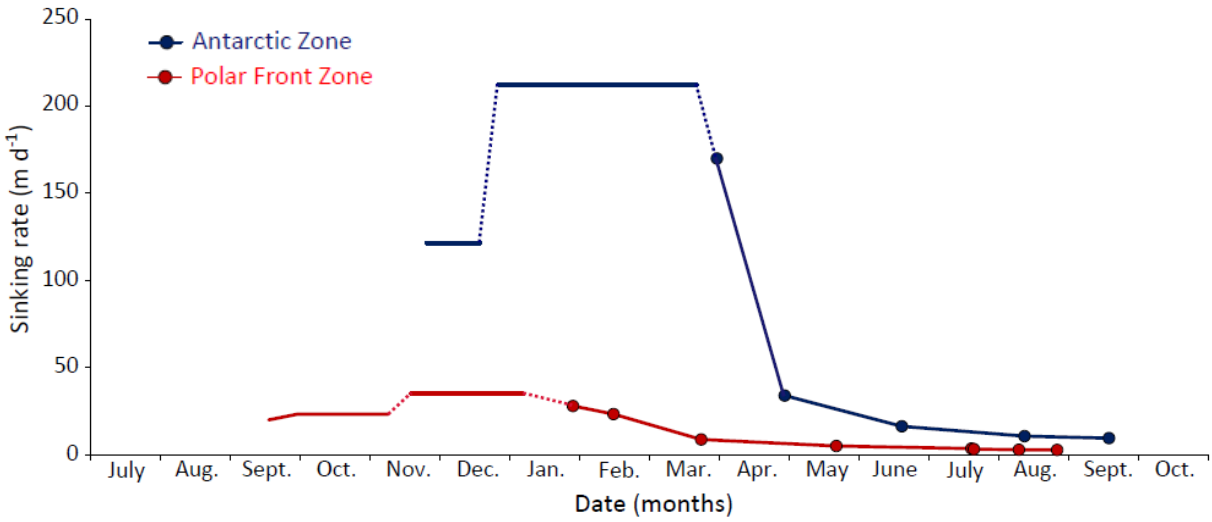

Figure 3.5. Seasonal variations of sinking velocities of particles estimated from $\delta^{30}Si$ signatures of settling diatoms in the Antarctic Zone (in blue) and in the Polar Front Zone (in red)

Since we have shown that winter BSi fluxes originate from late summer, in order to sustain such fluxes over the whole winter the sinking velocities of particles should be low. We have calculated these rates (W_{winter}) by dividing the distance between the traps with the sum of the cup opening durations during the non-productive period. This implies an exponential decrease of the rates with time which might not reflect reality but this approach is supported by the winter $\delta^{30}Si$ signatures. Winter settling rates estimates decrease from 34 to 9.5 m d^{-1} at 61°S and from 23 to < 3 m d^{-1} at 54°S (*Fig. 3.5.*). These estimates correspond to sinking rates of single phytoplankton cells (from < 1 to tens of m d^{-1}; Turner, 2002) and strongly differ from the high velocities of marine snow. As already discussed previously, this low winter flux might be mainly composed of broken or partly dissolved diatoms that should sink as single cell or small aggregates.

The progressive lightening of $\delta^{30}Si$ signature in early spring is delayed between the shallowest and deepest trap (approximately 6 and 20 days at 61°S and 54°S respectively, *Fig. 3.4a., 3.4b.*) implying that particles have slower velocities than those of summer aggregates. Indeed, taking into account this delay and using the same relation than the one used to calculate W_{bloom}, We estimate sinking rates of spring particles (W_{spring}) of at least 121 and 23 m d^{-1} in the AZ and PFZ respectively. Even if these values were lower than those estimated for the summer bloom, they were still in the range of published values for sinking aggregates. Thus, it is possible that diatoms growing during the early spring bloom form smaller and more "fluffy" phytodetrital-aggregates than the dense and compact aggregates produced during the intense summer bloom. Indeed, particles produced during the growing stage of the bloom may be composed of relatively unprocessed and fresh material while later in the season, aggregates might become more compact and could contain more zooplankton mediated particles (Thornton, 2002). During their sedimentation throughout the water column, these spring "fluffy" aggregates may scavenge small and isotopically heavy particles that were retained in surface and intermediate waters during austral winter. Efficient adsorption of suspended particles by settling aggregates has already been observed in the ML (Passow et al., 2001; Iversen et al., 2010). This support the idea of a mixing between old and slow-sinking particles and fresh and fast-sinking aggregates in the cups, and also the progressive lightening of silicon isotopic composition of sinking particles associated to an increasing contribution of fresh and isotopically light diatoms.

Note that, in the PFZ W_{spring}, W_{bloom} and W_{winter} were systematically lower than those estimated for the AZ (*Fig. 3.5.*). Since phytoplankton populations were dominated by the same diatom species (*Fragilariopsis kerguelensis*; Rigual-Hernandez, personal communication) at both latitudes, differences in planktonic community structure cannot be reported to explain these observations. However, samples collected in 1999-2000 in the PFZ were very rich in small and lightly silicified fragments compared to those sampled in the AZ or during different years (Rigual-Hernandez, personal communication). These fragments originated probably from setae or spines of *Chaetoceros spp.,* and other thin-shelled species and could suggest that some type of intense "grazing event" might occur in the surface water that year. Note that these contrasted sinking velocities might also be due to a sampling artifact since the traps were located at a much lower depth in the PFZ (800 and 1500 m) than in the AZ (2000 and 3700 m). Indeed, as the particles sink through the water column, the organic matter is remineralized by microbial activity. This process might increase the relative content of minerals and the density excess of aggregates (ballast effect) that will accelerate their sedimentation

with depth (Martin et al., 1987; Armstrong et al, 2002; Iversen et al., 2010). However, given that all the particles already have very low POC contents, this may not be the dominant effect, and an alternate possible explanation is that the Antarctic Zone particles are denser owing to greater compaction during their physical and biological initial aggregation in the surface mixed layer.

The overall seasonal picture that emerges from our estimations of particle sinking rates is that both sites show higher sinking rates at times of higher fluxes (*Fig. 3.5.*). To the extent, that higher sinking rates allow particles to experience less degradation during their transit to the traps implying the possibility of more efficient POC transfer during high flux periods. This does appear to be the case for the Antarctic Zone, where POC/BSi ratios were found to be somewhat elevated during the summer high flux period, although POC contents were nonetheless very low (<1.5% of dry mass) and thus POC export also small (Rigual-Hernandez et al., 2015).

c) Mass and isotopic balance of BSi

Several studies have attempted to determine whether the Si-pool in the Southern Ocean surface waters operate in a steady-state or Rayleigh system. However, these studies generally represent only snapshots and do not reflect any temporal evolution (Varela et al., 2004; Cardinal et al., 2005; De La Rocha et al., 2011; Fripiat et al., 2011a, 2011c) or were focused on specific mesoscale structures (e.g. Cavagna et al., 2011). Here we have seasonal records of $\delta^{30}Si$ of exported biogenic silica from which we can infer information about the behavior of the system in the main zones of the Southern Ocean.

Since isotopic composition and concentration of DSi were measured in the ML at 61°S shortly after the date when moorings were implemented (1.9 ± 0.8 ‰ and 28.1 µmol L^{-1} respectively, Cardinal et al., 2005), and at 54°S 2 years after mooring implementation (1.99 ‰ and 11 µmol L^{-1} respectively, Cardinal et al., 2005), we can use these values as initial parameters to simulate the evolution of $\delta^{30}Si$ following a Rayleigh model (*Fig. 3.*6a. and 3.6c.) or a steady-state model (*Fig. 3.6b. and 3.6d.*) in both zones.

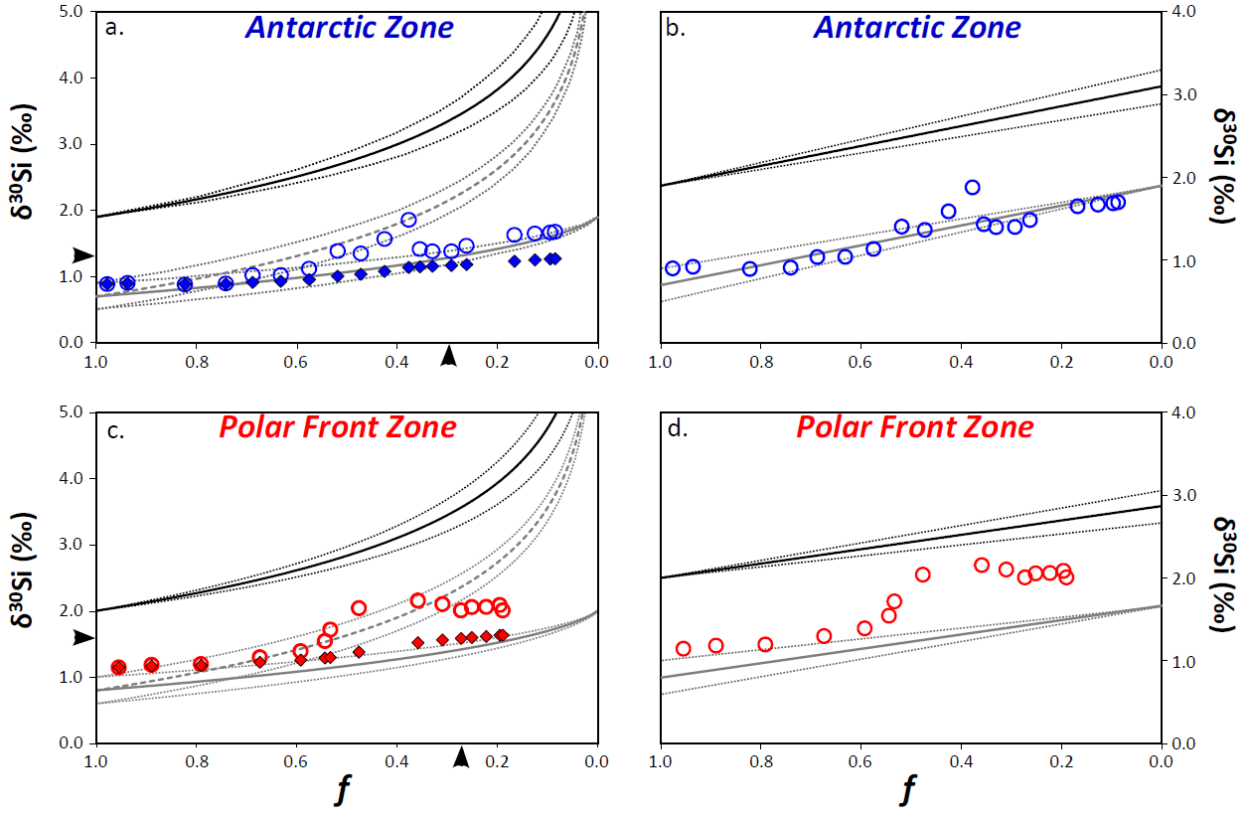

Figure 3.6. $\delta^{30}Si$ variations of settling biogenic silica in the Antarctic Zone (blue circles); the Polar Front Zone (red circles) described following a Rayleigh distillation model (a. and c.) or a steady state fractionnation model (b. and d.). The black line represent the evolution of $\delta^{30}Si$ of the remaining dissolved pool in the mixed layer (ML), gray lines are the evolution of $\delta^{30}Si$ of exported biogenic silica, with plain and dashed line associated to accumulated and instantaneous product respectively in the case of a Rayleigh distillation model. Dotted lines are error propagation of ± 1 sd of the fractionation factor and *f* is the fraction of silicic acid remaining in the pool. Diamonds represent the evolution of time integrated of measured $\delta^{30}Si$ and black arrows are the annual integrated $\delta^{30}Si$ (*Table 3.2.*) and its corresponding silicic acid utilization (see text for details).

The initial DSi standing stock integrated over the ML (97 m in the AZ and 76 m in the PFZ; Cardinal et al., 2005) was then 1.36 mol and 0.42 mol in the AZ and PFZ respectively. To simplify the calculations we assume that the ML depth did not vary during the year. Although this assumption may at first sight appear unrealistic in the Southern Ocean, it seems reasonable as monthly averaged ML depths integrated from 2002 to 2013 shows relatively low seasonal variations (from 50 to 100 m, *Fig. C8.*). Indeed, sporadic mixing events as the one observed in the AZ would not have a significant impact on such climatology. In the ACC, 50% of the BSi produced in the ML is dissolved above 2000 m (Holzer et al., 2014). By correcting our BSi fluxes from such dissolution, we can estimate the seasonal DSi consumption in the ML at 61°S and 54°S (equal to integrated corrected BSi collected in the cups) and thus the fraction of DSi-stock remaining in the ML (noted *f* in *equations 3.2.* to *3.6.*). Using the fractionation factor ($^{30}\varepsilon$) estimated by Fripiat et al. (2011c) for the ACC ($^{30}\varepsilon$ = -1.2 ± 0.2 ‰) and the

initial parameters measured by Cardinal et al. (2005), we can reconstruct the seasonal variations of $\delta^{30}Si$ following a closed or open model and compare the predicted values with our measured $\delta^{30}Si$ in the AZ (*Fig. 3.6a., 3.6b.*) and in the PFZ (*Fig. 3.6c., 3.6d.*). Note that we use only the shallower trap (2000 m and 800 m in the AZ and PFZ respectively) which present the longest $\delta^{30}Si$ record and that we do not consider cups that have collected particles before our initial parameters and that encompass the decreasing $\delta^{30}Si$ spring trend.

Most studies have suggested that turbulence diffusion and vertical mixing events lead the Southern Ocean surface waters to operate in an open system (Varela et al., 2004; Cardinal et al., 2005; Cavagna et al., 2011; De La Rocha et al., 2011; Fripiat et al. 2011a, 2011c) and that a Rayleigh model was unlikely to describe correctly $\delta^{30}Si$ variations in this ocean. Our results show that, south of the PF, the isotopic composition of exported BSi differs markedly from the one predicted by steady-state model, especially when the diatom bloom occurred in surface waters. Even if the ML did not represent strictly a closed system during the productive period, the dynamic of diatom blooms that consume DSi in surface water was better described by a Rayleigh fractionation law (*equations 3.2.* to *3.4.*, *Fig. 3.6a., 3.6c.*) as already observed by Fripiat et al. (2012). Indeed, during this period, the ML was highly stratified and nutrient uptake would greatly exceed new input from vertical mixing inducing a low Si-supply:Si-uptake ratio. During summer, the production of BSi progressed in a sequential mode over time, consuming substrate (here silicic acid) that was present at the beginning, and exporting instantaneous product (here exported BSi collected in our traps). Moreover, the time-integrated isotopic signature of exported BSi fit thoroughly the accumulated product (*Fig. 3.6a., 3.6c.*) both in the AZ and the PFZ. Occasionally, mixing event(s) disrupted the ML (e.g. in March in the AZ), resulted in an increase of the Si-supply:Si-uptake ratio combined to a lightening of the $\delta^{30}Si$ signal and shifted the system toward a more open mode dynamic (*Fig 3.6b.*). Thus, the seasonal variations of the $\delta^{30}Si$ of exported biogenic silica south of the PF could not be described by a single model but result from a combination of a closed and an open mode depending on the Si-supply:Si-uptake ratio of the system.

Considering that the system follows a Rayleigh fractionation law from the beginning of the production to the mixing event(s) (i.e. in March) in the AZ and to the end of the bloom (i.e. in June) in the PFZ, we can reconstruct the $\delta^{30}Si$ signature of silicic acid pool in the ML. Indeed, in the AZ, predicted $\delta^{30}Si_{DSi}$ was 2.1 ‰ which is very close to 1.9 ± 0.08 ‰ as measured in the ML at the same station 3 weeks before by Cardinal et al. (2005). Similarly, in the PFZ, the predicted $\delta^{30}Si_{DSi}$ was comparable to the one observed at the same period 2 years earlier (Cardinal et al., 2005). At the end of the AZ bloom,

the model predicted that 37 % of the initial pool of silicic acid (i.e. the 28.1 µmol L^{-1} measured by Cardinal et al., 2005) was not consumed by diatoms which correspond to 10.5 µmol L^{-1} that would remain in the ML early March 2002. This value is very consistent with the 10 µmol L^{-1} measured in February 1999 during the SOIREE experiment (Trull et al., 2001b). In the same way, 31 % of the initial DSi stock (i.e. 3.40 µmol L^{-1}) remained in the PFZ ML at the end of the productive period which felt in the range of H_4SiO_4 observed in March-April this zone (from 2 to 4 µmol L^{-1}, e.g. Trull et al., 2001b; Fripiat et al., 2011a). Finally, considering the lightening of the $\delta^{30}Si_{BSi}$ signal associated to the vertical mixing in March 2002, we can estimate that a silicic acid flux representing approximately 17 % of the DSi initial pool was brought from depth to the ML during this event. This 4.8 µmol L^{-1} supply seems to be realistic as Brzezinski et al. (2001) and Nelson et al. (2001) have measured a similar increase of DSi concentrations in the AZ surface waters between January and March 1998.

III.3.3. Biogeochemical dynamics of Si in the SAZ

a) Variations of Si isotopic composition of sinking diatoms

North of the SAF, the silicon isotopic composition of settling particles was 0.9 ± 0.03 ‰ at the end of winter, and reached a maximum of 1.8 ± 0.03 ‰ in March when the BSi export at 2000 m began to decrease (*Fig. 3.4c.*). The range of $\delta^{30}Si$ values was comparable to those measured in the AZ even though these 2 zones exhibit different DSi concentrations and phytoplankton composition assemblages in their own surface waters. This latitudinal trend was already observed in the Atlantic Sector of the Southern Ocean (Fripiat et al., 2012) and could result from a concomitant decline of silicon isotopic composition of surface seawater $\delta^{30}Si$ as observed for the same transect in late spring 2001 (Cardinal et al., 2005).

Since BSi fluxes were much lower and variable in the SAZ, the $\delta^{30}Si$ signature of sinking particles displayed a larger variability than in the AZ and PFZ (*Fig. 3.4.*). This variability could be associated to a greater instability of the ML. The surface layer in the SAZ is very weakly stratified (e.g. Sallée et al., 2006), which translates into both very deep ML (Fig. A5), and large intra-seasonal variability. Variability in the ML can arise from multiple sources including mesoscale activity (Rintoul & Trull, 2001), anomalous air-sea buoyancy fluxes (Schulz et al., 2012), or anomalous burst of wind-induced cross-frontal Ekman transport (Sallée et al., 2006). In addition to deepening the ML, cross-frontal transport impacts the nitrogen isotopic composition of nitrate in different parts of the SAZ (Sigman et al., 1999). Altogether, the weak stratification, and the burst of northward cross-frontal transport result in

temporary non optimal light conditions for phytoplankton growth, as well as pulses of new and isotopically light silicic acid in surface waters.

Even if the seasonal cycle of $\delta^{30}Si$ at 47°S was more scattered than in the two other zones, we however clearly see an increasing trend as the bloom developed in surface water (*Fig. 3.4c.*). Relating this trend to the strong seasonality of the MLD that occurs in the SAZ is tempting. Indeed, several studies have evidenced that the MLD in the SAZ exhibits large seasonal variability with deep mixed layers before November (> 400 m) and stable and shallow mixed layers (< 50 m) from December to March (Rintoul & Trull, 2001; Dong et al., 2008; Weeding & Trull, 2014; *Fig. C8.*). Thus, the combination of deep MLD (200 to > 500 m) and cross-frontal transport of surface waters in winter and early spring will prevent the development of diatoms, maintaining their relatively lighter silicon isotopic composition. On average, the $\delta^{30}Si$ values of settling particles increase slightly from 0.89 ± 0.05 ‰ in August to 1.10 ± 0.00 ‰ in November (*Fig. 3.4c.*). It was only in summer, when the ML is much shallower (≈ 35-45 m) and the stratification more stable, when phytoplankton experiences conditions suitable to grow that silicon isotopic composition of particles became significantly heavier (from 1.10 ± 0.00 ‰ in November to 1.80 ± 0.11 ‰, *Fig. 3.4c.*).

However, this trend could also be associated to the increasing relative abundance of diatoms frustules in the siliceous phytoplankton assemblages compared to other siliceous organisms such as silicoflagellates and/or radiolarians (from less than 60 % in August to more than 90 % in December, Rigual-Hernandez, unpublished results). Radiolarians are siliceous planktonic organisms that may have lower $\delta^{30}Si$ compared to diatoms but the scarcity of measurements does not allow us to determine precisely the range of radiolarian $\delta^{30}Si$. To our knowledge, only 2 studies have indirectly addressed this information. Ding et al. (1996) have measured light silicon isotopic composition (0.3 to -0.2 ‰) of sediments dominated by radiolarians, and using ultrasonic micro-separation of particles, Egan et al. (2012) have observed systematically lighter $\delta^{30}Si$ value (sometimes even negative) in the size fraction > 50µm characterized by the occurrence of these organisms. Then, because diatoms were not the dominant organisms that develop in the ML in the SAZ, the trend of silicon isotopic composition of BSi in early spring may reflect the concomitant effect of a shift in water ventilation and a change in the composition of settling particles.

b) Mass and isotopic balance of BSi

SAZ is a more active region than the ACC south of the SAF and isotopic reactions are unlikely to follow the same dynamics as in the AZ. The ML depth here displays a huge seasonal variability (see monthly averaged climatology in *Fig. C8.* and details in Weeding and Trull, 2014). Thus, we cannot estimate initial parameters for models using measured concentrations in the ML as we did previously in the AZ. The initial DSi standing stock was estimated by summing all the BSi fluxes collected in our 2000 m trap until the end of January and by correcting this value for the effects of dissolution as for the other traps (cf. above and Holzer et al., 2014). Indeed, Fripiat et al. (2011b) measured surface H_4SiO_4 concentrations close to 0 at this station during the SAZ-Sense program (January-February 2007) and concluded that all the Si pool has been consumed in the ML at this period of the year. Thus, we can consider that the BSi samples collected after this date were all representative of complete consumption of the DSi reservoir (i.e. with a f = 0). Taking into account this consideration, the initial $\delta^{30}Si_{DSi}$ should be similar to the final $\delta^{30}Si_{BSi}$ or to the final $\delta^{30}Si$ of accumulated biogenic silica if the system behaves following an open or a closed model respectively. Since these two delta values were different (1.86 ‰ and 1.65 ‰ in the case of the steady-state and the Rayleigh distillation model respectively), we have investigated these two situations and performed the same approach than south of the PF to investigate the seasonal evolution of the isotopic balance in the SAZ (*Fig. 3.7.*), using the -1.2 ± 0.2 ‰ fractionation factor compiled by Fripiat et al. (2011c) for the whole ACC.

Contrary to what we have observed previously, the seasonal variations of the $\delta^{30}Si$ of exported biogenic silica in this region could not be described by Rayleigh fractionation trend but seems to better match with an open model confirming a significant ventilation of surface waters by vertical mixing and/or lateral advection from the south (Rintoul & Trull, 2001). This observation is reinforced by the fact that the seasonal evolution of the BSi isotopic composition fits well with the steady-state fractionation model when using the 1.86 ‰ final $\delta^{30}Si_{BSi}$ as initial condition for the model (*Fig. 3.7b.*).

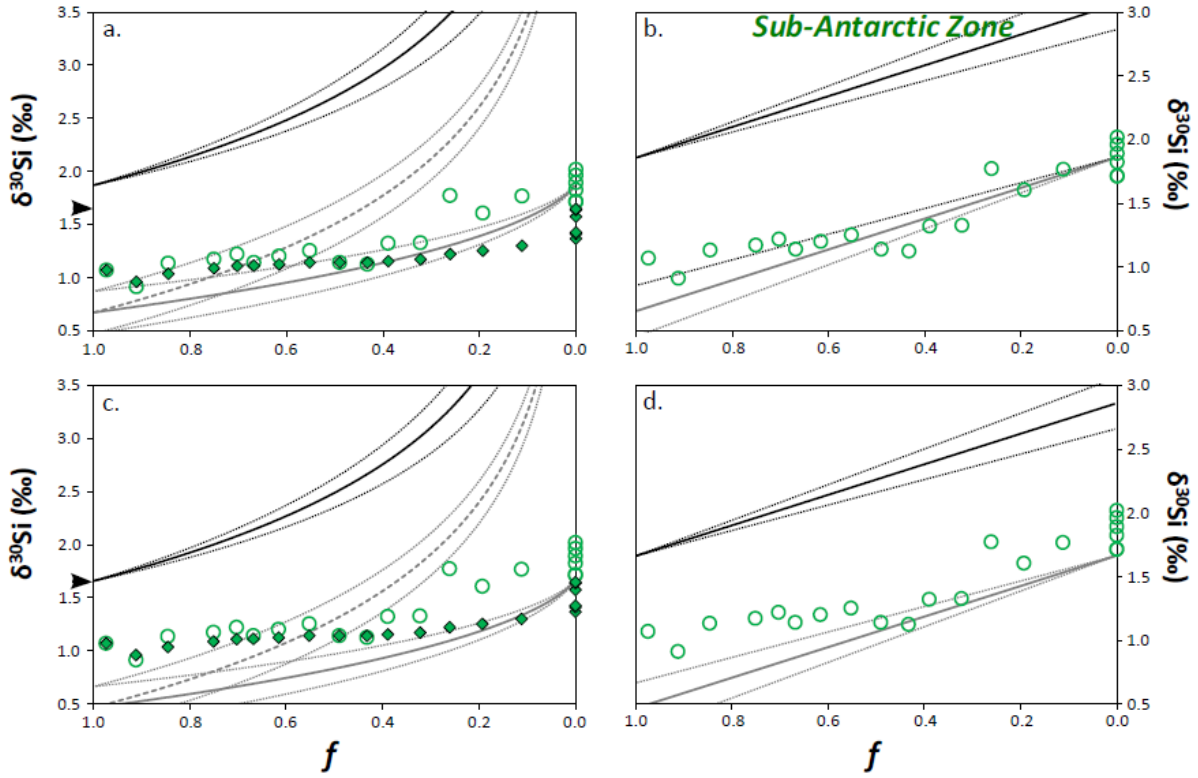

Figure 3.7. $\delta^{30}Si$ variations of settling biogenic silica in the Sub-Antarctic Zone (green circles) described following a Rayleigh distillation or a steady state fractionation models with a $\delta^{30}Si_{DSi}$ = 1.8616 ‰ as initial condition (a. and b., respectively) and with a $\delta^{30}Si_{DSi}$ = 1.6513 ‰ as initial condition (c. and d., respectively). The black line represent the evolution of $\delta^{30}Si$ of the remaining dissolved pool in the mixed layer (ML), gray lines are the evolution of $\delta^{30}Si$ of exported biogenic silica, with plain and dashed line associated to accumulated and instantaneous product respectively in the case of a Rayleigh distillation model. Dotted lines are error propagation of ± 1 sd of the fractionation factor and *f* is the fraction of silicic acid remaining in the pool. Diamonds represent the evolution of time integrated of measured $\delta^{30}Si$ and black arrows are the annual integrated $\delta^{30}Si$ (*Table 3.2.*) and its corresponding silicic acid utilization (see text for details).

This assumption was also clearly observed from July to early November 1999 when MLD reached very deep values (< 400 m; *Fig. C8.*), allowing nutrients to spread toward surface waters and maintaining a high Si-supply:Si-uptake ratio. In October, the predicted silicon isotopic composition of DSi was not significantly different from the corresponding $\delta^{30}Si_{DSi}$ measured in 2001 by Cardinal et al. (2005) at the same station (1.82 ‰ and 1.9 ± 0.06 ‰ respectively). In November, the $\delta^{30}Si$ of exported biogenic silica deviated markedly from the open model and remained in-between the two models until February. This coincides with the shoaling of MLD (< 50 m) and the occurrence of the maximum of phytoplankton biomass in surface waters (*Fig. C7.*). In some situations, $\delta^{30}Si_{BSi}$ may be controlled by processes which did not occur simultaneously with those controlling $\delta^{30}Si_{DSi}$. This may be the case for dynamic conditions where vertical mixings events can bring some isotopically light silicon into the ML

which results in a lower $\delta^{30}Si$ of exported biogenic silica as observed in November. The opposite effect would appear when a significant dissolution of BSi occurs in the ML, leaving the remaining silica enriched in the heaviest isotope as observed in January (*Fig. 3.7b.*). Then, because of its high mesoscale activity and its low DSi concentration in the ML, the silicon cycle in the SAZ could not be described by a Rayleigh fractionation model but behave more as an open system with specific events such as strong vertical mixing or higher BSi dissolution that could deviate the $\delta^{30}Si$ signature of biogenic silica from the predicted value.

III.3.4 Implication for interpretation of sedimentary records

From a palaeoceanographic perspective, diatom $\delta^{30}Si$ preserved in sediment core material can be used as a proxy of diatom silicic acid utilization, with high $\delta^{30}Si$ representing high nutrient consumption (De La Rocha et al., 1998; Varela et al., 2004; De La Rocha, 2006; Beucher et al., 2008; Egan et al., 2012; Ehlert et al., 2012; Etourneau et al., 2012). These studies linked the $\delta^{30}Si$ of opal with the isotopic signature of surface seawater and the extent of DSi depletion in the ML by using either the closed-system or open-system models. It is currently not obvious which model best describes the silicon mass and isotopic variations in the modern Southern Ocean and thus which one is the most appropriate to reconstruct surface biogeochemical processes from exported particle signatures.

In the SAZ, the isotopic signature of exported opal integrated over the whole season ($\int\delta^{30}Si$ = 1.65 ‰, *Table 3.2.*) corresponds to a complete Si depletion in the ML (f = 0) together when using the Rayleigh (*equation 3.4.*) or the steady state (*equation 3.6.*) fractionation laws. This estimation is not surprising regarding the Si-depleted characteristic of this zone (Trull et al., 2001b), and is well consistent with the fact that $\delta^{30}Si$ of exported BSi records the extent of DSi consumption in the ML (i.e. it reflects the period when diatoms are growing and drive H_4SiO_4 concentration in surface waters to its minimum annual value; Egan et al., 2012). Moreover, this integrated isotopic signature of exported opal fall well in the range of previous modern sedimentary records (e.g. from 1.65 to 2 ‰ during the Holocene, Beucher et al., 2008; and from 1.36 to 2.07 ‰ in core top material, Egan et al., 2012).

The high temporal resolution of our 54°S and 61°S datasets clearly highlights that, despite the occurrence of strong mixing event as observed is the AZ, the production and export of opal south of the PF is better describe by a closed-system model. Indeed, the Si-supply:Si-uptake ratio were likely

minimal as these zones could sustain very high regime of biogenic silica production (e.g. Closset et al., 2014). The isotopic signatures of exported opal integrated over the whole season can be associated to the accumulated product (*equation 3.4.*, $\int\delta^{30}Si$ = 1.59 ‰ and 1.29 ‰, in the PFZ and AZ respectively) and are consistent with the range of published core top records (from 1.21 to 1.68 ‰ in PFZ and from 1.14 to 1.58 ‰ in AZ, Egan et al., 2012). These integrated $\delta^{30}Si$ signatures can be associated to a strong depletion of the initial DSi pool (f = 26 % and 29%, in the PFZ and AZ respectively) and correspond to a remaining H_4SiO_4 concentration in the ML of 2.9 and 8.2 µmol L^{-1} in the PFZ and AZ respectively (*Fig. 3.6a., 3.6c.*), which are not significantly different to the values observed at the end of the productive period in the PFZ (from 1.8 to 4.0 µmol L^{-1}, Trull et al., 2001b; Fripiat et al., 2011a) and AZ (≈ 10 µmol L^{-1}, Brzezinski et al., 2001; Trull et al., 2001b). Note that, if we estimate the remaining DSi stock using the steady-state model, the calculated values would have been overestimated by 81 and 76 % in the PFZ and AZ ML (5.2 and 14.3 µmol L^{-1}, respectively). This support the idea that, despite its strong dynamic and seasonality, the ACC behave as a closed system regarding to the production (and ultimately the export) of biogenic silica. Moreover, the $\int\delta^{30}Si$ of exported particles that is preserved in the sediments likely reflects the Si consumption by diatoms and can be used to reconstruct past H_4SiO_4 concentrations prevailing at the end of the productive period.

III.4. Conclusions

Our study addressed the seasonal evolution of the silicon isotopic signature of sinking biogenic silica in different zones of the Southern Ocean. As already observed in previous studies (Varela et al., 2004; Fripiat et al., 2012), the $\delta^{30}Si$ signature of diatoms in our samples is well conserved through the water column and is closely linked to the Si consumption in surface waters, validating the use of this proxy to reconstruct past Si-utilization by diatoms in the ML.

We confirm and complete the seasonal increasing trend observed in the single previous work that has investigated the $\delta^{30}Si_{BSi}$ from the sediment traps samples in the AZ (Varela et al., 2004). Combining these results with 2 other datasets in the PFZ and the SAZ, we have highlighted that the SAZ has a distinct silicon isotope and mass balance than regions located south of the SAF. In this latter, the Si-supply:Si-uptake ratio was extremely low in summer and the system behaved mainly as a closed-system since the supply of silicic acid could not balance the strong DSi depletion by diatoms. During

this productive period, the $\delta^{30}Si_{BSi}$ increased exponentially as the silicic acid was consumed in surface waters. It was only during winter, when mixing events broke up the ML stratification that the Si-supply:Si-uptake ratio increased and that the system deviate from the ideal Rayleigh fractionation model and the $\delta^{30}Si_{BSi}$ stayed high and constant. These observations were highly consistent with the simulation proposed in the AZ and PFZ by Fripiat et al. (2012). Because of its high mesoscale activity and its low DSi concentrations in surface waters, the SAZ exhibit a higher BSi dissolution-production ratio and a higher Si-supply:Si-uptake ratio that may reduce the apparent fractionation factor. In these highly dynamic conditions, it seems apparent that the system could not be described by Rayleigh fractionation equations but was more related to a steady-state model. The $\delta^{30}Si_{BSi}$ was more variable but shown a clear increasing linear trend during the year.

The comparison of $\delta^{30}Si_{BSi}$ measured in the deep and shallow traps allowed us to estimate and monitor for the first time the seasonal variations of particles sinking rates in the AZ and PFZ. In these zones, fresh diatoms were exported relatively quickly as phytodetrital-aggregates during spring when biological activity increased in the ML. During the summer peak of production in surface water, aggregation and repackaging processes shifted the sinking velocities of particles up to 200 m d^{-1} in the AZ. Then, after the demise of the bloom, aggregates were degraded and diatoms were consumed and/or dissolved in the ML leading to a progressive decrease of their settling rates. This study provides by an original approach new data that contribute to corroborate previous hypothesis about the dynamic of the biological production and its export (e.g. Trull et al., 2008; Ebersbach et al., 2011; Laurenceau et al., 2014).

Using seasonal variations of $\delta^{30}Si_{BSi}$ of material collected in deep sediment traps, we had access to other information about processes occurring in the ML and infiltrated the biogeochemical cycle of silicon in the Southern Ocean. The silicon isotopic composition of settling diatoms is a sensitive tracer to quantify Si fluxes in surface and subsurface ocean, as we did for silicic acid consumption during the summer bloom in the AZ or for the amount of silicon supplied to the surface waters by vertical mixing events. This proxy is thus a precious tool to reconstruct both past and modern Si-utilization by diatoms, but also, by using a more conceptual approach, to identify other processes that affect the production and/or export of biogenic silica in surface waters and their influence of nutrient dynamics in the Southern Ocean. This study fits the overall effort to expand the available $\delta^{30}Si$ dataset and highlights once again the relevance to use silicon isotopes in a quantitative way. However, more efforts remain

regarding the modeling of processes involved in seasonal variations of $\delta^{30}Si$ to improve simulations of silicon isotopes and mass balance in the ocean.

Aknowledgements

The SAZ sediment trap program received support from the Australian Antarctic Climate and Ecosystems Cooperative Research Centre, Australian Antarctic Sciences Awards #1156 and #2256, the Australian Marine National Facility, the USA NSF Office of Polar Programs, and the Belgian Science and Policy Organisation. Sediment trap and deployments, augmented by surface biogeochemical and meteorological moorings, are ongoing at the 47°S site under the auspices of the Australian Integrated Marine Observing System (www.imos.org.au). Ocean color analyses and visualizations used in this paper were produced with the Giovanni online data system, developed and maintained by the NASA GES.

III.5. References

Abraham K., S. Opfergelt, F. Fripiat, A-J. Cavagna, J.T.M. de Jong, S.F. Foley, L. André, D. Cardinal (2008), δ30Si and δ29Si Determination on USGS BHVO-1 and BHVO-2 Reference Materails with a New Configuration on a Nu Plasma Multi-Collector ICP-MS, Geostandards and Geoanalytical Research, 32(2), 193-202.

Alldredge A.L., C.C. Gotschalk, S. MacIntyre (1987), Evidence for sustained residence of macrocrustacean fecal pellets in surface waters off Southern california, Deep-Sea Research, 34(9), 1641-1652.

Armstrong R.A., C. Lee, J.I. Hedges, S. Honjo, S.G. Wakeham, 2002. A new mechanistic model for organic carbon fluxes in the ocean based on the quantitative association of POC with ballast minerals. Deep-Sea Research II 49, 219-236.

Assmy P., V. Smetacek, M. Montresor, C. Klaas, J. Henjes, V.H. Strass, J.M. Arrieta, U. Bathmann, G.M. Berg, E. Breitbarth, B. Cisewski, L., Friedrichs, N. Fuchs, G.J. Herndl, S. Jansen, S. Krägefsky, M. Latasa, I. Peeken, R. Röttgers, R. Scharek, S.E. Schüller, S. Steigenberger, A. Webb, D. Wolf-Gladrow (2013), Thick-shelled, grazer-protected diatoms decouple ocean carbon and silicon cycles in the iron-limited Antarctic Circumpolar Current, Proceedings of the National Academy of Sciences, 110, 20633-20638.

Asper V.L., W.O. Smith Jr (2003), Abundance, distribution and sinking rates of aggregates in the Ross Sea, Antarctica, Deep-Sea Research I, 50, 131-150.

Beucher C.P., M.A. Brzezinski, J.L. Jones (2008), Sources and biological fractionation of Silicon isotopes in the Eastern Equatorial Pacific, Geochimica et Cosmochimica Acta, 72, 3063-3073, doi:10.1016/j.gca.2008.04.021.

Boyd P.W and T.W. Trull (2007), Understanding the export of biogenic particles in oceanic waters: Is there concensus?, Progress in Oceanography, 72, 276-312.

Boyd P.W, J. LaRoche, M. Gall, R. Frew, R.M.L. McKay (1999), Role of iron, light, and silicate in controlling algal biomass in subantarctic waters SE of New Zealand, Journal of Geophysical research, 104(C6), 13395-13408.

Boyd P.W., C.S. Law, C.S. Wong, Y. Nojiri, A. Tsuda, M. Levasseur, S. Takeda, R. Rivkin, P.J. Harrison, R. Strzepek, J. Gower, J. Barwell-Clarke, W. Crawford, D. Crawford, M. Hale, K. Harada, K. Johnson, H. Kiyosawa, I. Kudo, A. Marchetti, W. Miler, J. Needoba, J. Nishioka, H. Ogawa, J. Page, M. Robert, H. Saito, A. Sastri, N. Sherry, T. Soutar, N. Sutherland, Y. Taira, F. Whitney, S.-K.E. Wong, T. Yoshimura (2004) The decline and fate of an iron-induced subarctic phytoplankton bloom, Nature, 428, 549-553

Brzezinski M.A., D.M. Nelson, V.M. Franck, D.E. Sigmon (2001), Silicon dynamics within an intense open-ocean diatom bloom in the Pacific sector of the Southern Ocean, Deep-sea research II, 48, 3997-4018.

Brzezinski M.A., C.J. Pride, V.M. Frank (2002), A switch from Si(OH)4 to NO3- depletion in the glacial Southern Ocean, Geophysical research letters, 29(12), doi:10.1029/2001GL014349.

Buesseler K.O., A.N. Antia, M. Chen, S.W. Fowler, W.D. Gardner, O. Gustafsson, K. Harada, A.F. Michaels, M. Rutgers van der Loeff, M. Sarin, D.K. Steinberg, T. Trull (2007), An assessment of the use of sediment traps for estimating upper ocean particle fluxes, Journal of Marine Research, 65, 345-416.

Cardinal D., F. Dehairs, T. Cattaldo, L. André (2001), Geochemistry of suspended particles in the Subantarctic and Polar Frontal Zones south of Australia: Constraints on export and advection processes, Journal of geophysical research, 106(C12), 31637-31656.

Cardinal D., L.Y. Alleman, J. De Jong, K. Ziegler, L. André (2003), Isotopic composition of silicon measured by multicollector plasma source mass spectrometry in dry plasma mode, Journal of Analytical Atomic Spectrometry, 18, 213-218.

Cardinal D., L.Y. Alleman, F. Dehairs, N. Savoye, T.W. Trull, L. André (2005), Relevance of silicon isotopes to Si-nutrient utilization and Si-source assessment in Antarctic waters, Global biogeochemical cycles, 19(GB2007), doi:10.1029/2004GB002364.

Cardinal D., N. Savoye, T.W. Trull, F. Dehairs, E.E. Kopczynska, F. Fripiat, J-L. Tison, L. André (2007), Silicon isotopes in spring Southern Ocean diatoms: Large zonal changes homogeneity among size fractions, Marine Chemistry, 106, 46-62.

Cavagna A-J., F. Fripiat, F. Dehairs, D. Wolf-Gladrow, B. Cisewski, N. Savoye, L. André, D. Cardinal (2011), Silicon uptake and supply during a Southern Ocean iron fertilization experiment (EIFEX) tracked by Si isotopes, Limnology and Oceanography, 56(1), 147-160, doi:10.4319/lo.2011.56.1.0147.

Closset I., M. Lasbleiz, K. Leblanc, B. Quéguiner, A.-J. cavagna, M. Elskens, J. Navez, D. Cardinal (2014), Seasonal evolution of net and regenerated silica production around a natural Fe-fertilized area in the Southern Ocean estimated with Si isotopic approaches, Biogeosciences, 11, 5827-5846, doi:10.5194/bg-11-5827-2014.

De La Rocha C.L. (2006), Opal-based isotopic proxies of paleoenvironmental conditions, Global biogeochemical cycles, 20(GB4S09), doi:10.1029/2005GB002664.

De La Rocha C.L., M.A. Brzezinski, M.J. DeNiro (1997), Fractionation of silicon isotopes by marine diatoms during biogenic silica formation, Geochimica et Cosmochimica Acta, 61(23), 5051-5056.

De La Rocha C.L., M.A. Brzezinski, M.J. DeNiro, A. Shemesh (1998), Silicon-isotope composition of diatoms as an indicator of past oceanic change, Nature, 395, 680-683.

De La Rocha C.L., P. Bescont, A. Croguennoc, E. Ponzevera (2011), The silicon isotopic composition of surface waters in the Atlantic and Indian sectors of the Southern Ocean, Geochimica et Cosmochimica Acta, 75, 5283-5295, doi:10.1016/j.gca.2011.06.028.

De Salas M.F., R. Eriksen, A.T. Davidson, S.W. Wright (2011), Protistan communities in the Australian sector of the Sub-Antarctic Zone during SAZ-Sense, Deep-Sea Research II, 58, 2135-2149, doi:10.1016/j.dsr2.2011.05.032.

De Souza G. F., B. C. Reynolds, J. Rickli, M. Frank, M. A. Saito, L. J. A. Gerringa, B. Bourdon (2012), Southern Ocean control of silicon stable isotope distribution in the deep Atlantic Ocean, Global Biogeochemical Cycles, 26, GB2035, doi:10.1029/2011GB004141.

Demarest M.S., M.A. Brzezinski, C.P. Beucher (2009), Fractionation of silicon isotopes during biogenic silica dissolution, Geochimica et Cosmochimica Acta, 73, 5572-5583, doi:10.1016/j.gca.2009.06.019.

Ding T., S. Jiang, D. Wan, Y. Li, J. Li, H. Song, Z. Liu, X. Yao (1996), Silicon Isotope Geochemistry, Geological Publishing House, Beijing, China.

Dong S., J. Sprintall, S.T. Gille, L. Talley (2008), Southern Ocean mixed-layer depth from Argo float profiles, Journal of Geophysical Research, 113, C06013, doi:10.1029/2006JC004051.

Ebersbach F., T.W. Trull, D.M. Davies, S.G. Bray (2011), Controls on mesopelagic particle fluxes in the Sub-Antarctic and Polar Frontal Zones in the Southern Ocean south of Australia in summer – Perspectives from free-drifting sediment traps, Deep-sea research II, 58, 2260-2276, doi:10.1016/j.dsr2.2011.05.025.

Egan K.E., R.E.M. Rickaby, M.J. Leng, K.R. Hendry, M. Hermoso, H.J. Sloane, H. Bostock, A.N. Halliday (2012), Diatom silicon isotopes as a proxy for silicic acid utilisation: A Southern Ocean core top calibration, Geochimica et Cosmochimica Acta, 96, 174-192, doi:10.1016/j.gca.2012.08.002.

Elhert C., P. Grasse, E. Mollier-Vogel, T. Böschen, J. Franz, G.F. de Souza, B.C. Reynolds, L. Stramma, M. Frank (2012) Factors controlling the silicon isotope distribution in waters and surface sediments of the Peruvian coastal upwelling, Geochimica et Cosmochimica Acta, 99, 128-145

Etourneau J., C. Ehlert, M. Frank, P. Martinez, R. Schneider (2012) Contribution of changes in opal productivity and nutrient distribution in the coastal upwelling systems to Late Pliocene/Early Pleistocene climate cooling, Climate of the Past, 8, 1435-1445, doi:10.5194/cp-8-1435-2012

Fripiat F., A-J. Cavagna, F. Dehairs, S. Speich, L. André, D. Cardinal (2011a), Silicon pool dynamics and biogenic silica export in the Southern Ocean inferred from Si-isotopes, Ocean Science, 7, 533-547, doi:10.5194/os-7-533-2011.

Fripiat F., K. Leblanc, M. Elskens, A-J. Cavagna, L. Armand, L. André, F. Dehairs, D. Cardinal (2011b), Efficient silicon recycling in summer in both the Polar Frontal and Subantarctic Zones of the Southern Ocean, Marine ecology progess series, 435, 47-61, doi:10.3354/meps09237.

Fripiat F., A-J. Cavagna, N. Savoye, F. Dehairs, L. André, D. Cardinal (2011c), Isotopic constraints on the Si-biogeochemical cycle of the Antarctic Zone in the Kerguelen area (KEOPS), Marine Chemistry, 123, 11-22, doi:10.1016/j.marchem.2010.08.005.

Fripiat F., A-J. Cavagna, F. Dehairs, A. de Brauwere, L. André, D. Cardinal (2012), Processes controlling the Si-isotopic composition in the Southern Ocean and application for paleoceanography, Biogeosciences, 9, 2443-2457, doi:10.5194/bg-9-2443-2012.

Fry B. (2006) Stable Isotope Ecology, Springer, New York, pp 308

Georg R.B., B.C. Reynolds, M. Frank, A. N. Halliday (2006), New sample preparation techniques for the determination of Si isotopic compositions using MC-ICPMS, Chemical Geology, 235, 95-104.

Grasshoff K., K. Kremling, M. Ehrhardt (1999), Methods of Seawater Analysis 3rd edition completely Revised and Extended edition. Wiley-VCH. ISBN 3-527-29589-5.

Grigorov I., A. Rigual-Hernandez, S. Honjo, A.E.S. Kemp, L. Armand (2014), Settling fluxes of diatoms to the interior of the Antarctic circumpolar current along 170°W, Deep-Sea Research I, 93, 1-13.

Holzer M., F.W. Primeau, T. DeVries, R. Matear (2014), The Southern Ocean silicon trap: Data-constrained estimates of regenerated silicic acid, trapping efficiencies, and global transport paths, Journal of geophysical research, 119, 313-331, doi:10.1002/2013JC009356.

Honjo S., R. François, S. Manganini, J. Dymond, R. Collier (2000), Particle fluxes to the interior of the Southern Ocean in the Western Pacific sector along 170°W, Deep-Sea Research II, 47, 3521-3548.

Hughes H.J., C. Delvigne, M. Korntheuer, J. De Jong, L. André, D. Cardinal (2011), Controlling the mass bias introduced by anionic and organic matrices in silicon isotopic measurements, Journal of Analytical Atomic Spectrometry, 26, 1892-1896.

Iversen M.H. & H. Ploug (2010), Ballast minerals and the sinking carbon flux in the ocean: carbon-specific respiration rates and sinking velocity of marine snow aggregates, Biogeosciences, 7, 2613-2624, doi:10.5194/bg-7-2613-2010.

Iversen M.H. & H. Ploug (2013), Temperature effects on carbon-specific respiration rate and sinking velocity of diatom aggregates – potential implications for deep ocean export processes, Biogeosciences, 10, 4073-4085, doi:10.5194/bg-10-4073-2013.

Kopczynska E.E., F. Dehairs, M. Elskens, S. Wright (2001), Phytoplankton and microzooplankton variability between the Subtropical and Polar Fronts south of Australia: Thriving under regenerative and new production in late summer, Journal of geophysical research, 106(C12), 31597-31609.

Laurenceau E.C., T.W. Trull, D.M. Davies, S.G. Bray, J. Doan, F. Planchon, F. Carlotti, M-P. Jouandet, A-J. Cavagna, A.M. Waite, S. Blain (2014), The relative importance of phytoplankton aggregates and zooplankton fecal pellets to carbon export: insights from free-drifting sediment trap deployments in naturally iron-fertilised waters near the Kerguelen plateau, Biogeosciences Discussion, 11, 13623-13673.

MacDonnell A.M.P., K.O. Buesseler (2010), Variability in the average sinking velocity of marine particles, Limnology and Oceanography, 55(5), 2085-2096.

Martin J.H. (1990), Glacial-interglacial CO2 change: The iron hypothesis, Paleoceanography, 5(1), 1-13.

Mosseri J., B. Quéguiner, L. Armand, V. Cornet-Barthaux (2008), Impact of iron on silicon utilization by diatoms in the Southern Ocean: A case study of Si/N cycle decoupling in a naturally iron-enriched area, Deep-sea research II, 55, 801-819.

Nelson D.M., M.A. Brzezinski, D.E. Sigmon, V.M. Franck (2001), A seasonal progression of Si limitation in the Pacific sector of the Southern Ocean, Deep-sea research II, 48, 3973-3995.

Opfergelt S., P. Delmelle (2012), silicon isotopes and continental weathering processes: Assessing controls on Si transfer to the ocean, Comptes Rendus Geoscience, 344, 723-738, doi:10.1016/j.crte.2012.09.006.

Orsi A.H., T. Whiworth III, W.D. Nowlin Jr (1995), On the meridional extent and fronts of the Antarctic Circumpolar Current, Deep-Sea Research I, 42(5), 641-673.

Panizzo V., J. Crespin, X. Crosta, A. Shemesh, G. Massé, R. Yam, N. Mattielli, D. Cardinal (2014), Sea ice diatom contributions to Holocene nutrient utilization in East Antarctica, Paleoceanography, 29, 328-342, doi:10.1002/2014PA002609.

Parslow J.S., P.W. Boyd, S.R. Rintoul, F.B. Griffiths (2001), A persistent subsurface chlorophyll maximum in the Interpolar Frontal Zone south of Australia: Seasonal progression and implications for phytoplankton-light-nutrient interactions, Journal of geophysical research, 106(C12), 31543-31557.

Passow U., R.F. Shipe, A. Murray, D.K. Pak, M.A. Brzezinski, A.L. Alldredge (2001), The origin of transparent exopolymer particles (TEP) and their role in the sedimentation of particulate matter, Continental Shelf Research, 21, 327-346.

Quéguiner B. (2013), Iron fertilization and the structure of planktonic communities in high nutrient regions of the Southern Ocean, Deep-Sea Research II, 90, 43-54.

Ragueneau O., P. Tréguer, A. Leynaert, R.F. Anderson, M.A. Brzezinski, D.J. DeMaster, R.C. Dugdale, J. Dymond, G. Fischer, R. François, C. Heinze, E. Maier-Reimer, V. Martin-Jézéquel, D.M. Nelson, B. Quéguiner (2000), A review of the Si cycle in the modern ocean: recent progress and missing gaps in the application of biogenic opal as a paleoproductivity proxy, Global and Planetary Change, 26, 317-365.

Ragueneau O., N. Savoye, Y. Del Amo, J. Cotten, B. Tardiveau, A. Leynaert (2005), A new method for the measurement of biogenic silica in suspended matter of coastal waters: using Si:Al ratios to correct for the mineral interference, Continental Shelf Research, 25, 697-710.

Reynolds B.C., J. Aggarwal, L. André, D. Baxter, C. Beucher, M.A. Brzezinski, E. Engström, R.B. Georg, M. Land, M.J. Leng, S. Opfergelt, I. Rodushkin, H.J. Sloane, S.H.J.M. van den Boorn, P.Z. Vroon, D. Cardinal (2007), An inter-laboratory comparison of Si isotope reference materials, Journal of Analytical Atomic Spectrometry,22, 561-568, doi:10.1039/b616755a.

Rigual-Hernandez A.S., T.W. Trull, S.G. Bray, I. Closset, L.K. Armand (2015), Seasonal dynamics in diatom export fluxes to the deep sea in the Australian sector of the Antarctic Zone, Journal of Marine Systems, 142, 62-74.

Rintoul S.R., T.W. Trull (2001), Seasonal evolution of the mixed layer in the Subantarctic Zone south of Australia, Journal of geophysical research, 106(C12), 31447-31462.

Sallée J.B., N. Wienders, R. Morrow, K. Speer (2006), Formation of Subantarctic mode water in the Southeastern Indian Ocean, Ocean Dynamics, 56 , 525-542.

Sarmiento J.L., N. Gurber, M.A. Brzezinski, J.P. Dunne (2004), High-latitude controls of thermocline nutrients and low latitude biological productivity, Nature, 427, 56-60.

Schulz E.W., S.A. Josey, R. Verein (2012) First air-sea flux mooring measurements in the Southern Ocean, Geophysical Research Letters, 39, L16606, doi:10.1029/2012GL052290

Siegel D.A., T.C. Granata, A.F. Micheals, T.D. Dickey (1990), Mesoscale Eddy Diffusion, Particle Sinking, and the Interpretation of Sediment Trap Data, Journal of geophysical research, 95(C4), 5305-5311.

Sigman D.M., M.A. Altabet, D.C. McCorkle, R. François, G. Fischer (1999), The $\delta^{15}N$ of nitrate in the Southern Ocean: Consumption of nitrate in surface waters, Global Biogeochemical Cycles, 13(4), 1149-1166.

Sigmon D.E., D.M. Nelson, M.A. Brzezinski (2002), The Si cycle in the Pacific sector of the Southern Ocean: seasonal diatom production in the surface layer and export to the deep sea, Deep-sea research II, 49, 1747-1763.

Stemmann L., G.A. Jackson, G. Gorsky (2004) A vertical model of particle size distributions and fluxes in the midwater column that includes biological and physical processes – Part II: application to a three year survey in the NW Mediterranean Sea, Deep-Sea Research I, 51, 885-908

Thornton D. (2002), Diatom aggregation in the sea: mechanisms and ecological implications, European Journal of Phycology, 37(2), 149-161, doi: 10.1017/S0967086202003657.

Tréguer P.J., C.L. De La Rocha (2013), The World Ocean Silica Cycle, Annual Review of Marine Science, 5, 477-501.

Trull T., S.G. Bray, S.J. Manganini, S. Honjo, R. François (2001a), Moored sediment trap measurements of carbon export in the Subantarctic and Polar Frontal Zones of the Southern Ocean, south of Australia, Journal of geophysical research, 106(C12), 31489-31509.

Trull T., S.R. Rintoul, M. Hadfield, E.R. Abraham (2001b), Circulation and seasonal evolution of polar waters south of Australia: Implications for iron fertilization of the Southern Ocean, Deep-Sea Research II, 48, 2439-2466.

Trull T., S.G. Bray, K.O. Buesseler, C.H. Lamborg, S. Manganini, C. Moy, J. Valdes (2008), In situ measurement of mesopelagic particle sinking rates and the control of carbon transfer to the ocean interior during the Vertical Flux in the Global Ocean (VETIGO) voyages in the North Pacific, Deep-Sea Research II, 55, 1684-1695.

Turner J.T. (2002), Zooplankton fecal pellets, marine snow and sinking phytoplankton blooms, Aquatic microbial ecology, 27, 57-102.

Varela D.E., C.J., Pride, M.A. Brzezinski (2004), Biological fractionation of silicon isotopes in Southern Ocean surface waters, Global biogeochemical cycles, 18(GB1047), doi:10.1029/2003GB002140.

Van den Boorn S.H.J.M., P.Z. Vroon, M.J. Van Bergen (2009), Sulfur-induced offsets in MC-ICP-MS silicon-isotope measurements, Journal of Analytical Atomic Spectrometry, 24, 1111-1114.

Weeding B., T.W. Trull (2014), Hourly oxygen and total gas tension measurements at the Southern Ocean Time Series site reveal winter ventilation and spring net community production, Journal of Geophysical Research: Oceans, 119, 348-358, doi:10.1002/2013JC009302.

Yu E-F., R. François, M.P.Bacon, S. Honjo, A.P. Fleer, S.J. Manganini, M.M. Rutgers van der Loeff, V. Ittekot (2001), Trapping efficiency of bottom-tethered sediment traps estimated from the intercepted fluxes of ^{230}Th and ^{231}Pa, Deep-Sea Research I, 48, 865-889.

Synthèse et Perspectives

« C'est là un bien grand mystère […]
rien de l'univers n'est semblable si quelque part
on ne sait où,
un mouton que nous ne connaissons pas a,
oui ou non, mangé une rose… »

1. Synthèse des principaux résultats

Ce dernier chapitre synthétise les éléments de réponses apportés par ce travail de thèse aux principaux objectifs énoncés au début de ce manuscrit, et met en perspective les implications et les nouveaux questionnements soulevés lors de l'interprétation de ces jeux de données. Une meilleure compréhension du cycle biogéochimique du silicium dans l'Océan Austral implique de décrire et d'évaluer avec précision l'influence des principaux facteurs de contrôle des flux de silicium dans la couche de mélange et dans l'océan profond. L'utilisation des isotopes du silicium s'est déjà révélée être un outil puissant dans l'identification des sources de silicium et dans la quantification des taux de production et dissolution à l'échelle saisonnière (e.g. Fripiat et al., 2011a, 2011b). Cependant, il subsiste encore de nombreuses incertitudes en ce qui concerne la biogéochimie du silicium dans l'Océan Austral ainsi qu'au niveau du fonctionnement de son système isotopique. Ce travail de thèse s'est donc articulé autour de ces problématiques en combinant deux approches isotopiques, permettant ainsi d'intégrer différentes échelles de temps et donc d'étudier simultanément les différents processus impliqués dans le cycle biogéochimique du silicium. De plus, l'association à deux programmes internationaux (KEOPS et SAZ-project) a permis de produire un jeu de données conséquent, constitué de différents types d'échantillons (eau de mer, diatomées, particules sédimentaires), récoltés sur toute la colonne d'eau et dans les principales conditions environnementales rencontrées dans l'ACC (zones HNLC de l'AZ, de la PFZ, de la SAZ, et une zone naturellement fertilisée en fer). Les principales conclusions qui émanent de ce travail sont synthétisées ici.

1.1. Les zones naturellement fertilisées en fer : des usines actives de transformation du silicium

Les zones naturellement enrichies en fer de l'Océan Austral peuvent soutenir des taux de production de silice biogénique parmi les plus élevés de l'océan global et jusqu'à 15 fois plus élevés que dans les eaux limitées en fer avoisinantes (de 3.09 ± 0.01 mmoles m^{-2} j^{-1} dans la zone HNLC à 47.9 ± 0.4 mmoles m^{-2} j^{-1} dans la zone fertilisée). Ces régimes exceptionnels de production d'opale sont comparables à ceux observés dans les zones les plus productives de la planète telle que les panaches des fleuves ou les systèmes d'upwellings côtiers. Au contraire, les taux de productions sont relativement faibles en début de saison (en moyenne 10.2 mmoles m^{-2} j^{-1}) et homogènes quelles que soient les conditions environnementales.

1.2. Evolution saisonnière du cycle biogéochimique du silicium dans une zone naturellement fertilisée en fer de l'Océan Austral

Comme expliqué précédemment, la combinaison de différentes approches isotopiques nous permet de réviser le budget du cycle du silicium sur le plateau de Kerguelen en quantifiant les différents stocks et flux et en identifiant les différents processus en jeu. La conclusion principale de ce budget est que les apports hivernaux et ceux ayant lieu durant la saison de production sont compensés par l'accumulation de la BSi tout au long de l'été dans la ML et en subsurface, et par son export en fin de saison, lorsque la ML est déstabilisée. En comparant les conditions initiales en début de saison et les signatures isotopiques des masses d'eau, il apparaît que ces apports hivernaux proviennent des eaux profondes (UCDW) originaires de la partie sud-est du Plateau de Kerguelen. Ensuite au cours de la saison de croissance la même source de silicium, les eaux hivernales (du Plateau) peut être utilisée pour expliquer les signatures isotopiques des différentes stations localisées sur le Plateau (stations A3, TNS6, E1 à E5), suggérant que le bloom du plateau se disperse du sud vers le nord, et n'est pas ou très peu influencé par les populations côtières qui se développent à proximité des îles Kerguelen. Ces observations sont d'ailleurs en accord avec la circulation locale de surface décrite par Park et al. (2014) mais ne correspondaient pas nécessairement aux hypothèses utilisées dans les études actuelles (par ex. source de Si provenant des WW HNLC, Fripiat et al., 2011a ; De Brauwere et al., 2011). En début de printemps, comme en fin d'été, la dissolution du matériel particulaire pré-existant suffit à maintenir de faibles taux de production de BSi, le rapport dissolution/production (D/P) du système est élevé et on peut qualifier le régime de production de Si de « régénéré ». La BSi ne s'accumule donc que durant l'été, lorsque les taux de production sont particulièrement importants et que la production de Si dite « nouvelle » domine (faible rapport D/P). L'ensemble de la BSi produite est enfin exporté à la fin de l'automne lorsque la production redevient faible et que le système n'accumule plus de BSi (retour à un régime de production « régénéré » avec un rapport D/P élevé). On observe ainsi une transition saisonnière entre différents régimes de production de silice qui active la pompe de silicium et contribue au découplage entre les cycles biogéochimiques du Si et de N.

1.3. Découplage des cycles biogéochimique du silicium et de l'azote

Au début du printemps, les rapports stœchiométriques d'absorption (ρSi:ρN et ρSi:ρC) apparaissent plus élevés dans la zone fertilisée que dans la zone HNLC impliquant que, contrairement à ce qui est communément admis, le contrôle des rapports stœchiométriques est beaucoup plus

complexe et n'est pas uniquement influencé par la disponibilité en fer. Cependant, les travaux récents de Lasbleiz et al. (2014) ont montré que ces rapports pouvaient être biaisés par la présence d'organismes non siliceux (qui consomment C et N mais pas Si) et qu'ils étaient fortement influencés par la composition des communautés phytoplanctoniques. Une estimation des rapports d'uptake et des rapports particulaires spécifiques aux diatomées telle que proposée dans leur étude permettrait de mieux comprendre la réponse des diatomées face à la limitation ou à la fertilisation en micronutriments tel que le fer. Nos résultats confirment néanmoins que dans la zone fertilisée, les diatomées sont fortement silicifiées et possèdent des rapports d'uptake de Si légèrement plus élevés que ceux normalement attendus dans ces conditions (Brzezinski et al., 1985). Le découplage des cycles de Si et N observé dans les zones naturellement fertilisées en fer comme le plateau de Kerguelen (et peut-être dans les autres régions de l'ACC), résulterait de la combinaison d'une pompe de silicium particulièrement active pendant la période de production et de la reminéralisation plus efficace de la matière organique (et en particulier des nitrates) comparée à la silice. Durant le bloom phytoplanctonique, on aurait ainsi une production dite « nouvelle » de silice couplée à une production plutôt régénérée de la matière organique basée sur les produits de la nitrification, particulièrement active dans la zone d'étude (Dehairs et al., 2014 ; Cavagna et al., 2014). Ceci expliquerait donc les faibles concentrations de H_4SiO_4 mesurées en fin de saison alors que le stock de NO_3^- est encore relativement abondant.

1.4. Variations saisonnières et spatiales de l'équilibre isotopique du silicium : découplage des compartiments particulaire et dissous ?

En combinant les données isotopiques des deux campagnes KEOPS, on remarque que les signatures isotopiques des réservoirs dissous et particulaire ne sont pas directement reliées par un simple modèle ouvert ou fermé, comme nous étions tentés de le penser à partir des précédentes études. Dans ces régions fortement productives, l'activité à mésoéchelle (tourbillons, fronts etc.) favorise les échanges verticaux et horizontaux de nutriments. En effet, en profondeur, les signatures isotopiques des WW suivent une courbe de mélange entre les eaux de surface et les WW initiales. Dans la ML, le $\delta^{30}Si$ de l'acide silicique ne peut donc pas être décrit par un modèle de Rayleigh et se comporte plutôt comme un système ouvert. En revanche, la dissolution de la silice biogénique étant relativement faible dans les eaux de surface de l'ACC, les diatomées n'échangent que très peu avec le compartiment dissous. Leurs $\delta^{30}Si$ semblent donc être mieux décrits par un modèle fermé. Dans ce cas, en fonction du régime d'export de BSi (période d'accumulation en surface vs. période de déstabilisation de la ML et d'export en profondeur), le $\delta^{30}Si$ de la BSi correspond alternativement à un produit accumulé ou

instantané, ou peut se situer entre ces deux situations idéales. L'intensité du découplage entre ces deux compartiments dépendrait surtout de la variabilité des rapports D/P, Si-supply : Si-uptake, et de l'efficacité d'export du système comme cela a déjà suggéré par Fripiat et al., (2012). L'ensemble des résultats présentés dans ce travail montre que le découplage entre les $\delta^{30}Si_{DSi}$ et $\delta^{30}Si_{BSi}$ évolue en fonction des variations saisonnières et régionales de ces derniers paramètres. Ainsi, le découplage serait plus marqué pendant les périodes de forte production phytoplanctonique (l'été) et au sud du FP où les concentrations en H_4SiO_4 restent relativement élevées au moins une grande partie de l'année. En dehors de ces périodes de production et dans la SAZ, les deux réservoirs échangeraient suffisamment de silicium via une dissolution significative de la BSi et une production basée sur des sources régénérées pour fonctionner selon un système plutôt ouvert.

1.5. Reconstruire l'utilisation relative de silicium dans la couche de mélange

Comme il a déjà été observé auparavant la dissolution ne semble pas affecter la signature isotopique du flux de particules (Varela et al., 2004 ; Fripiat et al., 2012) qui est donc bien conservée sur toute la colonne d'eau et peut être directement reliée à la consommation en silicium dans les eaux de surface. Ceci valide une fois de plus l'utilisation de ce proxy pour reconstruire l'utilisation passée de Si par les diatomées dans la ML. L'étude des variations du $\delta^{30}Si$ du flux de particules a permis de mettre en évidence pour la première fois une consommation significative d'acide silicique par les organismes siliceux au nord du FP ainsi que de confirmer l'existence d'évènements de mélange vertical importants à la fin de l'été dans la AZ et de quantifier l'apport de DSi dans la ML issu de ces évènements.

1.6. Dynamique saisonnière du flux de diatomées estimée à partir des approches isotopiques, un nouvel outil d'analyse ?

La comparaison des signatures isotopiques du flux de particules à différentes profondeurs nous donne également accès à des informations complémentaires telles que l'estimation de la vitesse de chute des particules siliceuses. Au sud du PF, ces vitesses varient au cours de la saison, avec des particules chutant rapidement en été (jusqu'à 200 m j^{-1} dans l'AZ) probablement sous la forme d'agrégats, puis les vitesses de chute diminuent de façon exponentielle durant l'hiver lorsque les agrégats sont dégradés, et sont associées plutôt à un flux de diatomées solitaires et/ou détritiques (petits fragments). Au printemps, on retrouve un mélange entre les nouvelles particules qui chutent rapidement et qui « adsorberaient » (scavenging) sur leur passage les anciens fragments d'opale,

toujours en suspension dans la colonne d'eau. Notre étude met en évidence un continuum entre des particules sédimentant rapidement (« settling particles ») dominant les flux en période d'efflorescence et l'apport de particules sédimentant lentement, qui se rapprocheraient plus des particules en suspension (« suspended particles »). Ces résultats soutiennent les hypothèses précédentes de variations saisonnières des vitesses de chute des particules (Trull et al., 2008 ; Ebersbach et al., 2011, Laurenceau et al., 2014). La vitesse de chute des particules étant un paramètre particulièrement délicat à mesurer in-situ, très peu d'études se sont penchées sur ses variations temporelles et dans la colonne d'eau. L'utilisation des isotopes du silicium dans ce domaine représente donc une application originale, relativement simple et prometteuse de cet outil.

2. Développement analytique

Les objectifs de ce travail de thèse ne se concentrent pas sur le développement de nouveaux outils d'analyse, néanmoins, l'utilisation d'échantillons de natures différentes a nécessité l'adaptation et l'optimisation des techniques existantes. De plus, ces méthodes d'analyse ont été mises en place pour la première fois en routine au sein du laboratoire LOCEAN et sur le MC-ICP-MS du LSCE. Certaines améliorations techniques significatives sont donc ressorties de ces travaux.

- La nécessité de mesurer les taux de dissolution de BSi lors de l'estimation des flux de silicium dans la couche de mélange avait déjà été soulevée par Fripiat et al., 2011b. Cependant, ces flux extrêmement faibles, en particulier dans l'Océan Austral, sont souvent en dessous de la limite de détection de la méthode de dilution isotopique proposée par Fripiat et al. (2009) et ne sont donc pas directement mesurables. Afin d'augmenter la sensibilité de cette technique, nous avons combiné deux méthodes : la méthode « standard », avec un enrichissement en ^{30}Si à 10% de la concentration initiale de H_4SiO_4 pour la mesure du taux de production ; et une méthode « sensible », avec un enrichissement en ^{30}Si à 100% de la concentration initiale de H_4SiO_4 pour la mesure du taux de dissolution (on double la concentration initiale durant l'incubation). Cette méthode s'est révélée efficace puisque nous avons mesuré des taux de dissolution de l'ordre de 0.04 µmole j^{-1}, et que nous n'avons pas relevé de difficulté lors des préparations chimiques des échantillons, ni d'effet mémoire sur le HR-ICP-MS. Néanmoins, cette méthode « sensible » pourrait n'être applicable que dans les conditions où les diatomées ne sont pas limitées en Si (comme c'était le cas durant KEOPS-2). En effet, dans une région (ou lors d'une

période) où le stock de DSi est faible, le doublement de la concentration de d'acide silicique induit par la méthode risque d'augmenter artificiellement les taux de production de BSi. Dans ce cas, il faudra de nouveau optimiser le modèle à deux compartiments pour intégrer les taux de production mesurés dans les incubations « standards », et les taux de dissolution mesurés dans les incubations « sensibles » ou se contenter d'utiliser le modèle à un compartiment.

- Jusqu'à présent, plusieurs techniques ont été utilisées pour mesurer la composition isotopique du silicium de l'eau de mer. La plus sensible, rapide et moins risquée est celle que nous avons utilisée et qui s'organise en trois étapes : une préconcentration du silicium à l'aide de la méthode MAGIC (Reynolds et al., 2006), suivie d'une purification de l'échantillon sur une résine échangeuse d'ions (Georg et al., 2006), et enfin une analyse par MC-ICP-MS en plasma sec, avec dopage au magnésium et bracketing pour contrôler le biais de masse (Cardinal et al., 2003). Le principal inconvénient de cette méthode est qu'on ne peut pas s'affranchir complètement des anions tels que les sulfates (SO_4^{2-}) lors de l'étape de purification. Or, nous avons montré qu'à partir d'un rapport $SO_4^{2-}/Si > 5$, la présence des sulfates entraine un effet de matrice significatif et biaise la signature isotopique de l'échantillon vers des valeurs plus lourdes. Ainsi, à partir d'un certain volume d'échantillon d'eau de mer analysé (environ 30 ml), il est indispensable d'homogénéiser les matrices des échantillons et des standards utilisés pour le bracketing en dopant l'ensemble des solutions avec une solution de H_2SO_4, comme cela avait été préalablement proposé par Hughes et al. (2011) pour des eaux douces ou des solutions de sols. En ce qui concerne les eaux de mer de la région de Kerguelen, nous avons estimé que les nitrates et les phosphates n'étaient pas en concentration suffisamment importante pour perturber le signal isotopique. Néanmoins, lors de l'analyse d'eaux plus riches en anions (par exemple de fleuves ou de baies soumises à l'influence anthropique) il faudra probablement vérifier leur effet de matrice potentiel et adopter le même type d'approche en cas d'impact significatif sur la mesure du $\delta^{30}Si$.

- Dans le cadre de l'étude du cycle biogéochimique du silicium dans l'océan, on cherche à analyser uniquement la signature isotopique de l'eau de mer et de la silice biogénique. Les échantillons contenant une quantité significative de silice d'origine lithogène sont donc écartés. Pour la première fois, il a été possible d'estimer le $\delta^{30}Si$ de la BSi dans des échantillons présentant une « contamination » de LSi significative. Nous avons montré que, en utilisant la méthode de digestion de Ragueneau et al. (2005), et lorsque la concentration de LSi dans la deuxième digestion est suffisante, on peut corriger le $\delta^{30}Si$ de la première digestion avec le $\delta^{30}Si$ de la seconde pour estimer le $\delta^{30}Si$ de la BSi en s'affranchissant de la contamination lithogénique. Cette méthode s'est révélée concluante dans le cas

de nos échantillons relativement concentrés en LSi originaires de la SAZ. Cependant, pour des systèmes extrêmement riches en apports lithogènes tels que les estuaires, les fleuves ou les systèmes côtiers, l'emploi de cette méthode devra être préalablement testé. De plus, cette correction augmente sensiblement les barres d'erreur sur les mesures et peut probablement encore être optimisée.

- Au cours de ce travail de thèse, environ 500 échantillons ont été analysé à l'aide d'un MC-ICP-MS, Neptune^{+}, dont plus de la moitié ont été répliqués en totalité (préparation chimique et analyse isotopique). La reproductivité analytique (R_A = 0.06 ‰) de la machine au cours de ces trois années a été estimée par l'analyse de 167 réplicats d'une même solution d'un matériel de référence ayant une signature isotopique proche de celle de la BSi marine, la diatomite (δ^{30}Si = 1.26 ‰ ; Reynolds et al., 2007). Les échantillons de pièges à particules ont tous été répliqués au moins une fois nous permettant ainsi d'estimer une reproductivité globale de 0.05 ‰ (n = 129), les échantillons de la campagne KEOPS-2 ont été mesurés avec une reproductivité globale de 0.04 ‰ (n = 78) et de 0.06 ‰ (n = 108) pour l'eau de mer et la BSi, respectivement. Une reproductivité globale équivalente à la reproductivité analytique signifie que les principales limitations de cette méthode d'analyse ne proviennent pas de la préparation chimique des échantillons mais repose uniquement sur des limitations instrumentales. Ainsi, les techniques chimiques utilisées au cours de ce travail de thèse se révèlent être particulièrement propres et adaptées aux types d'échantillons étudiés. On peut noter que de telles reproductibilités sont significativement meilleures (d'un facteur 2 à 3) que les premières études mesurant les δ^{30}Si dans des eaux de mer il y a dix ans (Cardinal et al. 2005) ou même que d'études plus récentes (de Souza et al., 2012). Il est possible que cela soit dû à un meilleur contrôle de la matrice anionique. Une inter-calibration GEOTRACES à laquelle nous avons participé est en cours et devrait permettre de mieux comprendre les différences de reproductibilités et de justesse entre laboratoires, instruments et techniques de purification. Dans le futur, la sensibilité de la méthode pourrait donc être améliorée principalement à l'aide d'optimisations techniques du MC-ICP-MS telles que des systèmes d'introduction de l'échantillon permettant de réduire les interférences ou d'augmenter la stabilité du signal.

3. Conclusion générale

La composition isotopique du silicium est un traceur sensible pour quantifier les flux de Si en surface et subsurface de l'océan, comme par exemple le taux de consommation d'acide silicique dans la ML ou l'apport de DSi en surface lors d'évènements de mélange ponctuels. Ce paramètre est donc un outil précieux dans la quantification des flux passés et présents de Si dans la ML, mais permet également d'identifier d'autres processus qui influent sur la production et/ou l'export de la BSi et leur influence sur la dynamique des nutriments dans l'Océan Austral.

Cette thèse s'inscrit dans l'effort global visant à élargir l'ensemble des données et met en évidence une fois de plus la pertinence d'utiliser les isotopes du silicium de manière quantitative. Toutefois, des efforts supplémentaires demeurent quant à la compréhension des variations saisonnières de la signature isotopique de l'eau de mer et des particules, et des processus de régulation du cycle biogéochimique du silicium dans l'Océan Austral. Le développement de séries temporelles, telles que présentées dans le chapitre 3, et la production de jeu de données répartis sur la totalité de l'année semblent indispensables pour améliorer les simulations actuelles du cycle biogéochimique du Si et ses variations isotopiques dans l'ACC.

4. Perspectives

Ce travail de thèse a également conduit à de nouvelles interrogations scientifiques et de nouvelles perspectives de recherche :

4.1. Vers une redéfinition des modèles actuels…

Les principales conclusions des chapitres 2 et 3 nous amènent à constater qu'aucun des modèles théoriques actuels (Rayleigh ou steady-state) ne sont capables de reproduire totalement les variations saisonnières des isotopes du silicium dans l'Océan Austral et en particulier dans la zone naturellement fertilisée en fer de Kerguelen. En effet, ceux-ci décrivent l'évolution des valeurs de $\delta^{30}Si_{DSi}$ et $\delta^{30}Si_{BSi}$ uniquement en fonction de la consommation d'acide silicique dans la ML. Or il semble que l'équilibre

isotopique du silicium est particulièrement sensible à d'autres paramètres tels que le régime de production de BSi, ou l'efficacité d'export du système.

Ainsi, nous avons montré que lorsque les rapports Si-supply:Si-uptake et D/P sont faibles, et que le système accumule de la BSi (pendant la phase de croissance du bloom ou l'été dans l'AZ et la PFZ), l'apport de DSi ne peut pas compenser la consommation du stock par les diatomées et le $\delta^{30}Si_{BSi}$ s'alourdit alors de façon exponentielle. C'est seulement à la fin de l'automne, lorsque des évènements de mélange déstabilisent la colonne d'eau et que le rapport Si-supply:Si-uptake augmente, lorsque la production diminue et se base sur des sources régénérées de silicium (rapport D/P élevé), que la signature isotopique de la BSi se stabilise ou s'allège et fait dévier le signal des courbes théoriques de Rayleigh. Dans les régions caractérisées par une forte activité à méso-échelle ou dans la SAZ, le découplage entre les compartiments dissous et particulaire est moins prononcé puisque la présence de rapports D/P et Si-supply:Si-uptake élevé et l'injection d'acide silicique isotopiquement léger dans la ML tendent à faire évoluer les deux réservoirs selon un modèle plus ouvert. Jusqu'à aujourd'hui, trois exercices de modélisation (dont deux appliqués au système du Plateau de Kerguelen) ont été menés afin tenter de décrire ces variations saisonnières dans la ML et tentent de tester les différentes sources potentielles de Si ou testent l'effet du fractionnement isotopique pendant la dissolution de la silice (De Brauwere et al., 2012 ; Fripiat et al., 2012 ; Coffineau et al., 2014).

La définition des conditions initiales adéquates est une étape cruciale lors d'un exercice de modélisation. La campagne KEOPS-2 nous a permis d'échantillonner la zone naturellement fertilisée en fer du Plateau de Kerguelen juste avant et dans les premiers stades de développement du bloom phytoplanctonique. Les paramètres mesurés alors (concentration et composition isotopique de BSi et DSi) peuvent nous permettre d'entériner ou non les choix réalisés lors de l'étude de De Brauwere et al. (2012) sur la modélisation isotopique du cycle du silicium dans la région. Dans la ML les conditions initiales du modèle coïncident remarquablement bien avec les valeurs mesurées début novembre 2011 (station A3-1), exceptée pour la concentration de DSi qui est environ 30 % plus faible (22.9 µmoles L^{-1} vs. 33.9 µmoles L^{-}) que celle choisie pour initier le modèle (*Fig. II.1.*). En revanche, il n'y a aucune correspondance entre les conditions initiales mesurées dans le réservoir particulaire des WW durant KEOPS-2 et celles choisies par De Brauwere et al. (2012) à partir du jeu de données de janvier 2005. Les valeurs mesurées 27 jours après l'initiation du bloom (station A3-2) dévient toutes plus ou moins significativement du modèle, excepté en ce qui concerne le réservoir dissous des WW du Plateau (*Fig. II.1.*). Dans la ML le $\delta^{30}Si$ ne s'alourdit pas aussi rapidement que prédit dans le modèle, quelque soit le

réservoir considéré. De même le stock de BSi n'augmente pas de façon aussi importante, et par conséquent, le stock de DSi ne diminue pas de façon aussi drastique que la tendance annoncée par le modèle. Dans les WW, l'export n'a pas encore commencé 27 jours après le début du bloom et le réservoir de BSi des WW n'augmente que très peu.

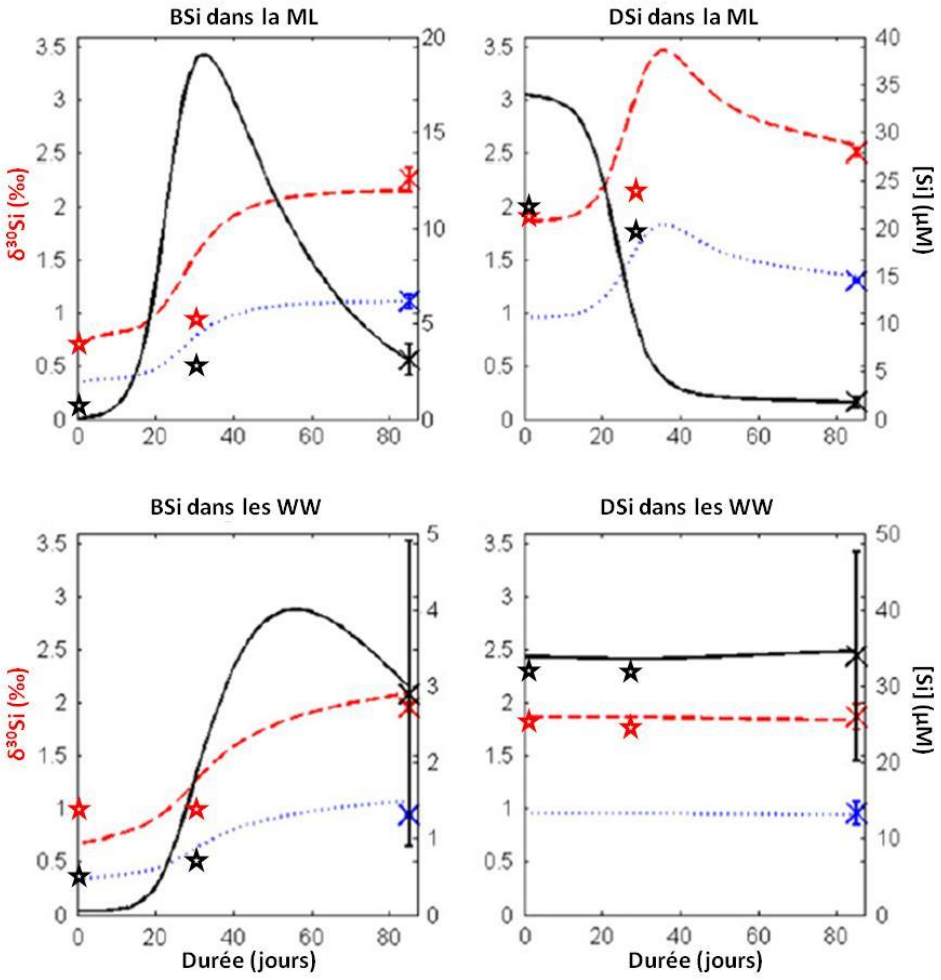

Figure II.1. Simulation de l'évolution de la composition isotopique (en rouge) et de la concentration totale de Si (en noir) dans les compartiments particulaire et dissous de la ML et des WW du Plateau de Kerguelen telle que modélisée par de Brauwere et al. 2012. Les étoiles représentent les valeurs mesurées en début de saison (A3-1 et A3-2 KEOPS-2) et en fin de saison (A3 KEOPS-1).

Les différences observées entre les mesures réalisées durant KEOPS-2 et les valeurs prédites par le modèle sont probablement en partie associées à une paramétrisation erronée et/ou approximative de ce dernier, en raison de l'absence de données en début de saison. En effet, sur la *figure II.2.*, on remarque que les taux de production, de dissolution et d'export de la BSi sont en réalité beaucoup plus

faibles que ceux utilisés par le modèle 27 jours après l'initiation du bloom. Dans cette configuration, les taux de production atteindraient donc un maximum significativement moins élevé que dans le modèle, mais se stabiliseraient sur une période beaucoup plus longue (environ 86 jours, chapitre 1). Ceci serait possible grâce à des apports de DSi depuis les WW pendant la période estivale, comme il a été discuté par Fripiat et al. (2011a) et dans le chapitre 1, et qui ne sont pas pris en compte dans ce modèle. De plus, des analyses de la composition isotopique du flux de particules au-dessus du Plateau de Kerguelen confirment l'existence de taux de consommation de DSi significatifs se traduisant par un alourdissement exponentiel du δ^{30}Si de la BSi exportée depuis le début du mois de décembre à mi-février (soit environ 70 jours ; Rembauville, communication personnelle). Ces mesures montrent également un allègement soudain de la composition isotopique du flux de particules au début du mois de janvier, traduisant un apport d'acide silicique isotopiquement léger associé à un évènement de mélange tel que celui décrit dans la AZ (chapitre 3) et confirmant la présence de ces échanges à travers la MLD pendant la période estivale.

De plus, dans le modèle de De Brauwere et al. (2012), le rapport D/P augmente progressivement en raison de l'action conjointe de la diminution du taux de production et de l'augmentation de la dissolution de la BSi au cours de la saison. Or, nous avons montré qu'au début de la période de croissance du bloom, la pompe de silicium reste relativement faible et la production de BSi peut être majoritairement basée sur des sources régénérées de Si. Le rapport D/P du système est donc encore relativement élevé (chapitre 1). Lorsque le système bascule dans un régime de production « nouvelle » de BSi, la pompe de silicium s'active et les rapports D/P se stabilisent autour de 0, ceci probablement pendant toute la période où le système accumule de la BSi (au moins 60 jours, chapitre 1). Puis ce rapport D/P ré-augmente en fin d'été, lorsque la production de BSi diminue drastiquement (*Fig. II.2.*).

Une meilleure prise en compte de ces paramètres et de leur évolution saisonnière permettra très probablement de réajuster ce modèle et d'identifier les processus qui jouent un rôle significatif dans le contrôle des variations saisonnières, spatiales et de la dynamique des isotopes du silicium dans une région naturellement fertilisée en fer telle que le Plateau de Kerguelen.

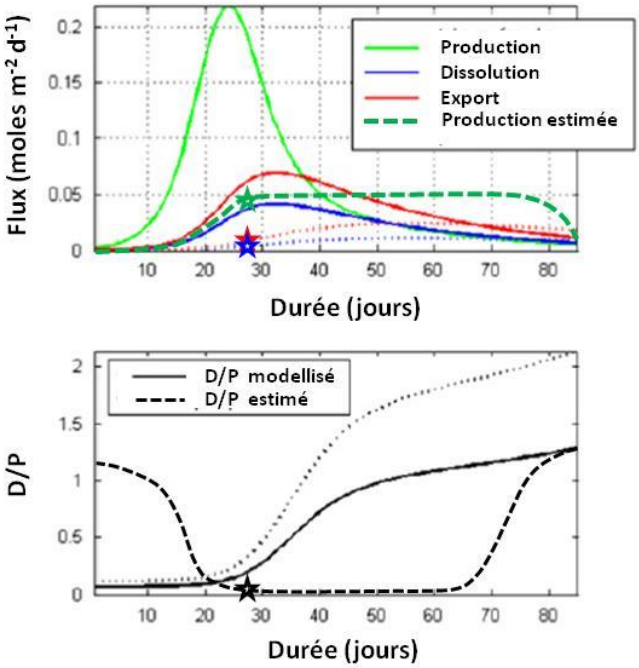

Figure II.2. Simulation de l'évolution des taux de production (en vert) de dissolution (en bleu) et d'export (en rouge) ainsi que l'évolution saisonnière du rapport Dissolution/Production (en noir) selon le modèle de De Brauwere et al. (2012). Les étoiles correspondent aux valeurs mesurées durant KEOPS-2 à la station A3 (Closset et al., 2014), et les courbes pointillées représentent les fluctuations probables des paramètres estimées à partir de ces travaux de thèse, et qui nécessitent une meilleure calibration dans le modèle.

De plus, la plupart des modèles se concentrent sur la période de croissance du bloom (environ 80 jours, généralement basée sur les estimations de Mongin et al., (2008) et ne modélisent pas le comportement du $\delta^{30}Si$ pendant la période non-productive qui peut néanmoins continuer à jouer un rôle dans le cycle océanique du silicium (à travers l'export et le recyclage de la BSi par exemple). Grace au jeu de données produit à partir des pièges à particules, nous avons maintenant des séries temporelles de la variation du $\delta^{30}Si$ de la BSi exportée dans les trois principales zones de l'Océan Austral beaucoup plus longues. En confrontant ces résultats avec les modèles saisonniers proposés par Fripiat et al. (2012), il nous sera possible d'optimiser ces modèles pour chacune des régions de l'ACC afin de mieux comprendre les processus qui contrôlent les variations de la composition isotopique de la BSi, en particulier en dehors des périodes de production (e.g. *Fig. II.3.*).

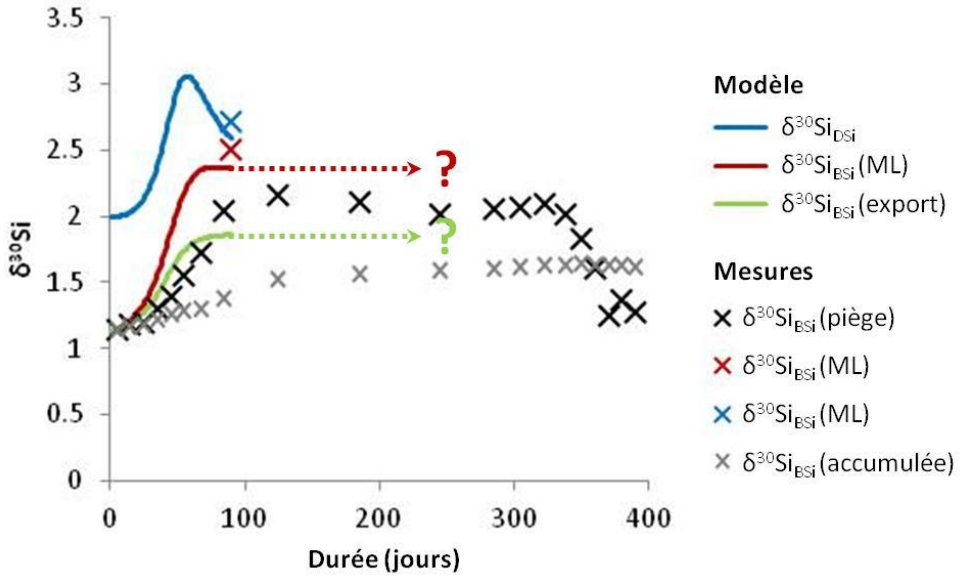

Figure II.3. Simulation de l'évolution de la composition isotopique de l'acide silicique (en bleu), de la BSi dans la ML (en rouge) et de la BSi exportée (en vert) pour la PFZ selon le modèle de Fripiat et al. (2012). Les points représentent les valeurs de la composition isotopique des particules collectées dans les pièges de la PFZ (en noir) ainsi que ses valeurs accumulées (en gris).

4.2. Vers une meilleure compréhension de la dynamique du fractionnement isotopique chez les diatomées…

La principale limite à l'étude et à la modélisation des équilibres isotopiques du silicium réside actuellement dans la définition du ou des facteur(s) de fractionnement et de ses facteurs de contrôle. Le facteur de fractionnement varie-t-il en fonction des régions, des populations phytoplanctoniques, ou au cours la saison ? D'après le chapitre 3, il semble que le facteur de fractionnement soit assez homogène entre les principales zones de l'ACC. Ceci est en accord avec le fait que le flux de particules siliceuses dans ces zones est systématiquement dominé par la même espèce de diatomée (*Fragilariopsis kerguelensis*, Rigual-Hernandes, personnal communication). En effet, il a été montré lors d'expériences d'incubation que différentes populations de diatomées fractionnaient différemment les isotopes du silicium lors de la production de BSi (Sutton et al., 2013). Cependant, les incertitudes importantes subsistant quant au calcul du $^{30}\varepsilon$ à partir des modèles théoriques (Rayleigh vs. steady state), et les écarts des $\delta^{30}Si_{BSi}$ observés en particulier en fin de saison, nous amènent à penser que le facteur de fractionnement ne serait pas constant au cours du temps, mais plutôt fonction de la cinétique d'uptake. En effet, le fractionnement isotopique du silicium ayant probablement lieu lors de transport du H_4SiO_4 par les SIT à travers la membrane des diatomées, celui-ci varie très probablement en fonction de la vitesse à laquelle le DSi est absorbé par la diatomée (V_{Si}), ce qui expliquerait en partie les variations saisonnières du $^{30}\varepsilon$ et le découplage entre les réservoirs

dissous et particulaire observés dans la région de Kerguelen. Afin de vérifier cette hypothèse, on pourrait par exemple mesurer les $\delta^{30}Si_{DSi}$ et $\delta^{30}Si_{BSi}$ ainsi que les taux de production et dissolution simultanément sur les mêmes échantillons, lors d'expériences d'incubations telles que celles effectuées durant la campagne KEOPS-2 (ceci implique néanmoins une logistique assez lourde, et limiterait probablement le nombre d'échantillons, de réplicats, de profondeurs et/ou de stations étudiées).

4.3. Vers une meilleure intégration des facteurs environnementaux propres à l'Océan austral…

Grâce aux avancées analytiques dans le domaine des isotopes stables, des travaux récents ont utilisé ces traceurs afin d'étudier plus précisément le couplage entre le cycles du Si et du C à partir d'archives sédimentaires prélevées dans l'Océan Austral (e.g. Panizzo et al., 2014). Cette étude a notamment mis en évidence l'influence de la glace de mer sur les variations passées de ces deux cycles biogéochimiques et comment elle peut potentiellement biaiser l'interprétation de ces enregistrements sédimentaires. Comme nous l'avons montré dans ce travail de thèse, il subsiste encore de nombreuses lacunes dans nos connaissances relatives au processus qui peuvent influencer les équilibres isotopiques et le transfert dans la colonne d'eau de ces proxies isotopiques ($\delta^{13}C$ et $\delta^{30}Si$).

Actuellement, un projet de recherche est en cours dans le cadre d'un poste d'ATER faisant suite à ce travail de thèse, afin de mieux comprendre le rôle de la banquise dans le (dé)couplage entre les cycles biogéochimiques du C et du Si ; ainsi que les processus influençant les proxies isotopiques tels que le $\delta^{13}C$ et $\delta^{30}Si$, depuis leur production en surface jusqu'à leur incorporation dans les sédiments. Pour cela, une série d'échantillons destinés à l'analyse des isotopes de C et de Si mais également de l'azote ($\delta^{15}N$) a été prélevé sur le plateau continental de la Terre Adélie (Campagne COCA-2012), une région où les processus physiques et biogéochimiques sont étroitement liés à la dynamique de la banquise. Ils représentent un échantillonnage complet de la colonne d'eau (eau de mer et particules collectées à 7 stations), un piège à particules situé dans une zone à fort taux de sédimentations (Fosse de d'Urville), programmé sur un an avec une résolution temporelle variable (5 jours durant l'été austral à 50 jours durant l'hiver) ainsi que plusieurs carottes d'interface situées à proximité de ce dernier. Les résultats préliminaires montrent une saisonnalité du flux de BSi extrêmement forte, caractérisée par un unique évènement de sédimentation massive restreint à une très courte durée (15 jours fin janvier-début février) et qui représente à lui tout seul plus de 90 % du flux annuel (*Fig. II.4.*).

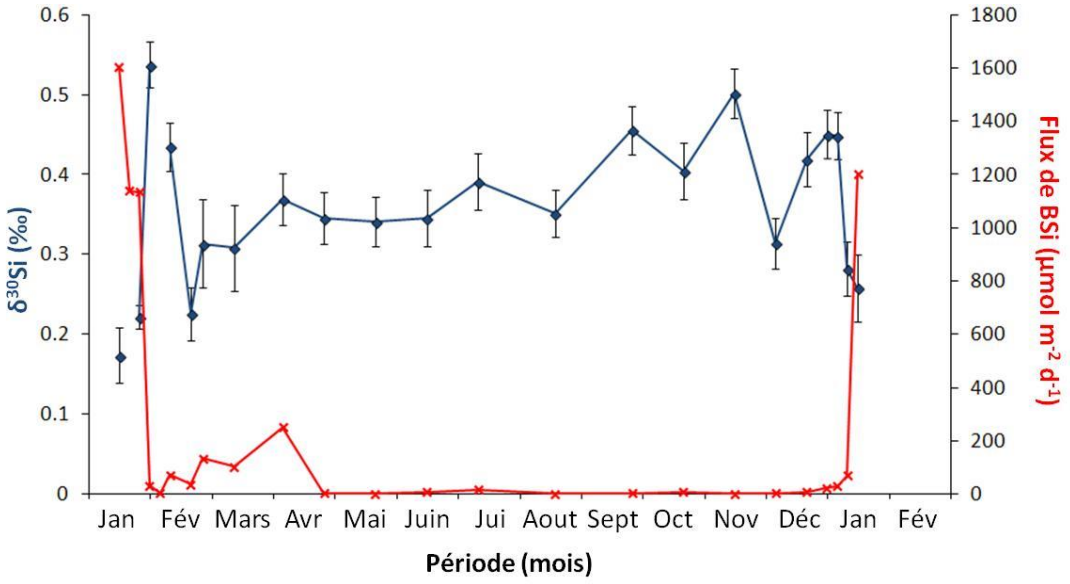

Figure II.4. Evolution saisonnière du flux de BSi (en rouge) et de la composition isotopique (en bleu) des particules collectées dans un piège situé en zone saisonnière de banquise sur le plateau continental de la Terre Adélie (Fosse de d'Urville).

Contrairement aux données issues des zones libres de glace présentées dans le chapitre 3 la majorité des variations du $\delta^{30}Si$ a lieu durant cette courte période de temps et oscille entre moins de 0.2 ‰ et plus de 0.5 ‰. Durant l'hiver, les valeurs de $\delta^{30}Si$ se maintiennent entre 0.3 ‰ et 0.4 ‰ et semblent se déstabiliser à nouveau à partir du début du printemps. Ces résultats sont à comparer avec la signature isotopique des diatomées d'eaux libres de glace avoisinantes (entre -0.93 ‰ et -0.06 ‰, résultats en cours d'analyse, non présentés ici) et celles issues de la glace de mer (de 0.41 ‰ à 0.86 ‰, Fripiat et al., 2007). En effet, la diversité des organismes récoltés dans ce type de pièges à particules est relativement importante et regroupe à la fois des individus caractéristiques du milieu phytoplanctonique et de la banquise (Closset, 2011). Il serait ainsi possible d'estimer une contribution des organismes issus de la glace de mer dans le flux de particules à partir des signatures isotopiques des différentes populations de diatomées, comme il a été proposé par Panizzo et al. (2014). L'analyse du $\delta^{30}Si$ dans les réservoirs dissous et particulaire (en cours) nous permettra également de mieux comprendre le rôle de la glace de mer dans le cycle côtier du Si et peut-être d'établir un budget du silicium sur le plateau continental de la Terre Adélie, tel qu'il a été construit pour le Plateau de Kerguelen. La Terre Adélie est une zone de formation des AABW qui a un rôle dominant dans les teneurs et $\delta^{30}Si$ des eaux de fond de l'océan mondial (de Souza et al., 2014) c'est donc une zone particulièrement importante à caractériser dans ce contexte. La comparaison de ces résultats avec des mesures des isotopes stables du C (et de l'N) nous permettra de franchir un pas de plus vers la compréhension des interactions entre les cycles biogéochimiques de ces différents éléments.

4.4. Vers une augmentation de la couverture spatio-temporelle des mesures…

Cette thèse s'est concentrée sur les eaux HNLC des trois principales zones de l'ACC ainsi que sur la région naturellement enrichie en fer du Plateau de Kerguelen. Cependant, très peu d'études se sont intéressées pour le moment aux autres régions fertilisées en fer de l'Océan Austral telles que la pointe de la Péninsule Antarctique (De la Rocha et al. (2011) se sont concentrés uniquement sur la signature isotopique des eaux de surface); ou encore aux zones situées sur le plateau continental antarctique. D'autres systèmes océaniques riches en organismes siliceux restent également fortement sous-échantillonnés en ce qui concerne les isotopes du silicium, comme c'est le cas notamment dans l'Atlantique Nord et dans l'Océan Arctique. Grâce aux avancées techniques et méthodologiques discutées dans ce manuscrit, il est aujourd'hui possible de mesurer la composition isotopique de réservoirs présentant des faibles concentrations de silicium (BSi et DSi), ouvrant ainsi la possibilité de se tourner vers l'étude de régions jusqu'à présent négligées, telles que au nord du PF dans l'Océan Austral ou encore l'Océan Indien. En effet, nous avons vu que les stocks de BSi et DSi sont particulièrement faibles dans la SAZ ; or cette région joue un rôle important dans la biogéochimie de l'océan global puisqu'elle représente une zone de formation d'eaux modales (SAMW et AAIW) et constitue un puits de CO_2 atmosphérique important.

Ce travail de thèse a également mis en évidence que la notion de saisonnalité est très importante dans la compréhension de la distribution et des variations du $\delta^{30}Si$ de l'eau de mer et des particules siliceuses. Or jusqu'à présent, aucune étude ne s'était concentrée sur un suivi annuel complet de l'évolution de la composition isotopique de la BSi et encore moins du DSi. La production de nouveaux jeux de données issues de séries temporelles à haute fréquence, à l'aide de pièges à particules par exemple ou d'instruments d'échantillonnage autonomes est donc indispensable afin d'améliorer les modèles actuels du cycle océanique du silicium.

5. Références bibliographiques

Brzezinski M. (1985) The Si:C:N ratio of marine diatoms: interspecific variability and the effect of some environmental variables. Journal of Phycology. 21:347-357

Cardinal D., L.Y. Alleman, J. De Jong, K. Ziegler, L. André (2003), Isotopic composition of silicon measured by multicollector plasma source mass spectrometry in dry plasma mode, Journal of Analytical Atomic Spectrometry, 18, 213-218.

Cardinal D., L.Y. Alleman, F. Dehairs, N. Savoye, T.W. Trull, L. André (2005), Relevance of silicon isotopes to Si-nutrient utilization and Si-source assessment in Antarctic waters, Global biogeochemical cycles, 19(GB2007), doi:10.1029/2004GB002364.

Cavagna A-J., F. Fripiat, M. Elskens, F. Dehairs, P. Mangion, L. Chirurgien, I. Closset, M. Lasleiz, L. Flores-Leiva, D. Cardinal, K. Leblanc, C. Fernadez, D. Lefèvre, L. Oriol, S. Blain, B. Quéguiner (2014), Biological productivity regime and associated N cycling in the vicinity of Kerguelen Island area, Southern Ocean, Biogeosciences Discussion, 11, 18073-18104.

Closset I. (2011) « Les derniers millénaires en Antarctique de l'Est : Calibration de nouveaux proxies climatiques, rapport de master 2, UPMC, 36 pages

Coffineau N., C. L. De la Rocha, P. Pondaven (2014), Exploring interacting influences on the silicon isotopic composition of the surface ocean: a case study from the Kerguelen Plateau, Biogeosciences, 11, 1371-1391.

De Brauwere A., Fripiat F., Cardinal D., Cavagna A.-J., De Ridder F., André L., Elskens M. (2012) Isotopic model of oceanic silicon cycling: the Kerguelen Plateau case study. Deep-Sea Research I. 70:42-59

Dehairs F., F. Fripiat, A.-J. Cavagna, T. W. Trull, C. Fernandez, D. Davies, A. Roukaerts, D. Fonseca Batista, F. Planchon, M. Elskens (2014), Nitrogen cycling in the Southern Ocean Kerguelen Plateau area: evidence for significant surface nitrification from nitrate isotopic compositions, Biogeosciences Discussion, 11, 13905-13955.

De La Rocha C.L., P. Bescont, A. Croguennoc, E. Ponzevera (2011), The silicon isotopic composition of surface waters in the Atlantic and Indian sectors of the Southern Ocean, Geochimica et Cosmochimica Acta, 75, 5283-5295, doi:10.1016/j.gca.2011.06.028.

De Souza G. F., B. C. Reynolds, J. Rickli, M. Frank, M. A. Saito, L. J. A. Gerringa, B. Bourdon (2012), Southern Ocean control of silicon stable isotope distribution in the deep Atlantic Ocean, Global Biogeochemical Cycles, 26, GB2035, doi:10.1029/2011GB004141.

Ebersbach F., T.W. Trull, D.M. Davies, S.G. Bray (2011), Controls on mesopelagic particle fluxes in the Sub-Antarctic and Polar Frontal Zones in the Southern Ocean south of Australia in summer – Perspectives from free-drifting sediment traps, Deep-sea research II, 58, 2260-2276, doi:10.1016/j.dsr2.2011.05.025.

Fripiat F., D. Cardinal, J.-L. Tison, A. Worby, L. André (2007) Diatom-induced silicon isotopic fractionation in Antarctic sea ice, Journal of Geophysical Research, 112, G02001, doi:10.1029/2006JG000244

Fripiat F., R. Corvaisier, J. Navez, M. Elskens, V. Schoemann, K. Leblanc, L. André, D. Cardinal (2009) Measuring production-dissolution rates of marine biogenic silica by ^{30}Si-isotope dilution using a high-resolution sector field inductively coupled plasma mass spectrometer, Limnology and Oceanography: Methods, 7, 470-478

Fripiat F., A-J. Cavagna, N. Savoye, F. Dehairs, L. André, D. Cardinal (2011a), Isotopic constraints on the Si-biogeochemical cycle of the Antarctic Zone in the Kerguelen area (KEOPS), Marine Chemistry, 123, 11-22, doi:10.1016/j.marchem.2010.08.005.

Fripiat F., K. Leblanc, M. Elskens, A-J. Cavagna, L. Armand, L. André, F. Dehairs, D. Cardinal (2011b), Efficient silicon recycling in summer in both the Polar Frontal and Subantarctic Zones of the Southern Ocean, Marine ecology progess series, 435, 47-61, doi:10.3354/meps09237.

Fripiat F., A-J. Cavagna, F. Dehairs, A. de Brauwere, L. André, D. Cardinal (2012), Processes controlling the Si-isotopic composition in the Southern Ocean and application for paleoceanography, Biogeosciences, 9, 2443-2457, doi:10.5194/bg-9-2443-2012.

Georg R.B., B.C. Reynolds, M. Frank, A. N. Halliday (2006), New sample preparation techniques for the determination of Si isotopic compositions using MC-ICPMS, Chemical Geology, 235, 95-104.

Hughes H.J., C. Delvigne, M. Korntheuer, J. De Jong, L. André, D. Cardinal (2011), Controlling the mass bias introduced by anionic and organic matrices in silicon isotopic measurements, Journal of Analytical Atomic Spectrometry, 26, 1892-1896.

Lasbleiz M., K. Leblanc, S. Blain, J. Ras, V. Cornet-Barthaux, S. Hélias Nunige, B. Quéguiner (2014), Pigments, elemental composition (C, N, P and Si), and stoichiometry of particulate matter in the naturally iron fertilized region of Kerguelen in the Southern Ocean, Biogeosciences, 11, 5931-5955, doi:10.5194/bg-11-5931-2014.

Laurenceau E.C., T.W. Trull, D.M. Davies, S.G. Bray, J. Doan, F. Planchon, F. Carlotti, M-P. Jouandet, A-J. Cavagna, A.M. Waite, S. Blain (2014), The relative importance of phytoplankton aggregates and zooplankton fecal pellets to carbon export: insights from free-drifting sediment trap deployments in naturally iron-fertilised waters near the Kerguelen plateau, Biogeosciences Discussion, 11, 13623-13673.

Mongin M., E. Molina, T.W. Trull (2008), Seasonality and scale of the Kerguelen plateau phytoplankton bloom: A remote sensing and modeling analysis of the influence of natural iron fertilization in the Southern Ocean, Deep-Sea Research II, 55, 880-892.

Panizzo V., J. Crespin, X. Crosta, A. Shemesh, G. Massé, R. Yam, N. Mattielli, D. Cardinal (2014), Sea ice diatom contributions to Holocene nutrient utilization in East Antarctica, Paleoceanography, 29, 328-342, doi:10.1002/2014PA002609.

Park Y.-H., I. Durand, E. Kestenare, G. Rougier, M. Zhou, F. d'Ovidio, C. Cotté, J.-H. Lee (2014), Polar Front around the Kerguelen Islands: An up-to-date determination and associated circulation of surface/subsurface waterJournal of Geophysical Research: Oceans, 119, doi:10.1002/2014JC010061.

Ragueneau O., N. Savoye, Y. Del Amo, J. Cotten, B. Tardiveau, A. Leynaert (2005), A new method for the measurement of biogenic silica in suspended matter of coastal waters: using Si:Al ratios to correct for the mineral interference, Continental Shelf Research, 25, 697-710.

Reynolds B., Frank M., Halliday A. (2006) Silicon isotope fractionation during nutrient utilization in the North Pacific. Earth and Planetary Science Letters. 244:431-443

Reynolds B.C., J. Aggarwal, L. André, D. Baxter, C. Beucher, M.A. Brzezinski, E. Engström, R.B. Georg, M. Land, M.J. Leng, S. Opfergelt, I. Rodushkin, H.J. Sloane, S.H.J.M. van den Boorn, P.Z. Vroon, D. Cardinal (2007), An inter-laboratory comparison of Si isotope reference materials, Journal of Analytical Atomic Spectrometry,22, 561-568, doi:10.1039/b616755a.

Sutton J.N., D.E. Varela, M.A. Brzezinski, C.P. Beucher (2013) Species-dependent silicon isotope fractionation by marine diatoms, Geochimica et Cosmochimica Acta, 104, 300-309

Trull T., S.G. Bray, K.O. Buesseler, C.H. Lamborg, S. Manganini, C. Moy, J. Valdes (2008), In situ measurement of mesopelagic particle sinking rates and the control of carbon transfer to the ocean interior during the Vertical Flux in the Global Ocean (VETIGO) voyages in the North Pacific, Deep-Sea Research II, 55, 1684-1695.

Varela D.E., C.J., Pride, M.A. Brzezinski (2004), Biological fractionation of silicon isotopes in Southern Ocean surface waters, Global biogeochemical cycles, 18(GB1047), doi:10.1029/2003GB002140.

Matériel Supplémentaire et Annexes

ANNEXES A

Table A1. Concentrations (BSi, µmol l^{-1}), production (ρSi, µmol l^{-1} d^{-1}) and dissolution (ρDiss, µmol l^{-1} d^{-1}) of biogenic silica over depth in the four contrasted KEOPS-2 stations.

Station *Date (2011)*	**PAR %**	**Depth m**	**BSi Concentration µmol l^{-1}**	**BSi Production µmol^{-1} d^{-1}**	**BSi Dissolution µmol^{-1} d^{-1}**
R-2					
26 Oct	75	6	0.32 ± *0.02*	0.04 ± *0.00*	0.04 ± *0.00*
	45	16	0.32 ± *0.02*	0.03 ± *0.00*	*na*
	25	28	0.35 ± *0.02*	0.04 ± *0.00*	0.04 ± *0.00*
	16	37	0.33 ± *0.02*	0.03 ± *0.00*	*na*
	4	64	0.39 ± *0.02*	0.03 ± *0.00*	0.07 ± *0.01*
	1	92	0.41 ± *0.02*	0.04 ± *0.00*	0.04 ± *0.00*
	0.3	116	0.39 ± *0.02*	0.02 ± *0.00*	0.06 ± *0.01*
F-L					
7 Nov	75	2	3.20 ± *0.16*	1.22 ± *0.12*	0.14 ± *0.01*
	25	9	3.50 ± *0.18*	1.08 ± *0.11*	*na*
	16	11	3.48 ± *0.17*	0.99 ± *0.10*	0.14 ± *0.01*
	4	20	3.45 ± *0.17*	0.88 ± *0.09*	*na*
	1	29	3.22 ± *0.16*	0.59 ± *0.06*	0.11 ± *0.01*
	0.3	36	2.90 ± *0.15*	0.07 ± *0.01*	0.11 ± *0.01*
	0.01	57	3.04 ± *0.15*	0.04 ± *0.00*	0.10 ± *0.01*
E-4W					
12 Nov	75	2	4.86 ± *0.24*	1.03 ± *0.10*	0.12 ± *0.01*
	25	9	4.79 ± *0.24*	1.19 ± *0.12*	*na*
	16	12	4.50 ± *0.23*	1.02 ± *0.10*	0.14 ± *0.01*
	4	21	4.38 ± *0.22*	0.97 ± *0.10*	*na*
	1	31	4.54 ± *0.23*	0.99 ± *0.10*	0.12 ± *0.01*
	0.3	39	3.73 ± *0.19*	0.45 ± *0.04*	0.13 ± *0.01*
	0.01	61	3.65 ± *0.18*	0.06 ± *0.01*	0.15 ± *0.01*
A3-2					
17 Nov	75	2	4.83 ± *0.24*	1.28 ± *0.13*	0.12 ± *0.01*
	25	12	4.77 ± *0.24*	1.18 ± *0.12*	*na*
	16	15	4.43 ± *0.22*	1.21 ± *0.12*	0.14 ± *0.01*
	4	27	4.40 ± *0.22*	1.32 ± *0.13*	*na*
	1	38	4.53 ± *0.23*	1.28 ± *0.13*	0.09 ± *0.01*
	0.3	48	4.11 ± *0.21*	0.17 ± *0.02*	0.21 ± *0.02*
	0.01	77	4.17 ± *0.21*	0.04 ± *0.00*	0.16 ± *0.02*

Table A2. Concentrations (BSi, µmol l^{-1}), production (ρSi, µmol l^{-1} d^{-1}) and dissolution (ρDiss, µmol l^{-1} d^{-1}) of biogenic silica over depth in the KEOPS-2 lagrangian survey stations.

Station *Date (2011)*	PAR %	Depth m	BSi Concentration µmol l^{-1}	BSi Production µmol $^{-1}$ d^{-1}	BSi Dissolution µmol $^{-1}$ d^{-1}
E-1					
30 Oct	75	4	1.36 ± *0.07*	0.25 ± *0.03*	0.09 ± *0.01*
	25	11	1.34 ± *0.07*	0.28 ± *0.03*	*na*
	16	19	1.43 ± *0.07*	0.28 ± *0.03*	0.07 ± *0.01*
	4	45	1.55 ± *0.08*	0.26 ± *0.03*	*na*
	1	64	1.75 ± *0.09*	0.24 ± *0.03*	0.17 ± *0.02*
	0.3	81	1.17 ± *0.06*	0.02 ± *0.00*	0.19 ± *0.02*
	0.01	129	1.69 ± *0.08*	0.01 ± *0.00*	*na*
E-3					
4 Nov	75	4	1.19 ± *0.06*	0.18 ± *0.02*	0.16 ± *0.02*
	25	21	1.20 ± *0.06*	0.20 ± *0.02*	*na*
	16	27	1.23 ± *0.06*	0.17 ± *0.02*	0.11 ± *0.01*
	4	48	1.17 ± *0.06*	0.12 ± *0.01*	*na*
	1	68	1.46 ± *0.07*	0.12 ± *0.01*	0.20 ± *0.02*
	0.3	86	1.17 ± *0.06*	0.01 ± *0.00*	0.19 ± *0.02*
	0.01	137	1.16 ± *0.06*	0.00 ± *0.00*	0.21 ± *0.02*
E-4E					
14 Nov	75	2	3.07 ± *0.15*	0.62 ± *0.06*	*na*
	25	10	2.93 ± *0.15*	0.57 ± *0.06*	*na*
	16	13	3.10 ± *0.16*	0.63 ± *0.06*	*na*
	4	24	3.19 ± *0.16*	0.64 ± *0.06*	*na*
	1	34	2.91 ± *0.15*	0.61 ± *0.06*	*na*
	0.3	42	2.91 ± *0.15*	0.26 ± *0.03*	*na*
	0.01	67	1.77 ± *0.09*	0.01 ± *0.00*	*na*
E-5					
19 Nov	75	3	2.87 ± *0.14*	0.57 ± *0.06*	0.12 ± *0.01*
	25	16	2.80 ± *0.14*	0.52 ± *0.05*	*na*
	16	22	2.90 ± *0.15*	0.63 ± *0.06*	0.15 ± *0.01*
	4	38	3.16 ± *0.16*	0.49 ± *0.05*	*na*
	1	54	2.90 ± *0.15*	0.29 ± *0.03*	0.11 ± *0.01*
	0.3	68	2.87 ± *0.14*	0.03 ± *0.00*	0.14 ± *0.01*
	0.01	108	1.11 ± *0.06*	0.00 ± *0.00*	0.14 ± *0.01*

SUPPLEMENTARY METHOD B

Controlling the mass bias introduced by sulfate in Si measurements by MC-ICP-MS

The cation-exchange purification technique used here does not remove anions (in our case, mostly Cl^-, SO_4^{2-} and to a lesser extent NO_3^-) from solutions. In this case, the addition of a known artificial matrix in excess in both the sample and standard solution can be used to dilute the natural concentration of the contaminant and to homogenize sample and standard matrices (doping method, Georg et al., 2006 ; Hughes et al., 2011). Indeed, dissimilar matrices will affect differently the plasma and ionization efficiency and will induce artificial bias in the delta measurements, invalidating the use of the standard-sample bracketing technique.

In our samples, Cl^- originating from seawater can be neglected compared to Cl^- added as HCl (Merck Suprapur) to dissolve the brucite; and as solutions were analyzed in a HCl matrix largely in excess (up to 0.5 mol L^{-1}) compared to natural Cl^- concentration. Similarly, the occurrence of NO_3^- in seawater was resolved by the use of HNO_3 (Merck Suprapur, 0.5 mol L^{-1}) as a solvent in both the samples and standards. For KEOPS-2 surface samples, sulfate concentrations measured by ionic chromatography after purification could be significant to generate a shift in isotopic measurements (SO_4^{2-}/Si up to 20). Van den Boorn et al. (2009) has recently reported that the presence of sulfate in rock digestion solutions can induce a significant offset (up to +1.4 ‰) in silicon isotopic measurements when SO_4^{2-}/Si ratios > 0.02.

To test the effect of sulfate on silicon measurements, we doped 4 Diatomite purified solutions with variable amounts of H_2SO_4 (Merck, Suprapur) to yield solutions with SO_4^{2-}/Si ratios ranging from 0 to 19. The sulfate-doped Diatomite solutions were then analyzed for silicon isotope composition using the sulfate-free standard-sample bracketing technique. These solutions were analyzed using the same configuration as for the KEOPS-2 samples and the procedure was replicated 6 times on separated MC-ICP-MS analytical sessions.

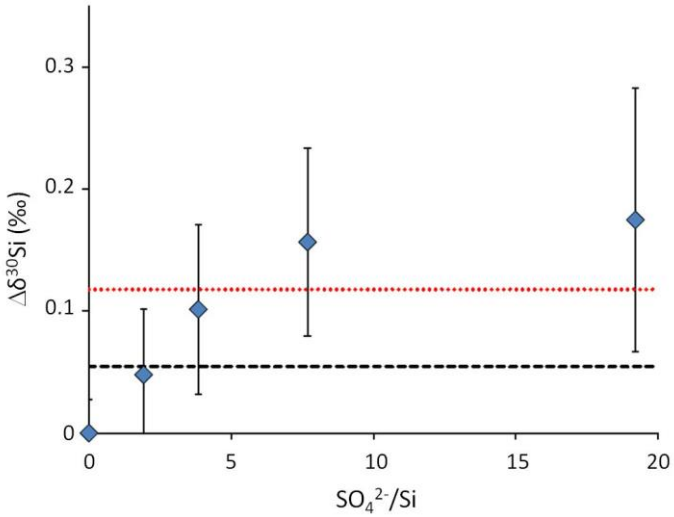

Figure B1. Effect of sulfate (expressed as SO_4^{2-}/Si ratios) on silicon isotope measurements ($\Delta\delta^{30}Si$ = offset in $\delta^{30}Si$ of sulfate-doped Diatomite relative to pure standard). Error bars represent 1sd. Black dashed and red dotted lines are the +1sd and +2sd from the initial (non-doped) value, respectively.

The results of the experiment show a clear positive relation between the silicon isotopic composition of Diatomite and SO_4^{2-}/Si ratio of the solution (*Fig. B1.*), with the increase of $\delta^{30}Si$ signatures becoming significant (+0.2 ‰) when SO_4^{2-}/Si ratios > 8. Moreover, we observe a degradation of the analytical reproducibility with increasing SO_4^{2-}/Si ratios with standard deviations up to five times higher in the most sulfate-concentrated solution, suggesting a strong decline of the measurement quality.

Doping both standard and Diatomite solutions with H_2SO_4 (final concentration 1mmol L^{-1}) would impose similar SO_4^{2-}/Si ratios in the sample and the standard solutions and should prevent any matrix effect. Indeed, we observe that the doping procedure does not induce any bias on Diatomite reference material measurements that have a $\delta^{30}Si$ signature similar to the published values (1.27 ± 0.06 ‰, n = 50 ; compared to $\delta^{30}Si$ = 1.26 ‰, Reynolds et al., 2007).

Thus, as proposed by Hughes et al. (2011) for river waters, samples and standards solutions used for seawater isotopic analyses must be doped with sulfate when their SO_4^{2-}/Si ratios > 8 in order to control the sulfate matrix effect during MC-ICP-MS measurements. In our study, it concerned every surface samples where we used a preconcentration (MAGIC) volume > 50 ml. However, to run the MC-ICP-MS in the same matrix conditions for all samples, we decided to apply this procedure for all KEOPS-2 seawater samples. Thus, after cationic exchange purification (Georg et al., 2006) and prior to MC-ICP-

MS measurements, sulfuric acid (H4SO4, Merck Suprapur) was added to both the standard and the samples in order to reach the same final SO_4^{2-} concentration (1 mmol L^{-1}, see *Table B1.*).

Table B1. Running concentrations for isotopic analysis of seawater sample

	Si	**HCl**	**HNO_3**	**H_2SO_4**	**Mg**
Concentrations	2-2.5 ppm	0.5 mol L^{-1}	0.5 mol L^{-1}	1 mmol L^{-1}	2-2.5 ppm

Supplementary references

Georg R.B., B.C. Reynolds, M. Frank, A. N. Halliday (2006), New sample preparation techniques for the determination of Si isotopic compositions using MC-ICPMS, Chemical Geology, 235, 95-104.

Hughes H.J., C. Delvigne, M. Korntheuer, J. De Jong, L. André, D. Cardinal (2011), Controlling the mass bias introduced by anionic and organic matrices in silicon isotopic measurements, Journal of Analytical Atomic Spectrometry, 26, 1892-1896.

Reynolds B.C., J. Aggarwal, L. André, D. Baxter, C. Beucher, M.A. Brzezinski, E. Engström, R.B. Georg, M. Land, M.J. Leng, S. Opfergelt, I. Rodushkin, H.J. Sloane, S.H.J.M. van den Boorn, P.Z. Vroon, D. Cardinal (2007), An inter-laboratory comparison of Si isotope reference materials, Journal of Analytical Atomic Spectrometry,22, 561-568, doi:10.1039/b616755a.

Van den Boorn S.H.J.M., P.Z. Vroon, M.J. Van Bergen (2009), Sulfur-induced offsets in MC-ICP-MS silicon-isotope measurements, Journal of Analytical Atomic Spectrometry, 24, 1111-1114.

ANNEXES B

Table B2. Silicic acid, biogenic silica concentrations and δ^{30}Si of DSi and BSi for all KEOPS-2 samples.

Station	Depth (m)	$[H_4SiO_4]$ ($\mu mol\ L^{-1}$)	$\delta^{30}DSi$ (‰)	[BSi] ($\mu mol\ L^{-1}$)	$\delta^{30B}Si$ (‰)	
A3-1	11	22,89 ± 1,60	1,96 ± *0,07*	1,26 ± 0,21	0,77 ± *0,06*	*
CTD#004	42	22,83 ± 1,60	2,01 ± *0,03*	1,35 ± 0,05	0,82 ± *0,07*	*
20/10/2011	104	23,88 ± 1,67	1,99 ± *0,02*	1,18 ± 0,34	0,72 ± *0,09*	*
50°S 37.77	152	32,77 ± 2,29	1,73 ± *0,05*	0,75 ± 0,09	0,96 ± *0,08*	*
72°E 04.82	173	31,55 ± 2,21	1,76 ± *0,03*	0,58 ± 0,07	1,05 ± *0,03*	*
	204	36,41 ± 2,55	1,71 ± *0,03*	0,51 ± 0,06	1,21 ± *0,10*	*
	227	41,26 ± 2,89	1,58 ± *0,04*			
	253	44,90 ± 3,14	1,62 ± *0,04*			
	279	46,12 ± 3,23	1,49 ± *0,03*			
	354	60,68 ± 4,25	1,41 ± *0,02*			
	474	70,39 ± 4,93	1,38 ± *0,00*			
TNS8	12	17,91 ± 1,25	2,36 ± *0,04*	1,31 ± 0,27	0,86 ± *0,03*	*
CTD#008	41	18,41 ± 1,29		1,12 ± 0,14	1,04 ± *0,03*	*
21/10/2011	102	19,59 ± 1,37	2,24 ± *0,03*	1,52 ± 0,44	0,96 ± *0,03*	*
49°S 27.77	150	21,65 ± 1,52	2,16 ± *0,03*	1,39 ± 0,16	1,05 ± *0,04*	*
72°E 14.41	205	26,80 ± 1,88	1,93 ± *0,03*	1,09 ± 0,13	1,08 ± *0,04*	*
	254	41,92 ± 2,93	1,50 ± *0,02*			
	305	54,55 ± 3,82	1,34 ± *0,02*			
	405	65,15 ± 4,56	1,29 ± *0,02*			
	505	71,72 ± 5,02	1,21 ± *0,02*			
	606	72,46 ± 5,07				
	707	70,05 ± 4,90	1,25 ± *0,04*			
	910	80,81 ± 5,66	1,11 ± *0,03*			
	1000	76,33 ± 5,34	1,24 ± *0,04*			
TNS06	11	16,42 ± 1,15	2,41 ± *0,03*	1,38 ± 0,01	1,11 ± *0,02*	*
CTD#10	42	16,56 ± 1,16		1,54 ± 0,11	1,30 ± *0,03*	*
22/10/2011	103	16,64 ± 1,16	2,41 ± *0,03*	1,53 ± 0,01	1,34 ± *0,04*	*
48°S 46.78	184	31,31 ± 2,19	1,71 ± *0,02*	0,46 ± 0,05	1,38 ± *0,04*	*
72°E 16.77	204	35,35 ± 2,47	1,50 ± *0,02*	0,56 ± 0,06	1,41 ± *0,03*	*
	255	43,94 ± 3,08	1,36 ± *0,02*			
	306	52,53 ± 3,68	1,42 ± *0,02*			
	407	61,50 ± 4,30				
	509	69,33 ± 4,85	1,30 ± *0,03*			
	610	73,26 ± 5,13				
	813	80,10 ± 5,61	1,26 ± *0,03*			
	1526	88,38 ± 6,19	1,05 ± *0,03*			
	1886	95,96 ± 6,72	0,95 ± *0,02*			

Table B2. (continued) Silicic acid, biogenic silica concentrations and $\delta^{30}Si$ of DSi and BSi for all KEOPS-2 samples.

Station	Depth (m)	$[H_4SiO_4]$ ($\mu mol\ L^{-1}$)	$\delta^{30}DSi$ (‰)	[BSi] ($\mu mol\ L^{-1}$)	$\delta^{30B}Si$ (‰)	
TNS01	11	8,96 ± 0,63	2,32 ± *0,04*	0,24 ± 0,03	1,35 ± *0,04*	*
CTD#15	41	8,96 ± 0,63	2,18 ± *0,03*	0,24 ± 0,02	1,27 ± *0,04*	*
23/10/2011	102	9,95 ± 0,70	2,26 ± *0,04*	0,26 ± 0,03	1,31 ± *0,03*	*
46°S 49.99	153	13,40 ± 0,94	2,23 ± *0,11*	0,08 ± 0,01		*
71°E 30.06	202	17,65 ± 1,24	1,89 ± *0,03*	0,08 ± 0,01		*
	253	26,20 ± 1,83	1,86 ± *0,03*			
	304	32,62 ± 2,28	1,66 ± *0,03*			
	405	45,45 ± 3,18	1,57 ± *0,04*			
	506	54,55 ± 3,82				
	606	57,49 ± 4,02	1,39 ± *0,05*			
	809	71,01 ± 4,97	1,31 ± *0,06*			
	1520	80,81 ± 5,66	1,00 ± *0,03*			
	2282	97,60 ± 6,83	1,02 ± *0,15*			
R2	21	12,94 ± 0,91	2,21 ± *0,04*	0,30 ± 0,03	0,73 ± *0,04*	*
CTD#17&20	40	12,94 ± 0,91	2,30 ± *0,06*	0,41 ± 0,08	0,78 ± *0,06*	*
26/10/2011	80	11,96 ± 0,84	2,18 ± *0,04*	0,29 ± 0,03	0,96 ± *0,01*	*
50°S 21.52	90			0,93 ± 0,02	1,18 ± *0,06*	
66°E 43.00	100	12,98 ± 0,91	2,27 ± *0,02*	0,27 ± 0,03	1,37 ± *0,03*	*
	126	13,37 ± 0,94	2,38 ± *0,04*	0,17 ± 0,02	1,52 ± *0,03*	*
	151	12,88 ± 0,90	2,14 ± *0,06*	0,13 ± 0,01	1,34 ± *0,04*	*
	203	21,74 ± 1,52	1,92 ± *0,04*	0,42 ± 0,01		
	253	29,95 ± 2,10	1,80 ± *0,03*			
	356	37,20 ± 2,60	1,60 ± *0,03*			
	404	48,31 ± 3,38	1,37 ± *0,04*			
	507	57,00 ± 3,99	1,29 ± *0,06*	0,16 ± 0,00	1,71 ± *0,04*	
	609	61,35 ± 4,29	1,19 ± *0,01*	0,05 ± 0,00	1,71 ± *0,14*	
	708		1,28 ± *0,04*			
	812	71,01 ± 4,97	1,22 ± *0,03*	0,11 ± 0,00	1,86 ± *0,04*	
	911	74,03 ± 5,18	1,23 ± *0,03*			
	1011	78,27 ± 5,48	1,08 ± *0,01*	0,05 ± 0,00	1,85 ± *0,05*	
	1520	85,86 ± 6,01	1,07 ± *0,04*	0,10 ± 0,00	2,01 ± *0,10*	
	1832	90,91 ± 6,36	1,06 ± *0,03*			
	2000			0,02 ± 0,02		
	2473	119,57 ± 8,37	1,13 ± *0,03*	0,08 ± 0,00	2,09 ± *0,06*	
	2500		1,14 ± *0,03*			

Table B2. (continued) Silicic acid, biogenic silica concentrations and δ^{30}Si of DSi and BSi for all KEOPS-2 samples.

Station	Depth (m)	$[H_4SiO_4]$ (µmol L^{-1})	δ^{30}DSi (‰)	[BSi] (µmol L^{-1})	δ^{30B}Si (‰)	
E1	21	15,92 ± 1,11	2,26 ± *0,04*	1,61 ± 0,05	1,16 ± *0,09*	*
CTD#27&30	41	15,92 ± 1,11	2,27 ± *0,00*	1,45 ± 0,11	1,18 ± *0,06*	*
30/10/2011	60			1,30 ± 0,09		
48°S 29.88	81	8,70 ± 0,61	2,23 ± *0,02*	1,60 ± 0,25	1,20 ± *0,00*	*
72°E 10.66	101	16,58 ± 1,16	2,20 ± *0,01*	1,53 ± 0,18	1,20 ± *0,04*	**
	125	17,11 ± 1,20	2,02 ± *0,12*	1,59 ± 0,18	1,23 ± *0,02*	*
	151	20,32 ± 1,42	1,99 ± *0,02*	1,42 ± 0,16	1,30 ± *0,06*	*
	182	28,88 ± 2,02	1,84 ± *0,06*	0,49 ± 0,06	1,32 ± *0,02*	**
	253		1,57 ± *0,03*			
	303	52,94 ± 3,71	1,44 ± *0,03*	0,70 ± 0,01	1,37 ± *0,01*	
	403	63,64 ± 4,45	1,35 ± *0,03*			
	455	70,05 ± 4,90	1,29 ± *0,03*			
	505	70,05 ± 4,90	1,27 ± *0,04*	0,47 ± 0,05	1,56 ± *0,12*	
	605	76,46 ± 5,35	1,28 ± *0,03*			
	636	76,46 ± 5,35	1,20 ± *0,03*	0,41 ± 0,01	1,57 ± *0,09*	
	707	76,46 ± 5,35	1,23 ± *0,04*			
	808	80,10 ± 5,61	1,12 ± *0,03*			
	913	80,10 ± 5,61	1,18 ± *0,03*			
	1011	83,33 ± 5,83	1,01 ± *0,03*	0,33 ± 0,03	1,71 ± *0,00*	
	1498	88,38 ± 6,19	0,98 ± *0,03*	0,22 ± 0,01	1,74 ± *0,02*	
	1780			0,20 ± 0,00	1,79 ± *0,02*	
	2042	101,06 ± 7,07	1,18 ± *0,02*	0,52 ± 0,01	1,83 ± *0,12*	
TEW1	10	7,46 ± 0,52	2,75 ± *0,01*	6,33 ± 0,55	2,04 ± *0,02*	*
CTD#35	31	12,94 ± 0,91	2,39 ± *0,06*	3,30 ± 0,24	1,86 ± *0,03*	*
31/10/2011	51	14,93 ± 1,04	2,16 ± *0,03*	2,75 ±		*
49°S 08.99	71	16,42 ± 1,15	2,19 ± *0,03*	1,88 ± 0,01	1,66 ± *0,03*	*
69°E 50.01	80		1,88 ± *0,04*			
TEW3	16	19,90 ± 1,39		0,63 ± 0,01	0,47 ± *0,03*	*
CTD#38	41	19,90 ± 1,39	2,31 ± *0,03*	0,92 ± 0,08	0,79 ± *0,03*	*
31/10/2011	61	11,96 ± 0,84	2,33 ± *0,03*	0,78 ± 0,09	0,57 ± *0,03*	*
48°S 47.95	76	8,70 ± 0,61	2,01 ± *0,04*	0,70 ± 0,08	0,56 ± *0,04*	*
71°E 01.06	111	24,74 ± 1,73	1,86 ± *0,03*	0,56 ± 0,06	0,74 ± *0,04*	*
	183	28,34 ± 1,98		0,39 ± 0,04	1,26 ± *0,04*	*
	253	40,11 ± 2,81				
	277	41,18 ± 2,88				
	404	58,82 ± 4,12	1,95 ± *0,05*			
	545	75,14 ± 5,26	1,41 ± *0,02*			
E2	11	11,96 ± 0,84	2,34 ± *0,06*	1,87 ± 0,05	1,23 ± *0,04*	*
CTD#43	41	18,41 ± 1,29	2,42 ± *0,12*	1,00 ± 0,04	1,27 ± *0,06*	*
01/11/2011	102	17,65 ± 1,24	2,22 ± *0,03*	1,14 ± 0,02	1,21 ± *0,03*	*
48°S 31.41	153	20,32 ± 1,42	1,99 ± *0,02*	0,96 ± 0,11	1,25 ± *0,02*	*
72°E 04.63	204	46,01 ± 3,22		0,48 ± 0,06	1,42 ± *0,09*	*
	254	36,36 ± 2,55				
	305	58,82 ± 4,12				
	406	68,98 ± 4,83	1,30 ± *0,03*			
	507	73,80 ± 5,17	1,02 ± *0,03*			
	609	75,24 ± 5,27	1,22 ± *0,01*			
	813	72,95 ± 5,11	1,21 ± *0,03*			
	1016	83,33 ± 5,83	1,08 ± *0,03*			
	2020	75,24 ± 5,27	0,93 ± *0,04*			

Table B2. (continued) Silicic acid, biogenic silica concentrations and δ^{30}Si of DSi and BSi for all KEOPS-2 samples.

Station	Depth (m)	$[H_4SiO_4]$ (µmol L^{-1})	δ^{30}DSi (‰)	[BSi] (µmol L^{-1})	δ^{30B}Si (‰)	
TEW8	10	6,97 ± 0,49		2,58 ± 0,33	1,57 ± *0,03*	*
CTD#47	41	11,44 ± 0,80	2,47 ± *0,03*	2,33 ± 0,31	1,62 ± *0,03*	*
02/11/2011	102	20,62 ± 1,44	2,08 ± *0,03*	0,74 ± 0,12	1,34 ± *0,03*	*
48°S 28.05	152	23,71 ± 1,66	1,89 ± *0,03*	0,47 ± 0,05	1,34 ± *0,04*	*
75°E 00.19	202	26,20 ± 1,83	1,79 ± *0,03*	0,22 ± 0,03	1,38 ± *0,04*	*
	254	32,09 ± 2,25	1,66 ± *0,03*			
	304	37,97 ± 2,66	1,48 ± *0,03*			
	405	53,48 ± 3,74	1,45 ± *0,03*			
	507	57,67 ± 4,04				
	609	66,87 ± 4,68	1,40 ± *0,03*			
	809	66,67 ± 4,67	1,33 ± *0,01*			
	1011	76,07 ± 5,33				
	2812	133,84 ± 9,37	1,07 ± *0,00*			
E3	11	15,42 ± 1,08	2,40 ± *0,11*	1,22 ± 0,03	1,12 ± *0,04*	*
CTD#50&55	42	15,42 ± 1,08	2,29 ± *0,03*	1,54 ± 0,18	1,08 ± *0,06*	*
04/11/2011				1,98 ± 0,19		
48°S 42.07	71	17,91 ± 1,25	2,16 ± *0,04*	1,19 ± 0,14	1,26 ± *0,09*	*
71°E 58.02	102	22,83 ± 1,60	2,15 ± *0,04*	0,81 ± 0,09	1,35 ± *0,04*	*
	125	17,79 ± 1,25		1,83 ± 0,21	1,38 ± *0,06*	*
	153	19,25 ± 1,35	2,06 ± *0,04*	1,33 ± 0,15	1,28 ± *0,02*	*
	203	28,88 ± 2,02	1,92 ± *0,01*	0,42 ± 0,05	1,31 ± *0,06*	*
	225			0,58 ± 0,01	1,45 ± *0,02*	*
	252	40,64 ± 2,84	1,63 ± *0,04*			
	304	49,28 ± 3,45	1,32 ± *0,04*			
	404	69,36 ± 4,86	1,23 ± *0,07*	0,38 ± 0,01	1,51 ± *0,04*	
	505	69,57 ± 4,87	1,36 ± *0,02*			
	606	74,03 ± 5,18	1,24 ± *0,01*	0,46 ± 0,02	1,58 ± *0,06*	
	707	78,88 ± 5,52	1,26 ± *0,03*			
	800	82,52 ± 5,78		0,17 ± 0,02	1,66 ± *0,02*	
	910	82,52 ± 5,78	1,24 ± *0,07*			
	1012	77,88 ± 5,45	1,16 ± *0,03*	0,27 ± 0,01	1,68 ± *0,06*	
	1214	78,85 ± 5,52	1,18 ± *0,20*	0,26 ± 0,01	1,63 ± *0,07*	
	1500			0,22 ± 0,01	1,70 ± *0,04*	
	1908	82,52 ± 5,78	1,06 ± *0,04*			
	2000		1,12 ± *0,03*			

Table B2. (continued) Silicic acid, biogenic silica concentrations and δ^{30}Si of DSi and BSi for all KEOPS-2 samples.

Station	Depth (m)	$[H_4SiO_4]$ (µmol L^{-1})	δ^{30}DSi (‰)	[BSi] (µmol L^{-1})	δ^{30B}Si (‰)	
F-L	11	7,61 ± 0,53	2,79 ± *0,03*	3,00 ± 0,28	1,56 ± *0,18*	*
CTD#63&68	35	8,70 ± 0,61	2,53 ± *0,08*	3,54 ± 0,26	1,60 ± *0,02*	*
07/11/2011	55			1,88 ± 0,16	1,66 ± *0,05*	
48°S 37.27	61	9,95 ± 0,70	2,39 ± *0,02*	2,33 ± 0,80	1,59 ± *0,03*	*
74°E 48.44	80	14,42 ± 1,01	2,12 ± *0,07*	0,51 ± 0,06	1,38 ± *0,03*	*
	101	17,79 ± 1,25	1,97 ± *0,01*	0,34 ± 0,03	1,50 ± *0,12*	**
	126	19,71 ± 1,38	1,97 ± *0,03*	0,23 ± 0,03	1,47 ± *0,03*	*
	151	21,15 ± 1,48	1,66 ± *0,03*	0,24 ± 0,03	1,50 ± *0,04*	*
	202		1,66 ± *0,04*			
	225			0,13 ± 0,01	1,55 ± *0,09*	
	252	31,40 ± 2,20	1,71 ± *0,04*			
	303	37,20 ± 2,60	1,49 ± *0,04*			
	404	46,86 ± 3,28	1,31 ± *0,08*	0,14 ± 0,00	1,68 ± *0,04*	
	506	63,19 ± 4,42	1,24 ± *0,04*			
	607	60,87 ± 4,26	1,28 ± *0,04*	0,14 ± 0,00	1,74 ± *0,03*	
	707	70,39 ± 4,93	1,25 ± *0,03*			
	911	76,46 ± 5,35	1,25 ± *0,05*			
	1013	71,01 ± 4,97	1,26 ± *0,02*			
	1215	72,46 ± 5,07	1,26 ± *0,04*	0,22 ± 0,00	1,84 ± *0,05*	
	1772	101,94 ± 7,14	1,04 ± *0,04*	0,17 ± 0,01	1,86 ± *0,07*	
	2200			0,23 ± 0,00	1,90 ± *0,09*	
	2741	135,36 ± 9,48	1,10 ± *0,01*			
	3000		1,16 ± *0,03*			
E4W	10	11,96 ± 0,84	2,26 ± *0,03*	3,88 ± 0,22	0,93 ± *0,10*	*
CTD#81&87	41	18,91 ± 1,32	2,22 ± *0,03*	3,92 ± 0,57	0,75 ± *0,07*	*
12/11/2011	70	20,90 ± 1,46	2,20 ± *0,03*	1,91 ± 0,41	0,69 ± *0,04*	*
48°S 45.93	94	24,64 ± 1,72	1,87 ± *0,03*	0,43 ± 0,05	0,70 ± *0,03*	*
71°E 25.50	126	24,15 ± 1,69	1,89 ± *0,03*	0,38 ± 0,04	0,82 ± *0,03*	*
	153	24,64 ± 1,72	1,78 ± *0,04*	0,72 ± 0,08	1,14 ± *0,03*	*
	175			0,79 ± 0,00	1,11 ± *0,03*	
	203	36,71 ± 2,57	1,67 ± *0,03*			
	252	45,89 ± 3,21	1,42 ± *0,03*			
	304	49,76 ± 3,48	1,31 ± *0,03*	0,62 ± 0,01	1,48 ± *0,04*	
	406	61,35 ± 4,29	1,28 ± *0,03*			
	507	68,60 ± 4,80				
	607	75,24 ± 5,27	1,22 ± *0,01*	0,63 ± 0,03	1,70 ± *0,08*	
	708	76,46 ± 5,35	1,29 ± *0,03*			
	811	77,67 ± 5,44	1,32 ± *0,10*	0,60 ± 0,06	1,67 ± *0,02*	
	909	76,46 ± 5,35	1,25 ± *0,08*			
	1011	81,31 ± 5,69	1,20 ± *0,03*			
	1214	97,09 ± 6,80	1,01 ± *0,03*			
	1384	101,94 ± 7,14	1,01 ± *0,03*			

Table B2. (continued) Silicic acid, biogenic silica concentrations and $\delta^{30}Si$ of DSi and BSi for all KEOPS-2 samples.

Station	Depth (m)	$[H_4SiO_4]$ (µmol L^{-1})	$\delta^{30}DSi$ (‰)	[BSi] (µmol L^{-1})	$\delta^{30B}Si$ (‰)	
E4E	20	12,44 ± 0,87	2,48 ± *0,03*	2,94 ± 0,05	1,32 ± *0,06*	*
CTD#94&97	51	8,70 ± 0,61	2,57 ± *0,04*	2,43 ± 0,43	1,40 ± *0,04*	*
14/11/2011	93	18,41 ± 1,29	2,25 ± *0,04*	2,31 ± 0,39	1,46 ± *0,06*	*
48°S 42.93	103	20,62 ± 1,44	2,21 ± *0,02*	0,67 ± 0,08	1,35 ± *0,03*	*
72°E 33.76	126	22,68 ± 1,59	2,14 ± *0,03*	0,75 ± 0,09	1,39 ± *0,03*	*
	152	24,74 ± 1,73	1,83 ± *0,03*	0,69 ± 0,08	1,28 ± *0,03*	*
	181	27,81 ± 1,95	1,80 ± *0,04*			
	253	49,73 ± 3,48	1,53 ± *0,03*			
	303	54,01 ± 3,78	1,27 ± *0,02*			
	404	64,71 ± 4,53	1,35 ± *0,01*			
	505	75,72 ± 5,30	1,21 ± *0,02*			
	606	74,03 ± 5,18	1,29 ± *0,04*			
	706	78,88 ± 5,52	1,24 ± *0,03*			
	912	77,67 ± 5,44	1,20 ± *0,05*			
	1012	80,10 ± 5,61	1,18 ± *0,10*			
	1265	83,74 ± 5,86	1,16 ± *0,04*			
	1518	89,81 ± 6,29	1,11 ± *0,04*			
	1827	95,87 ± 6,71	1,09 ± *0,03*			
	2027	89,81 ± 6,29	0,97 ± *0,03*			
	2212	91,41 ± 6,40	1,21 ± *0,06*			
A3-2	11	19,40 ± 1,36	2,25	3,83 ± 0,49	1,01 ± 0,03	*
CTD#107	40	19,40 ± 1,36	2,10	4,06 ± 0,42	0,93 ± 0,02	**
16/11/2011	81	20,40 ± 1,43	2,07	3,55 ± 0,36	0,92 ± 0,07	*
50°S 37.46	126	19,71 ± 1,38	2,10	4,33 ± 0,83	1,00 ± 0,05	*
72°E 03.34	150	19,71 ± 1,38	1,92	3,58 ± 0,26	1,03 ± 0,05	**
	176	24,60 ± 1,72	1,89	2,04 ± 0,31	1,01 ± 0,09	*
	202	31,90 ± 2,23	1,69	0,85 ± 0,06	1,02 ± 0,08	*
	270	40,64 ± 2,84	1,62	0,72 ± 0,14	1,34 ± 0,07	
	303	45,45 ± 3,18	1,51 0,03			
	350			0,82 ± 0,09	1,49 ± 0,09	
	405	63,10 ± 4,42	1,45 0,03			
	460			3,09 ± 0,02	1,72 ± 0,05	
	513	80,21 ± 5,61	1,34 0,03			
E5	11	12,94 ± 0,91	2,44 ± *0,10*	1,75 ± 0,19	1,26 ± *0,03*	*
CTD#113&114	41	12,94 ± 0,91	2,58 ± *0,05*	3,44 ± 1,46	1,39 ± *0,00*	*
18/11/2011	55			1,64 ± 0,04		
48°S 24.69	82	12,94 ± 0,91	2,36 ± *0,04*	2,44 ± 0,07	1,46 ± *0,08*	*
71°E 53.99	102	21,39 ± 1,50		0,95 ± 0,11	1,42 ± *0,03*	**
	126	18,01 ± 1,26		0,73 ± 0,08	1,44 ± *0,03*	*
	152	23,12 ± 1,62		0,66 ± 0,08	1,37 ± *0,03*	*
	202	22,75 ± 1,59	2,12 ± *0,04*			
	220			1,01 ± 0,04	1,40 ± *0,05*	
	252	38,65 ± 2,71	1,66 ± *0,03*			
	302	50,24 ± 3,52	1,49 ± *0,04*			
	404	62,32 ± 4,36	1,37 ± *0,04*	2,30 ± 0,08	1,43 ± *0,01*	
	507	69,08 ± 4,84	1,36 ± *0,04*			
	606	71,50 ± 5,00	1,41 ± *0,04*			
	707	84,39 ± 5,91	1,20 ± *0,04*			
	800			0,35 ± 0,01	1,62 ± *0,00*	
	911	90,17 ± 6,31	1,20 ± *0,05*			
	1011	88,44 ± 6,19	1,23 ± *0,04*	0,25 ± 0,02	1,66 ± *0,08*	
	1214	88,24 ± 6,18	1,15 ± *0,03*			
	1500			0,17 ± 0,02	1,69 ± *0,09*	
	1922	112,72 ± 7,89	1,11 ± *0,04*			

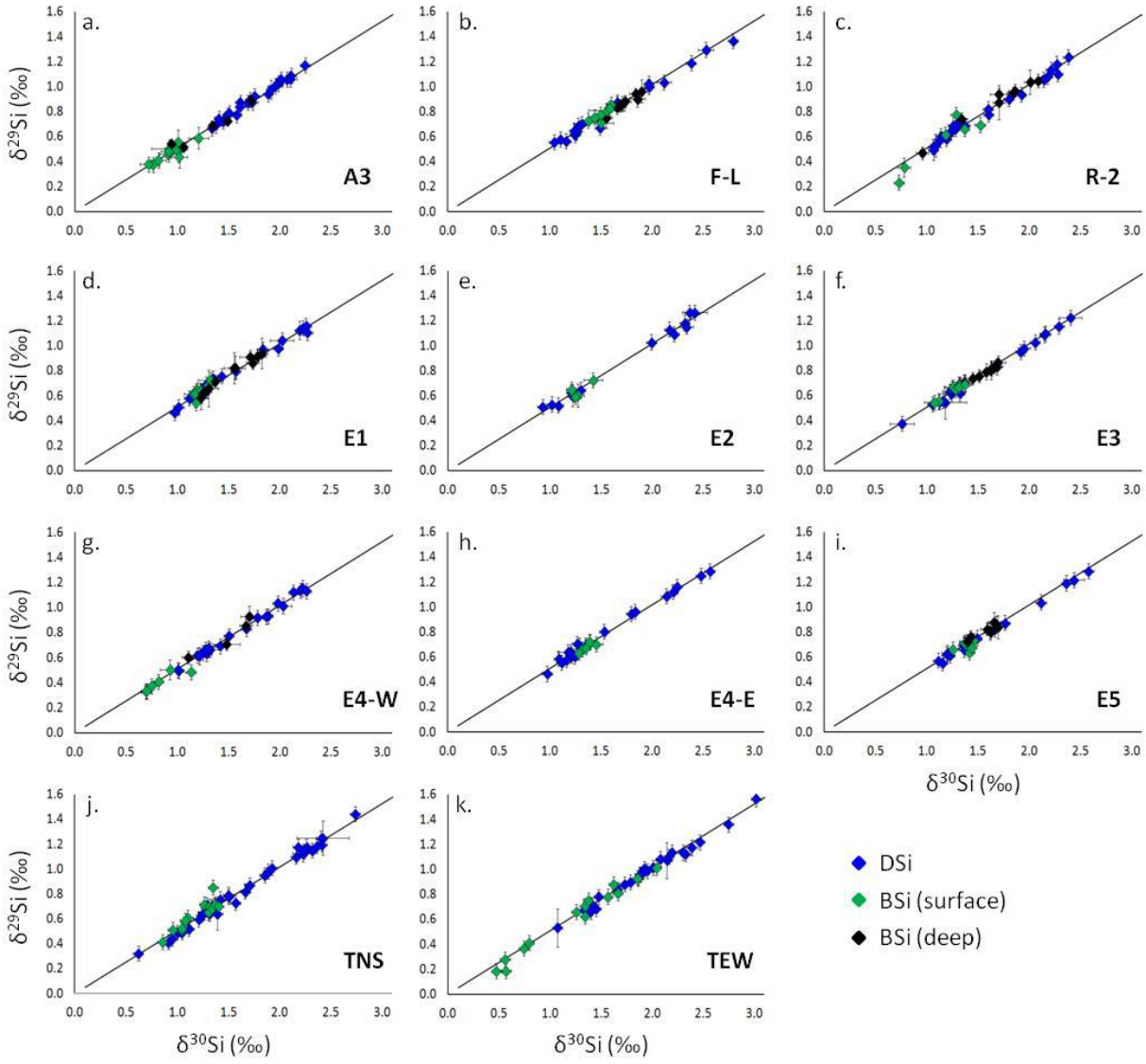

Figure B2. $\delta^{29}Si$ versus $\delta^{30}Si$ of samples measured by Neptune^{+} MC-ICP-MS in dry plasma mode. DSi samples are in blue, surface BSi samples (collected using nuclepore membrane filtration) are in green, and deep BSi samples (collected with in situ pumps) are in black. Error bars represent the average standard deviation of duplicates (±1 sd) and the line shows the theoretical kinetic fractionation law between ^{29}Si and ^{30}Si (y = 0.51x, as calculated following Young et al., 2002).

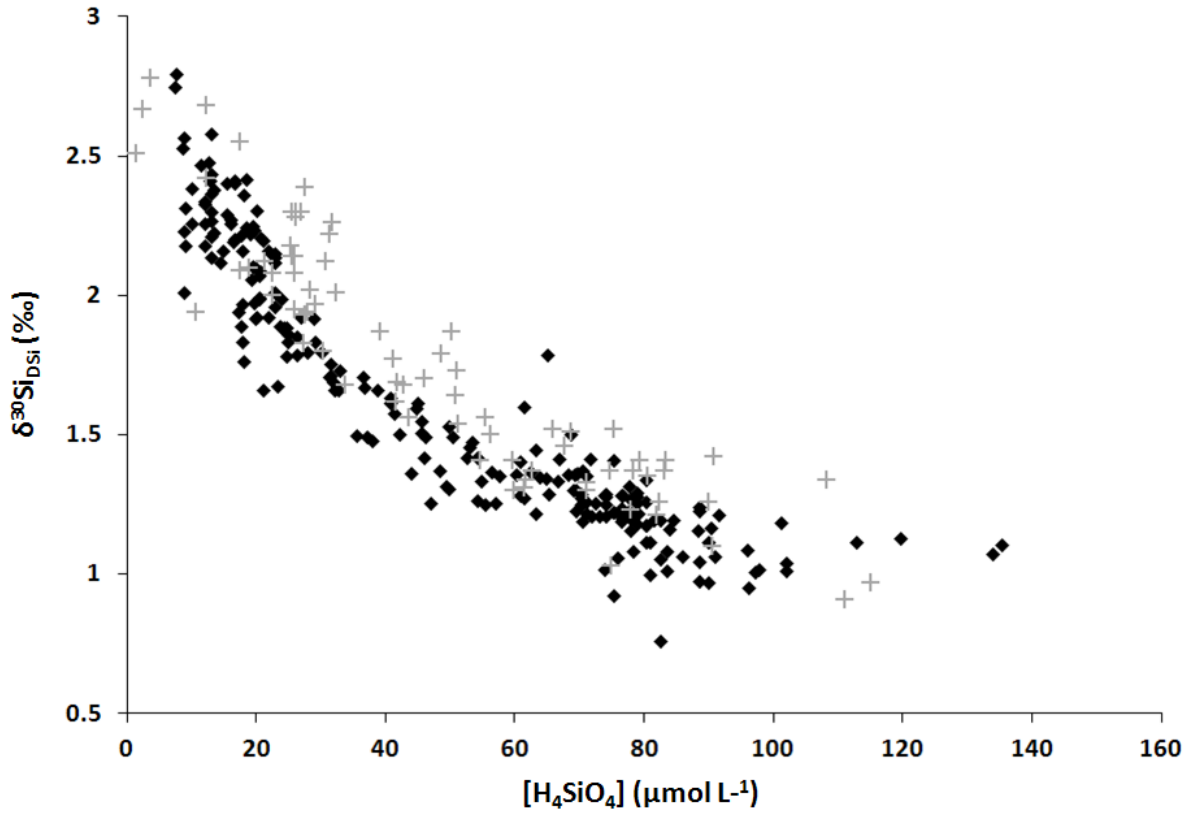

Figure B3. All KEOPS-2 (black diamonds) and KEOPS-1 (grey crosses) silicic acid $\delta^{30}Si$ plotted against the silicic acid concentration

SUPPLEMENTARY METHOD C

Correction of $\delta^{30}Si$ values from lithogenic contamination

Since the alkaline digestion also dissolves LSi, and because it has a silicon isotopic signature significantly different from BSi (-2.3 to +0.1 ‰ compared to -0.3 to +2.6 ‰ for living diatoms; Opfergelt and Delmelle, 2012), it is essential to estimate accurately the amount of LSi that contributes to the Si in each solution used for isotopic measurements. Using the 2-step digestion adapted from Ragueneau et al. (2005), we found a negligible proportion of LSi for all samples collected by the 54°S and 61°S moorings (< 1.5 % and 1 % of BSi in the first leaching respectively). These values are consistent with those estimated by Bray et al. (unpublished results) from analysis of total lithogenic SiO_2 in samples collected in parallel with those for silicon isotopic determination. However, since surface production in the SAZ is not dominated by diatoms, opal fluxes measured in the traps located at 47°S were much lower. There, the relative proportion of LSi dissolved during the 1st leaching (on average 3.54 %, 4.9 % and 6.38 % at 1000 m, 2000 m and 3800 m respectively) is theoretically sufficient to bias significantly the final $\delta^{30}Si$ signature of biogenic silica. Indeed, for these LSi inputs, and assuming an extreme light LSi end-member value of -2.3 ‰ for $\delta^{30}Si_{LSi}$, we calculated a maximum interference in the isotopic signals introduced by the lithogenic phase ranging from -0.08 to -0.15 ‰. Such a contribution cannot be neglected since it is higher than our overall precision for $\delta^{30}Si$ determination (0.05 ± 0.03 ‰). In some samples collected in the SAZ there was enough Si in the 2nd digestion to measure the $\delta^{30}Si$. Thus we propose a method using this second $\delta^{30}Si$ ($\delta^{30}Si_{L2}$) to correct the lithogenic interference on the $\delta^{30}Si$ signature of BSi in the 1st digestion ($\delta^{30}Si_{L1}$). Two basic assumptions have to be made to apply such a correction:

(1) All the BSi has been digested during the first digestion, so the second digestion is not biased by any interference.

(2) Dissolution of LSi does not fractionate, so the $\delta^{30}Si_{L2}$ is similar to the $\delta^{30}Si$ of lithogenic silica that has been dissolved during the first digestion.

In our case, the relatively high $\delta^{30}Si_{L2}$ (e.g. +0.69 ‰ on average at 1000m, n = 6) could indicate an experimental artifact due to incomplete dissolution of biogenic silica during the first digestion, so the first assumption may not be valid. However, by plotting the $\delta^{30}Si_{L2}$ vs. Si:Al ratio measured in the second digestion, it is possible to estimate the silicon isotopic signature of lithogenic silica. *Figure C1.* shows that, as expected in the case of a BSi contamination in the second digestion, samples with Si:Al

ratios close to the crustal ratio have low $\delta^{30}Si_{L2}$ whereas samples with higher Si:Al ratios have $\delta^{30}Si_{L2}$ closer to that of diatoms. Using this positive relationship (R^2 = 0.63, p value < 0.01) and the mean Si:Al ratio of continental crust (3.92; Wedepohl, 1995), we can estimate a $\delta^{30}Si$ for "pure" LSi dissolved in the second digestion ($\delta^{30}Si_{LSi(2)}$) of -0.38 ± 0.27 ‰.

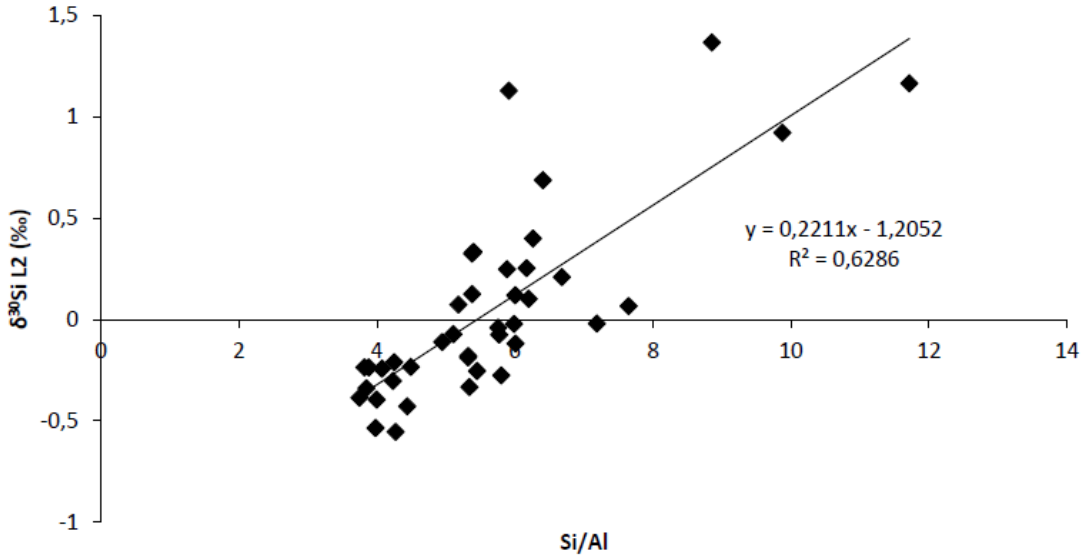

Figure C1 Correlations between the silicon isotopic signature of the 2nd digestion ($\delta^{30}Si_{L2}$) and Si:Al ratio of the solution in the Sub-Antarctic Zone moorings.

The second assumption may be also violated since the occurrence of fractionation during dissolution of LSi is still uncertain. Concerning BSi, Demarest et al. (2009) have shown that dissolution of fresh diatoms and sediment trap siliceous material in seawater release preferentially light silicon isotope with a fractionation factor of ε = -0.55 ‰. However, both in situ and experimental studies suggest that sedimentary opal is not affected by a silicon isotope fractionation during dissolution (Egan et al., 2012; Wetzel et al., 2014). According to Wetzel et al. (2014) this major difference may be linked to the opal's age and depend principally on its chemical properties such as different aluminium content. Lithogenic and biogenic silica display different solubility with BSi being more easily dissolvable because of its amorphous structure while lithogenic silica is more crystalline (Tréguer & De la Rocha, 2013). The effects of Si isotopic fractionation during dissolution of to these materials might be different and have not been examined so far for LSi. Therefore we use the $^{30}\varepsilon$ of -0.55 ‰ estimated by Demarest et al. (2009) to calculate the $\delta^{30}Si$ of "pure" lithogenic silica dissolved in the first digestion ($\delta^{30}Si_{LSi(1)}$). We then consider that dissolution of LSi in our digestion occurred in a closed-system and could be

explained by a Rayleigh fractionation law (*equations 3.2.* to *3.4.*). Indeed, the dissolved silicon produced during the 40' digestion is unlikely to interact significantly with the substrate and there was no new inputs of LSi and BSi.

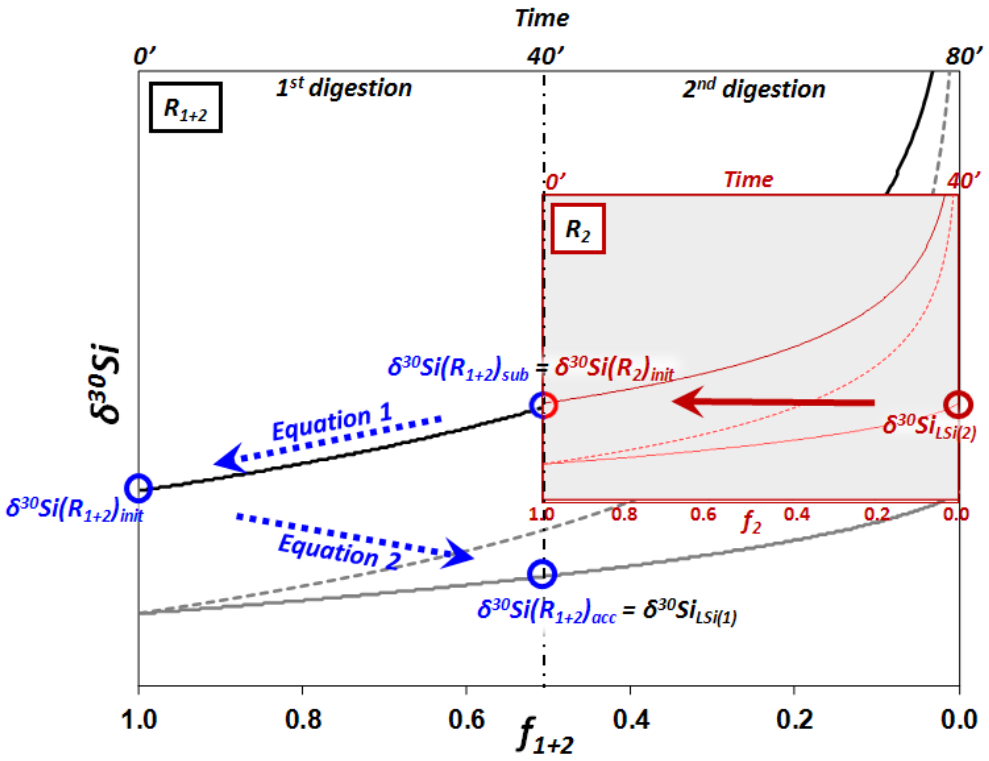

Figure C2. Scheme view of the calculation of the silicon isotopic signature of lithogenic silica dissolved in the 1st digestion ($\delta^{30}Si_{LSi(1)}$). R_{1+2} and R_2 are two different Rayleigh fractionation models describing the dynamic of silicon isotopes in lithogenic silica (LSi) during the two digestions (in black) and during the 2nd one respectively (in red). Thick lines represent the evolution of $\delta^{30}Si$ of the remaining particulate lithogenic pool, thin lines are the evolution of $\delta^{30}Si$ of accumulated lithogenic dissolved product and dashed lines the instantaneous lithogenic dissolved product. *f* is the fraction of LSi remaining in the tube. The $\delta^{30}Si$ measured in the 2nd digestion corresponds to the initial $\delta^{30}Si$ of LSi in this 2nd digestion ($\delta^{30}Si(R_2)_{init}$) which is also the LSi that remain after the 1st digestion ($\delta^{30}Si(R_{1+2})_{sub}$). Using Rayleigh distillation equations, we can calculate the initial $\delta^{30}Si$ of LSi ($\delta^{30}Si(R_{1+2})_{init}$) and the $\delta^{30}Si$ of dissolved lithogenic product that accumulate at the end of the 1st digestion ($\delta^{30}Si_{LSi(1)}$), see text for details.

In our case, each digestion could be described by one distinct closed-system (R_1 and R_2 for digestion 1 and 2 respectively, see *Fig. C2*) and the combination of these 2 digestions represents another Rayleigh system (R_{1+2}). The $\delta^{30}Si_{LSi(2)}$ calculated previously (-0.38 ± 0.27 ‰) is the $\delta^{30}Si$ of the accumulated product in R_2 and is similar to the initial $\delta^{30}Si$ of the source ($\delta^{30}Si(R_2)_{init}$) since, at the end of the digestion, $f_2 = 1$ (*equation 3.3.*). In the R_{1+2} closed-system, $\delta^{30}Si(R_2)_{init}$ is the $\delta^{30}Si$ of the residual substrate after the 1st digestion ($\delta^{30}Si(R_{1+2})_{res1}$). Note that here, f_{1+2} ranged from 0.35 to 0.51 indicating that approximately half of the LSi considered in the R_{1+2} model has been dissolved during the 1st

digestion. Using this $\delta^{30}Si(R_{1+2})_{res1}$ and *equation 3.2.*, we calculated the $\delta^{30}Si$ of the source ($\delta^{30}Si(R_{1+2})_{init}$) and then the $\delta^{30}Si$ of the product that was accumulated at the end of the 1st digestion ($\delta^{30}Si(R_{1+2})_{acc}$), i.e. when f_{1+2} in R_{1+2} model corresponds to the fraction of LSi remaining after the 1st digestion (*equation 3.3.*). This $\delta^{30}Si(R_{1+2})_{acc}$ is the $\delta^{30}Si$ value of the LSi that was dissolved in the 1st digestion taking into account potential effects of fractionation during its dissolution. Then, we used this value to correct the silicon isotopic composition estimated in the 1st digestion as follows:

$$\delta^{30}Si_{(BSi)} = \delta^{30}Si_{(L1)} - \frac{(\%LSi \times \delta^{30}Si_{LSi(1)})}{1-\%LSi} \quad \text{(C.1.)}$$

with $\delta^{30}Si_{(L1)}$ and $\delta^{30}Si_{LSi(1),}$ the silicon isotopic composition measured in the 1st digestion and estimated for lithogenic silica respectively; and %LSi the relative proportion of LSi dissolved during the 1st leaching. By applying this correction, we are confident that our $\delta^{30}Si$ values correspond to the biogenic SiO_2 component only.

Corrected and uncorrected $\delta^{30}Si$ are provided in *Figure C3*. On average, the correction yields a difference of +0.09, +0.13 and +0.18 ‰ for the 47°S sediment traps at 1000, 2000 and 3800m respectively.

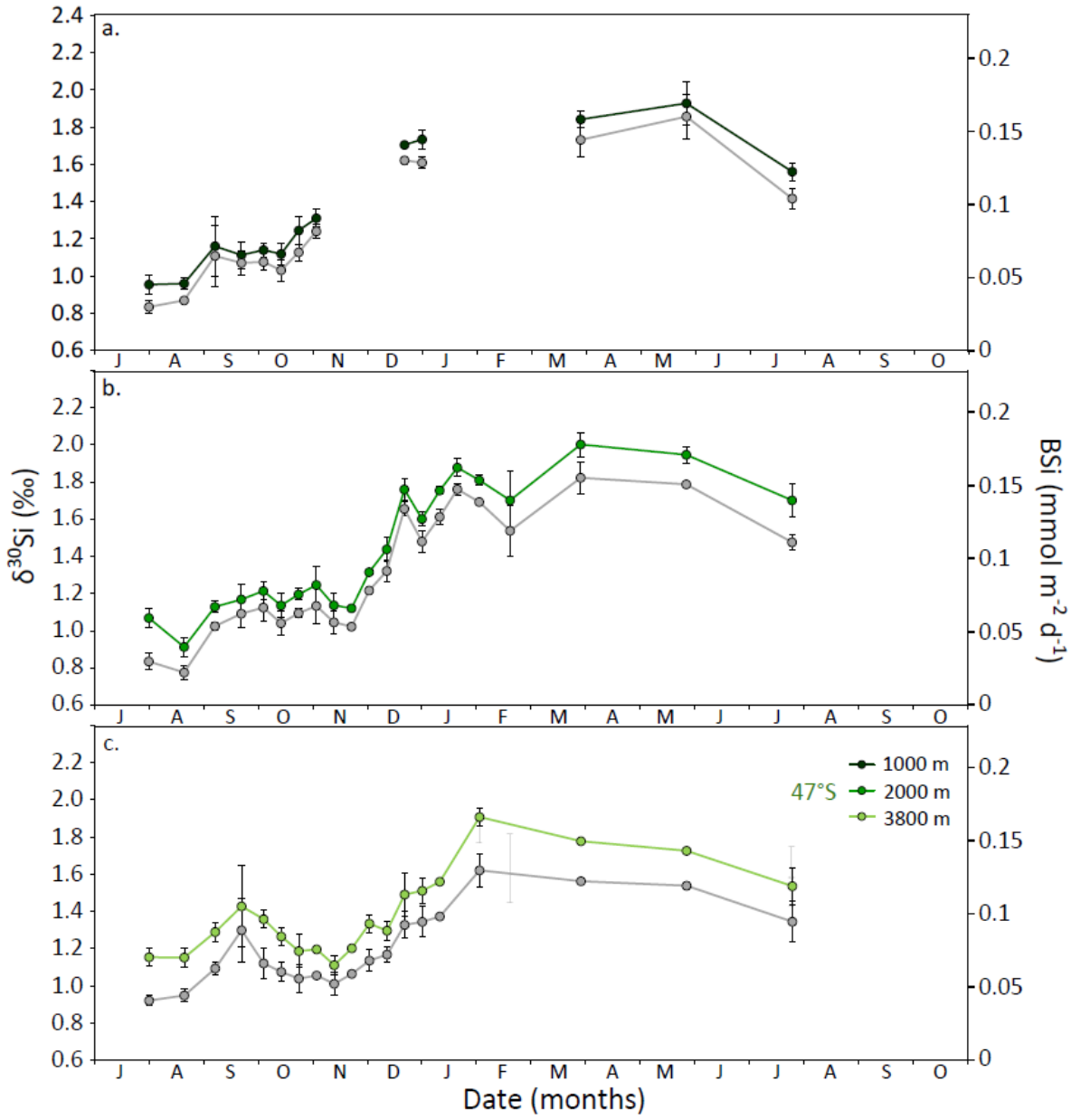

Figure C3. Seasonal variations of silicon isotopic composition (δ^{30}Si in ‰) of settling biogenic silica in the Sub-Antarctic Zone without (in grey) and with (in green) correction for potential lithogenic silica contamination in the 1000 m (a.), 2000 m (b.) and 3800 m (c.) sediment traps.

Supplementary references

Demarest M.S., M.A. Brzezinski, C.P. Beucher (2009), Fractionation of silicon isotopes during biogenic silica dissolution, Geochimica et Cosmochimica Acta, 73, 5572-5583, doi:10.1016/j.gca.2009.06.019.

Egan K.E., R.E.M. Rickaby, M.J. Leng, K.R. Hendry, M. Hermoso, H.J. Sloane, H. Bostock, A.N. Halliday (2012), Diatom silicon isotopes as a proxy for silicic acid utilisation: A Southern Ocean core top calibration, Geochimica et Cosmochimica Acta, 96, 174-192, doi:10.1016/j.gca.2012.08.002.

Opfergelt S., P. Delmelle (2012), silicon isotopes and continental weathering processes: Assessing controls on Si transfer to the ocean, Comptes Rendus Geoscience, 344, 723-738, doi:10.1016/j.crte.2012.09.006.

Ragueneau O., N. Savoye, Y. Del Amo, J. Cotten, B. Tardiveau, A. Leynaert (2005), A new method for the measurement of biogenic silica in suspended matter of coastal waters: using Si:Al ratios to correct for the mineral interference, Continental Shelf Research, 25, 697-710.

Tréguer P.J., C.L. De La Rocha (2013), The World Ocean Silica Cycle, Annual Review of Marine Science, 5, 477-501.

Wedepohl H. (1995), The composition of the continental crust, Geochimica et Cosmochimica Acta, 59(7), 1217-1232.

Wetzel F., G.F. de Souza, B.C. Reynolds (2014), What controls silicon isotope fractionation during dissolution of diatom opal?, Geochimica et Cosmochimica Acta, 131, 128-137, doi:10.1016/j.gca.2014.01.028.

ANNEXES C

Table C1. Mass and BSi flux, and $\delta^{30}Si$ (uncorrected and corrected) for all sediment trap samples

	Cup #	Mid-point Date	Duration (d)	Mass flux (mg m^{-2} d^{-1})	Bsi flux (µmol m^{-2} d^{-1})	$\delta^{30}Si$ (‰)	Corrected $\delta^{30}Si$ (‰)
	1	Nov. 30, 2001	8	47,75	548,73	**1,499 ± *0,04***	
	2	Dec. 08, 2001	8	77,89	1025,64	**1,123 ± *0,03***	
	3	Dec. 16, 2001	8	325,70	4092,22	**0,901 ± *0,01***	
	4	Dec. 24, 2001	8	508,62	6888,87	**0,919 ± *0,00***	
	5	Jan. 01, 2002	8	1151,14	19399,45	**0,894 ± *0,04***	
	6	Jan. 09, 2002	8	1068,62	13822,24	**0,91 ± *0,05***	
Mooring AZ	7	Jan. 17, 2002	8	656,16	9077,99	**1,038 ± *0,02***	
lat 60° 44.43 S	8	Jan. 25, 2002	8	702,20	9533,48	**1,039 ± *0,04***	
long 139° 53.97 E	9	Feb. 02, 2002	8	665,81	9581,76	**1,135 ± *0,03***	
2000 m	10	Feb. 10, 2002	8	595,49	9643,17	**1,405 ± *0,01***	
	11	Feb. 18, 2002	8	534,06	7828,84	**1,366 ± *0,04***	
	12	Feb. 26, 2002	8	524,35	8037,91	**1,588 ± *0,02***	
	13	Mar. 06, 2002	8	586,02	8186,67	**1,879 ± *0,06***	
	14	Mar. 14, 2002	8	285,35	3776,18	**1,434 ± *0,05***	
	15	Mar. 22, 2002	8	289,89	4222,66	**1,398 ± *0,06***	
	16	Mar. 30, 2002	8	262,60	6426,24	**1,4 ± *0,04***	
	17	Apr. 08, 2002	10	264,45	4079,95	**1,485 ± *0,05***	
	18	May 08, 2002	50	129,74	2598,38	**1,65 ± *0,06***	
	19	June 29, 2002	54	65,38	1022,38	**1,671 ± *0,06***	
	20	Aug. 22, 2002	55	55,64	753,68	**1,686 ± *0,09***	
	21	Sept. 29, 2002	20	42,37	658,59	**1,699 ± *0,08***	
	1	Nov. 30, 2001	8	38,44	507,74	**1,784 ± *0,05***	
	2	Dec. 08, 2001	8	30,87	336,03	**1,608 ± *0,04***	
	3	Dec. 16, 2001	8	99,22	1177,68	**1,31 ± *0,01***	
	4	Dec. 24, 2001	8	231,16	2722,97	**1,047 ± *0,06***	
	5	Jan. 01, 2002	8	872,52	11799,52	**0,961 ± *0,06***	
Mooring AZ	6	Jan. 09, 2002	8	1157,16	13881,88	**0,957 ± *0,06***	
lat 60° 44.43 S	7	Jan. 17, 2002	8	828,23	15215,19	**1,046 ± *0,04***	
long 139° 53.97 E	8	Jan. 25, 2002	8	489,81	7504,09	**1,106 ± *0,04***	
3700 m	9	Feb. 02, 2002	8	490,59	7975,33	**1,172 ± *0,02***	
	10	Feb. 10, 2002	8	419,02	8550,12	**1,283 ± *0,02***	
	11	Feb. 18, 2002	8	583,74	9498,12	**1,479 ± *0,03***	
	12	Feb. 26, 2002	8	580,88	8411,15	**1,527 ± *0,03***	
	13	Mar. 06, 2002	8	849,49	14260,79	**1,917 ± *0,07***	
	14	Mar. 14, 2002	8	368,64	5500,59	**1,585 ± *0,08***	
	15	Mar. 22, 2002	8	218,21	5408,66	**1,403 ± *0,03***	
	16	Mar. 30, 2002	8	257,53	3749,60	**1,252 ± *0,08***	
	17	Apr. 08, 2002	10	257,11	4361,15	**1,521 ± *0,07***	
	18	May 08, 2002	50	117,74	2020,77	**1,822 ± *0,02***	

***Table C1.* (continued)** Mass and BSi flux, and $\delta^{30}Si$ (uncorrected and corrected) for all sediment trap samples

	Cup #	Mid-point Date	Duration (d)	Mass flux (mg m^{-2} d^{-1})	Bsi flux (µmol m^{-2} d^{-1})	$\delta^{30}Si$ (‰)	Corrected $\delta^{30}Si$ (‰)
	1	July 31, 1999	20	45,93	896,98	**2,054 ± *0,03***	
	2	Aug. 20, 1999	20	71,78	1196,59	**2,058 ± *0,05***	
	3	Sept. 06, 1999	15	81,43	1508,70	**2,085 ± *0,04***	
	4	Sept. 21, 1999	15	25,13	330,61	**2,005 ± *0,08***	
	5	Oct. 04, 1999	10	44,52	821,37	**1,827 ± *0,03***	
	6	Oct. 14, 1999	10	101,12	1878,13	**1,596 ± *0,07***	
Mooring PFZ	7	Oct. 24, 1999	10	58,17	922,75	**1,242 ± *0,07***	
lat 53° 44.84 S	8	Nov. 03, 1999	10	106,27	1233,59	**1,357 ± *0,03***	
long 141° 45.49 E	9	Nov. 13, 1999	10	121,90	1637,35	**1,273 ± *0,04***	
800 m	10	Nov. 23, 1999	10	294,39	3783,70	**1,144 ± *0,04***	
	11	Dec. 03, 1999	10	514,81	5457,26	**1,181 ± *0,03***	
	12	Dec. 13, 1999	10	724,41	8223,51	**1,194 ± *0,09***	
	13	Dec. 23, 1999	10	660,58	9810,51	**1,297 ± *0,04***	
	14	Jan. 02, 2000	10	510,96	6785,33	**1,39 ± *0,04***	
	15	Jan. 12, 2000	10	338,73	4048,45	**1,543 ± *0,04***	
	17	Feb. 03, 2000	15	104,37	596,06	**1,714 ± *0,04***	
	18	Feb. 21, 2000	20	193,93	2381,65	**2,039 ± *0,04***	
	19	Mar. 01, 2000	60	131,98	1639,98	**2,153 ± *0,07***	
	20	May 31, 2000	60	50,14	681,62	**2,1 ± *0,04***	
	21	July 30, 2000	60	36,86	515,67	**2,006 ± *0,05***	
	1	July 31, 1999	20	102,10	1143,50	**2,124 ± *0,02***	
	2	Aug. 20, 1999	20	59,60	1151,80	**2,111 ± *0,04***	
	3	Sept. 06, 1999	15	78,47	1749,74	**2,133 ± *0,03***	
	4	Sept. 21, 1999	15	51,00	1052,78	**2,156 ± *0,03***	
	6	Oct. 14, 1999	10	56,89	948,38	**2,015 ± *0,02***	
Mooring PFZ	7	Oct. 24, 1999	10	44,49	717,70	**1,846 ± *0,05***	
lat 53° 44.84 S	8	Nov. 03, 1999	10	28,42	451,42	**1,605 ± *0,04***	
long 141° 45.49 E	9	Nov. 13, 1999	10	16,53	225,15	**1,432 ± *0,05***	
1500 m	10	Nov. 23, 1999	10	43,97	495,39	**1,233 ± *0,06***	
	11	Dec. 03, 1999	10	63,88	806,06	**1,149 ± *0,04***	
	12	Dec. 13, 1999	10	174,73	2441,53	**1,241 ± *0,03***	
	13	Dec. 23, 1999	10	524,60	7596,19	**1,268 ± *0,08***	
	14	Jan. 02, 2000	10	1038,53	14047,39	**1,314 ± *0,11***	
	15	Jan. 12, 2000	10	773,06	11892,85	**1,327 ± *0,08***	
	16	Jan. 22, 2000	10	269,74	4919,70	**1,497 ± *0,13***	
	17	Feb. 03, 2000	15	40,94	496,17	**1,715 ± *0,06***	
	18	Feb. 21, 2000	20	12,18	157,78	**1,895 ± *0,03***	
	20	May 31, 2000	60	7,06	144,63	**1,849 ± *0,05***	

Table C1. **(continued)** Mass and BSi flux, and $\delta^{30}Si$ (uncorrected and corrected) for all sediment trap samples

	Cup #	Mid-point Date	Duration (d)	Mass flux (mg m^{-2} d^{-1})	Bsi flux (µmol m^{-2} d^{-1})	$\delta^{30}Si$ (‰)	Corrected $\delta^{30}Si$ (‰)
	1	July 31, 1999	20	19,65	16,50	0,83 ± *0,03*	**0,95 ± *0,05***
	2	Aug. 20, 1999	20	27,08	37,81	0,87 ± *0,01*	**0,96 ± *0,03***
	3	Sept. 06, 1999	15	45,86	80,35	1,11 ± *0,17*	**1,16 ± *0,16***
	4	Sept. 21, 1999	15	57,54	81,30	1,07 ± *0,06*	**1,11 ± *0,07***
Mooring SAZ	5	Oct. 04, 1999	10	66,52	85,10	1,08 ± *0,05*	**1,14 ± *0,04***
lat 46° 45.55 S	6	Oct. 14, 1999	10	65,88	69,38	1,03 ± *0,06*	**1,12 ± *0,06***
long 142° 4.22 E	7	Oct. 24, 1999	10	89,79	73,74	1,13 ± *0,05*	**1,25 ± *0,08***
1000 m	8	Nov. 03, 1999	10	73,90	61,35	1,24 ± *0,04*	**1,31 ± *0,05***
	13	Dec. 23, 1999	10	32,57	42,74	1,63 ± *0,02*	**1,71 ± *0,01***
	14	Jan. 02, 2000	10	38,53	46,59	1,62 ± *0,03*	**1,74 ± *0,05***
	19	Mar. 01, 2000	60	39,60	57,50	1,74 ± *0,09*	**1,85 ± *0,04***
	20	May 31, 2000	60	46,95	86,94	1,87 ± *0,12*	**1,94 ± *0,12***
	21	July 30, 2000	60	12,98	11,53	1,42 ± *0,06*	**1,57 ± *0,05***
	1	July 31, 1999	20	18,76	17,74	0,83 ± *0,05*	**1,07 ± *0,05***
	2	Aug. 20, 1999	20	35,05	41,53	0,77 ± *0,04*	**0,91 ± *0,05***
	3	Sept. 06, 1999	15	40,19	59,05	1,03 ± *0,02*	**1,13 ± *0,03***
	4	Sept. 21, 1999	15	49,85	84,47	1,09 ± *0,07*	**1,17 ± *0,08***
	5	Oct. 04, 1999	10	46,52	64,46	1,13 ± *0,08*	**1,22 ± *0,05***
	6	Oct. 14, 1999	10	38,05	46,61	1,04 ± *0,06*	**1,14 ± *0,07***
	7	Oct. 24, 1999	10	53,61	70,06	1,10 ± *0,02*	**1,20 ± *0,03***
	8	Nov. 03, 1999	10	72,50	85,02	1,14 ± *0,10*	**1,25 ± *0,10***
Mooring SAZ	9	Nov. 13, 1999	10	64,42	83,32	1,05 ± *0,06*	**1,14 ± *0,07***
lat 46° 45.55 S	10	Nov. 23, 1999	10	60,57	76,82	1,02 ± *0,02*	**1,12 ± *0,01***
long 142° 4.22 E	11	Dec. 03, 1999	10	46,42	57,92	1,22 ± *0,02*	**1,32 ± *0,02***
2000 m	12	Dec. 13, 1999	10	47,62	65,57	1,33 ± *0,06*	**1,44 ± *0,07***
	13	Dec. 23, 1999	10	54,67	82,22	1,67 ± *0,04*	**1,77 ± *0,06***
	14	Jan. 02, 2000	10	51,32	90,97	1,49 ± *0,06*	**1,61 ± *0,04***
	15	Jan. 12, 2000	10	59,77	108,83	1,62 ± *0,04*	**1,77 ± *0,02***
	16	Jan. 22, 2000	10	64,49	149,85	1,77 ± *0,03*	**1,89 ± *0,05***
	17	Feb. 03, 2000	15	45,61	94,08	1,70 ± *0,01*	**1,82 ± *0,03***
	18	Feb. 21, 2000	20	24,82	38,03	1,54 ± *0,14*	**1,71 ± *0,16***
	19	Mar. 01, 2000	60	58,32	87,62	1,83 ± *0,09*	**2,02 ± *0,07***
	20	May 31, 2000	60	44,24	66,63	1,80 ± *0,02*	**1,96 ± *0,04***
	21	July 30, 2000	60	52,42	55,19	1,48 ± *0,04*	**1,72 ± *0,09***
	1	July 31, 1999	20	17,94	16,71	0,92 ± *0,03*	**1,16 ± *0,05***
	2	Aug. 20, 1999	20	29,49	28,81	0,95 ± *0,03*	**1,16 ± *0,05***
	3	Sept. 06, 1999	15	35,76	34,54	1,10 ± *0,04*	**1,30 ± *0,05***
	4	Sept. 21, 1999	15	47,83	68,07	1,31 ± *0,17*	**1,44 ± *0,22***
	5	Oct. 04, 1999	10	47,46	37,76	1,12 ± *0,09*	**1,37 ± *0,05***
	6	Oct. 14, 1999	10	28,97	56,01	1,08 ± *0,05*	**1,27 ± *0,05***
Mooring SAZ	7	Oct. 24, 1999	10	41,32	52,33	1,04 ± *0,08*	**1,19 ± *0,09***
lat 46° 45.55 S	8	Nov. 03, 1999	10	45,46	51,75	1,06 ± *0,00*	**1,20 ± *0,02***
long 142° 4.22 E	9	Nov. 13, 1999	10	37,37	43,92	1,01 ± *0,06*	**1,11 ± *0,05***
3800 m	10	Nov. 23, 1999	10	42,64	48,67	1,07 ± *0,00*	**1,21 ± *0,01***
	11	Dec. 03, 1999	10	21,53	23,99	1,14 ± *0,06*	**1,34 ± *0,05***
	12	Dec. 13, 1999	10	21,74	27,42	1,17 ± *0,04*	**1,30 ± *0,05***
	13	Dec. 23, 1999	10	36,42	54,04	1,33 ± *0,07*	**1,50 ± *0,12***
	14	Jan. 02, 2000	10	70,17	99,09	1,35 ± *0,08*	**1,52 ± *0,07***
	15	Jan. 12, 2000	10	40,22	48,54	1,38 ± *0,00*	**1,57 ± *0,02***
	17	Feb. 03, 2000	15	30,91	39,74	1,63 ± *0,09*	**1,92 ± *0,05***
	19	Mar. 01, 2000	60	57,80	81,38	1,57 ± *0,00*	**1,79 ± *0,01***
	20	May 31, 2000	60	47,62	65,57	1,55 ± *0,02*	**1,74 ± *0,01***
	21	July 30, 2000	60	23,85	30,63	1,35 ± *0,11*	**1,55 ± *0,10***

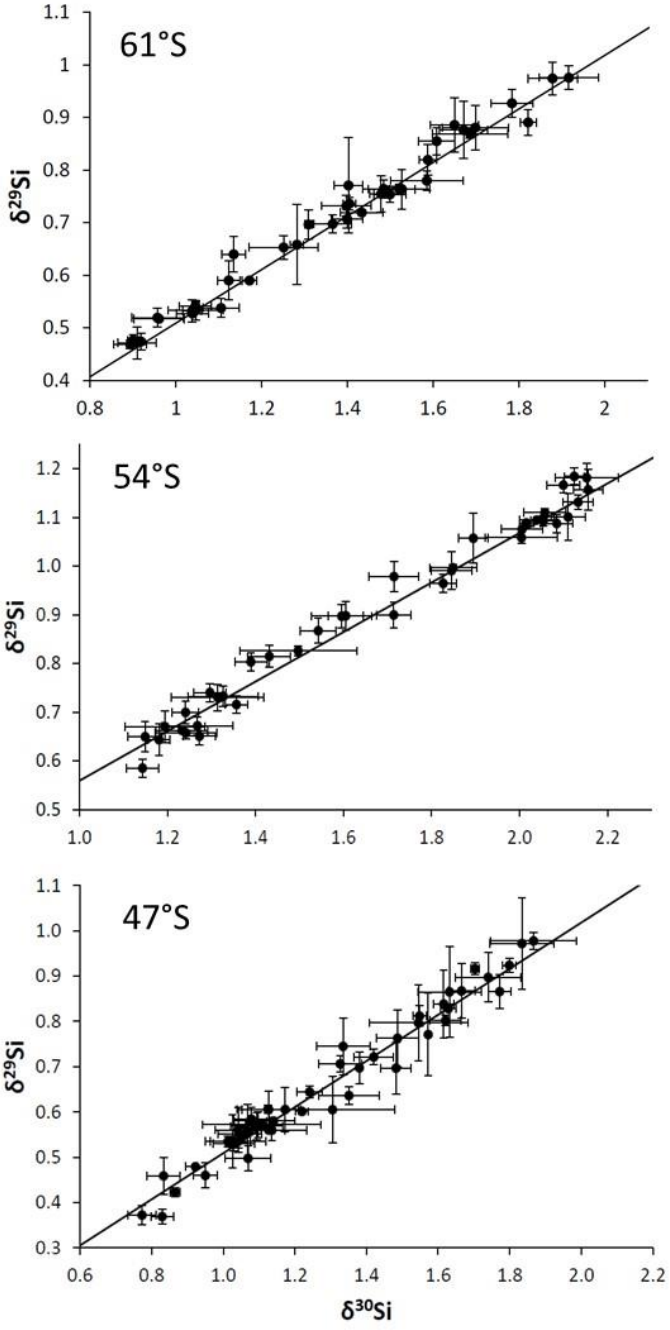

Figure C4. $\delta^{29}Si$ versus $\delta^{30}Si$ of samples measured by Neptune^{+} MC-ICP-MS in dry plasma mode in the Antarctic Zone (a.), The Polar Front Zone (b.) and the Sub-Antarctic Zone (c.). Error bars represent the average standard deviation of duplicates (±1 sd) and the line shows the theoretical kinetic fractionation law between ^{29}Si and ^{30}Si (y = 0.51x, as calculated following Young et al., 2002).

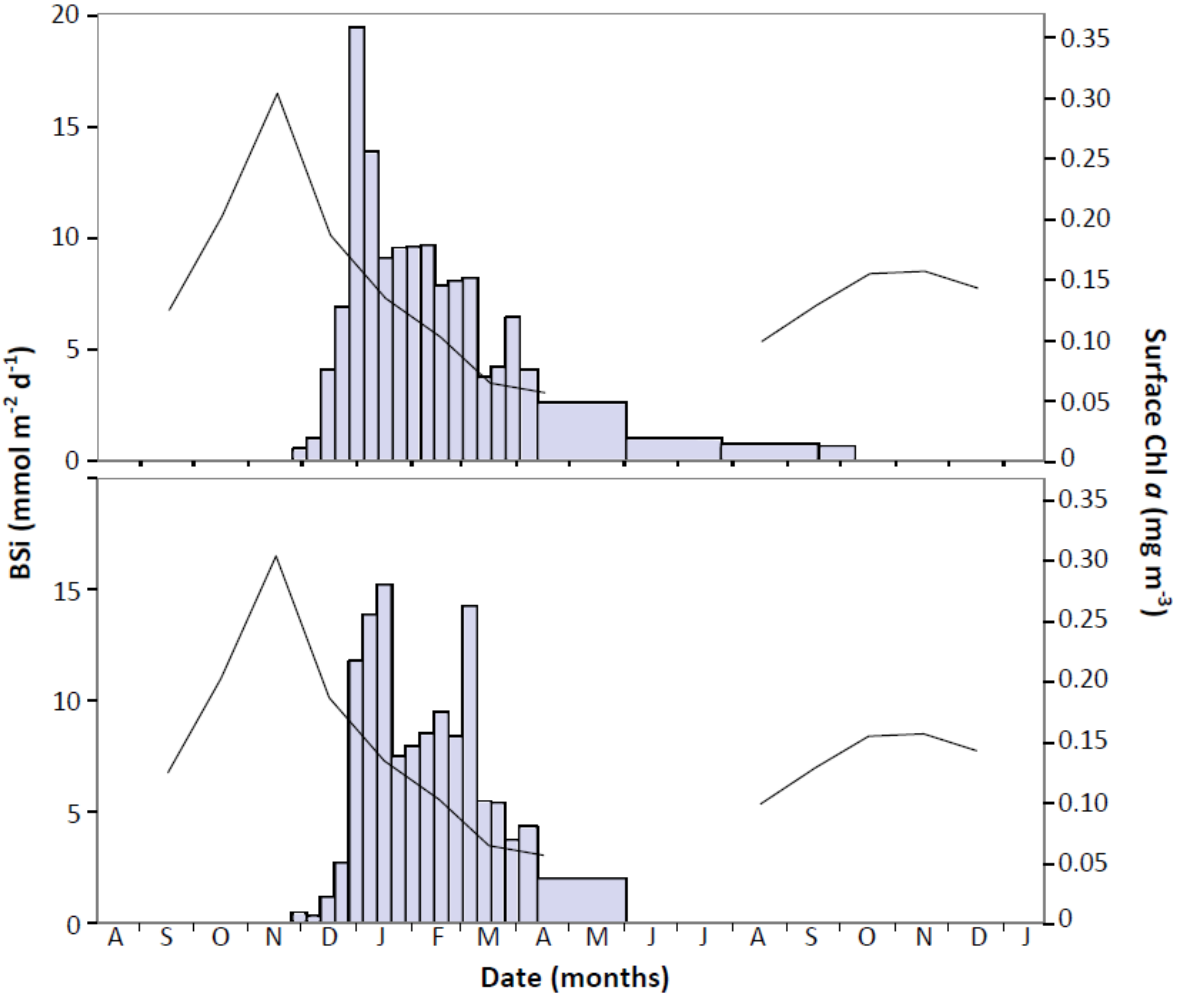

Figure C5. Seasonal variation of the biogenic silica flux (blue bars, mmol m^{-2} d^{-1}) in relation to monthly mean chlorophyll a concentration (black line, mg m^{-3}) in the Antarctic Zone, extracted from the NASA's Giovanni program (Acker & Leptoukh, 2007)

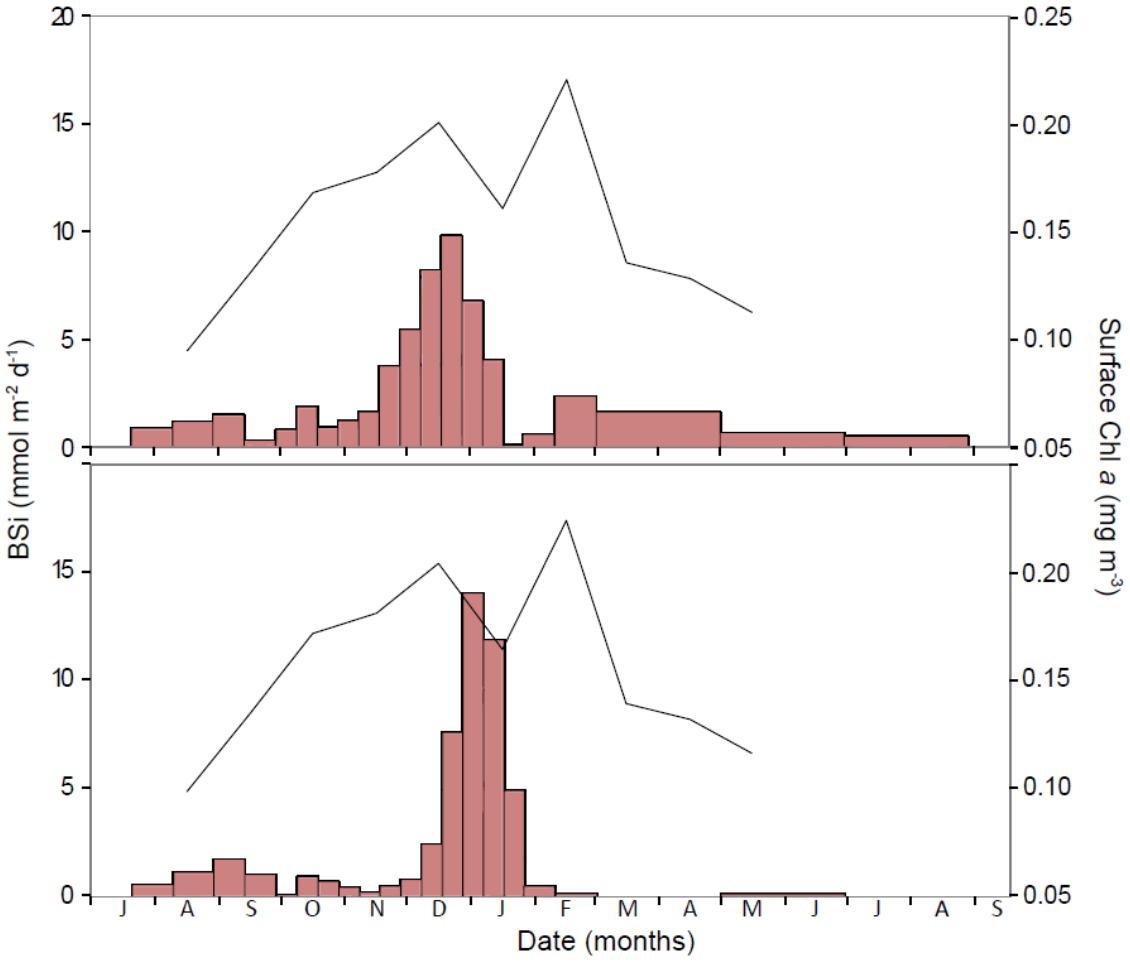

Figure C6. Seasonal variation of the biogenic silica flux (red bars, mmol m^{-2} d^{-1}) in relation to monthly mean chlorophyll a concentration (black line, mg m^{-3}) in the Polar Front Zone, extracted from the NASA's Giovanni program (Acker & Leptoukh, 2007).

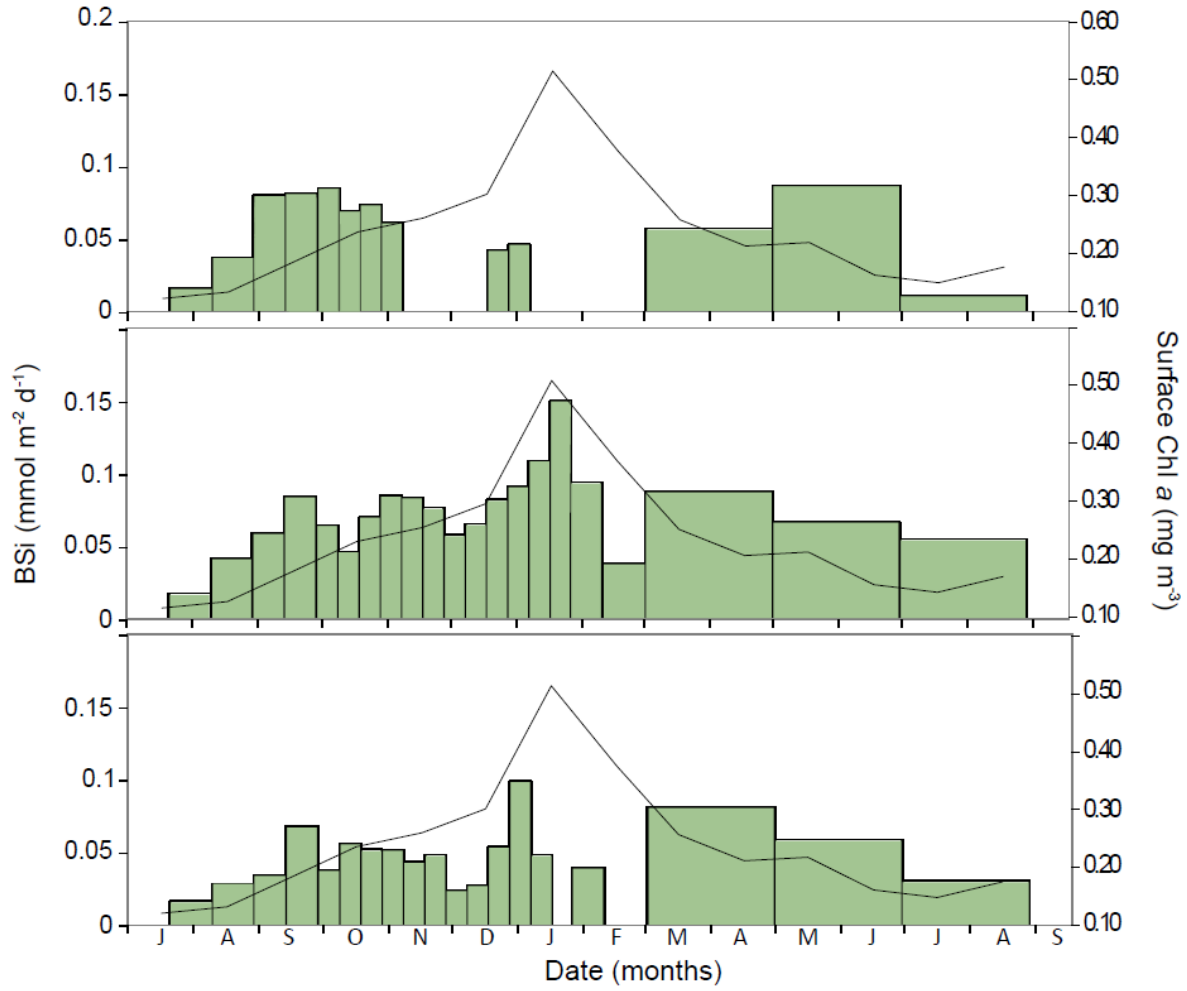

Figure C7. Seasonal variation of the biogenic silica flux (green bars, mmol m^{-2} d^{-1}) in relation to monthly mean chlorophyll a concentration (black line, mg m^{-3}) in the Sub-Antarctic Zone, extracted from the NASA's Giovanni program (Acker & Leptoukh, 2007).

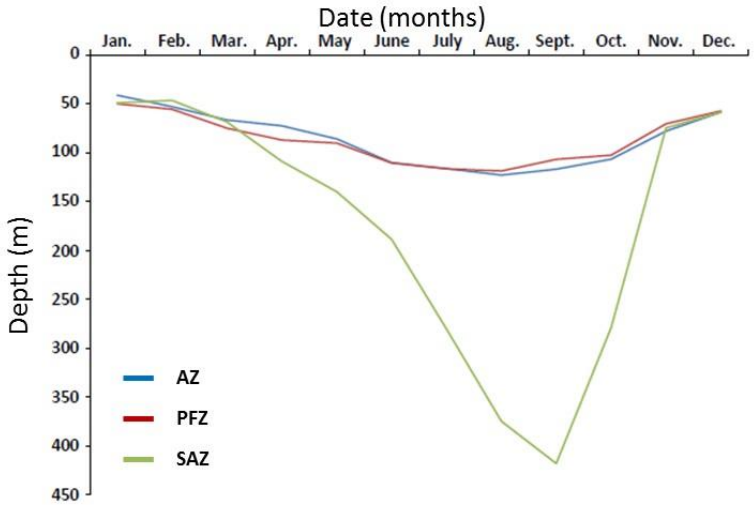

Figure C8. Seasonal variation of the monthly mean mixed layer depth in the Antarctic Zone (in blue), the Polar Front Zone (in red) and the Sub-Antarctic Zone (in green). Mixed layer depths (MLD) were extracted from the Argo dataset (www.argo.ucsd.edu). We calculated the MLD on individual Argo profile with a surface-density-difference criterion of $\sigma \leq 0.03$ kg m^{-3} (Sallée et al., 2006; where σ is the potential density referenced to the surface) and mapped monthly meridional sections along SR3 using all available data within 2° longitude of 143° E. The extensive coverage provided by the Argo dataset enabled us to obtain monthly sections of MLD on half-degree grid.

Journal of Marine Systems 142 (2015) 62–74

Contents lists available at ScienceDirect

Journal of Marine Systems

journal homepage: www.elsevier.com/locate/jmarsys

Seasonal dynamics in diatom and particulate export fluxes to the deep sea in the Australian sector of the southern Antarctic Zone

Andrés S. Rigual-Hernández [a,*], Thomas W. Trull [b,c], Stephen G. Bray [b], Ivia Closset [d], Leanne K. Armand [a]

[a] Department of Biological Sciences, Macquarie University, North Ryde, NSW 2109, Australia
[b] Antarctic Climate and Ecosystems Cooperative Research Centre, University of Tasmania, Hobart, Tasmania 7001, Australia
[c] CSIRO Oceans and Atmosphere Flagship, Hobart, Tasmania 7001, Australia
[d] Sorbonne Universités (UPMC, Univ Paris 06)-CNRS-IRD-MNHN, LOCEAN Laboratory, 4 place Jussieu, F-75005 Paris, France

ARTICLE INFO

Article history:
Received 13 June 2014
Received in revised form 6 October 2014
Accepted 8 October 2014
Available online 18 October 2014

Keywords:
Diatom flux
Particulate flux
Sediment traps
Southern Ocean

ABSTRACT

Particle fluxes were recorded over a one-year period (2001-02) in the southern Antarctic Zone in the Australian Sector of the Southern Ocean. Here, we present the results on the seasonal and vertical variability of biogenic particle and diatom valve fluxes. Total mass and diatom fluxes were highly seasonal, with maxima registered during the austral summer and minima during winter. Biogenic opal dominated sedimentation, followed by carbonate, and very low levels of organic carbon (annual average 1.4%). The strong correlation between opal and organic carbon at both depth levels suggests that a significant fraction of organic matter exported to the deep sea was associated with diatom sedimentation events. Seasonal diatom fluxes appear driven principally by changes in the flux of *Fragilariopsis kerguelensis*. The occurrence of the sea-ice affiliated diatoms *Fragilariopsis cylindrus* and *Fragilariopsis curta* in both sediment traps is considered to correspond to the sedimentation of a diatom bloom advected from an area under the influence of sea ice. Highest fluxes of the subsurface-dwelling species *Thalassiothrix antarctica* registered at the end of the summer bloom were linked to a drop of the light levels during the summer-autumn transition. This study provides the first annual observation on seasonal succession of diatom species in the Australian sector of the Antarctic Zone, and corresponds, in terms of magnitude and seasonality of diatom fluxes, to those in neighbouring sectors (Pacific and eastern Atlantic).

1. Introduction

Diatoms are unicellular algae with an absolute requirement for silicic acid to form their frustules. They constitute a major component of phytoplankton communities, being responsible for ~40% of all marine carbon fixation (Nelson et al., 1995). Diatoms are the main contributors to the silica-rich deposits in deep-sea sediments and are thought to influence the present and past global climate via their influence on the biological pump of CO_2 from the atmosphere into the ocean interior (Matsumoto et al., 2002; Nelson et al., 1995; Sarmiento et al., 1998). The composition of phytoplankton communities and abundance of diatoms within them are related to specific ecological parameters of the water masses where they live (e.g., temperature, sea-ice cover and nutrient availability), and hence in the case of diatoms, their frustules can be used as biotic proxies for palaeoenvironmental and palaeoceanographic reconstructions.

In order to evaluate the role of diatoms in the biological pump and the cycling of silicon, it is essential to thoroughly understand their ecology and the processes that the living biocoenoses undergo from their initial production in the euphotic zone to their eventual preservation in the ocean sediments (e.g. Grigorov et al., 2014; Varela et al., 2004). This knowledge is also required to validate paleorecontructions based on the diatom sedimentary record (e.g. Armand and Leventer, 2010; Leventer et al., 1993; Taylor and Sjunneskog, 2002).

The Southern Ocean is regarded as having one of the highest diatom biomasses of the global ocean. Despite its high-nutrient low chlorophyll (HNLC) regime, massive diatom blooms occur every year during spring and summer associated with specific areas, such as oceanographic fronts (e.g. Honjo et al., 2000; Moore and Abbott, 2000), coastal areas of Antarctica (e.g. Arrigo et al., 1999; Bathmann et al., 1991; Wefer et al., 1988) and the retreating sea ice edge (e.g. Smith and Nelson, 1986; Sullivan et al., 1988). As a result of this relatively high diatom productivity (Pondaven et al., 2000), large amounts of biogenic silica accumulate in the Southern Ocean sediments, mainly south of the Antarctic Polar Front (APF), where about 30% of the global opal marine accumulation occurs (Tréguer and De la Rocha, 2013).

Moored sediment traps are one of the few available tools for monitoring particle fluxes in the open ocean over extended periods of time. They provide a means to determine the magnitude and timing of phytoplankton blooms, document species succession and estimate the remineralization of labile components throughout the water column. The use of sediment traps has contributed significantly to our understanding of diatom ecology in the Southern Ocean and coastal Antarctic systems (e.g. Leventer and Dunbar, 1987, 1996; Fischer et al., 1988;

* Corresponding author.
E-mail address: andres.rigualhernandez@mq.edu.au (A.S. Rigual-Hernández).

http://dx.doi.org/10.1016/j.jmarsys.2014.10.002
0924-7963/

Abelmann and Gersonde, 1991; Ishikawa et al., 2001; Suzuki et al., 2001; Pilskaln et al., 2004; Ichinomiya et al., 2008; Romero and Armand, 2010). However, these studies are scattered in space and time, and large regions of the Southern Ocean, including the Australian Sector, remain undocumented.

During the Australian multidisciplinary ACE CRC SAZ Project (Trull et al., 2001a), the main hydrological zones of the Australian sector of the Southern Ocean were instrumented with sediment trap mooring lines. The central goal of this experiment was to determine the origin, composition and fate of particulate matter transported to the ocean interior. This research yielded important results, including the demonstration that particulate organic carbon (POC) export in the Southern Ocean is similar to the global ocean median (Bray et al., 2000; Trull et al., 2001b).

Here, as part of the ACE CRC SAZ project, we report on the biogenic particle fluxes registered by two sediment traps deployed in the southern Antarctic Zone (60° 44.43′S; 139°E 53.97′S) over a year (November 2001 to September 2002) in order to (1) document the magnitude, composition and seasonal distribution patterns of the settling particle fluxes, with particular focus on diatoms and their specific composition; and (2) assess the effects of dissolution and physical processes in the water column on the diatom assemblage composition by comparing the assemblages registered by the 2000 and 3700 m sediment traps. An improved understanding of diatom ecology and changes that the diatom assemblages undergo during their sinking through the water column should lead to a better interpretation of proxy records in the Southern Ocean.

1.1. Oceanographic setting

The Antarctic Circumpolar Current (ACC) flows eastward around Antarctica driven by strong westerly winds connecting the Pacific, Atlantic and Indian Oceans. Several circumpolar jets or fronts divide the ACC into distinct zones (Fig. 1a), each one characterized by specific hydrological and biochemical properties (Orsi et al., 1995). The fronts coincide with strong current cores of the ACC defined by contours of sea surface height (SSH). Each of these fronts consists of multiple branches or filaments, where their position varies rapidly over time (Sokolov and Rintoul, 2002, 2007, 2009a,b). From north to south, these fronts and zones are the Subtropical Front (STF), the Subantarctic Zone (SAZ), the Subantarctic Front (SAF), the Polar Frontal Zone (PFZ), the Polar Front (PF), the Antarctic Zone (AZ) and the Southern ACC Front (SACCF) (Sokolov and Rintoul, 2009a, b).

The surface waters of the Australian sector of the Southern Ocean are nitrate and phosphate rich and their concentrations remain fairly uniform across the ACC (Bostock et al., 2013). In contrast, silicic acid (Si) content shows a marked south to north gradient. Highest Si concentrations are reached south of the Polar Front Zone (up to 70 μM), whereas the Subantarctic Zone waters exhibits low Si values (1 to 5 μM) (Bostock et al., 2013; Coale et al., 2004). Despite the relatively high macronutrient concentrations, Southern Ocean surface waters are often characterized by relatively low phytoplankton biomass. Light limitation related to deep mixing (Sakshaug and Holm-Hansen, 1984) and extremely low concentrations of trace metals such as iron (Boyd et al., 2000; De Baar et al., 1995; Fitzwater et al., 2000; Johnson et al., 1997; Martin et al., 1990) seem to be the main causes for this "high-nitrate, low-chlorophyll" (HNLC) regime.

Sea ice seasonality off East Antarctica is considered linked to patterns of oceanic currents, which in turn are related to sea floor topography (Massom et al., 2013). Seasonal sea-ice advance occurs from early autumn through early spring followed by retreat from late spring through summer (Kimura and Wakatsuchi, 2011; Massom et al., 2013).

Our study site, station 61 S (60° 44.43′S; 139° 53.97′E), is located within the southern Antarctic Zone (AZ-S; Parslow et al., 2001), between the southern branch of the PF (59°S) and the southern front of the SAACF (Rintoul and Bullister, 1999; Rintoul and Sokolov, 2001). The mooring site is within the same region where the first open-ocean iron enrichment experiment in the Southern Ocean (Southern Ocean Iron Release Experiment - SOIREE) was conducted (Boyd et al., 2000) and can be considered representative of the region between the PF and the SACCF (between 54°S and 62°S) (Trull et al., 2001c). Despite surface waters rich in macronutrients (i.e. silicate, phosphate and nitrate), the algal biomass accumulation is considered low (<0.5 μg/L) (Parslow et al., 2001; Popp et al., 1999; Trull et al., 2001c). Copepods, mainly large calanoid copepodites, dominate the zooplankton community at the study site. Grazing pressure is considered low (<1% of the phytoplankton standing stock removed per day) and is thought not to greatly influence the development of the annual bloom (Zeldis, 2001). Very low iron concentrations (0.1-0.2 nM; Sohrin et al., 2000; Boyd et al., 2000) appear to be responsible for the low primary production. The study area is far from the influence of coastal waters and just north of the maximum winter sea-ice extent (Fig. 1b; Massom et al., 2013).

2. Material and Methods

2.1. Field experiment

Site 61 S was instrumented with a mooring line equipped with three McLane Parflux time series sediment traps (Honjo and Doherty, 1988) placed at 1000, 2000 and 3700 m depth in a water column of 4393 m (Fig. 1c). Each trap was paired with an Aanderaa current meter and temperature sensor. The trap sampling cups were filled with a buffered solution of sodium tetraborate (1 g L^{-1}), sodium chloride (5 g L^{-1}), strontium chloride (0.22 g L^{-1}), and mercury chloride (3 g L^{-1}). Cup rotation intervals were synchronized between traps and were established based on anticipated mass fluxes. The shortest sampling intervals were 8 days and correspond with the austral summer and autumn, whereas the longest interval was 55 days corresponding with austral winter (Table 1). No samples were recovered from the shallowest trap owing to equipment malfunction. The two deeper traps completed their collection sequence as programmed without any instrumental failures providing a continuous time-series for 317 days (November 30, 2001 to September 29, 2002) divided into 21 collecting intervals. Owing to the low particle fluxes registered at the onset and end of the experiment insufficient material remained for diatom analysis of cup 1 of the 2000 m trap and cups 1, 2, 19, 20 and 21 of the 3700 m trap (Table 1). After recovery, sediment trap cups were removed, capped on board and stored at 4 °C in the dark until they were processed. The original samples were sieved through a 1 mm nylon mesh in order to remove the largest swimmers, and only the fraction <1 mm was analyzed. Then, they were split into 10 equal fractions using a McLane WSD-10 wet-sample divider. One complete split was used for microplankton analysis. A detailed description of the geochemical analytical procedures is given by Trull et al. (2001b); Bray et al. (2000). Component fluxes are reported for individual cups along with average values over the collection or deployment period for each component (Table 1). As the collection period was shorter than a calendar year, annual mean estimates were determined and are presented in Table 1. These annual estimates take into account the fact that the unobserved days occurred in winter when fluxes were low, and were obtained by using the flux for the last winter cup (#21 in 2002) to represent mean daily fluxes during the unobserved period.

In order to investigate the correlation between time series, a correlation matrix was calculated (Table 2).

2.2. Siliceous microplankton sample preparation and analysis

Each diatom fraction sample was refilled with distilled water to 40 ml, from which 10 ml was subsampled and buffered with a solution of sodium carbonate and sodium hydrogen carbonate (pH 8) and kept refrigerated for future calcareous nannoplankton analysis. The remaining

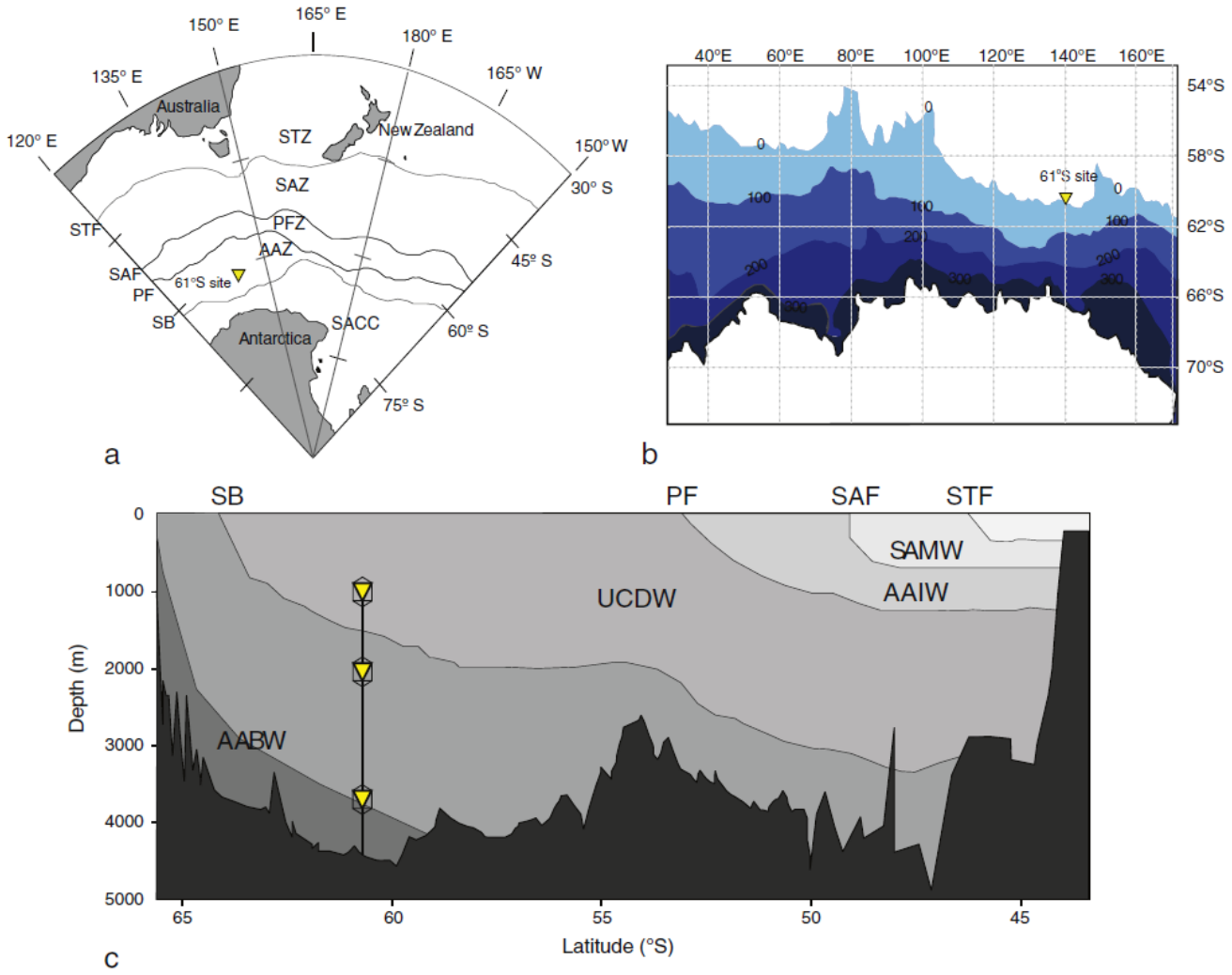

Fig. 1. a. Location of the sediment trap mooring line in the Antarctic Zone of the Australian sector of the Southern Ocean. Fronts (STF - Subtropical Front, SAF - Subantarctic Front, PF - Polar Front, SB - Southern Boundary), regions (STZ – Subtropical Zone, SAZ – Subantarctic Zone, PFZ – Polar Front Zone, ACC – Antarctic Zone and SACCZ - Zone south of the ACC) and maximum extension of winter sea ice (Max WSI) are shown. Triangle represents the position of 61°S mooring during the experiment (Nov. 2001 – Sep. 2002). b. Mean sea ice season duration map for the East Antarctic sector (1979/80-2009/10), with contours for 100, 200 and 300 days marked (modified from Massom et al., 2013). c. Schematic diagram of the Australian sector of the Southern Ocean depicting the bathymetry, main water masses and mooring configuration. SAMW – Subantarctic Mode Water, AAIW – Antarctic Intermediate Water, UCDW – Upper Circumpolar Deep Water, LCDW – Lower Circumpolar Deep Water and AABW – Antarctic Bottom Water. Figure is adapted from Bostock et al. (2013).

30 ml was treated with hydrogen peroxide, potassium permanganate and concentrated hydrochloric acid in order to clean the sample of organic matter and calcareous components following the methodology of Romero et al. (1999, 2000). The resulting sediment slurry was stored in bottles filled with distilled water. Microscopic slides were prepared following the decantation method outlined by Flores and Sierro (1997). This method produces random settling of the diatoms for quantitative microscopic purposes. The dried cover-slip was permanently mounted onto a glass slide with Norland optical adhesive 61 mounting medium (Refractive index: 1.56).

Qualitative and quantitative analyses were performed using a Olympus BH-2 compound light optical microscope at 1000x magnification with phase-contrast illumination. A minimum of 400 specimens were counted per sample. Each diatom valve was identified to the lowest taxonomic level possible. Scanning Electron Microscope observations of selected samples were used to verify taxonomic identifications made with the LM. The recommendations of Schrader and Gersonde (1978) were used as a basis for the counting of diatom valves. We did not include the counts of the girdle bands of *Dactyliosolen antarcticus* in the determination of relative abundances.

The microplankton counts were transformed into daily fluxes of specimens m^{-2} d^{-1} following the formula of Sancetta and Calvert (1988); Romero et al. (2009):

$$F = \frac{Nx\left(\frac{A}{a}\right)xVxS}{dxT}$$

where "F" is the daily flux of specimens, "*N*" the number of specimens, "A" the total area of a Petri dish, "a" the analysed area, "V" the dilution volume, "S" the split of the cup, "d" the number of days of collection and "T" the aperture area of the sediment trap.

The diatom species diversity was estimated applying Shannon's diversity index (H′) to the relative abundance data ($H' = -\sum p_i \log_2 p_i$, where $p = n1/N$, $n1 =$ number of specimens of one taxon and N the total number of specimens). Large values of H indicate greater diversity.

The annualized diatom valve flux for the 2000 m sediment trap was estimated following the same procedure as for the component fluxes (Table 1).

Table 1
Daily export fluxes of total mass flux, biogenic silica ($BSiO_2$), calcium carbonate ($CaCO_3$), particulate organic carbon (POC) and diatom valves registered at the 61°S site from November 2001 through October 2002. Mass fluxes listed as zero were too small to measure (<1 mg). *Average diatom fluxes for the 2000 and 3700 m traps have been estimated for different sampling intervals (309 and 172 days, respectively).

	Sampling period	Length	Total Mass Flux	$BSiO_2$		$CaCO_3$		POC		POC/PN	Diatoms
Cup	mid point	days	mg m^{-2} d^{-1}	mg m^{-2} d^{-1}	%	mg m^{-2} d^{-1}	%	mg m^{-2} d^{-1}	%	molar ratio	10^6 valves m^{-2} d^{-1}
61_2000											
1	Nov. 30, 2001	8	48	26	54	14	30	0.7	1.5	6.6	-
2	Dec. 08, 2001	8	78	47	61	17	22	1.7	2.2	6.1	9
3	Dec. 16, 2001	8	326	198	61	62	19	6.9	2.1	5.4	82
4	Dec. 24, 2001	8	509	326	64	140	28	6.4	1.3	3.5	85
5	Jan. 01, 2002	8	1151	856	74	44	4	26.9	2.3	7.4	408
6	Jan. 09, 2002	8	1069	796	75	170	16	14.8	1.4	4.9	200
7	Jan. 17, 2002	8	656	478	73	60	9	11.3	1.7	6.1	159
8	Jan. 25, 2002	8	702	541	77	38	5	11.0	1.6	6.1	296
9	Feb. 02, 2002	8	666	520	78	39	6	12.0	1.8	6.5	184
10	Feb. 10, 2002	8	595	469	79	24	4	8.2	1.4	6.2	295
11	Feb. 18, 2002	8	534	425	80	20	4	6.2	1.2	6.5	149
12	Feb. 26, 2002	8	524	418	80	19	4	4.7	0.9	6.5	152
13	Mar. 06, 2002	8	586	471	80	15	3	6.9	1.2	7.2	120
14	Mar. 14, 2002	8	285	230	81	11	4	3.2	1.1	6.6	71
15	Mar. 22, 2002	8	290	253	87	7	3	3.2	1.1	6.8	66
16	Mar. 30, 2002	8	263	218	83	8	3	2.6	1.0	6.1	87
17	Apr. 08, 2002	10	264	220	83	7	3	2.2	0.8	6.4	97
18	May. 08, 2002	50	130	102	78	5	4	1.2	1.0	5.9	47
19	Jun. 29, 2002	54	65	52	79	2	4	0.7	1.0	6.6	10
20	Aug. 22, 2002	55	56	44	78	2	4	0.8	1.5	6.6	19
21	Sep. 29, 2002	20	42	34	81	2	4	0.5	1.3	7.2	6
Annualised values			**232**	**178**	**76**	**17**	**7.4**	**3.3**	**1.4**	**6.1**	**67**
Annual flux			**85 g m^{-2} y^{-1}**	**65 g m^{-2} y^{-1}**		**6 g m^{-2} y^{-1}**		**1.2 g m^{-2} y^{-1}**			**24 10^9 valves m^{-2} y^{-1}**
61_3700											
1	Nov. 30, 2001	8	38	25	64	9	23	0.4	1.1	7.4	-
2	Dec. 08, 2001	8	31	17	54	9	28	0.4	1.2	6.4	-
3	Dec. 16, 2001	8	99	51	52	29	30	1.4	1.4	6.7	4
4	Dec. 24, 2001	8	231	148	64	59	26	1.4	0.6	2.6	12
5	Jan. 01, 2002	8	873	656	75	87	10	17.3	2.0	6.8	118
6	Jan. 09, 2002	8	1157	886	77	154	13	19.8	1.7	6.9	479
7	Jan. 17, 2002	8	828	611	74	166	20	9.4	1.1	4.6	354
8	Jan. 25, 2002	8	490	376	77	34	7	6.4	1.3	6.4	169
9	Feb. 02, 2002	8	491	384	78	32	6	6.5	1.3	6.1	385
10	Feb. 10, 2002	8	419	335	80	19	4	6.0	1.4	7.0	281
11	Feb. 18, 2002	8	584	475	81	36	6	6.2	1.1	6.2	254
12	Feb. 26, 2002	8	581	473	81	31	5	5.2	0.9	5.5	238
13	Mar. 06, 2002	8	849	737	87	23	3	7.6	0.9	6.5	326
14	Mar. 14, 2002	8	369	233	63	18	5	3.3	0.9	6.5	44
15	Mar. 22, 2002	8	218	174	80	8	4	2.6	1.2	7.3	32
16	Mar. 30, 2002	8	258	198	77	10	4	2.5	1.0	7.2	43
17	Apr. 08, 2002	10	257	202	79	9	3	2.3	0.9	6.9	32
18	May. 08, 2002	50	118	98	83	5	4	1.2	1.0	6.3	8
19	Jun. 29, 2002	54	0	0	83	0	4	0.0	1.0	6.3	-
20	Aug. 22, 2002	55	0	0	83	0	4	0.0	1.0	6.3	-
21	Sep. 29, 2002	20	0	0	83	0	4	0.0	1.0	6.3	-
Annualised values			**188**	**146**	**78**	**17**	**9**	**2.3**	**1.2**	**6.2**	**62**
Annual flux			**69 g m^{-2} y^{-1}**	**53 g m^{-2} y^{-1}**		**6 g m^{-2} y^{-1}**		**0.9 g m^{-2} y^{-1}**			**23 10^9 valves m^{-2} y^{-1}**

The temporal overlap of diatom fluxes between 2000 m and the 3700 m traps occurred between December-May (172 days) (Table 1). This overlap was used to estimate the sinking velocities of diatom valves and to track the alteration of settling diatom assemblages between traps. The sinking settling velocities for the main diatom taxa were calculated from the time lag between associated peaks in both traps and the vertical distance between traps. We used a squared-chord distance as the metric for assessing the similarity between the diatom assemblages of both traps (Ortiz and Mix, 1997). Squared chord distance values can range between 0.0 and 2.0, with 0.0 indicating identical proportions of species within the assemblages being compared.

Table 2
Correlation matrix (R^2) for the total mass and bulk compound fluxes at both sediment traps.

2000 m	Total Mass Flux	$BSiO_2$	$CaCO_3$	POC
Total Mass Flux	-			
$BSiO_2$	0.99	-		
$CaCO_3$	0.37	0.30	-	
POC	0.86	0.83	0.24	-
3700 m				
Total Mass Flux	-			
$BSiO_2$	0.99	-		
$CaCO_3$	0.61	0.54	-	
POC	0.87	0.83	0.63	-

2.3. Satellite imagery, meteorological and oceanographic data

Weekly mean sea surface temperature (SST) data for the period 2001 to 2002 was extracted from the NOAA Optimum Interpolation Sea Surface Temperature Analysis database (Reynolds et al., 2002). The monthly averages of the upper 300 m thermal structure for the 2001–2002 period (Fig. 2) were obtained for the sampling location from the World Ocean Atlas 2009 (Locarnini et al., 2010). The maximum

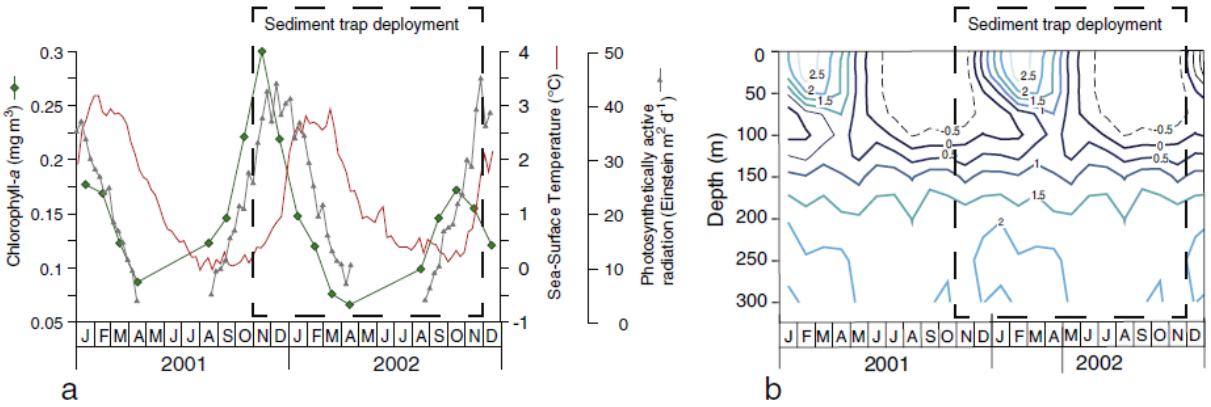

Fig. 2. (a) Monthly mean chlorophyll-*a* concentration (mg m^{-3}), sea surface temperature (SST) (°C) and photosynthetically active radiation (Einstein m^{-2} d^{-1}) for the period November 2001 to September 2002. No data was available from April to August in 2001 and 2002. (b) Seasonal variation in the vertical structure of temperature (°C) at the 61°S site.

weekly SST mean during the field experiment was 2.94 °C degrees occurring in March 2002, whereas the minimum was 0.12 °C at the beginning of October 2002. Changes of the weekly mean SST mirrored the seasonal changes in the vertical structure of the water column temperature profile. A pattern of stratification during austral summer months and vertical homogeneity in autumn and winter was noted during the field experiment (Fig. 2).

Satellite-derived monthly chlorophyll-*a* concentration and photosynthetically active radiation (PAR) estimates were obtained from NASA's Giovanni program (Acker and Leptoukh, 2007) (Fig. 2). The pigment concentration record was then used as a proxy for surface algal biomass accumulation. The overall chlorophyll-*a* levels were low (0.07-0.30 mg/m^3) and similar to previous observations in the study area (Trull et al., 2001c). The increase in the algal biomass commenced in September 2001 and reached its highest levels in November 2001, coinciding with a maximum in the insolation levels (Fig. 2). Pigment concentration declined through summer and reached its lowest levels in autumn and winter (March to August 2002).

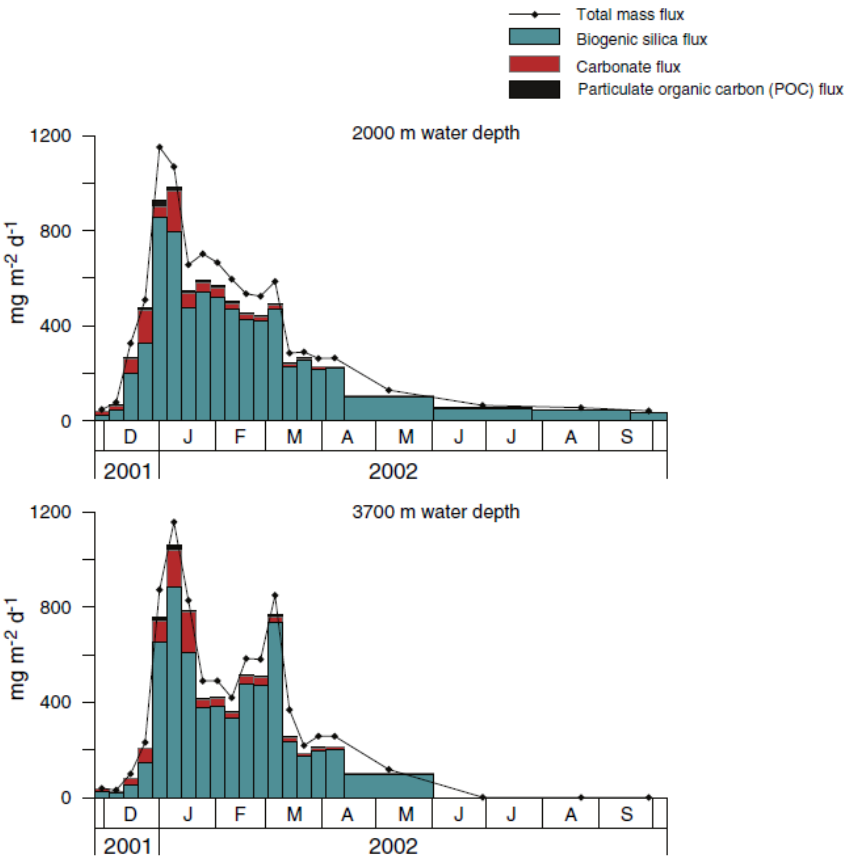

Fig. 3. Temporal variability of the total mass and major biogenic fluxes for <1 mm fraction at 2000 and 3700 m water depth from November 2001 through to November 2002 at the 61°S site.

3. Results

3.1. Bulk composition

Total fluxes of particulates at both traps were highly seasonal, with maxima registered during the austral summer (up to 1151 mg m^{-2} d^{-1} at 2000 m and 1157 mg m^{-2} d^{-1} at 3700 m) and almost negligible fluxes during winter (up to 42 mg m^{-2} d^{-1} at 2000 m and below detection limits at 3700 m) (Fig. 2). The fluxes of total particulates at 2000 and 3700 m depth showed similar seasonal variations and were closely correlated ($R^2 = 0.82$; Fig. 4). Particulate fluxes were slightly higher at 2000 m (261 ± mg m^{-2} d^{-1} = deployment average ± standard deviation) than at 3700 m (216 ± 337 mg m^{-2} d^{-1}). Biogenic silica (SiO_2) was the dominant bulk component, regardless of the sampling period or depth (deployment average = 76% at 2000 and 78% at 3700 m). The highest relative contribution of opal was registered from the end of summer through early-autumn at both depths (Table 1). Secondary contributors were carbonate ($CaCO_3$) (7% at 2000 m and 9% at 3700 m) and particulate organic carbon (POC) (1.4% at 2000 m and 1.2% at 3700 m). The relative concentration of carbonate and POC was at its highest in austral spring and summer (Table 1). The fluxes of all components were closely correlated. The results of the correlation matrix are given in Table 2. Total mass flux showed a strong correlation with POC at both sediment traps ($R^2 = 0.86$ at 2000 m and $R^2 = 0.87$ at 3700 m). $BSiO_2$ fluxes were also highly correlated with POC at both depths ($R^2 = 0.83$), whereas $CaCO_3$ and POC fluxes exhibited the lowest values ($R^2 = 0.24$ at 2000 m and $R^2 = 0.63$ at 3700 m).

The molar POC/PN ratios were relatively low (Table 1), and thus similar to surface Southern Ocean particles and phytoplankton (Copin-Montegut and Copin-Montegut, 1983).

3.2. Composition of the biogenic opal fraction

The biogenic opal fraction was composed of diatoms, silicoflagellates, radiolarians and the dinoflagellate *Actiniscus pentasterias*. Diatoms were, numerically, the dominant siliceous plankton group registered by the traps with a mean flux between 67 x 10^6 and 76 x 10^6 valves m^{-2} day^{-1} at 2000 m (annualized mean and deployment average, respectively). Mean diatom flux at the 3700 m trap yielded higher values (deployment average = 132 x 10^6 valves m^{-2} day^{-1}) due to the lower sampling duration (172 days) over the winter season (Table 1). Silicoflagellates and radiolarians were three and four orders of magnitude lower than diatoms (not shown), whereas only one specimen of *A. pentaserias* was indentified in the lower trap. At both depth levels, total diatom fluxes showed strong seasonal variations that closely followed total mass seasonality with Pearson correlation coefficients of r = 0.88 for 2000 m and r = 0.81 for 3700 m (Fig. 4). Diatom frustules from 61 taxa were identified over the entire experiment and are listed in Table 3 together with their relative contribution for the whole sampling period. The seasonal changes in the diatom flux and main species at mooring site 61°S are plotted in Fig. 5.

Diversity index values (H′) followed the same seasonal trend as total diatom flux at both depths, with highest values registered during austral summer and lowest during winter (Fig. 5). The squared-chord distance between the sediment trap diatom assemblages at 2000 and 3700 m was 0.003, indicating highly similar proportions of species within depths.

The dominant species of the diatom assemblage was *Fragilariopsis kerguelensis* with a mean flux between 53 x 10^6 and 60 x 10^6 valves m^{-2} day^{-1} at 2000 m (annualized mean and deployment average, respectively). This species contribution ranged from 37% to 96% of the total assemblage at 2000 m (average relative contribution for the overlapping period between traps = 72%; Table 3) and from 31% to 82% at 3700 m (average relative contribution for the overlapping period between traps = 68%) (Table 3). The diatom flux peaks at both depths can be attributed to an increased flux of *F. kerguelensis*, with exception to a peak in late January at 2000 m when *Fragilariopsis pseudonana* dominated the settling assemblage (39%). Secondary contributors to the diatom assemblage at 2000 and 3700 m were *Thalassiosira lentiginosa* (average relative contribution for the overlapping period between

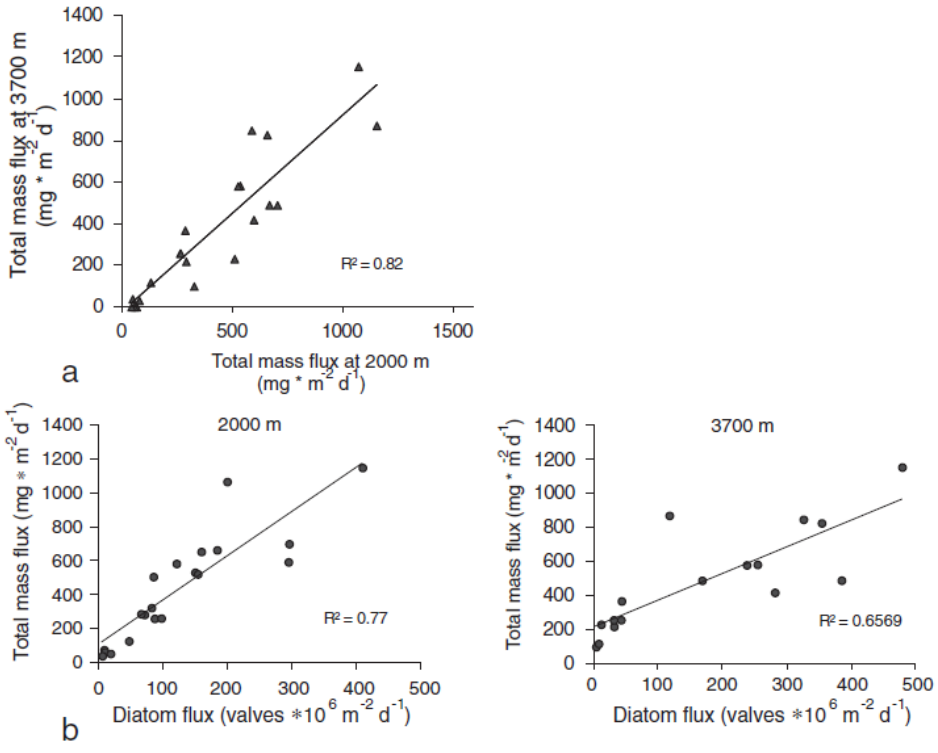

Fig. 4. Correlation between (a) mass flux (mg m^{-2} day^{-1}) at 2000 and 3700 m, and (b) mass flux (mg m^{-2} day^{-1}) and diatom valve flux (10^6 m^{-2} day^{-1}) at 2000 and 3700 m.

Table 3
Integrated fractional abundances of the diatom taxa found at the 2000 and 3700 m sediment traps at station 61°S.

	2000 m		3700 m
	Average 309 days	Average 172 days	Average 172 days
Actinocyclus spp.	0.01	0.01	0.03
Actinocyclus actinochilus (Ehrenberg) Simonsen	0.02	0.01	0.00
Asteromphalus hookeri Ehrenberg	0.17	0.20	0.48
A. hyalinus Karsten	0.16	0.26	0.29
A. parvulus Karsten	0.19	0.32	0.35
Asteromphalus spp.	0.01	0.01	0.01
Azpeitia tabularis (Grunow) Fryxell et Sims	0.68	0.57	0.74
Chaetoceros aequatorialis var. *antarcticus* Manguin	0.02	0.03	0.06
Ch. atlanticus Cleve	0.16	0.29	0.37
Ch. dichaeta Ehrenberg	0.11	0.19	0.16
Ch. peruvianus Brightwell	0.00	0.00	0.01
Chaetoceros sp. A	0.08	0.14	0.11
Chaetoceros sp. B	0.07	0.13	0.19
Chaetoceros spp.	0.15	0.27	0.32
Chaetoceros Hyalochaete resting spores	0.14	0.25	0.14
Corethron spp.	0.01	0.01	0.00
Dactyliosolen antarcticus Castracane			
Eucampia antarctica (Castracane) Mangin	0.13	0.14	0.20
Fragilariopsis curta (Van Heurck) Hustedt	0.57	1.00	1.11
F. cylindrus(Grunow) Krieger	0.16	0.29	0.10
F. kerguelensis (O'Meara) Hustedt	79.91	72.41	68.34
F. obliquecostata (van Heurck) Heiden	0.02	0.03	0.05
F. pseudonana (Hasle) Hasle	2.03	3.64	1.43
F. rhombica (O'Meara) Hustedt	0.93	1.58	2.13
F. ritscheri Hustedt	0.07	0.13	0.11
F. separanda Hustedt	2.10	2.85	2.03
F. cf. *sublineata* (Van Heurck) Heiden	0.03	0.04	0.03
Haslea trompii (Cleve) Simonsen	0.01	0.01	0.02
Navicula directa Smith) Ralfs in Pritchard	0.33	0.58	1.06
Nitzschia sicula var. *bicuneata* (Castracane) Grunow	0.06	0.10	0.14
*Pleurosigma directum*Grunow in Van Heurck	0.02	0.03	0.03
Pseudo-nitzschia <3 μm transapical axis	0.40	0.72	1.41
*P-n. heimii*Manguin	0.01	0.02	0.02
Pseudo-nitzschia spp.	0.11	0.19	0.08
Porosira pseudodenticulata (Hustedt) Jousé	0.02	0.03	0.03
Proboscia spp.	0.00	0.00	0.01
Rhizosolenia antennata (Ehrenberg) Brown f. *semispina* Sundström	0.00	0.00	0.02
Rhizosolenia bergonii Peragallo	0.00	0.00	0.02
Rhizosolenia sp. f. 1A (Armand et Zielinski)	0.01	0.01	0.02
Rhizosolenia spp.	0.09	0.07	0.02
Stellarima stellaris (Roper) Hasle et Sims	0.00	0.00	0.02
Thalassionema nitzschioides f. *capitulata* (Castracane) Moreno-Ruiz	0.06	0.09	0.11
T. nitzschioides f. *lanceolata* (Grunow) Pergallo et Pergallo	0.05	0.02	0.02
Thalassiosira gravida Cleve	0.03	0.05	0.11
T. gracilis var. *gracilis* (Karsten) Hustedt	3.65	6.08	7.41
T. gracilis var. *expecta* (Van Landingham) Frxyell et Hasle	0.42	0.65	1.30
T. lentiginosa (Janisch) Fryxell	4.97	4.63	6.77
T. leptopus (Grunow ex Van Heurck) Hasle et G.Fryxell	0.01	0.01	0.54
T, lineata group	0.11	0.14	0.36
T. maculata Fryxell et Johansen	0.05	0.02	0.02
T. oestrupii (Ostenfeld) Hasle	0.01	0.02	0.01
T. oliveriana(O'Meara) Makarova et Nikolaev	0.67	0.37	0.42
T. tumida (Janisch) Hasle	0.12	0.07	0.10
Thalassiosira spp. < 20 μm	0.37	0.62	0.29
Thalassiosira spp. > 20 μm	0.04	0.05	0.00
Thalassiosira sp. A	0.18	0.22	0.01
Thalassiosira sp. B	0.02	0.03	0.08
Thalassiothrix antarctica Schimper ex Karsten	0.20	0.18	0.58
Tropidoneis group	0.04	0.05	0.12
Other centrics	0.07	0.07	0.02
Other pennates	0.01	0.01	0.01

traps = 5% and 7%, respectively), *Thalassiosira gracilis* var. *gracilis* (6% and 7%), *Fragilariopsis separanda* (3% and 2%), *Fragilariopsis pseudonana* (4% and 1%), *Fragilariopsis rhombica* (2% and 2%), *Fragilariopsis curta* (1% and 1%) and *Azpeitia tabularis* (1% and 1%) (Table 3 and Fig. 5). It is worth noting that some large and/or entangled frustules of some diatom taxa, such as *Thalassiothrix* (Hallegraeff, 1986), could have been be retained in the 1 mm screen mesh, and therefore, underrepresented in this study.

Scanning electron microscope (SEM) pictures of some of the most relevant taxa are shown in Fig. 6.

3.3. Diatom settling velocities

The calculation of the sinking velocities of the main diatom taxa was only possible for the "particle bloom" period, i.e. from December to March, when distinct peaks were registered in both sediment traps

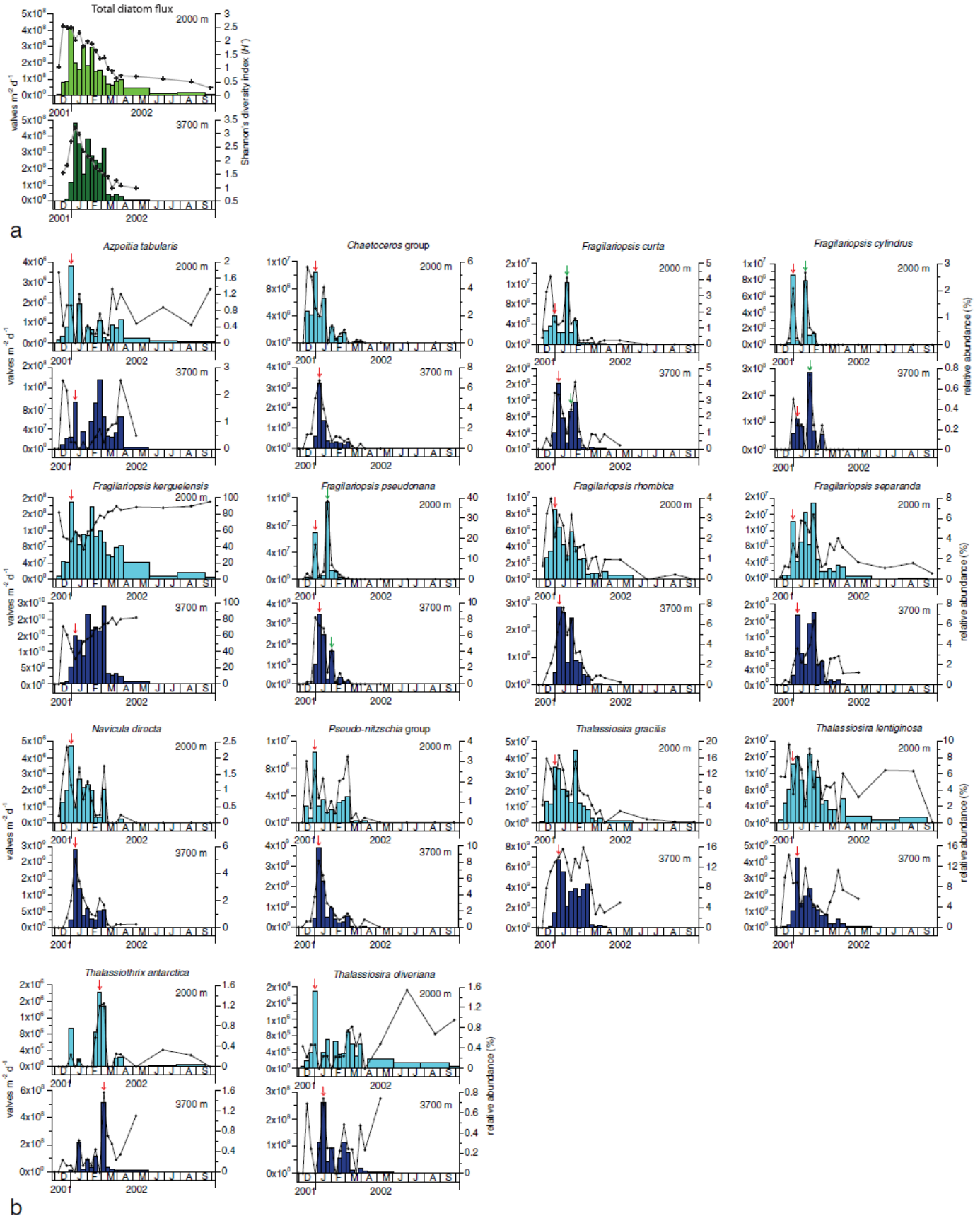

Fig. 5. Seasonal variation of (a) total diatom flux and Shannon's diversity index (H′) and (b) flux and relative abundance of the main diatom species at 2000 and 3700 m sediment traps. The arrows indicate the associated peaks of valve flux at both depths used to calculate the sinking velocities.

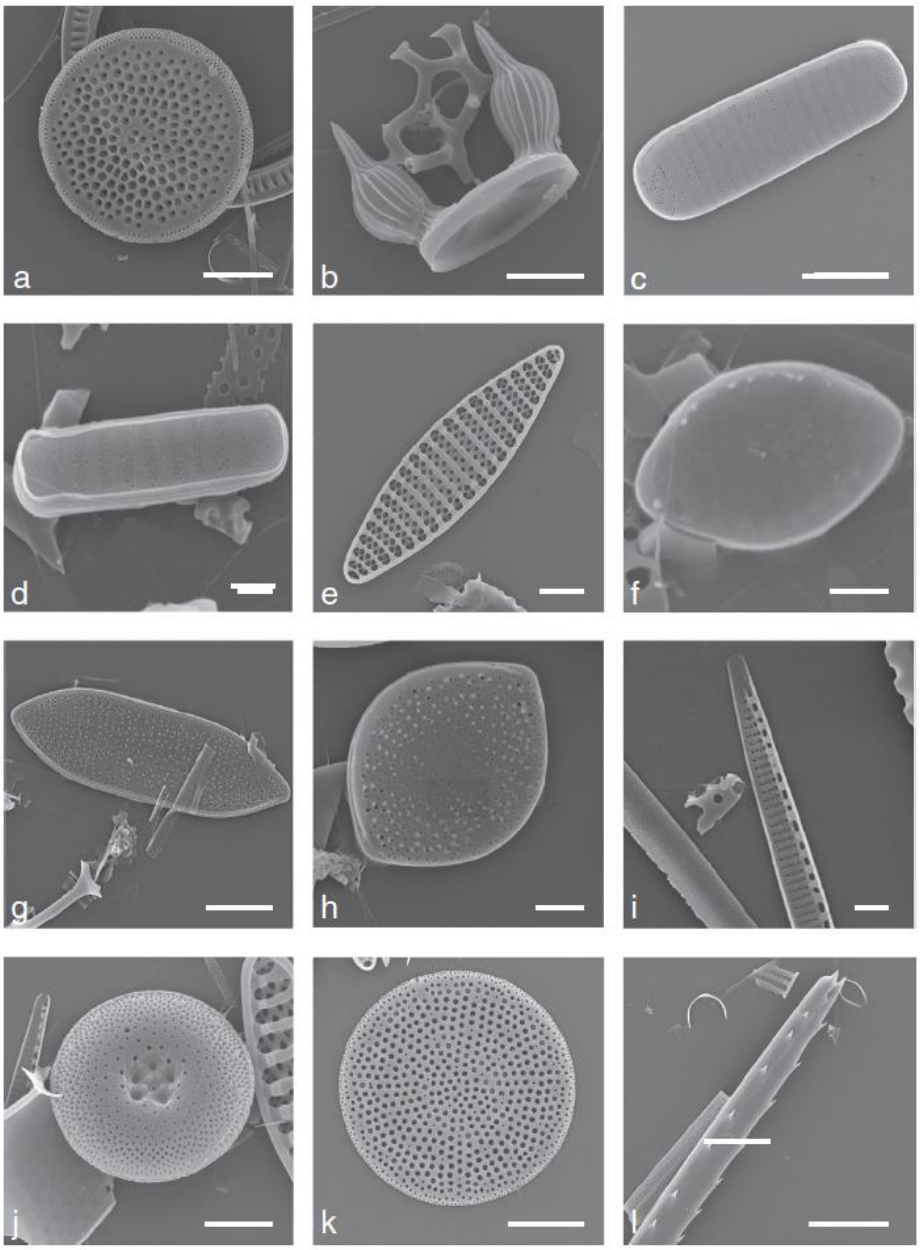

Fig. 6. SEM photos of some of the most relevant diatom taxa collected by the sediment traps at site 61°S. (a) *Azpeitia tabularis*. (b) *Chaetoceros atlanticus* (resting stage). (c) *Fragilariopsis curta*. (d) *Fragilariopsis cylindrus*. (e) *Fragilariopsis kerguelensis*. (f) *Fragilariopsis pseudonana*. (g) *Fragilariopsis rhombica*. (h) *Fragilariopsis separanda*. (i) *Pseudo-nitzschia* spp. (j) *Thalassiosira gracilis* var. *gracilis*. (k) *Thalassiosira lentiginosa*. (l) *Thalassiothrix antarctica*. Scale bars: d, f = 1 μm; h, i = 2 μm; c, e, j = 5 μm; a, b, g, k, l = 10 μm.

(Fig. 5). The precision of the calculations is limited by the duration of the sampling intervals during this period (8 days). The majority of the taxa exhibited an offset of a single sampling interval (8 days) between the 2000 and 3700 m traps, suggesting and average settling speed of 210 m d^{-1}.

4. Discussion

4.1. Quality check of downward particle fluxes

The use of sediment traps has greatly enhanced our understanding of particle transfer in open ocean environments. However, laboratory and field experiments have shown that the measurement of downward particle fluxes can be subject to several hydrodynamic biases (e.g. Baker et al., 1988; Gardner, 1980; Yu et al., 2001). Therefore, an assessment of the trapping efficiency is needed prior to interpreting the results of any sediment trap experiment.

Our mooring line at site 61°S was maintained taut by the distribution of floats along the line and at the mooring head. Measured mean current speeds at both trap levels were always lower than 10 cm s^{-1} that is, as a rule of thumb, considered the threshold at which trapping efficiency decreases significantly (e.g. Baker et al., 1988; Heussner et al., 2006; Honjo et al., 1992; Yu et al., 2001). On the basis of global comparisons, these conditions suggest that fluxes registered by the traps were unlikely to be significantly biased by under- or over-trapping (Honjo., 1996; Yu et al., 2001).

4.2. Variability of total mass flux and composition of particles

The seasonal variability of the vertical particle transfer at site 61°S appears principally controlled by seasonal changes in the euphotic zone productivity. A significant increase in chlorophyll-*a* concentration from October 2001, approximately two months before any significant warming or stratification occurs (Fig. 2), is in line with an increase in

incident insolation from the beginning of spring. Taking into account that pigment concentration at the sea surface reached its highest levels during November 2001 (Fig. 2), and that maximum total particle and diatom fluxes were registered at the beginning of January 2002 (Figs. 3 and 5), a time lag of about two months between peak production in the surface waters and onset of particle export in the study area can be assumed. This feature is in agreement with the observations of Buesseler et al. (2001) in the Pacific Sector of the Southern Ocean who reported a similar delay in the delivery of the surface bloom to the ocean interior. Contrastingly, algal biomass reached its annual minimum during the austral winter (June-September) (Fig. 2) and very low particle and diatom export fluxes were registered by the traps (Fig. 3 and 5). These low chlorophyll-*a* concentration and flux values appear to be driven by two factors: (i) insufficient sunlight as a result of the low solar angle and shortened day length that reduced the ability to increase biomass and (ii) intense vertical mixing that transported phytoplankton below their critical depth, i.e. depth at which the rate of photosynthesis equals the rate of respiration (Fig. 2).

In terms of particle composition, silica-rich and carbonate-poor particulate fluxes registered by the traps mirrored the dominance of diatoms in the waters south of the Antarctic Zone, south of Tasmania. The composition of the settling material is consistent with that of the surface sediments in the region. Opal content in the surface sediments of the Southern Ocean increases from north to south, being the dominant component south of the APF. In contrast, $CaCO_3$ is dominant north of the SAF and decreases southward (Honjo et al., 2000).

Total mass and POC fluxes provided the strongest correlation at both sediment traps (Table 2). As $BSiO_2$ dominated the mass fluxes throughout the sampling period, changes in the $BSiO_2$ flux directly affected POC fluxes, suggesting that diatom valve sedimentation plays an important role in controlling the organic carbon export to depth at the AZ site. On the other hand, the small $CaCO_3$ fluxes and lower correlation values with POC at both sediment traps suggest that $CaCO_3$ had a lesser influence on the POC export. However, as the carrying capacity of POC per $CaCO_3$ unit could not be quantified, the role of $CaCO_3$ in controlling the transfer of organic carbon to depth remains unknown.

4.3. Seasonal trend of diatom fluxes and species composition

The annual diatom fluxes registered by the 2000 m sediment trap (Table 1) fall within the range of those estimated by Fischer et al. (2002) in the AZ of the eastern Atlantic (20 x 10^6 valves m^{-2} d^{-1}) and those reported by Grigorov et al. (2014) in the Ross Sea Gyre (93 x 10^6 valves m^{-2} day^{-1}). The diatom fluxes recorded at site 61°S are therefore comparable in magnitude to previously reported diatom data sets of the AZ in the Southern Ocean.

Although several factors, such as grazing, dissolution and lateral advection, can influence diatom flux (Boltovskoy et al., 1993), the similar seasonal patterns, with a two month offset between primary productivity and diatom flux variations (Figs. 2 and 5a) suggest that the primary signal of the phytoplankton bloom in the overlying water masses is registered by the traps. About two-thirds of the annual diatom export fluxes at each trap depth were registered during January and February (Fig. 5). A markedly seasonal pattern is characteristic of high latitude systems (e.g. Wefer et al., 1988; Dunbar et al., 1998; Honjo et al., 2000; Fischer et al., 2002; Pilskaln et al., 2004; Romero and Armand, 2010) and illustrates the opportunistic character (r selection) of the dominant species during the summer bloom. As a consequence of this rapid diatom biomass increase, silica in the AZ-S is often stripped out the mixed layer by mid-summer (Trull et al., 2001c).

The temporal variations in the composition of diatom assemblages mirrored the changes of the hydrographic conditions in the AZ-S, south of Tasmania. Overall, the major diatom taxa recorded at our mooring site are typical of living and fossil assemblages representing open ocean waters of the Antarctic Zone (Romero and Armand, 2010; Crosta et al., 2005, respectively).

The seasonal diatom flux was mainly driven by changes in the flux of the large, heavily-silicified and bloom-forming *F. kerguelensis*, a prominent member of the diatom assemblages in the iron-limited Southern Ocean waters (Abelmann et al., 2006; Smetacek, 1999). Large abundances of *F. kerguelensis* in phytoplankton blooms have also been previously reported in our study area during the SOIREE experiment (Gall et al., 2001; Trull and Armand, 2001), in the AZ of the south-west Atlantic (Hart, 1934) and in the vicinity of open-ocean fronts in the Atlantic and Pacific sectors (Bathmann et al., 1997; Grigorov et al., 2014; Laubscher et al., 1993). The relative contribution of *F. kerguelensis* at both 61 S traps (68-80%; Table 1) is consistent with its distribution in the Southern Ocean surface sediments where its maximum abundances (70-83%) are found between the Polar Front and the maximum summer sea-ice edge (Crosta et al., 2005). Fischer et al. (2002); Grigorov et al. (2014) reported lower relative abundance and fluxes of this species in sediment traps in the AZ of the Atlantic sector (29%; 6 x 10^6 valves m^{-2} d^{-1}) and in the Ross Sea Gyre (22%; 20 x 10^6 valves m^{-2} d^{-1}), respectively. However, these sites were under the influence of seasonal ice, where sea-ice affiliated taxa such as smaller *Fragilariopsis* species and *Chacetoceros* spp., are known to often dominate the diatom assemblages (Armand et al., 2005).

At the onset of the summer particle "bloom", H´ rises significantly due to the burst of reproduction and sedimentation of most of the diatom taxa (Fig. 5a). The small and rapidly dividing diatoms *Chaetoceros* group, *Fragilariopsis pseudonana*, *Fragilariopsis rhombica*, *Fragilariopsis separanda* and *Pseudo-nitzschia* spp., together with the cool open ocean species *Thalassiosira gracilis*, are major contributors to the bulk of the spring-summer maximum (Fig. 5). The majority of these diatoms correspond to the Group 1 defined by Quéguiner (2013), consisting of slightly silicified and fast-growing species that undergo rapid species succession during productive periods. The biomass accumulation of such diatoms is thought to be controlled principally by nutrient availability rather than grazing pressure. This concept agrees well with the observations of Zeldis (2001) who reported low grazing impact over the bloom development during the SOIREE experiment. At the end of their growth season, these bloom-forming species are considered to undergo mass mortality resulting in the formation of aggregates that rapidly sink from the euphotic zone (Assmy et al., 2013).

The AZ-S site is remote from the direct influence of sea-ice in summer (Massom et al., 2013; Fig. 1b), which makes the occurrence of the sea-ice affiliated diatoms *Fragilariopsis cylindrus* and *Fragilariopsis curta* during January (Fig. 5b) puzzling. The distribution of *F. cylindrus* in the modern Southern Ocean is constrained to the north by the maximum summer sea ice edge (Armand et al., 2005; Esper et al., 2010; Semina, 2003), whereas *F. cylindrus* appears limited by the maximum extension of sea ice during winter (Armand et al., 2005; Esper et al., 2010). Likely explanations for the presence of these species at site 61°S are either (i) the occurrence of an iceberg in the vicinity of our study area or (ii) the advection of a transient bloom produced in a region under the influence of sea ice. Rich sea-ice affiliated diatom communities have been found in association with free-drifting icebergs (e.g. Smith et al., 2011), however this explanation is unlikely since our site is remote from any known iceberg pathway (Gladstone et al., 2001). Taking into account a time lag of about two months between peak production and particle export, a healthy and neutrally buoyant bloom could cover a much larger distance than that estimated for a sinking particle (detailed in 4.5). Sea-ice coverage west of ~90°E can reach latitudes well above 61°S (Massom et al., 2013; Fig. 1b). We hypothesize that the pulses of *F. curta* and *F. cylindrus* could correspond to the sedimentation of a diatom bloom that was either advected from an area upstream the ACC under the influence of seasonal sea ice or transported northward by Antarctic Surface Water currents (AASW) produced by the seasonal retreat of the sea ice, south of our study.

Enhanced fluxes of the large and thick-walled *F. kerguelensis* persisted for a longer period (until April) than those of Group 1 (sensu Quéguiner, 2013) most likely contributing to the progressive reduction

of silicic acid concentrations in the mixed layer throughout the summer. A similar pattern was reported by Assmy et al. (2013) both inside and outside the iron-fertilized bloom during the European Iron Fertilization Experiment (EIFEX). *Fragilariopsis kerguelensis* is considered a "sinking-silica species" (Assmy et al., 2013) largely responsible for the decoupling of silicon and carbon cycles in the iron-limited ACC.

At the end of the diatom export maximum (i.e. February-March), *Thalassiothrix antarctica* contributed more significantly to the flux via increased abundances (Fig. 5b). This species is a large, slow-growing diatom distributed within discrete layers of the water column (Kemp et al., 2000). Such diatoms are considered k-strategists (Kemp and Villareal, 2013) and fall within Group 2 defined by Quéguiner (2013). High abundances of *Thalassiothrix antarctica* have been reported within and south of the APF (Bracher et al., 1999; Laubscher et al., 1993) and associated to a subsurface chlorophyll maximum in the PFZ south of Tasmania (Gomi et al., 2010; Kopczynska et al., 2001; Parslow et al., 2001) and in Prydz Bay (Quilty et al., 1985). We suspect that *Thalassiothrix antarctica* develops in parallel to Group 1 diatoms, as a result of them inhabiting the pycnocline discontinuity, exploiting deep nutrients and undergoing low rates of primary productivity under low-light conditions (Kemp et al., 2000, 2006; Quéguiner, 2013). The abrupt drop of the photosynthetically active radiation levels to less than half their peak values from February to March (Fig. 2a) and/or the occurrence of a vertical mixing event may have produced both light and/or nutrient limitation leading to the rapid flocculation and sinking of *T. antarctica* during the summer-autumn transition.

Post-March diatom export decreases significantly (Fig. 5a) due to the reduction to lowest levels of light and the concomitant intensification of mixing of the water column (Fig. 2a,b). The "post-bloom" diatom assemblage is characterized by low diversity values (Fig. 5a) mainly due to the high relative abundance of *F. kerguelensis* (up to 96% in September). The remaining assemblage is subsequently composed of large and heavily silicified centrics such as *Thalassiosira lentiginosa*, *Azpeitia tabularis* and *Thalassiosira oliveriana*. These are typical open ocean diatoms (Crosta et al., 2005; Romero et al., 2005) with presumed lower nutrient requirements than the summer bloom-forming species.

4.4. Transfer to depth

Our results suggest that a fast and relatively undisturbed downward transport of particles occurred between 2000 and 3700 m (Figs. 3 and 4). The similar BSi and POC content in both traps (Table 1) indicates that little silica dissolution and remineralization occurred between 2000 and 3700 m. Such a result is consistent with previous sediment trap studies that reported minimal alteration of the silica and organic carbon fluxes below the mesopelagic-bathypelagic boundary (~2000 m) (Honjo et al., 2008; Takahashi, 1986). However, the high Si/C at both depth levels also implies that organic matter is recycled faster than opal before reaching the traps, and this must occur at mesopelagic depths. We interpret this as the remineralization of the settling material by the microbial community and by the zooplankton that preferentially feed on organic matter (Honjo, 2009). High Si/C ratios are characteristic of the iron-limited systems of the Southern Ocean where large and highly silicified species (e.g. *Fragilariopsis kerguelensis*) dominate the diatom assemblages. In this regard, the average POC content (1.4%) of our samples at 2000 m is very low, and the average BSi/POC molar ratio for the entire collection period was less than 0.1 for both traps, in comparison to an average of ~1 for a compilation of deep Southern Ocean traps (Honjo et al., 2008) and a median of ~2 for a global compilation (Lampitt and Antia, 1997). This makes it clear that the trap samples have experienced very strong losses of organic carbon, consistent with previous studies suggesting that Southern Ocean waters south of the Polar Front can be described as low carbon export regimes (Lam and Bishop, 2007).

The sinking velocities of the major diatom taxa during the "particle bloom" indicate rapid sedimentation of the diatom assemblages between the upper and lower traps (210 m d^{-1}). These settling speeds are very similar to those estimated by Honjo et al. (2000) in the AZ of the Pacific Sector and are equal, or greater than, those observed in high productivity areas at lower latitudes (Honjo, 1996). In contrast, based on the time delay between samples with similar silicon isotopic signatures at different depths at site 61 S, Closet et al. (unpublished results) estimated the settling velocities outside the production period to be 120 m d^{-1} or less. These observations suggests that sinking rates of diatom valves at site 61 S are related to flux size, perhaps because higher fluxes lead to the formation of fast-sinking aggregates (e.g. Alldredge and Gotschalkt, 1989). This concept is consistent with the observations of Grigorov et al. (2014) on sediment trap material from the Pacific Sector of the Southern Ocean who reported abundant diatom aggregates at times of peak flux and mainly individual cells and small chains outside the production period. Moreover, the formation of aggregates would also explain the enhanced POC export (Table 1) in association with high fluxes of Group 1 diatoms during the production period (Assmy et al., 2013).

The pulse of *Thalassiothrix antarctica* in early March at both depths coincides with an upturn of the POC fluxes (Table 1). *Thalassiothrix antarctica* cells are about 60 times larger (in estimated biovolume) than *F. kerguelensis* (Cornet-Barthaux et al., 2007), and therefore, have the potential to contribute significantly to the annual organic carbon export even at background concentrations (Goldman, 1993; Goldman and McGillicuddy, 2003; Quéguiner, 2013).

During winter, the lower sinking rates and high area/volume ratios of single diatom cells may facilitate the recycling of the valves and remineralization of organic matter in the upper water column. The enrichment of dissolution-resistant diatoms (e.g. *Fragilariopsis kerguelensis*, *Thalassiosira oliveriana*, *Azpeitia tabularis*) during the winter months observed in our traps could, therefore, be partially related to enhanced, selective dissolution of more lightly silicified species (e.g. *Pseudo-nitzschia* spp., *Fragilariopsis pseudonana*, *Chaetoceros* spp.).

With regard to the comparison of the annual diatom assemblage between traps, their highly similar abundance proportions, as revealed by the low squared chord distance score, indicate that both traps registered diatom assemblages from the same source. Moreover, the latter results further support the idea that silica BSi dissolution below 2000 m is minimal at the AZ-S site.

Conclusions

The main objective of our study was to document the variability in the magnitude, timing and composition of particle and diatom export fluxes to the deep sea in the southern Antarctic Zone (AZ-S) within the Australian sector of the Southern Ocean. To examine this issue, we studied the year-round dynamics of particle flux from November 2001 through September 2002. The overall fluxes of biogenic particles to the mid- and deep water column in the AZ-S were markedly seasonal with peak fluxes occurring during the austral summer and very low export during winter. This seasonal pattern is mediated by algal productivity. Comparison of satellite and particle flux data suggests a delay of about two months between peak production and onset of particle export. The biogenic opal fraction largely dominates the export throughout the year, and is mainly delivered by diatoms. Carbonate and organic carbon are secondary components.

Diatom seasonal fluxes followed the seasonality of the biogeochemical particle fluxes at both depths and their magnitude (67-76 x 10^6 valves m^{-2} day^{-1}) is similar to previously published data recorded in the AZ of other sectors of the Southern Ocean. The diatom assemblages recovered at our mooring site are typical of the open ocean waters of the Antarctic Zone (Crosta et al., 2005) and their seasonal succession agrees well with the conceptual scheme proposed by Quéguiner (2013) for the POOZ (Permanently Open Ocean Zone) and the PFZ (Polar Frontal Zone). *Fragilariopsis kerguelensis* is, by far, the most dominant diatom species in the sediment trap samples. The occurrence of the sea-ice affiliated species *F. cylindrus* and *F. curta* may correspond to

the sedimentation of a diatom bloom advected from an area under the influence of sea ice upstream the ACC. The sedimentation pulse of the deep-dwelling species *Thalassiothrix antarctica* during the February-March transition appears to have been triggered by an abrupt drop of the light levels and/or a vertical mixing event.

Finally, the good correlation between the total mass fluxes at both sediment traps and their similar diatom species composition suggests fast and undisturbed settling of particles through the deep water column at the AZ-S site.

Acknowledgements

This project is supported through funding from the Australian Government´s Australian Antarctic Science Grant Program (Project number 4078) and Macquarie University. The SAZ Project is grateful for logistical and equipment support from ANARE and the Australian Antarctic Division (T. Trull, ASAC grants 1156 and 2256), the CSIRO Division of Marine Research Oceans and Climate Program, Geosciences Australia, and New Zealand's National Institute of Water and Atmospheric Research (NIWA). The officers, crews, and scientific staff of the Aurora Australis voyages are thanked for their professionalism and dedication. Anne-Marie Ballegeer is greatly acknowledged for her comments during the preparation of the manuscript. The authors acknowledge the assistance and support of Nicole Vella and Debra Birch from the Macquarie University Microscopy Unit for performing scanning electron microscopy experiments. Robert O'Malley provided remote sensing support during analysis. The chlorophyll-*a* data used in this paper were produced with the Giovanni online data system, developed and maintained by the NASA GES DISC. Dr Anne-Marie Ballegeer is acknowledged for her suggestions and technical support. Critical comments and suggestions from two anonymous reviewers helped to improve the manuscript.

References

Abelmann, A., Gersonde, R., 1991. Biosiliceous particle flux in the Southern Ocean. Mar. Chem. 35, 503–536.
Abelmann, A., Gersonde, R., Cortese, G., et al., 2006. Extensive phytoplankton blooms in the Atlantic Sector of the glacial Southern Ocean. Paleoceanography 21, PA1013.
Acker, J.G., Leptoukh, G., 2007. Online analysis enhances use of NASA Earth science data. EOS Trans. AGU 88, 14–17.
Alldredge, A.L., Gotschalkt, C.C., 1989. Direct observations of the mass flocculation of diatom blooms: characteristics, settling velocities and formation of diatom aggregates. Deep-Sea Res. (1 Oceanogr. Res. Pap.) 36 (2), 469–530.
Armand, L.K., Leventer, A., 2010. Palaeo sea ice distribution and reconstruction derived from the geological record. In: Thomas, D.N., Dieckmann, G.S. (Eds.), Sea Ice. Wiley-Blackwell Publishing Ltd, Oxford, pp. 469–530.
Armand, L.K., Crosta, X., Romero, O.E., et al., 2005. The biogeography of major diatom taxa in Southern Ocean surface sediments: 1. Sea ice related species. Palaeogeogr. Palaeoclimatol. Palaeoecol. 223, 93–126.
Arrigo, K.R., Robinson, D.H., Worthen, D.L., et al., 1999. Phytoplankton community structure and the drawdown of nutrients and CO_2 in the Southern Ocean. Science 283, 365–367.
Assmy, P., Smetacek, V., Montresor, M., 2013. Thick–shelled, grazer–protected diatoms decouple ocean carbon and silicon cycles in the iron–limited Antarctic Circumpolar Current. PNAS 110 (51), 20633–20638.
Baker, E.T., Milburn, H.B., Tennant, D.A., 1988. Field assessment of sediment trap efficiency under varying flow conditions. J. Mar. Res. 46, 573–592.
Bathmann, U., Fischer, G., Müller, P.J., et al., 1991. Short–term variations in particulate matter sedimentation off Kapp Norvegia, Weddell Sea, Antarctica: relation to water mass advection, ice cover, plankton biomass and feeding activity. Polar Biol. 11, 185–195.
Bathmann, U.V., Scharek, R., Klaas, C., Dubischar, C.D., Smetacek, V., 1997. Spring development of phytoplankton biomass and composition in major water masses of the Atlantic sector of the Southern Ocean. Deep Sea Research Part II: Topical Studies in Oceanography 44, 51–67.
Boltovskoy, D., Alder, V.A., Abelmann, A., 1993. Annual flux of Radiolaria and other shelled plankters in the eastern equatorial Atlantic at 853 m: seasonal variations and polycystine species-specific responses. Deep-Sea Res. (1 Oceanogr. Res. Pap.) 40 (9), 1863–1895.
Bostock, H.C., Barrows, T.T., Carter, L., et al., 2013. A review of the Australian–New Zealand sector of the Southern Ocean over the last 30 ka (Aus-INTIMATE project). Quat. Sci. Rev. 74, 35–57.
Boyd, P., Watson, J., Law, C.S., et al., 2000. Phytoplankton bloom upon mesoscale iron fertilisation of polar Southern Ocean waters. Nature 407, 695–702.
Bracher, A.U., Kroon, B.M.A., Lucas, M.I., 1999. Primary production, physiological state and composition of phytoplankton in the Atlantic Sector of the Southern Ocean. Mar. Ecol. Prog. Ser. 190, 1–16.
Bray, S., Trull, T.W., Manganini, S., 2000. SAZ Project Moored Sediment Traps: Results of the 1997–1998 Deployments. Antarct. Coop. Res. Cent., Hobart, Tasmania, Australia (128 pp.).
Buesseler, K.O., Ball, L., Andrews, J., et al., 2001. Upper ocean export of particulate organic carbon and biogenic silica in the Southern Ocean along 170°W. Deep-Sea Res. (2 Top. Stud. Oceanogr.) 48 (19–20), 4275–4297.
Coale, K.H., Johnson, K.S., Chavez, F.P., et al., 2004. Southern Ocean iron enrichment experiment: Carbon cycling in high- and low-Si waters. Science 304 (5669), 408–414.
Copin-Montegut, C., Copin-Montegut, G., 1983. Stoichiometry of carbon, nitrogen, and phosphorus in marine particulate matter. Deep-Sea Res. (1 Oceanogr. Res. Pap.) 30 (1), 31–46.
Cornet-Barthaux, V., Armand, L.K., Quéguiner, B., 2007. Biovolume and biomass measurements of key Southern Ocean diatoms. Aquat. Microb. Ecol. 48 (3), 295–308.
Crosta, X., Romero, O., Armand, L.K., et al., 2005. The biogeography of major diatom taxa in Southern Ocean sediments: 2. Open ocean related species. Palaeogeogr. Palaeoclimatol. Palaeoecol. 223, 66–92.
De Baar, H.J.W., de Jong, J.T.M., Bakker, D.C.E., et al., 1995. Importance of iron for phytoplankton blooms and carbon dioxide drawdown in the Southern Ocean. Nature 373, 412–415.
Dunbar, R.B., Leventer, A.R., Mucciarone, D.A., 1998. Water column sediment fluxes in the Ross Sea, Antarctica: atmospheric and sea ice forcing. J. Geophys. Res. 103 (30), 741–759.
Esper, O., Gersonde, R., Kadagies, N., 2010. Diatom distribution in southeastern Pacific surface sediments and their relationship to modern environmental variables. Palaeogeogr. Palaeoclimatol. Palaeoecol. 287, 1–27.
Fischer, G., Fütterer, D., Gersonde, R., et al., 1988. Seasonal variability of particle flux in the Weddell Sea and its relation to ice cover. Nature 335, 426–428.
Fischer, G., Gersonde, R., Wefer, G., 2002. Organic carbon, biogenic silica and diatom fluxes in the marginal winter sea-ice zone and in the Polar Front Region: interannual variations and differences in composition. Deep-Sea Res. (2 Top. Stud. Oceanogr.) 47, 1721–1745.
Fitzwater, S.E., Johnson, K.S., Gordon, et al., 2000. Trace metal concentrations in the Ross Sea and their relationship with nutrients and phytoplankton growth. Deep-Sea Res. (2 Top. Stud. Oceanogr.) 47, 3159–3179.
Flores, J.A., Sierro, F.J., 1997. A revised technique for the calculation of calcareous nannofossil accumulation rates. Micropaleontology 43, 321–324.
Gall, M.P., Boyd, P.W., Hall, J., et al., 2001. Phytoplankton processes. Part 1: Community structure during the Southern Ocean Iron Release Experiment (SOIREE). Deep-Sea Res. (1 Oceanogr. Res. Pap.) 48, 2551–2570.
Gardner, W.D., 1980. Sediment trap dynamics and calibration: a laboratory evaluation. J. Mar. Res. 38, 17–39.
Gladstone, R.M., Bigg, G.R., Nicholls, K.W., 2001. Iceberg trajectory modelling and meltwater injection in the Southern Ocean. J. Geophys. Res. 106 (9), 19903–19915.
Goldman, J.C., 1993. Potential role of large oceanic diatoms in new primary production. Deep-Sea Res. (1 Oceanogr. Res. Pap.) 40 (1), 159–168.
Goldman, J.C., McGillicuddy, D.J., 2003. Effect of large marine diatoms growing at low light on episodic new production. Limnol. Oceanogr. 48 (3), 1176–1182.
Gomi, Y., Fukuchi, M., Taniguchi, A., 2010. Diatom assemblages at subsurface chlorophyll maximum layer in the eastern Indian sector of the Southern Ocean in summer. J. Plankton Res. 32 (7), 1039–1050.
Grigorov, I., Rigual-Hernandez, A.S., Honjo, S., et al., 2014. Settling fluxes of diatom frustules to the interior of the Antarctic Circumpolar Current along 170°W. Deep-Sea Res. (1 Oceanogr. Res. Pap.) 93, 1–13.
Hallegraeff, G.M., 1986. Taxonomy and morphology of the marine plankton diatoms *Thalassionema* and *Thalassiothrix*. Diatom Res. 1, 57–80.
Hart, T., 1934. On the phytoplankton of the South-West Atlantic and the Bellinghausen Sea, 1929–31. Discov. Rep. 8, 1–268.
Heussner, S., Durrieu De Madron, X., Calafat, A., et al., 2006. Spatial and temporal variability of downward particle fluxes on a continental slope: Lessons from an 8-yr experiment in the Gulf of Lions (NW Mediterranean). Mar. Geol. 234, 63–92.
Honjo, S., 1996. Fluxes of particles to the interior of the open oceans. In: Ittekkot, V., et al. (Eds.), Particle Flux in the Ocean. John Wiley, New York, pp. 91–154.
Honjo, S., 2009. Biological pump and particulate fluxes. In: Steele, J.H., Thorpe, S.A., Turekian, K.K. (Eds.), Encyclopaedia of ocean sciences. Academic Press, San Diego, CA, pp. 371–375.
Honjo, S., Doherty, K.W., 1988. Large aperture time-series sediment traps; design objectives, construction and application. Deep-Sea Res. 35 (1), 133–149.
Honjo, S., Spencer, D.W., Gardner, W.D., 1992. A sediment trap intercomparison experiment in the Panama Basin, 1979. Deep-Sea Res. (1 Oceanogr. Res. Pap.) 39, 333–358.
Honjo, S., Francois, R., Manganini, S., et al., 2000. Particle fluxes to the interior of the Southern Ocean in the Western Pacific sector along 170 degrees W. Deep-Sea Res. (2 Top. Stud. Oceanogr.) 47 (15–16), 3521–3548.
Honjo, S., Manganini, S.J., Krishfield, R.A., et al., 2008. Particulate organic carbon fluxes to the ocean interior and factors controlling the biological pump: A synthesis of global sediment trap programs since 1983. Prog. Oceanogr. 76 (3), 217–285.
Ichinomiya, M., Gomi, Y., Nakamachi, M., et al., 2008. Temporal variations in the abundance and sinking flux of diatoms under fast ice in summer near Syowa Station, East Antarctica. Polar Sci. 2, 33–40.
Ishikawa, A., Wasiyama, N., Tanimura, A., et al., 2001. Variation in the diatom community under fast ice near Syowa Station, Antarctica, during the austral summer of 1997/98. Polar Biosci. 14, 10–23.
Johnson, K.S., Gordon, R.M., Coale, K.H., 1997. What controls dissolved iron concentrations in the world ocean? Mar. Chem. 57 (3–4), 137–161.

Kemp, A.E.S., Villareal, T.A., 2013. High diatom production and export in stratified waters – A potential negative feedback to global warming. Prog. Oceanogr. 119, 4–23.
Kemp, A.E.S., Pike, J., Pearce, R.B., et al., 2000. The "Fall dump" a new perspective on the role of a "shade flora" in the annual cycle of diatom production and export flux. Deep-Sea Res. (1 Oceanogr. Res. Pap.) 47, 2129–2154.
Kemp, A.E.S., Pearce, R.B., Grigorov, I., 2006. Production of giant marine diatoms and their export at oceanic frontal zones:implications for Si and C flux from stratified oceans. Global Biogeochem. Cycles 20 (4), GB4S04.
Kimura, N., Wakatsuchi, M., 2011. Large-scale processes governing the seasonal variability of Antarctic sea-ice area. Tellus 63A, 828–840.
Kopczynska, E.E., Dehairs, F., Elskens, M., et al., 2001. Phytoplankton and microzooplankton variability between the Subtropical and Polar Fronts south of Australia: Thriving under regenerative and new production in late summer. J. Geophys. Res. 106, 31597–31609.
Lam, P.J., Bishop, J.K.B., 2007. High biomass low export regimes in the southern ocean. Deep-Sea Res. (2 Top. Stud. Oceanogr.) 54 (5–7), 601–638.
Lampitt, R.S., Antia, A.N., 1997. Particle flux in deep seas: regional characteristics and temporal variability. Deep-Sea Res. (1 Oceanogr. Res. Pap.) 44 (8), 1377–1403.
Laubscher, R.K., Perissinotto, R., McQuaid, C.D., 1993. Phytoplankton production and biomass at frontal zones in the Atlantic Sector of the Southern Ocean. Polar Biol. 13, 471–481.
Leventer, A., Dunbar, R.B., 1987. Diatom flux in McMurdo Sound, Antarctica. Mar. Micropaleontol. 12, 49–64.
Leventer, A., Dunbar, R.B., 1996. Factors influencing the distribution of diatoms and other algae in the Ross Sea. J. Geophys. Res. 101, 18489–18500.
Leventer, A., Dunbar, R.B., DeMaster, D.J., 1993. Diatom Evidence for Late Holocene Climatic Events in Granite Harbor, Antarctica. Paleoceanography 8, 373–386.
Locarnini, R.A., Mishonov, A.V., Antonov, J.I., 2010. *World Ocean Atlas 2009*, Volume 1: Temperature 1. U.S. Government Printing Office, Washington, D.C.
Martin, J.H., Fitzwater, S.E., Gordon, R.M., 1990. Iron deficiency limits phytoplankton growth in Antarctic waters. Global Biogeochem. Cycles 4, 5–12.
Massom, R., Reid, P., Stammerjohn, S., et al., 2013. Change and Variability in East Antarctic Sea Ice Seasonality, 1979/80–2009/10. PLoS ONE 8 (5), e64756.
Matsumoto, K., Sarmiento, J.L., Brzezinski, M.A., 2002. Silicic acid leakage from the Southern Ocean: A possible explanation for glacial atmospheric pCO2. Global Biogeochem. Cycles 16, 1031.
Moore, J.K., Abbott, M.R., 2000. Phytoplankton chlorophyll distributions and primary production in the Southern Ocean. J. Geophys. Res. 105, 28709–28722.
Nelson, D.M., Tréguer, P., Brzezinski, M.A., et al., 1995. Production and dissolution of biogenic silica in the ocean: Revised global estimates, comparison with regional data and relationship to biogenic sedimentation. Global Biogeochem. Cycles 9, 359–372.
Orsi, A.H., Whitworth III, T., Nowlin Jr., W.D., 1995. On the meridional extent and fronts of the Antarctic Circumpolar Current. Deep-Sea Res. (1 Oceanogr. Res. Pap.) 42, 641–673.
Ortiz, J.D., Mix, A.C., 1997. Comparison of Imbrie-Kipp transfer function and modern analog temperature estimates using sediment trap and core top foraminiferal faunas. Paleoceanography 12, 175–190.
Parslow, J., Boyd, P., Rintoul, S.R., et al., 2001. A sub-surface chlorophyll maximum in the Polar Frontal Zone south of Australia: seasonal evolution and implications for phytoplankton-light-nutrient interactions. J. Geophys. Res. 106, 31543–31550.
Pilskaln, C.H., Manganini, S.J., Trull, T., et al., 2004. Geochemical particle fluxes in the Southern Indian Ocean seasonal ice zone: Prydz Bay region, east Antarctica. Deep-Sea Res. (1 Oceanogr. Res. Pap.) 50, 307–332.
Pondaven, P., Ragueneau, O., Tréguer, P., et al., 2000. Resolving the `opal paradox' in the Southern Ocean. Nature 405, 168–172.
Popp, B.N., Trull, T., Kenig, F., et al., 1999. Controls on the carbon isotopic composition of Southern Ocean phytoplankton. Global Biogeochem. Cycles 13 (4), 827–843.
Quéguiner, B., 2013. Iron fertilization and the structure of planktonic communities in high nutrient regions of the Southern Ocean. Deep-Sea Res. I (1 Oceanogr. Res. Pap.) 90, 43–54.
Quilty, P., Kerry, K.R., Marchant, H.J., 1985. A seasonally recurrent patch of Antarctic planktonic diatoms. Search (ANZAAS) 16, 48.
Reynolds, R.W., Rayner, N.A., Smith, T.M., et al., 2002. An improved in situ and satellite SST analysis for climate. J. Clim. 15, 1609–1625.
Rintoul, S.R., Bullister, J.L., 1999. A late winter Hydrographic section from Tasmania to Antarctica. Deep-Sea Res. (1 Oceanogr. Res. Pap.) 46, 1417–1454.
Rintoul, S.R., Sokolov, S., 2001. Baroclinic transport variability of the Antarctic Circumpolar Current south of Australia (WOCE repeat section SR3). J. Geophys. Res. 106, 2795–2814.
Romero, O.E., Armand, L.K., 2010. Marine diatoms as indicators of modern changes in oceanographic conditions. Cambridge University Press, Cambridge pp. 373–400.
Romero, O.E., Lange, C.B., Fischer, et al., 1999. Variability in export production documented by downward fluxes and species composition of marine planktonic diatoms: observations from the tropical and equatorial Atlantic. In: Fischer, G., Wefer, G. (Eds.), The Use of Proxies in Paleoceanography, Examples from the South Atlantic. Springer, Berlin, Heidelberg, pp. 365–392.
Romero, O.E., Fischer, G., Lange, C.B., et al., 2000. Siliceous phytoplankton of the western equatorial Atlantic: sediment traps and surface sediments. Deep-Sea Res. (2 Top. Stud. Oceanogr.) 47, 1939–1959.
Romero, O., Armand, L.K., Crosta, X., et al., 2005. The biogeography of major diatom taxa in Southern Ocean sediments: 3. Tropical/Subtropical species. Palaeogeogr. Palaeoclimatol. Palaeoecol. 223, 49–65.
Romero, O., Thunell, R.C., Astor, Y., et al., 2009. Seasonal and interanual dynamics in diatom production in the Cariaco Basin, Venezuela. Deep-Sea Res. (1 Oceanogr. Res. Pap.) 56, 571–581.
Sakshaug, E., Holm-Hansen, O., 1984. Factors governing pelagic production in polar oceans. In: Holm-Hansen, O., Bolis, L., Gilles, R. (Eds.), Marine Phytoplankton and ProductivityLecture Notes on Coastal and Estuarine Studies vol. 8. Springer, Berlin, pp. 1–18.
Sancetta, C., Calvert, S.E., 1988. The annual cycle of sedimentation in Saanich Inlet, British Columbia: implications for the interpretation of diatom fossil assemblages. Deep-Sea Res. 35 (1), 71–90.
Sarmiento, J.L., Hughes, T.M.C., Stouffer, R.J., et al., 1998. Simulated response of the ocean carbon cycle to anthropogenic climate warming. Nature 393, 245–249.
Schrader, H.J., Gersonde, R., 1978. Diatoms and silicofagellates. Micropaleontological counting methods and techniques: an exercise on an eight metres section of the Lower Pliocene of Capo Rosello, Sicily. Utrecht Bull. Micropaleontol. 17, 129–176.
Semina, H.J., 2003. SEM-studied diatoms of different regions of the World Ocean. Iconogr. Diatomol. 10, 1–362.
Smetacek, V., 1999. Diatoms and the ocean carbon cycle. Protist 250, 25–32.
Smith Jr., W.O., Nelson, D.M., 1986. Importance of ice edge phytoplankton production in the Southern Ocean. Bioscience 36 (4), 251–257.
Smith Jr., K.L., Sherman, A.D., Shaw, T.J., et al., 2011. Carbon export associated with free-drifting icebergs in the Southern Ocean. Deep-Sea Res. (2 Top. Stud. Oceanogr.) 58 (11–12), 1485–1496.
Sohrin, Y., Iwamoto, S., Matsui, M., et al., 2000. The distribution of Fe in the Australian sector of the Southern Ocean. Deep-Sea Res. (1 Oceanogr. Res. Pap.) 47, 55–84.
Sokolov, S., Rintoul, S.R., 2002. Structure of southern ocean fronts at 140 E. J. Mar. Syst. 37, 151–184.
Sokolov, S., Rintoul, S.R., 2007. Multiple Jets of the Antarctic Circumpolar Current South of Australia. J. Phys. Oceanogr. 37, 1394–1412.
Sokolov, S., Rintoul, S.R., 2009a. Circulation structure and distribution of the Antarctic Circumpolar Current fronts: 1. Mean circumpolar paths. J. Geophys. Res. 114, C11018.
Sokolov, S., Rintoul, S.R., 2009b. Circulation structure and distribution of the Antarctic Circumpolar Current fronts: 2. Variability and relationship to sea surface height. J. Geophys. Res. 114, C11019.
Sullivan, C.W., McClain, C.R., Comiso, J.C., Smith, W.O., 1988. Phytoplankton standing crops within an Antarctic ice edge assessed by satellite remote sensing. J. Geophys. Res. 93, 12487–12498.
Suzuki, H., Sasaki, H., Fukuchi, M., 2001. Short-term variability in the flux of rapidly sinking particles in the Antarctic Marginal Ice Zone. Polar Biol. 24, 697–705.
Takahashi, K., 1986. Seasonal fluxes of pelagic diatoms in the subarctic Pacific, 1982–1983. Deep-Sea Res. 33, 1225–1251.
Taylor, F., Sjunneskog, C., 2002. Postglacial marine diatom record of the Palmer Deep, Antarctic Peninsula (ODP Leg 178, Site 1098) 2. Diatom assemblages. Paleoceanography 17 (PAL 2-1-PAL 2-12).
Tréguer, P.J., De La Rocha, C.L., 2013. The world ocean silica cycle. Annu. Rev. Mar. Sci. 5, 477–501.
Trull, T., Armand, L., 2001. Insights into Southern Ocean Carbon export from the δ 13 C of particles and dissolved inorganic carbon during the SOIREE iron release experiment. Deep-Sea Res. (2 Top. Stud. Oceanogr.) 48, 2655–2680.
Trull, T., SedwickF, P.N., Griffiths, F.B., et al., 2001a. Introduction to special section: SAZ Project. J. Geophys. Res. 106, 31425–31429.
Trull, T., Bray, S., Manganini, S., et al., 2001b. Moored sediment trap measurements of carbon export in the Subantarctic and Polar Frontal Zones of the Southern Ocean, south of Australia. J. Geophys. Res. 106, 31489–31510.
Trull, T., Rintoul, S.R., Hadfield, M., et al., 2001c. Circulation and seasonal evolution of polar waters south of Australia: Implications for iron fertilization of the Southern Ocean. Deep-Sea Res. (1 Oceanogr. Res. Pap.) 48, 2439–2466.
Varela, D.E., Pride, C.J., Brzezinski, M.A., 2004. Biological fractionation of silicon isotopes in Southern Ocean surface waters. Global Biogeochem. Cycles 18, GB1047.
Wefer, G., Fischer, G., Füetterer, D., Gersonde, R., 1988. Seasonal particle flux in the Bransfield Strait. Antartica. Deep Sea Res. Part A (Oceanogr. Res. Pap.) 35, 891–898.
Yu, E.F., Francois, R., Bacon, M.P., et al., 2001. Trapping efficiency of bottom-tethered sediment traps estimated from the intercepted fluxes of ^{230}Th and ^{231} Pa. Deep-Sea Res. (1 Oceanogr. Res. Pap.) 48 (3), 865–889.
Zeldis, J., 2001. Mesozooplankton community composition, feeding, and export production during SOIREE. Deep-Sea Res. (2 Top. Stud. Oceanogr.) 48, 2615–2634.